CELL FUNCTIONS AND MOLECULAR MECHANISMS OF ZINC TRANSPORTERS IN *NEUROSPORA CRASSA*

A thesis submitted in partial fulfillment of the requirements

for the award of the degree of

DOCTOR OF PHILOSOPHY

by

SERENA NGIIMEI D

Department of Biosciences and Bioengineering

Indian Institute of Technology Guwahati,

Guwahati-781039, Assam, India

November 2023

भारतीय प्रौद्योगिकी संस्थान गुवाहाटी
INDIAN INSTITUTE OF TECHNOLOGY GUWAHATI
Department of Biosciences and Bioengineering

Statement

I do hereby declare that the content embodied in this thesis entitled **"Cell functions and molecular mechanisms of zinc transporters in *Neurospora crassa*"** is the result of investigation carried out by me in the Department of Biosciences and Bioengineering, Indian Institute of Technology, Guwahati, India, under the guidance of Prof. Ranjan Tamuli. The research presented in this thesis is original and has not been submitted in part or full for any degree or diploma to any other institute or university to the best of my knowledge and belief.

IIT, Guwahati

November, 2023

Serena Ngiimei D

Enrolment No.: 176106005
Department of Biosciences and Bioengineering
Indian Institute of Technology Guwahati,
Guwahati-781039, Assam, India

भारतीय प्रौद्योगिकी संस्थान गुवाहाटी
INDIAN INSTITUTE OF TECHNOLOGY GUWAHATI
Department of Biosciences and Bioengineering

Certificate

This is to certify that the research conducted for the thesis titled **"Cell functions and molecular mechanisms of zinc transporters in *Neurospora crassa*"** by **Serena Ngiimei D** (176106005) was carried out at the Indian Institute of Technology Guwahati, under my direct supervision. The research presented in this thesis is entirely original and has not been submitted, either in part or in full, for the attainment of any other degree or diploma from any other academic institution or university.

IIT, Guwahati

November, 2023

Dr. Ranjan Tamuli
Professor
Department of Biosciences and Bioengineering
Indian Institute of Technology Guwahati,
Guwahati-781039, Assam, India

Dedicated

to

my loving parents

K Daniel Ngiimei & M Rose Mary

Contents

List of Figures

List of Tables

Abbreviations

ANOVA	Analysis of Variance
bp	Base pair
BLAST	Basic Local Alignment Tool
BOD	Biological Oxygen Demand
CD	Circular dichroism
°C	Degree Celsius
CDD	Conserved Domain Database
cDNA	complementary Deoxyribonucleic Acid
CFW	Calcofluor White
cm	Centimetre
DNA	Deoxyribonucleic Acid
ExPASy	Expert Protein Analysis System
FGS	Fructose, Glucose, Sorbose
FGSC	Fungal Genetics Stock Centre
g	Gram
g	Relative Centrifugal Force
GFP	Green Fluorescent Protein
h	Hour
hph	Hygromycin B Resistance Gene
Jm-2	Joule per square metre
KV	Kilovolt
kb	Kilo base pair
kDa	Kilo Dalton
LG	Linkage Group
m	Metre
M	Molar
mA	Milliampere
MEGA	Molecular Evolutionary Genetic Analysis
µg	Microgram
µl	Microlitre
µm	Micrometre
µM	Micromolar
ml	Millilitre
mm	Millimetre
mM	Millimolar
N	Normal
NCBI	National Centre for Biotechnology Information
NCU	*Neurospora crassa* unit
NEB	New England Biolab
ng	Nanogram
NIH	National Institute of Health
NLS	Nuclear localization signal
nM	Nanomolar
NMR	Nuclear magnetic resonance
Ω	ohm
OD	Optical Density
ORF	Open Reading Frame
%	Percent
p	Probability
PCR	Polymerase Chain Reaction
pm	Picometre
psi	Pound-force per square inch
qRT-PCR	Quantitative Real-Time Polymerase Chain Reaction
RIP	Repeat Induced Point Mutation
RNA	Ribonucleic Acid
rpm	Revolution per minute
RT-PCR	Reverse Transcription Polymerase Chain Reaction
s	Second
SCM	Synthetic Crossing Media
SOC	super optimal broth with Catabolite repression
STRING	Search tool for the retrieval of interacting genes/proteins
UCR	University of California Riverside
UK	United Kingdom
USA	United States of America
UV	Ultraviolet
VGN	Vogel's Glucose Medium
V	Volt
w/v	weight per volume
w/w	weight per weight
UCR	University of California Riverside
YPD	Yeast Peptone Dextrose

Acknowledgments

I am filled with gratitude and immense joy as I extend my heartfelt thanks to every person who has lent their support and encouragement throughout this remarkable journey.

First and foremost, praises and thanks to God, the Almighty for His showers of blessings throughout my life and my research work, to complete this research successfully.

I would like to extend my deepest respect and gratitude to my supervisor, ***Prof. Ranjan Tamuli****, for giving me the opportunity to do research and for the invaluable guidance throughout this research. Without his constant motivation and meticulous supervision, this thesis would have remained but a distant dream. I hold dear the occasions when my experiments encountered challenges, for it was during these moments that I truly appreciated the patience and support of my mentor. His skillful guidance steered me toward the paths where I could uncover the answers I sought, and I am deeply thankful for his patience in reviewing the multiple iterations of my thesis. His nurturing research environment played a crucial role in making my Doctoral journey a priceless journey of enlightenment and growth.*

I would also like to thank my Doctoral committee members ***Prof. Aiyagari Ramesh*** *(Department of Biosciences and Bioengineering),* ***Dr. Kusum K Singh*** *(Department of Biosciences and Bioengineering), and* ***Dr. Uttam Manna*** *(Department of Chemistry) for their insightful suggestions and constructive criticisms of my work, which have eventually made it possible for me to complete my thesis.*

I also express my heartfelt gratitude to both the current and former Directors of the Indian Institute of Technology Guwahati (IITG) for bestowing upon me the privilege of conducting my

doctoral research within the vibrant and naturally rich campus they have nurtured. I also extend my sincere appreciation to the current and past Heads of the Department of Biosciences and Bioengineering, as well as all the dedicated staff members of the department, for their support in terms of access to essential analytical instruments and laboratory facilities, which were instrumental in the successful completion of my thesis.

I would like to convey my profound respects to the taxpayers of our nation, whose contributions have enabled various funding agencies, including the Ministry of Human Resources Development (MHRD), the Department of Science and Technology (DST), and the Department of Biotechnology (DBT) of the Government of India, to provide me with the necessary fellowships and project funding to my supervisor. It is through their generous support that my supervisor and I were inspired to bring our research endeavors to fruition in the form of this thesis.

I would also like to thank the Fungal Genetics Stock Centre (FGSC), University of Missouri, Kansas City, USA, for readily providing Neurospora strains. I am also grateful to ***Dr. Shirisha Nagotu****, OBCAL Lab, BSBE department, IIT Guwahati, Assam, India, for the S. cerevisiae strains BY4742 and YJL056C, which were needed for my research work.*

I extend my special thanks to all the RT Lab members, past and present, who have collectively guided me toward becoming a more experienced researcher through their invaluable contributions and collaborative spirit. This gratitude extends to Rahul, Surabhi, Sangeeta, Krishna, Megha, Rebecca, Shomina, Priyanuj, and Ambika as well as the alumni members of this group – Dr. Rekha Deka, Dr. Ravi Kumar, Dr. Vijaya Laxmi, Dr. Ananya Barman, Dr. Dibakar Gohain, Dr. Ajeet Kumar, Dr. Avishek Roy, Dr. Anand Tiwari, Dr. Christy K Marak, Dr. Darshana Baruah, Shalini, Nayan, Divya, Mohit, Aravind, and Abhilash. I treasure the times I spent in the lab with my lab mates, especially the lighter, more memorable times during tea breaks.

*I express my heartfelt gratitude to my friends at IITG - **Christy**, **Lhingcy**, **Moite**, **Emily**, and **Megha**. Their friendship, encouragements, and shared moments of joy have been a constant source of strength during this demanding journey. They made the challenges more manageable and the achievements more meaningful. My sincere gratitude also goes out to my friends **Wejeanliu**, **Monica**, **Victor** and **Solace**, who have continuously inspired and encouraged me to set higher goals and go farther. Their encouragement has been a driving force in my academic pursuits. I am also deeply grateful to **Mr. T. T. Haokip** (Joint Registrar, IITG) and his family for their generosity, warm hospitality, and guidance in nurturing not only my academic development but also my spiritual growth.*

*I am extremely grateful to my parents **(K Daniel Ngiimei** and **M Rose Mary)** and my grandparents **(Apou Karaiba** and late **Apai Kina)** for their boundless love, unceasing prayers, selfless care, and the countless sacrifices they've made to raise and educate me. Their encouragement has shaped the person I am today, empowering me to embark on the journey of pursuing my Ph.D. I reserve my sincerest, deepest thanks to my younger siblings **(Disunga**, **Rapunga**, **Maningdouba**, **Khangshung)**, beloved cousins, and relatives. Their unwavering support, invaluable prayers, and unconditional love have been the driving forces propelling me forward throughout my entire life.*

Lastly, I would like to express my gratitude to everyone who helped me, whether directly or indirectly, to finish this research work.

IIT Guwahati *Serena Ngiimei D*

Abstract

In this thesis work, I studied the cellular functions and molecular mechanisms of zinc resistance-conferring 1 (ZRC-1), meiotic sister chromatid 2 (MSC-2), and zinc-regulated gene 17 (ZRG-17) that are members of the cation diffusion facilitator (CDF) family of zinc transporters in *Neurospora crassa*. The Δ*zrc-1* mutant was unable to grow under high zinc conditions (≥ 0.5 mM). However, the expression of *zrc-1* was elevated ~3-fold under low zinc conditions in comparison to normal and high zinc concentrations. The Δ*msc-2* mutant showed colony growth and aerial hyphae similar to wild type and the expression of *msc-2* was independent of zinc. Furthermore, the double mutant Δ*zrc-1*; Δ*msc-2* and Δ*zrc-1*; Δ*zrg-17* showed additive phenotypes of both the parental single mutants. However, the phenotypic defects such as slow growth rate, defective in asexual sporulation, and inability to degrade cellulose of the Δ*zrg-17* single mutant were restored in the Δ*msc-2*; Δ*zrg-17* double mutant, which showed phenotypes similar to the wild type. The double mutant Δ*zrc-1*; Δ*zrg-17* showed severe growth defects, stunted aerial hyphae, short septa, and defects in conidiation. In addition, the Δ*zrc-1*; Δ*msc-2* and Δ*zrc-1*; Δ*zrg-17* double mutants showed sensitivity to DTT-induced ER stress and were unable to grow in the medium containing cellulose. Furthermore, zinc-responsive activator protein 1 (ZAP-1) was also studied to understand the molecular mechanism and the interaction of the CDF zinc transporters with the transcription factor. The *zap-1* of *N. crassa* was found to be crucial for survival under low zinc conditions and ZAP-1 was localized in nucleus under all zinc conditions tested. The double mutants Δ*zap-1*; Δ*zrc-1*, Δ*zap-1*; Δ*msc-2*, and Δ*zap-1*; Δ*zrg-17* showed slow growth under low zinc like Δ*zap-1* indicating that ZAP-1 might be functioning upstream of *zrc-1*, *msc-2,* and *zrg-17*. Furthermore, expression analysis of the CDF family of zinc transporter, *zrc-1*, *msc-2, zrg-17*, and *zrt-3* in Δ*zap-1* mutant showed very low-level expressions compared to expression in wild type, indicating that the ZAP-1 transcription factor regulates the CDF zinc transporters under low zinc conditions.

Synopsis

Thesis title: **Cell functions and molecular mechanisms of zinc transporters in *Neurospora crassa***

Objectives:

1. To investigate the cellular roles of the CDF family of zinc transporters *zrc-1* and *msc-2* in *Neurospora crassa*,
2. To study the genetic interaction of *zrc-1*, *msc-2* and *zrg-17* in *Neurospora crassa*, and
3. To investigate the role of ZAP-1 transcription factor in regulating CDF zinc transporters in *Neurospora crassa*

Chapter 1: Introduction to the zinc signaling system and the model filamentous fungus *Neurospora crassa*

Chapter 2: Materials and Methods

Chapter 3: Investigating the cellular roles of the CDF family zinc transporters *zrc-1* and *msc-2* in *Neurospora crassa*

Chapter 4: Investigating the genetic interaction of *zrc-1*, *msc-2* and *zrg-17* in *Neurospora crassa*

Chapter 5: Investigating the role of ZAP-1 transcription factor in regulating CDF zinc transporters in *Neurospora crassa*

Chapter 6: Conclusions and future perspectives

Bibliography

Chapter 1: Introduction to the zinc signaling system and the model filamentous fungus *Neurospora crassa*

Chapter 1 briefly describes the significance of zinc in the biological system, how the zinc transporters maintain optimal zinc levels vital for eukaryotic cells to function properly, and how this is achieved. This chapter also elaborates on the history and biology of the model filamentous fungus *Neurospora crassa*. Zinc is an essential trace element and a structural component of numerous proteins, including growth factors, cytokines, receptors, intracellular signaling enzymes, and transcription factors involved in cellular signaling pathways and their biological activity. Zinc participates in many enzymatic and metabolic functions in the body, and regulates the activity of more than 300 enzymes(Gaither and Eide 2001b; Eide 2006; Cousins et al. 2006; Yamasaki et al. 2007; Cuajungco et al. 2021; Clemens 2022). In addition, all organisms must also ensure zinc homeostasis despite the constantly changing extracellular environment to avoid zinc over-accumulation. The amount of total zinc needed for the optimum growth of eukaryotic cells ranges from 0.1−1 mM (Palmiter and Findley 1995; Suhy et al. 1999; MacDiarmid et al. 2000; Outten and O'Halloran 2001). There are robust pathways that maintain zinc homeostasis while ensuring an adequate supply of zinc for various signaling processes.

The maintenance of zinc homeostasis is regulated by various transporter proteins that maintain the Zn^{2+} levels (Eide 2006). In eukaryotes, zinc transporter proteins belong to two major groups of protein, namely the Zrt- Irt-like protein family (ZIP) and cation diffusion facilitator (CDF)/zinc transporter (ZnT) family. The ZIP family proteins enable the uptake or release of zinc from intracellular stores, whereas the transport of zinc out of the cell or into the lumens of intracellular compartments that is accomplished by the CDF family members (Eide 2006; Kambe et al. 2017).

The CDF family of zinc transporters plays a role in zinc homeostasis from prokaryotes to eukaryotes. These zinc transporters possess a unique ability to transport metal ions, including zinc, from the cytoplasm to the lumen of intracellular organelles or outside the cell (Paulsen and Saier 1997; Gaither and Eide 2001b; Nies 2003; Kambe et al. 2004; Cousins et al. 2006). The CDF family is involved in the zinc transport inside the cell, via a Zn^{2+}/ H^{+} antiport mechanism, until an ambient zinc level is reached. The CDF proteins also tightly regulate the export and import of zinc into the cellular compartments to maintain zinc homeostasis and prevent zinc toxicity. In *Saccharomyces cerevisiae*, the transmembrane proteins Meiotic sister chromatid -2 (Msc2p) and zinc-regulated gene 17 (Zrg17p) form a heteromeric complex in the endoplasmic reticulum (ER) and mediate zinc transport into the ER under low zinc conditions (Ellis et al. 2005). Alternatively, when zinc is high in the cytosol, zinc resistance-conferring 1 (Zrc1p) transports the extra zinc into vacuoles for storage and thereby serves as a suppressor of zinc toxicity (Miyabe et al. 2001). The zinc-activated protein 1 (Zap1p) transcription factor regulates the majority of the zinc transporters under the low zinc condition (Zhao and Eide 1997). Previous studies showed that Zap1p upregulates the expression of ~80 genes in *S. cerevisiae* (Lyons et al. 2000; Wu et al. 2008). Under the zinc-limiting conditions, Zap1p binds to an eleven-base pair consensus sequence known as zinc-responsive element (ZRE), which is found in one or more copies in the promoter region of the target genes (Zhao et al. 1998). Moreover, Zap1p undergoes auto-regulation by itself via a positive feedback loop by sensing zinc (Zhao and Eide 1997; Bird et al. 2000a; Yao et al. 2023).

N. crassa is a filamentous fungus extensively used as a model organism for several decades to understand numerous aspects of eukaryotic cell biology, genetics, biochemistry, and molecular biology (Perkins 1992; Davis 2000; Davis and Perkins 2002). In *N. crassa*, the regulations of zinc transporters and maintenance of zinc homeostasis are still largely unknown. Previous studies

(Kiranmayi and Mohan 2006; Montanini et al. 2007) showed the presence of nine putative CDF family proteins in *N. crassa*. Except for ZRG-17, the cellular roles of the CDF proteins are unexplored in *N. crassa* (Tiwari et al. 2018). Additionally, the expression of *zrg-17* was upregulated under low zinc (Tiwari et al. 2018), indicating the importance of zinc transporters for the proper growth and development of *N. crassa.* I studied the *zrg-17* knockout mutant that showed several zinc suppressible phenotypes such as slow growth rate, short aerial hyphae, and defects in asexual sporulation. In addition, I found that ZRG-17 is critical for ER stress tolerance and cellulose degradation under low zinc conditions. I also studied the cell functions of two other CDF zinc transporters ZRC-1 and MSC-2 in *N. crassa*. Furthermore, I studied the interactions between *zrc-1*, *msc-2,* and *zrg-17* to understand the significance of their genetic interaction in growth and development, and tolerance to various conditions such as ER stress, pH stress, temperature sensitivity, osmotic stress, and azole stress. Moreover, I identified the homolog of the *S. cerevisiae* Zap1p in *N. crassa* and investigated the transcriptional regulation of zinc transporters in response to low zinc in *N. crassa*.

Chapter 2: Material and Methods

Chapter 2 describes the materials and methods used in my thesis work. The *N. crassa* strains used in this study were either obtained from the Fungal Genetics Stock Center (FGSC, University of Missouri, Kansas City, MO 64110) or generated in our laboratory. The *S. cerevisiae* strains wild type (BY4742) and *zap1Δ* (YJL056C) were a kind gift from Dr. Shirisha Nagotu (IIT Guwahati, India). The growth and maintenance of the *N. crassa* strains were done using the media and procedures as described previously (Westergaard and Mitchell 1947; Davis and de Serres 1970). Chemicals and reagents were procured from the standard suppliers, and used after autoclave or filter sterilization whenever required. Cloning, PCR, Reverse Transcriptase PCR, Real-Time PCR, and other molecular biology experiments

were carried out by following the manufacturer's instructions or the generally accepted techniques as outlined by Sambrook and Russell (2001).

Chapter 3: Investigating the cellular roles of the CDF family zinc transporters *zrc-1* and *msc-2* in *Neurospora crassa*

In this Chapter, I discussed the cellular roles of the zinc transporters *zrc-1* and *msc-2* in *N. crassa*. The sequence analysis revealed that the *N. crassa* ZRC-1 and MSC-2 exhibited 39.14% and 44.93% sequence identities to the *S. cerevisiae* Zrc1p and Msc2p, respectively. The ZRC-1 and MSC-2 proteins exhibit the typical features of the other classical CDF proteins, including six transmembrane helices, a histidine-rich cytoplasmic loop, and a long C-terminal domain (≥100 aa) (Kolaj-Robin *et al.* 2015). I also performed homology modeling of the putative three-dimensional structure of the *N. crassa* ZRC-1 and MSC-2. The predicted structure revealed that the zinc-binding motif DD-HD (Lu and Fu 2007) is partially conserved in ZRC-1 and MSC-2 as HD-HD motif. This HD-HD motif was also found conserved in mammalian zinc transporters (ZnT1- ZnT8), where Zn^{2+} efficiently binds to HD-HD (Hoch et al. 2012).

Furthermore, I investigated the functions of ZRC-1 and MSC-2, in the vegetative growth, asexual, and sexual development of *N. crassa*. The strain lacking *zrc-1* was unable to produce aerial hyphae at high zinc concentrations, whereas the wild type was able to grow at higher concentrations of zinc. In addition, the Δ*zrc-1* mutant showed a significantly slow colony growth rate and sparse branching pattern under high zinc concentrations (≥ 0.5 mM). The Δ*msc-2* mutant exhibited no significant differences in growth compared to the wild type. Taken together, these suggest that ZRC-1 is critical for survival under high zinc conditions in *N. crassa*. The expression analysis of *zrc-1* and *msc-2* under different concentrations of zinc was also determined. The expression of *zrc-1* was ~3-

fold elevated in low zinc than in the high zinc conditions. In the promoter analysis, putative ZRE consensus sequence (-ACCYYNAAGGT-) at the promoter region of *zrc-1* was identified, indicating that ZAP-1 might play a role in *zrc-1* regulation. Moreover, there were no significant differences in the expression of *msc-2* in all zinc concentrations (VG, LZVG1, and LZVG1000). These results suggested that the cell functions of MSC-2 and ZRC-1 are conserved in *N. crassa* similar to the *S. cerevisiae*.

Chapter 4: Investigating the genetic interaction of *zrc-1*, *msc-2* and *zrg-17* in *Neurospora crassa*

In this chapter, I described the genetic interaction between *zrc-1*, *msc-2*, and *zrg-17*. I generated double mutants of *zrc-1*, *msc-2* and *zrg-17* genes to study their genetic interactions. The Δ*zrc-1*; Δ*msc-2*, Δ*msc-2*; Δ*zrg-17* and Δ*zrc-1*; Δ*zrg-17* double mutants were generated by crossing their respective single mutants of opposite mating types. The double mutants were tested on the Vogel's Glucose (VG) medium containing different concentrations of zinc for vegetative development. The Δ*zrc-1*; Δ*zrg-17* double mutant showed severe defects in growth and asexual reproduction compared to wild type. Similarly, Δ*zrc-1*; Δ*msc-2* double mutant showed phenotypes like the parental Δ*zrc-1* single mutant in high zinc condition. In contrast, the Δ*msc-2*; Δ*zrg-17* double mutant rescued the phenotypic defects of the Δ*zrg-17* single mutant, suggesting an antagonistic interaction between *msc-2* and *zrg-17*.

The Δ*zrc-1;* Δ*zrg-17* double mutant showed stunted aerial hyphae, a shorter inter-septal distance that results in more septation, and shorter hyphal width. Moreover, Δ*zrc-1;* Δ*zrg-17* showed conidiation defects, including early and enhanced immature conidiation and inappropriate conidiation in submerged culture, which was correlated with the elevated expression of the conidiation-specific *con-10* gene. Therefore, the CDF zinc transporters and genetic interactions between *zrc-1* and *zrg-17* regulate the development of septa and proper conidiation in *N. crassa*.

The Δ*zrc-1*; Δ*msc-2* and Δ*zrc-1*; Δzrg-*17* double mutants showed slight decrease in aerial hyphae height under DTT induced ER stress and these double mutants were not able to utilize cellulose, producing negligible or no biomass. Furthermore, the protein concentrations and the glucose released in the supernatant of the double mutants were determined. The inability of the Δ*zrc-1*; Δ*msc-2* and Δ*zrc-1*; Δzrg-*17* double mutants to grow in the cellulose-containing medium was correlated with the decreased in protein concentration and lower cellulase activity in the double mutants. These results suggested the involvement of CDF zinc transporters and their genetic interactions in normal growth, tolerance to stress conditions, and cellulose utilization in *N. crassa*.

Chapter 5: Investigating the role of ZAP-1 transcription factor in regulating CDF zinc transporters in *Neurospora crassa*

Chapter 5 describes the identification and investigation of the cell functions of the *N. crassa zap-1* under different zinc conditions. The Zap1 transcriptional activator controls the expression of a large number of genes in response to low zinc levels in *S. cerevisiae*, *A. fumigatus*, *C. albicans*, and *C. gattii* (Eide 2021). The sequence analysis revealed that the NCU02699 is the closest homolog to the *S. cerevisiae* Zap1p. The sequence analysis of *N. crassa* ZAP-1 and its orthologs showed sequence homology in the C-terminal, particularly at the zinc finger domains. Furthermore, phylogenetic analysis revealed the similarities of ZAP-1 to the *Madurella mycetomatis* MmZafA , which is hypothesized to regulate the expression of genes involved in maintaining zinc homeostasis and is important for initiating the process of grain formation that results in mycetoma (du Pré et al. 2022). The three-dimensional protein structure of ZAP-1 was also predicted using the structure of AD2 (predicted by NMR and CD, Wang et al. 2006) of *S. cerevisiae* Zap1p as the template. The predicted structure showed similarity of ZF2 and ZF3 of ZAP-1 in *N. crassa* with the ZF1 and ZF2 zinc fingers of the AD2 (which is crucial for binding to zinc (Bird et al. 2000b), indicating the conservation of the

activation domains. In comparison to other zinc-binding sites of the *S. cerevisiae* Zap1p, zinc bound to ZF1 and ZF2 (AD2) is extremely labile, which might be an important factor in their effectiveness in sensing zinc (Qiao et al. 2006). Taken together, the *N. crassa* ZAP-1 might be regulated by zinc like that of its *S. cerevisiae* homolog Zap1p.

The Δ*zap-1* knockout mutant was not able to grow in low zinc, however, this phenotype was rescued as the concentrations of zinc increased. Furthermore, the Δ*zap-1* mutant carrying the *zap-1* transgene was able to complement the slow growth phenotypes of Δ*zap-1* mutant under low zinc. Therefore, this study revealed that the *zap*-1 gene is crucial for survivability under low zinc conditions in *N. crassa*. I also found that the *N. crassa* ZAP-1 was localized in the nucleus under all the zinc conditions tested. To further understand the functional importance of ZAP-1 in *N. crassa*, I determined how zinc regulates *zap-1* expression by qRT-PCR. The *zap-1* gene expression is elevated (~6 fold) under low zinc conditions.

I also performed interspecies complementation of the *S. cerevisiae zap1Δ* mutant using the *N. crassa zap-1* allele. The transformant zap*1Δ + Nczap1* was able to complement the growth defect of *zap1Δ* under zinc-limiting conditions. Despite the structural differences between the *N. crassa* ZAP-1 and the *S. cereviseae* Zap1p, this data suggested interspecies functional conservation of the homologs of the ZAP-1 transcriptional activator that responds to zinc in *N. crassa*.

The genetic interactions among the CDF zinc transporters *zrc-1*, *mzc-2*, and *zrg*-17 were studied by generating the Δ*zap-1*; Δ*zrc-1*, Δ*zap-1*; Δ*msc-2*, and Δ*zap-1*; Δ*zrg-17* double mutants. The phenotypes of the double mutants were studied under various concentrations of zinc. In normal zinc conditions, the double mutants showed phenotypes similar to the wild type. However, under low zinc conditions the Δ*zap-1*; Δ*zrc-1*, Δ*zap-1*; Δ*msc-2*, and Δ*zap-1*; Δ*zrg-17* double mutants showed

restricted growth similar to Δ*zap-1*, suggesting that *zap-1* is epistatic to *zrc-1*, *mzc-2*, and *zrg-17*. This genetic interaction suggested that ZAP-1 might be the primary transcriptional activator functioning under low zinc conditions in *N. crassa*. Therefore, I studied the expression of the zinc transporters *zrc-1*, *msc-2*, *zrg-17*, and *zrt-3* in the Δ*zap-1* knockout mutant under low zinc conditions. The expression of *zrc-1*, *msc-2*, *zrg-17*, and *zrt-3* were reduced in the Δ*zap-1* mutant compared to wild type. This indicated that except ZAP-1, no other transcriptional activator could activate the zinc transporters. Therefore, ZAP-1 acts as the primary regulator of the zinc transporters under low zinc conditions in *N. crassa*.

Chapter 6: Conclusions and future perspectives

This chapter describes the conclusion and future prospects of the current research work. In this study, I investigated the cellular roles of *zrc-1*, *msc-2* and *zrg-17* members of zinc transporter belonging to CDF family, using their knockout mutant strains. The Δ*zrc-1* mutant exhibited slow growth rate under high zinc (≥ 0.5 mM) conditions. However, the expression of *zrc-1* gene was elevated under low zinc conditions, suggesting the importance of *zrc-1* under low zinc in *N. crassa*. Furthermore, the wild type like growth rate of the Δ*msc-2;* Δ*zrg-17* double mutant indicates antagonistic interaction while the Δ*zrc-1;* Δ*zrg-17* double mutant exhibits additive phenotype resulting in severe growth defects, irregular septation, and defects in conidiation as well as inability to grow in medium containing cellulose. In addition, the *zap-1* gene was found to be crucial for survival under low zinc conditions in *N. crassa* and ZAP-1 was localized in the nucleus under all the zinc conditions. Furthermore, *zap-1* gene expression was elevated (~6 fold) under low zinc conditions, depicting the functional importance of *zap-1* in *N. crassa*. Interspecies complementation of the *S. cerevisiae zap1Δ* mutant with the *N. crassa zap-1* allele indicated functional conservation of the homologs of ZAP-1 transcriptional activator. Moreover, the slow growth of Δ*zap-1*; Δ*zrc-1*, Δ*zap-1*; Δ*msc-2*, and Δ*zap-1*; Δ*zrg-17* double

mutant under low zinc conditions suggested that *zap-1* might function upstream of *zrc-1*, *msc-2,* and *zrg-17*. The low-level expression of *zrc-1*, *msc-2*, *zrg-17* and *zrt-3* gene in Δ*zap-1* mutant indicates that ZAP-1 might be the primary regulator of the zinc transporters under low zinc conditions in *N. crassa*.

Future perspectives

Further studies on the regulation and functional significance of these transporters will deepen our understanding of their roles in *N. crassa*. The future direction of this research work will be:

(i) A protein localization study of ZRC-1 and MSC-2 under varying zinc concentrations will help us understand the molecular mechanism of these transporters regulating the zinc level inside the cell in *N. crassa*.

(ii) Protein-protein interaction study of MSC-2 and ZRG-17 by Co-Immunoprecipitation (CoIP) and co-localization will further validate the interaction of these two proteins.

(iii) Expression analysis of cellulose-degrading enzymes (cellobiose dehydrogenase) such as *cbh-1* (NCU07340), *gh6-2* (NCU09680) and *gh5-1* (NCU00762) in the Δ*zrc-1*; Δ*msc-2* and Δ*zrc-1*; Δ*zrg-17* double mutants will help understand the role of CDF zinc transporters in degrading cellulose.

(iv) The protein-DNA interaction of the transcriptional factor ZAP-1 with the CDF zinc transporters genes, by chromatin immunoprecipitation (ChIP), followed by electrophoretic mobility shift assay (EMSA) will help determine the specific binding sequence of ZAP-1 in the promoter of target genes.

1

INTRODUCTION TO THE ZINC SIGNALING SYSTEM AND THE MODEL FILAMENTOUS FUNGUS *NEUROSPORA CRASSA*

1.1 Overview of the significance of zinc in the biological system

Zinc is an essential trace element, and plays a pivotal role in many biological functions. It is the second most abundant trace metal found in eukaryotic organisms and indispensable for various vital processes, including growth, development, immune responses, and metabolism (Chasapis et al. 2012; Maret 2013, 2017). Furthermore, zinc plays an essential role in the growth and development of microorganisms, plants, and animals, making it an integral element in every aspect of life forms (Drinker and Collier 1926; Mäser et al. 2001; Kaur et al. 2014; Alah et al. 2021; Clemens 2021; Eide 2021). The importance of zinc as an essential transition metal ion was first reported for requirement in cultivating *Aspergillus niger* (Raulin 1869). In addition, the presence of zinc in plant and animal tissue was reported and suggested to have some biological functions (Drinker and Collier 1926). Later, the effects of zinc deficiency were described in rats (Todd et al. 1933) and humans (Prasad et al. 1963), demonstrating that zinc deficiency leads to testicular atrophy, hair loss, hyperkeratinization of the epidermis, and growth retardation (Prasad et al. 1961, 1963). Furthermore, zinc supplementation aids to recovery from acute diarrhea and the common cold in children (Todd et al. 1933; Prasad et al. 1961, 1963).

The unique features of zinc may be the reason for its widespread use. Firstly, zinc is not a redox active metal, in contrast to iron or copper, which are subject to Fenton chemistry, hence DNA or proteins cannot potentially be harmed by free radical cascades (Vallee and Auld 1990; Coleman 1992). Secondly, zinc is a borderline Lewis acid, allowing it to interact effectively with various ligands (Berg and Shi 1996). For instance, zinc prefers to bind to a wide range of ligand types, such as sulphur from cysteine, nitrogen from histidine, and oxygen from glutamate, aspartate, and water (Berg and Shi 1996). Thirdly, zinc is kinetically labile, and therefore, it can undergo ligand exchange reactions promptly (Krezoski et al. 1988; Berg and Shi 1996). Finally, zinc-binding domains in a protein tend

to evolve rapidly by forming a tetrahedral site, and it exhibits flexibility for binding to zinc over other metal ions. These tetrahedral sites, formed by the synergy of ligands (cysteine and histidine), possess an optimized and tighter binding affinity to zinc than other metal ions (Krezoski et al. 1988; Vallee and Auld 1990; Berg and Shi 1996; Krężel and Maret 2016).

The preference for zinc over other metal ions reinforces the possibility that zinc may participate in several essential functions in cellular processes, particularly the structural and catalytic roles zinc plays in proteins. Likewise, the activities of zinc-binding proteins are influenced by the amount of zinc present inside the cell, like the interprotein zinc-binding sites, which react to zinc in a concentration-dependent manner (Kochańczyk et al. 2014; Lee et al. 2015). The importance of zinc in regulating the protein function by binding to the zinc-binding motifs was first reported in *Xenopus laevis* as a transcription factor (TF) IIIA (TFIIIA), and the zinc-binding motifs were known as zinc-finger consisting of conserved cysteine and histidine ligands (Miller et al. 1985). There are presently different classes of zinc-binding domains, and these classes are diverse with respect to their functionality as well as structure. Some of them are the transcription factor IIIA (Cys_2His_2), steroid-thyroid receptor (Cys_8), Gal4 family (Cys_6), RING finger ($Cys_3HisCys_4$), retroviral-nucleocapsid ($Cys_2HisCys$), plant homeodomain *PHD* ($Cys_3HisCys_3$), LIM domain ($Cys_2HisCys_5$), and GATA-1 (Cys_4) (Klug and Schwabe 1995; Berg and Shi 1996; Cassandri et al. 2017). Proteins that require zinc for structural and catalytic functions can modify their zinc affinities by combining certain ligands (Cys and His) (Andreini et al. 2008). Currently, 4500 Cys_2His_2 (C_2H_2) type zinc finger domains have been discovered in 564 human proteins, indicating that at least 3% of the genes encode zinc proteins in the human genome (Vallee and Auld 1990; Berg and Shi 1996; Maret 2004). Additionally, the zinc-finger domain is the most extensively utilized DNA-binding motif found in eukaryotic transcriptional factors (Cassandri et al. 2017).

1.1.1 Cellular zinc concentration and its impact on protein function

Zinc present within mammalian biological systems are categorized into three distinct forms based on its molecular behavior (Costello et al. 2011). The first category includes the non-exchangeable, non-reactive immobile zinc that are tightly bound to proteins, constituting approximately 54% of the zinc pool (Kochańczyk et al. 2014; Lee et al. 2015). The second form is the mobile reactive zinc that are loosely bound to ligands, constituting approximately 44.7% (Lee et al. 2015). Lastly, the third category, includes the free zinc that are the reactive pool of zinc, making up less than 1% of the total zinc pool (Lee et al. 2015). The cell signaling cascades are triggered by the reactive mobile zinc or free zinc rather than the non-exchangeable, non-reactive immobile zinc (Maret 2015). The concentration of total zinc within a eukaryotic cell is substantial, often falling within the range of 0.1 to 1 mM (Palmiter and Findley 1995; Suhy et al. 1999; Outten and O'Halloran 2001; Kochańczyk et al. 2014). However, depending on the specific cell types, the actual quantity of bioavailable Zn^{2+} (free zinc) varies widely, ranging from picomolar (pM) to nanomolar (nM) levels (Krężel and Maret 2006; Vinkenborg et al. 2009). The transient binding of Zn^{2+} to different proteins can be caused by a brief increase in the concentration of free Zn^{2+} ions, slightly over the required level, presumably due to localized zinc fluxes, which can affect how the proteins function through various mechanisms or pathways (Figure 1.1) (Maret 2013, 2017). Likewise, a reduction in free Zn^{2+} below a threshold level is toxic to cells and causes protein dysfunction, primarily because there are not enough metal cofactors and signal transducers present (Figure 1.1) (Maret 2013; Lee et al. 2015).

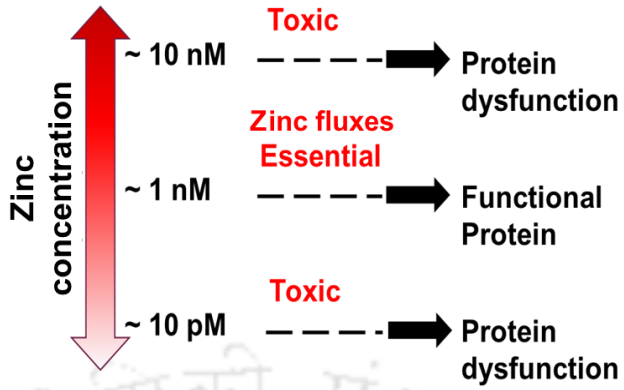

Figure 1.1 Effects of free Zn^{2+} concentration on protein function. Depending on the cell types, the concentration of zinc in cell varies ranging from 10^{-11} to 10^{-8} M. Extremely low and high Zn^{2+} concentrations have an adverse effect on the proteins and leading negative impact on the cell. High concentration of Zn^{2+} causes an irreversible protein damage, such as aggregation, which impairs the functionality of several proteins. However, low concentration of Zn^{2+} is harmful to the cell since zinc serves as an important metal cofactor and plays a significant role in signal transduction pathways. The maintenance of optimum level of Zn^{2+} inside the cell significantly impacts protein functionality. Adapted from Lee et al. (2015).

1.1.2 The requirement for zinc transporter in the cell

The inability of zinc to cross the cellular membranes indicates that transporter proteins are required, some of these proteins also acquire their zinc during transportation through the secretory routes. These transporter proteins should be tightly regulated to prevent the adverse effects of zinc deficiency or toxicity. For example, the packaging of insulin granules in pancreatic cells depends on the availability of a high amount of zinc in secretory vesicles, and the transport of zinc into the secretory vesicles for the synthesis, storage, and function is achieved by the zinc transporter that is exclusively expressed in the beta cells of the pancreatic islet β-cells (Dodson and Steiner 1998; Chimienti et al. 2005; Pound et

al. 2009; Nicolson et al. 2009; Wijesekara et al. 2010; Myers 2015). In addition, zinc-dependent enzymes are necessary for the addition of phosphoethanolamine groups to glycosylphosphatidylinositol (GPI) anchors in the endoplasmic reticulum (ER) (Sevlever et al. 2001). Furthermore, zinc signaling also modulates NMDA and GABA receptors in mammalian brain cells (Cuajungco and Lees 1997; Mocchegiani et al. 2005; Amico-Ruvio et al. 2011). Besides, a low concentration of zinc is detrimental to the cell, because zinc is an important metal cofactor and signal transducer. However high levels of zinc also detrimental to the cells, and may cause protein aggregations that ultimately lead to protein dysfunction (Cousins et al. 2006; Kambe et al. 2008). It has also been reported that the neuronal cell death during cerebral ischemia was due to the harsh effect of zinc toxicity in rats (Koh 2001). In addition to being toxic to neurons, high intracellular zinc concentrations are harmful to astrocytes, which constitute the majority of the glial cells in human brain (Nolte et al. 2004). Therefore, maintaining cellular zinc homeostasis in various cellular compartments within the controlled physiological range is essential for the efficient functioning of cells and cellular organelles, including the cytoplasm, endoplasmic reticulum (ER), and subcellular organelles. To maintain zinc homeostasis, a network of zinc transporter proteins for transportation, storage, and distribution of zinc has been developed in the cells (Frausto 1991; Gaither and Eide 2001b).

1.2 Overview of the zinc transporters protein families

Several proteins bind to extra zinc to prevent unfavorable reactions, transport zinc through membranes and cellular compartments, or sense zinc concentrations to control the level of zinc in the cells. The resistance nodulation cell division (RND) family of zinc exporters are found in few gram-negative bacteria like *Ralstonia metallidurans* CH34, and this RND exporters family enables efficient export of zinc across the cytoplasmic membrane and the outer membrane of the cell (Hantke 2001). In addition, the ATP-binding cassette (ABC) family of zinc transporters that are involved in zinc

transport, found only in bacteria (Higgins 1992). The ABC transporters are major membrane-crossing transporters that bind and hydrolyze ATP to transport solutes across membranes, and the ZnuABC transporter complex functions as a high-affinity zinc uptake in *Escherichia coli* (Patzer and Hantke 1998). Similar to the ABC-type transporter, the P-type ATPases found in both prokaryotes and eukaryotes, function to transport solutes by binding and hydrolysis of ATP (Scarborough 2002). The *ZntA* gene encodes a P-type ATPase family of protein that transports zinc outside of the cell in *E. coli* (Rensing et al. 1997), while the Hma2 and Hma4 members of the P-type ATPaseses in *Arabidopsis thaliana* play a role in zinc translocation from the root cells into the xylem and phloem tissue (Hussain et al. 2004). In the eukaryotic system the concentrations of zinc in the cytoplasm and cellular organelles are regulated by two primary zinc transporter families, the Zrt-, Irt-like Protein (ZIP) or solute carrier 39 (SLC39) (Guerinot 2000; Eide 2004) and cation diffusion facilitator CDF or zinc transporters (ZnT) or solute carrier 30 (SLC30) proteins (Kambe et al. 2004; Palmiter and Huang 2004).

1.2.1 Zrt-, Irt-like Protein (ZIP) or Solute Carrier 39 (SLC39) family of zinc transporter

The ZIP (Zrt-, Irt-like Protein) family derives its name from the initial members identified specifically, the zinc-regulated transporters Zrt1 and Zrt2 in yeast (Zhao and Eide 1996b, a), and the iron-regulated transporter (Irt) which serves as the primary cation transporter for iron uptake in the roots of *Arabidopsis thaliana* (Eide et al. 1996). SLC39 (solute carrier 39) is the systematic designation that belongs to the ZIP family in mammals (Jeong and Eide 2013). ZIP transporters are present at every level of phylogeny, including bacteria, fungi, plants, and mammals (Eng et al. 1998; Eide 2004; Jeong and Eide 2013). An essential characteristic of the ZIP family is the transport of zinc and/or other metal ion substrates into the cytoplasm from the extracellular environment or organellar lumen (Palmiter and Huang 2004; Bafaro et al. 2017). Most ZIP proteins have similar predicted topologies and contain

eight putative transmembrane domains (TMD), the N- and C-termini of the protein reside in the extracytoplasmic face of the membrane (Figure 1.2) (Eide 2004, 2006). While the majority of TMD loops are rather short, TMD 3 and 4 usually have a longer loop region containing a histidine-rich domain with the sequence $(HX)_n$, where n = 3 and 5, is frequently found in this region (Figure 1.2) (Eide 2004, 2006). Zinc absorption by ZIP1 and ZIP2, demonstrated by biochemical transport experiments, is energy-independent (Gaither and Eide 2000, 2001c). A $Zn^{2+}/[HCO^{-}_{3}]_2$ symport mechanism has been suggested by the study of HCO^{-}_{3} stimulated zinc absorption by ZIP2 (Gaither and Eide 2000). Additionally, an electroneutral $Zn^{2+}/[HCO^{-}_{3}]_2$ symport for ZIP8 has also been reported (Liu et al. 2008). Furthermore, the X-ray crystal structures and the full-length ZIP in an inward-open metal-bound state of bacterial homolog, *Bordetella bronchiseptica* (BbZIP), was reported (PDB ID:5TSB) (Zhang et al. 2016, 2017). In the BbZIP structure, the eight TMDs are divided into two units, with the first unit consisting of TMDs 2, 3, 7, and 8 constituting the binuclear metal binding center in-between the first and second units, which include TMDs 1, 4, 5, and 6 (Zhang et al. 2017). However, functional evidence also indicates that ZIP members can bind various metals with diverse specificities, affinities, and kinetics (Dempski 2012), suggesting that the function and transport mechanism of ZIP transporters are not fully known yet.

There are a total of 14 ZIPs in humans, each having a unique tissue/cellular distribution and physiological function (Jeong and Eide 2013). In particular, the ZIP4 transporter plays a crucial role in embryonic development and is the only enzyme that can absorb zinc from food (Eide 2004). Acrodermatitis enteropathica (AE), a fatal genetic condition is also caused by dysfunctional ZIP4 mutations (Küry et al. 2002; Wang et al. 2002), and pancreatic cancer have been linked to ZIP4 overexpression (Li et al. 2007). Additionally, ZIP10 has been shown to play a role in physiological and pathological processes such as immunity (Hojyo et al. 2014) and tumor formation (Pal et al. 2014;

Ma et al. 2021), including breast cancer (Takatani-Nakase et al. 2014), and gastric adenocarcinomas (Ren et al. 2023).

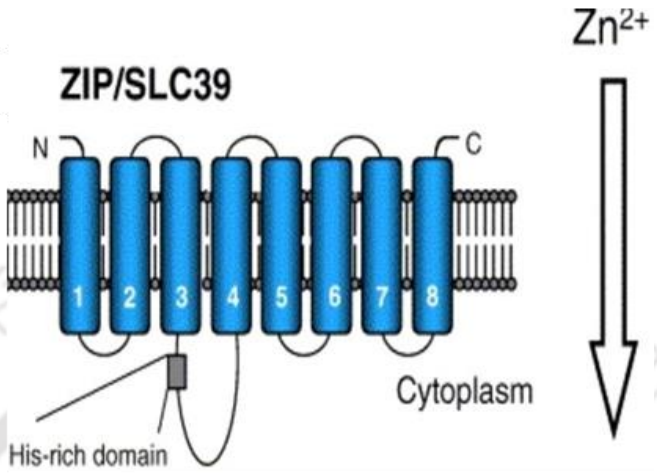

Figure 1.2 Predicted membrane topology of ZIP/SLC39 family of transporter. The ZIP family of transporter have eight putative transmembrane domains that are indicated in blue, and numbered (1-8). Both the N- and C- terminals are located in the extracytoplasmic face of the membrane. The histidine-rich domain between the TMD 3 and 4 is also indicated. The arrow indicates the direction of zinc transported from the outer membrane into the cytosol/ cytoplasm. Adapted from Eide (2006).

1.2.2 Cation diffusion facilitator (CDF) or zinc transporters (ZnT) or solute carrier 30 (SLC30) family of zinc transporters

The ZnT (zinc transporter) family of protein is also commonly known as the CDF (cation diffusion facilitator) family of transporter (Nies and Silver 1995). SLC30 (solute carrier 30) is the systematic designation that belongs to this family in mammals (Gaither and Eide 2001a; Eide 2004). Similar to the ZIP transporters, the CDF transporters are present at all levels of phylogeny (Palmiter and Huang 2004). The primary characteristic of the CDF family is the ability to transport metal ions, such as zinc, from the cytoplasm into the lumen of intracellular organelles or outside of the cell, consequently, CDF

proteins function opposite to ZIP transporters (MacDiarmid et al. 2000; Palmiter and Huang 2004; Eide 2006; Fang et al. 2008). Based on their evolutionary relationships, the CDF transporters are divided into three groups namely Zn-CDF, Zn/Fe-CDF, and Mn-CDF, and the zinc transporter proteins are a member of the Zn-CDF group (Montanini et al. 2007). In mammals, there are at least 10 ZnT members of Zn-CDF transporters (ZnT1 - ZnT10), and each of these serves different physiological functions (Table 1.1) (Kambe et al. 2004; Palmiter and Huang 2004; Fukada and Kambe 2011).

1.2.2.1 Structure and mechanism of transport of zinc by ZnT/CDF zinc transporters

The CDF transporters, except ZnT5 and its homologs, have similar predicted membrane topologies consisting of six TMDs with both N- and C-terminal located in the intracellular region and a distinctive histidine-rich loop between the TMDs 4 and 5 in the cytoplasm (Figure 1.3 A) (Paulsen and Saier 1997; Kolaj-Robin et al. 2015; Cotrim et al. 2019). The histidine-rich loop might function as an indicator of zinc selectivity, a sensor of cytosolic zinc levels, and a regulator of zinc transport activity (Figure 1.3 A) (Podar et al. 2012; Tanaka et al. 2013). An understanding of how these transporters is revealed by the three-dimensional structure of YiiP of *E. coli* member of CDF transporter, which has been determined by X-ray crystallography (PDB ID:3h90) (Lu and Fu 2007).

YiiP, also known as a ferrous iron efflux (FieF) protein, is an integral membrane protein belonging to the CDF family and functions to move Zn^{2+} and Cd^{2+} across cytoplasmic membranes of *E. coli* (Paulsen and Saier 1997; Grass et al. 2005). Yiip along with ZitB are the two CDF antiporters of *E. coli* that regulate zinc homeostasis due to their ability to transport Zn^{2+} in a proton-dependent manner (Grass et al. 2005). YiiP has six TMDs with N- and C- termini in the cytosol and functions as a homodimer, these six TMDs are further divided into two distinct subdomains: i) the TMDs 1, 2, 4, and 5 create a tightly bound four-helix bundle and an intramembranous zinc-binding site, generated by four conserved hydrophilic residues which are three aspartic acids and one histidine residues of

TMDs 2 and 5, known as the "DD-HD" motif and ii) the second subdomain is a bundle of two TMDs 3 and 6 (Lu and Fu 2007; Cotrim et al. 2019). The zinc-binding tetrahedral motif DD-HD is crucial for the coordination and stabilizing of Zn^{2+} ions, because when the aspartic acid residues in the DD-HD motif are mutated and replaced by cysteine (a residue that bind to Zn^{2+}) and alanine (a residue that does not bind to Zn^{2+}), these mutations disrupt the zinc transport activity (Wei and Fu 2006). Therefore, the DD-HD motif is crucial for binding to zinc and proper functioning of zinc transporters. The human orthologs, ZnTs (1 -10) have an HD-HD binding site at TMDs 2 and 5 (Figure 1.2) instead of a DD-HD motif, and the difference in the one histidine residue at TMD 2 instead of the aspartic acid residue enables the human ZnTs to be highly selective for Zn^{2+} (Hoch et al. 2012; Cotrim et al. 2019). In the YiiP protein, the DD-HD motif is able to bind to both Zn^{2+} as well as $Cd^{2+,}$ and altering the first aspartate in the DD-HD motif to histidine (HD-HD) makes the motif responsive to only Zn^{2+} (Hoch et al. 2012). This alteration makes the ZnTs selective to Zn^{2+} only, and selectivity against Cd^{2+} was eliminated with no impact on zinc transport (Hoch et al. 2012). Alteration in the amino acid residues in the HD-HD motif, changes the metal selectivity, for example, the Znt10 in humans contains the ND-HD motif, where an asparagine is present in the first residue instead of histidine, making the protein a manganese transporter (Quadri et al. 2012; Tuschl et al. 2012). Furthermore, the DD-DD aspartate pattern, found in the ZnT homologs in plants, allows the protein to transport manganese (Gustin et al. 2011).

Previously it was reported that an antiport mechanism used by the CDF transporters to export divalent cations (Kolaj-Robin et al. 2015). The YiiP protein of *E. coli* export zinc in a manner where a proton is imported/ traded in 1:1 zinc to proton exchange stoichiometry (Figure1.3 B) (Chao and Fu 2004a). In this mechanism, YiiP binds Zn^{2+} or H^{+} in both inward- and outward-facing conformations, and the extracellular proton acts as an initiator for the export of Zn^{2+} from the cytosol (Coudray et al.

2013). The ZnT transporters of human transport zinc via the zinc/ proton (Zn^{2+}/H^{+}) exchange mechanism (Figure 1.3 B) (Ohana et al. 2009), thus the ZnT transporters mechanism of zinc transport is conserved among the CDF members, and have been characterized based on the structural characteristics of YiiP. Therefore, despite their name, CDF proteins, do not act as diffusion facilitators, but zinc is transported using the gradient of other ions, as secondary active transporters (Chao and Fu 2004a, b).

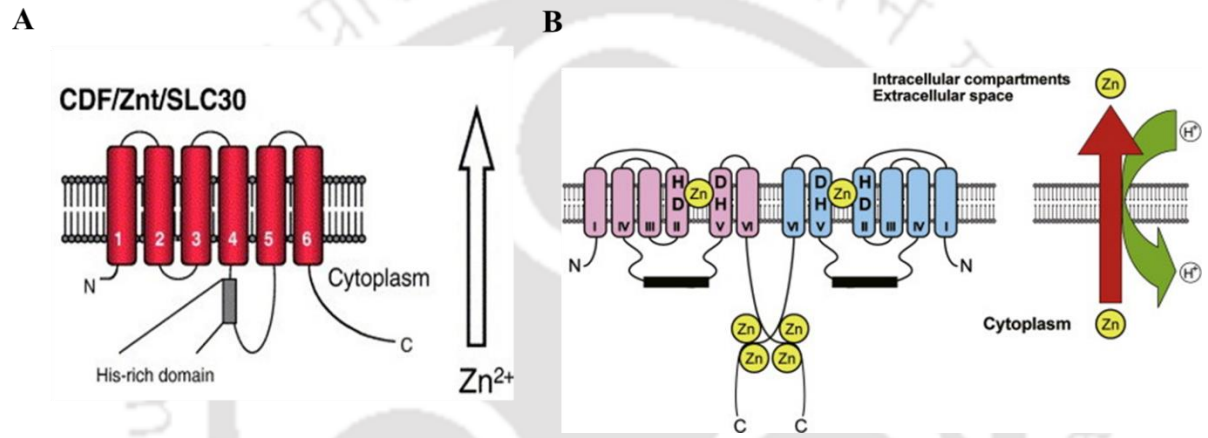

Figure 1.3 Predicted membrane topologies and zinc-binding sites, in ZnT/CDF/SLC30 transporters. A. The ZnT/CDF/SLC30 family of zinc transporter have six putative transmembrane domains that are indicated in red, and numbered (1-6). Both the N- and C- terminals resides in the cytosol. There is a histidine-rich domain between the TMD 4 and 5 is and the arrow indicates the direction of zinc transported from cytosol/ cytoplasm into the organelle to be stored or outside the membrane (adapted from Eide 2006). **B.** The predicted transmembrane topologies of ZnT transporters and the zinc binding sites of ZnT transporters. The TMDs are indicated in violet and blue (numbered as I to VI), and ZnTs forms homodimers like the bacterial homologue YiiP. Based on the X-ray structure of YiiP (Lu and Fu 2007), the ZnT transporters are predicted to have a zinc-binding site that is made up of two histidine (H) and two aspartic acid (D) residues within the TMDs II and V, forming

HD-HD motif, as well as a binuclear zinc binding site in the cytoplasmic C-terminal region. The thick black line between TMDs IV and V indicates a histidine-rich loop that may function as a zinc-binding site or regulate zinc transport activity. ZnT transporters are functional Zn^{2+}/H^{+} exchangers. The red and green arrow on the right side indicates the direction of zinc transport. Adapted from Kambe (2012).

1.2.2.2 Implications of ZnT/SLC30 zinc transporters in human

A wide range of research findings have established the connections between variations in ZnT/SLC30 transporters and several human genetic disorders (Hirano et al. 2008; Fukada and Kambe 2011; Fukada et al. 2011). The localization and functions of ZnT (SLC30) proteins in the body and cells (Figure 1.4), as well as the physiological events and health issues linked to them are listed below (Table 1.1).

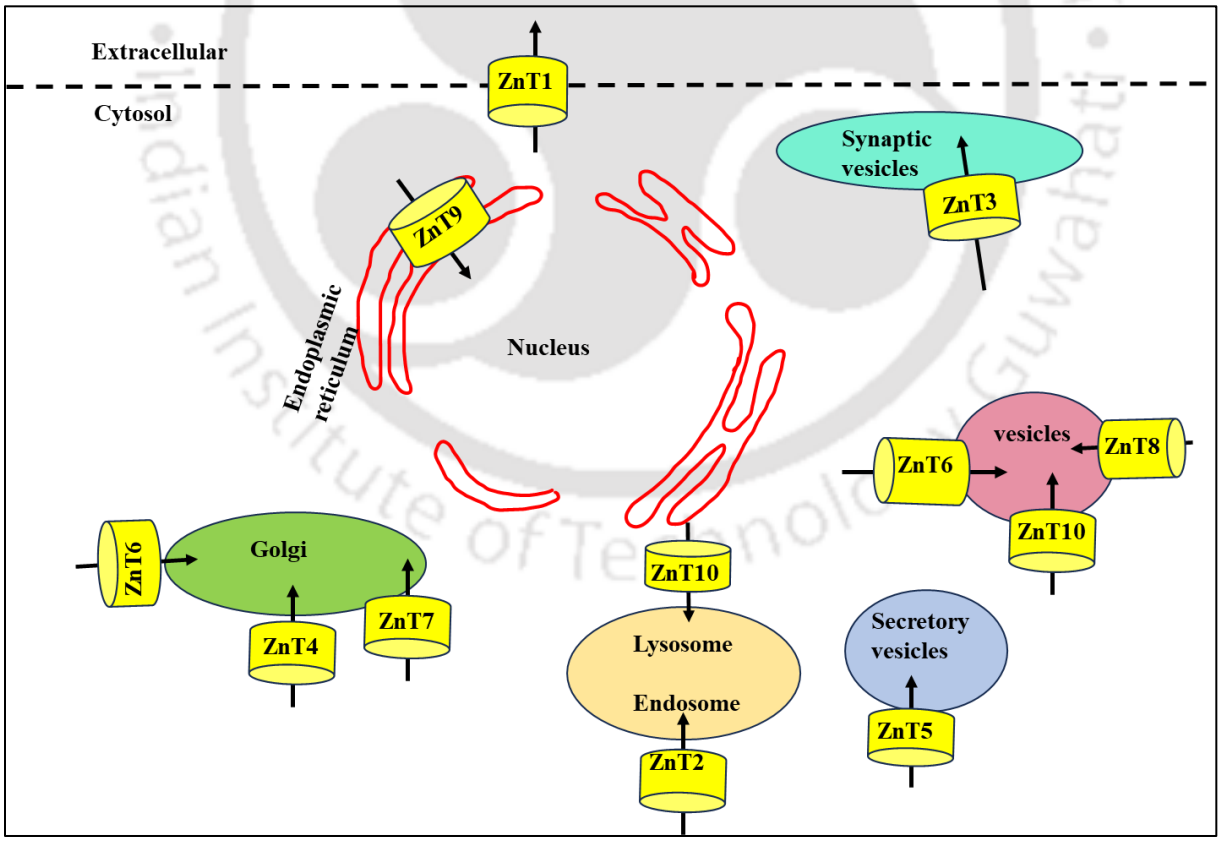

Figure 1.4 Subcellular localization of ZnT/SLC30 zinc transporters in the mammalian cell. The localization of ZnT/SLC30 zinc transporters (indicated in yellow) are depicted here (described in table 1.1). The arrows indicate direction of the transport. Adapted from Baltaci and Yuce (2018).

Table 1.1 The localization and functions of the ZnT/SLC30 proteins within the body and cell, and physiological processes and health problems, associated with ZnT/SLC30 proteins

Protein name	Probably localization and functions in cell	Physiological events and health problems
ZnT1 (SLC30A1)	Found in Cell membrane and pumping zinc out of the enterocytes across the basolateral membrane (Wang et al. 2009; Kimura and Kambe 2016)	Failure of embryonic development in homozygous *znt1* knockout mice (Andrews et al. 2004), Elevated body mass index correlates with high ZnT1 expression (Olesen et al. 2016)
ZnT2 (SLC30A2)	Gather zinc in lysosomes and endosomes (Palmiter et al. 1996a; Chaigne-Delalande and Lenardo 2014)	Present in maternal milk and mutation leads to neonatal zinc deficiency (Itsumura et al. 2013)
ZnT3 (SLC30A3)	Transports zinc to synaptic vesicles (Palmiter et al. 1996b; McAllister and Dyck 2017)	In the development of spatial memory and shaping of behavior (Martel et al. 2011), aging and Alzheimer-related cognitive loss (Adlard et al. 2010)
ZnT4 (SLC30A4)	Transport zinc to the trans Golgi network (TGN) (McCormick and Kelleher 2012)	Zinc in milk, smaller mammary glands, and reduced milk production (McCormick and Kelleher 2012)

ZnT5 (SLC30A5)	Early secretory pathway and the Golgi apparatus (Kambe et al. 2002; Suzuki et al. 2005)	Poor growth and low bone density dure to defect in maturation of osteoblasts (Inoue et al. 2002), delayed in mast cell-mediated allergic reactions (Nishida et al. 2009)
ZnT6 (SLC30A6)	Transports cytoplasmic zinc to vesicles and golgi apparatus in mice (Huang et al. 2002), hippocampus and neocortex of mice (Zhang et al. 2010)	Cognitive impairment in Alzheimer and pick's patients (Lovell et al. 2006)
ZnT7 (SLC30A7)	Transport zinc from the cytoplasm to the golgi apparatus (Huang et al. 2007), beta cells of osteoblast cells and pancreas (Suzuki et al. 2005)	Insulin signal pathway (Huang et al. 2007)
ZnT8 (SLC30A8)	Located in the pancreatic beta cells' secretary vesicle membrane. (Chimienti et al. 2005)	Reduce insulin secretion causing diabetic or glucose intolerant (Wijesekara et al. 2010)
ZnT9 (SLC30A9)	Localized in the cytoplasm and it is also found in nucleus/ER (Kambe et al. 2015)	Increased body mass index and obesity (Noh et al. 2014)
ZnT10 (SLC30A10)	In the golgi apparatus/endosomes at the cellular level and in the brain, liver, and retina at the tissue level (Patrushev et al. 2012; Huang and Tepaamorndech 2013)	Memory loss in Alzheimer patients (Bosomworth et al. 2013), Parkinson's disease, polycythemia, chronic liver cirrhosis and hypermagnesemia (Quadri et al. 2012; Tuschl et al. 2012)

1.3 Zinc transport mechanism in fungi

Zinc has long been recognized to be necessary for the growth of microorganisms, particularly fungi (Raulin 1869). It plays an important role in the structure and function of numerous enzymes, nucleic acid metabolism, and cell division (Eide 1998). Likewise, zinc has long been regarded as an important factor in host-pathogen interactions (Alamir et al. 2021). The mammalian host uses several cellular zinc importers and exporters to sequester intracellular zinc as a mechanism of nutritional immunity, thus, the virulence of pathogenic fungus is also greatly influenced by zinc uptake (Alamir et al. 2021). The most common of these pathogens are *Aspergillus fumigatus*, *Candida albicans*, and *Cryptococcus gattii*, which are all opportunistic and cause disease for those with compromised immune system (Brown et al. 2012).

1.3.1 Zinc transportation in *Saccharomyces cerevisiae*

The fungus *S. cerevisiae* has played a pioneering role in investigating the molecular mechanisms governing zinc homeostasis. In *S. cerevisiae*, the initial transport of zinc into the cytoplasm is facilitated by ZIP transporters localized in the plasma membrane, including Zrt1p (Zhao and Eide 1996a), Zrt2p (Zhao and Eide 1996b), and Fet4p (iron transporter) (Waters and Eide 2002). The Zrt3p protein, a ZIP transporter, mobilizes zinc reserves in the vacuole to deliver zinc to the cytoplasm and other organelles in response to a shortage of zinc (Figure 1.5) (MacDiarmid et al. 2000). Alternately, when zinc levels in the cytoplasm become too high, the CDF transporters, Zrc1p (zinc resistance conferring) and Cot1p (cobalt transporter) function in transferring the extra zinc from the cytosol into the vacuole (Figure 1.5) (Kamizono et al. 1989; Conklin et al. 1992; Miyabe et al. 2001). These suggested that the combinatorial role of Zrt3p, Zrc1p, and Cot1p zinc transporters in the vacuole are important for maintaining intracellular zinc homeostasis in *S. cerevisiae*. Additionally, members of CDF zinc transporters Msc2p (meiotic sister chromatid recombination) and Zrg17p (zinc regulated

gene), both localized in the endoplasmic reticulum (ER), form the heterodimeric complex, and transports zinc into the ER, which is important for the proper functioning of the ER (Figure 1.5) (Ellis et al. 2004, 2005). Majority of these zinc transporter genes are regulated by the zinc-responsive transcription factor, Zap1p (Figure 1.5) (Eide 2020). The Zap1p up-regulates genes under low zinc conditions by binding to the promoter region of the target genes (discussed in section 1.6).

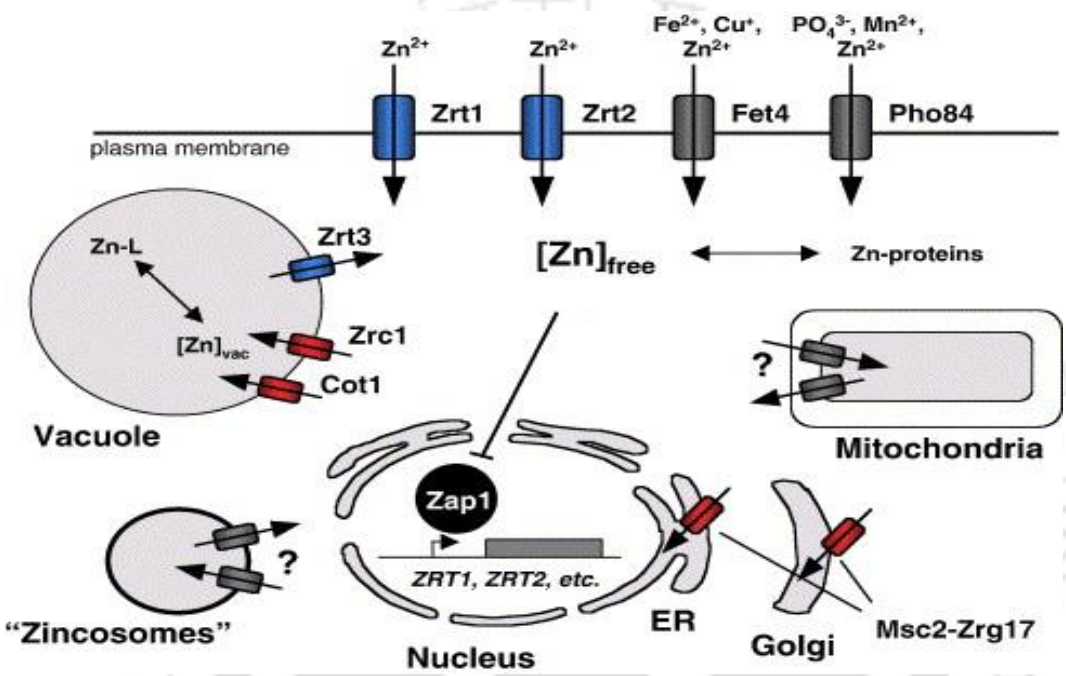

Figure 1.5 An overview of zinc transport and trafficking in *S. cerevisiae*. The ZIP transporter proteins (shown in blue) transport zinc into cells through the plasma membrane (Zrt1p and Zrt2p) or out of subcellular organelles (Zrt3p) when cytosolic zinc concentration is low or depleted. In addition, the ZnT/CDF transporter proteins (shown in red) transport zinc out of cells through the plasma membrane or into subcellular organelles (Zrc1p, Cot1p, Msc2p, and Zrg17p) when zinc concentration is high or excessive (Eide 2006; Kambe et al. 2021)**.** The putative transporters or known transporter related proteins from other families are shown in gray. The zinc responsive transcription factor Zap1p (shown in black) is responsible for the up-regulation of several target genes under low zinc (Eide

2009). To assist storage, the Zn^{2+} in the vacuole is probably attached to a ligand (L). Adapted from Eide (2006).

1.3.2 Zinc transportation in *Aspergillus fumigatus*

The regulation of zinc uptake is of crucial importance for the physiology and virulence of *A. fumigatus*, a pathogen that infiltrates the lungs of susceptible individuals and causes pulmonary aspergillosis (Kousha et al. 2011). In *A. fumigatus*, two ZIP family of zinc transporters ZrfA and ZrfB show sequence homology to the Zrt1p and Zrt2p of *S. cerevisiae*, and regulated by zinc in the environment (Vicentefranqueira et al. 2005). However, unlike ZIP protein of *S. cerevisiae*, the ZrfA and ZrfB of *A. fumigatus*, exhibit sensitivity to environmental pH and primarily function in acidic zinc-deficient conditions (Vicentefranqueira et al. 2005). Another, ZIP transporter, ZrfC show zinc-dependent regulation and play a major role in zinc uptake under alkaline conditions (Amich et al. 2014). Moreover, studies conducted with immunocompromised mice demonstrated that ZrfC serves as the primary zinc transporter in host tissues, and partially facilitates growth of the fungus in the presence of calprotectin, which is an antimicrobial Zn/Mn-chelating protein synthesized in large quantities by neutrophils, even in immunosuppressed animals, indicating that ZrfC essential to grow under alkaline zinc-limiting environment in *A. fumigatus* (Amich et al. 2014).

1.3.3 Zinc transportation in *Cryptococcus gattii*

The basidiomycete yeast *C. gattii* is the primary cause of cryptococcosis, which can result in pneumonia and meningitis (Chaturvedi and Chaturvedi 2011). In *C. gattii*, four genes belonging to the ZIP family of zinc transporters ZIP1, ZIP2, ZIP3, and ZIP4 have been identified (Schneider et al. 2015). The *C. gattii* Zip1 and Zip2 transporters are homologs of the *S. cerevisiae* Zrt1p and Zrt2p, and zinc concentration regulate their expression (Schneider et al. 2012). Furthermore, Zip1 and Zip2 are

the major zinc transporter protein in *C. gattii* and is required for growth and virulence under low zinc conditions in acidic as well as alkaline pH (Schneider et al. 2015).

1.4 Zinc-responsive transcription factor Zap1

In *S. cerevisiae*, the zinc-responsive transcription factor known as Zap1p (zinc-responsive activator protein 1) was first identified and reported (Zhao and Eide 1997). Zap1p is the key player in response to zinc deprivation in *S. cerevisiae* (Zhao and Eide 1997). Zap1p functions as a transcriptional activator for the majority of its target genes, increasing expression when zinc levels are low (Eide 2009). However, Zap1p might also serves as a repressor, either by directly or indirectly regulating the expression of the target gene (Eide 2009). Zap1p binds to zinc-responsive elements (ZREs) in the promoters of its target genes and regulates the expression (Zhao et al. 1998). The consensus sequence of ZRE is ACCTTNAAGGT, however, Zap1-binding sites might differ from this consensus sequence and some of the Zap1-regulated genes might have multiple ZREs in their promoters, while the majority only have one binding site (Zhao et al. 1998; Lyons et al. 2000; Eide 2009).

1.4.1 Structure and mechanism of action of Zap1p of *S. cerevisiae*

The Zap1p of *S. cerevisiae* is an 880 amino acid long protein with a molecular weight of 93 kDa. The Zap1p protein contains seven C_2H_2-type zinc finger (ZnF) domains located at the C-terminal end of the protein (Znf1−7; Figure 1.6), the zinc finger 3−7 (Znf3–Znf7) comprises the DNA binding domains (Bird et al. 2000a, b). Two activation domains, AD1 and AD2, are also present in Zap1p, mapped between amino acid residues 332−402 for AD1 and 611–641 for AD2, respectively, and both the Znf1 and Znf2 domains are part of AD2 (Figure 1.6) (Zhao and Eide 1997; Bird et al. 2000b). For proper expression of zinc-responsive genes, by Zap1p, zinc regulation of both AD1 and AD2 is required (Herbig et al. 2005). When the concentration of zinc is high in the cells, both AD1 and AD2

are bounded by zinc resulting in the inactivation of Zap1p, whereas if the concentration of zinc is low in the cells, the zinc bound to AD1 and AD2 is released and Zap1p becomes active again resulting in the expression of genes (Bird et al. 2003). These findings suggest that Zap1p is a direct sensor of zinc and the protein is found in the nucleus irrespective of the concentration of zinc ions in the cell (Bird et al. 2000a). In addition, AD1 is primarily responsible for the zinc-responsiveness of a majority of Zap1-regulated genes, while AD2 is required for the expression of a small number of Zap1p downstream genes (Frey and Eide 2011, 2012; Frey et al. 2011). However when exposed to heat stress and extreme zinc deficiency, AD1 becomes inefficient and AD2 becomes more active and important in maintaining Zap1p activity (Frey and Eide 2011), this could be due to the presence of the two zinc finger domains Znf1 and Znf2 in AD2 (Yao et al. 2023). In addition to the activation domains AD1 and AD2, the DNA binding domain DBD is also crucial for the activation of downstream genes (Bird et al. 2000a, b; Yin et al. 2022; Yao et al. 2023).

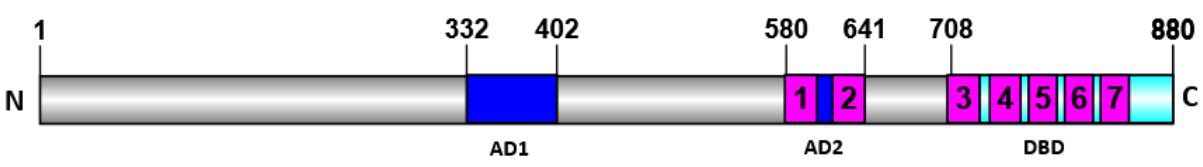

Figure 1.6 Functional domains of the zinc-responsive transcription factors, Zap1p of *S. cerevisiae*. The Zap1p protein is 880 amino acids long, containing seven zinc finger domains numbered 1−7 (shown in purple boxes). The zinc fingers 3−7, mapped between amino acids residues 705−880, comprises the DNA binding domain (DBD) (Bird et al. 2000a). Additionally, two transcription activation domains, AD1 and AD2 (shown in blue boxes) are also found in Zap1p and the zinc finger 1 and 2 is present within the AD2 (Eide 2020).

1.4.2 Zap1-mediated control of cellular responses to variations in zinc levels in *S. cerevisiae*

Under zinc starvation, several zinc homeostasis genes, including the high-affinity zinc uptake transporter gene *ZRT1* and the low-affinity zinc uptake transporter gene *ZRT2* (Zhao and Eide 1997), the vacuolar zinc transporters *ZRT3* and *ZRC1* (Miyabe et al. 2000; MacDiarmid et al. 2003), and the ER localized CDF zinc transporter *ZRG17* (Wu et al. 2011) are all under the regulation of Zap1p (Figure 1.5). Additionally, Zap1p controls its own expression at the transcriptional level by binding to a ZRE within its own promoter, which causes auto-regulation under the low zinc condition and an increased level of *ZAP1* transcripts and protein (Figure1.5) (Zhao et al. 1998; Eide 2020). The increased level of *ZAP*1 further inducs the expression of the target genes and the subsequent accumulation of the zinc transporters, including ZIP and CDF transporters, which aid in the ability to maintain zinc homeostasis (Figure1.5) (Zhao et al. 1998; Eide 2020). The production of Zap1p decreases when the concentration of zinc inside the cell reaches the optimum level, and the expression of the target genes also decrease to prevent zinc cytotoxicity, therefore Zap1p also functions as a transcriptional repressor (Bird et al. 2004).

Zap1p also regulates the expression of alcohol dehydrogenase isozymes (*ADH1* and *ADH3*) by repressing their expressions for zinc conservation in the cells (Lyons et al. 2000; Bird et al. 2006). ADHs are among the most abundant zinc-binding proteins in the cell (Gygi et al. 1999; Auld and Bergman 2008). When the cell is under zinc depleted state, Zap1p down regulates *ADH1* and *ADH3* expression by means of intergenic transcripts or non-coding RNA. The Zap1p binds to the ZRE present in the promoters of *ADH1* and *ADH3*, producing non-coding RNA, which results in the inability of the other transcription factor to bind and regulate the expression of *ADH* genes (Bird et al. 2006). Importantly, multiple studies have shown the significance the Zap1p transcription factor for the pathogenicity of fungus in their mammalian hosts (Moreno et al. 2007; Nobile et al. 2009; Schneider

et al. 2012; du Pré et al. 2022). The orthologs of Zap1 are found in *Aspergillus fumigatus* (Moreno et al. 2007; Amich and Calera 2014; Vicentefranqueira et al. 2018), *Candida albicans* (Kim et al. 2008; Nobile et al. 2009), *Candida glabrata* (Gaspar-Cordeiro et al. 2022), *Cryptococcus gattii* (Schneider et al. 2012), *Fusarium oxysporum* (López-Berges 2020), and *Madurella mycetomatis* (du Pré et al. 2022).

1.5 Introduction to *Neurospora crassa* as the model organism

1.5.1 A brief history and biology of *Neurospora crassa* as an excellent model organism

Neurospora also referred to as "nerve spores" because of its nerve-like striations on the sexual spore (ascospores), serves as a prominent model organism in genetics, biochemistry, and molecular biology, facilitating research into various aspects of eukaryotic cell biology for many decades, earning its reputation as the “organism behind molecular revolution” (Perkins 1992; Davis and Perkins 2002; Riquelme et al. 2011; Baker et al. 2012). *Neurospora crassa*, a member of the phylum Ascomycota, was initially identified as the causative agent of orange bread mold in French bakeries. It was initially documented under different names *Oidium aurantiacum* (Payen 1843) and *Penicillium sitophilum* (Montagne 1843). In the mid-1920s, Shear and Dodge categorized *N. crassa* as a heterothallic fungus with two mating types, *A* and *a*, and the presence of eight asci (sexual structures) (Shear and Dodge 1927; Perkins 1992). Later, in the mid-1930s, Carl Lindegren and Bernard Lodge demonstrated Mendelian inheritance in the individual asci, emphasizing the similarity of the rules governing inheritance and reproduction in fungi to those in higher plants and animals (Dodge 1939; Perkins 1992). Subsequently, in 1941, Beadle and Tatum's pioneering research with *N. crassa* produced the first biochemical mutants and introduced the famous "one gene-one enzyme" hypothesis (Beadle and Tatum 1941), which demonstrated that a specific gene controls the production of a particular enzyme

and significantly advanced the understanding of genetics. Thus, this groundbreaking work earned Beadle and Tatum the Nobel Prize in Physiology or Medicine in 1958, leaving a profound effect on the fields of genetics and molecular biology. Thereafter, *N. crassa* has established itself as a prime eukaryotic model organism in understanding various aspects of biological processes such as physiological regulation through circadian rhythm (Dunlap 1999; Loros and Dunlap 2001; Dunlap and Loros 2004), Epigenetic regulation through DNA methylation (Davis and Perkins 2002; Aramayo and Selker 2013), and RNA interference (RNAi) post-transcriptional gene silencing in fungi was first deciphered in *N. crassa* (Cogoni and Macino 1999a, b). Furthermore, *N. crassa* serves as the model organism in the study for biotechnological ethanol production from lignocellulosic sources (Dogaris et al. 2013) and host-virus interactions (Honda et al. 2020). The establishment of the Fungal Genetic Stock Center (FGSC) in 1960 marked a pivotal moment, ensuring that strains from earlier studies would be accessible to future generations of researchers (McCluskey 2003; McCluskey et al. 2010b). By 2003, the sequencing of *N. crassa* was successfully accomplished, revealing a genome size of 43 Mb and encompassing 10,082 protein-coding genes distributed across seven chromosomal linkage groups (LG I-VII) (Galagan et al. 2003). The availability of the complete genome sequence paved the way for a high-throughput knockout project aimed at creating gene replacement mutants for all genes, enabling the possibility of conducting numerous studies (Colot et al. 2006). The filamentous fungus, *N. crassa* is a heterotroph that uses a variety of carbon and nitrogen sources, simple salts, a few trace elements, and biotin (Davis and de Serres 1970). The genome defense mechanisms of *N. crassa* are diverse and include a reversible post-transcriptional gene silencing (PTGS) mechanism known as "quelling" (Romano and Macino 1992) that occurs during the vegetative phase, a fungal-specific transcriptional gene silencing (TGS) mechanism called "repeat-induced point mutation" (RIP)

(Cambareri et al. 1989), which occurs after fertilization and before karyogamy, and another PTGS mechanism called "meiotic silencing" which occurs during the sexual phase (Shiu et al. 2001).

1.5.2 Life cycle of *Neurospora crassa*

The multicellular fungus *N. crassa* exhibits a complex life cycle having both asexual and sexual phases, depending on environmental conditions (Figure 1.7) (Raju 1992; Springer 1993). When cultivated under nutrient-rich conditions, *N. crassa* undergoes asexual cycle, forming branched, multinucleate vegetative hyphae that further grow parallel to the surface of solid medium (Springer 1993). The hyphae contain incomplete cross walls called septa, that allow the movement of organelles between compartments (Schmit and Brody 1976; Springer 1993). Repeated fusion between the hyphal filaments gives rise to a complex network of hyphae known as the mycelium (Springer and Yanofsky 1989; Springer 1993). Under nutrient scarcity or exposure to an air-water interface, mycelium develop specialized aerial hyphae, which in turn, give rise to conidiophores, ultimately producing uninucleate asexual spores known as microconidia or multinucleate macroconidia (Springer 1993).

N. crassa is a heterothallic filamentous fungus with two non-switching mating types, *mat A* and *mat a*, determined by alternate DNA sequences known as idiomorphs present at a single mating type locus (LG I). The sexual phase is initiated in response to nitrogen starvation, light exposure, and cold temperatures, leading to the development of female reproductive structures called protoperithecia (Raju 1992). The protoperithecium (female sexual structure), comprises of coiled multicellular hyphae called ascogonium, which is enveloped by surrounding hyphae (Nelson and Metzenberg 1992; Bistis et al. 2003). From the protoperithecium, a specialized hyphae known as trichogyne originates and undergoes chemotropic growth towards male cells of the opposite mating type, which can be microconidia, macroconidia, or hyphal fragments (Bistis 1981). Following the fusion or plasmogamy, between the trichogyne and the male cell, the male nucleus is transported through the trichogyne into

the protoperithecium, initiating the development of the multicellular sexual structure known as the "perithecium," which is a matured protoperithecium (Aramayo and Selker 2013); at this stage, the male and female coexist as a dikaryon within a specialized structure called the ascogenous hypha without immediate fusion (Bistis 1981; Springer 1993). Subsequently, these paired male and female nuclei undergo synchronous mitotic divisions at the tip of a specialized hook-shaped structure called the "crozier". Within the crozier, the central cell, known as the "ascus mother cell," undergoes karyogamy followed by two sequential meiotic divisions and a post-meiotic mitosis, resulting in the formation of eight spindle-shaped sexual spores known as ascospores, arranged linearly within the narrow ascus (Figure 1.7) (Raju 1992; Bistis et al. 2003; Aramayo and Selker 2013). Once mature, the ascospores are ejected through an opening called the "ostiole" at the tip of the perithecium (Springer 1993; Bistis et al. 2003; Kim et al. 2012). These released ascospores eventually germinate upon heat activation and give rise to their vegetative hyphae (Figure 1.6) (Raju 1992).

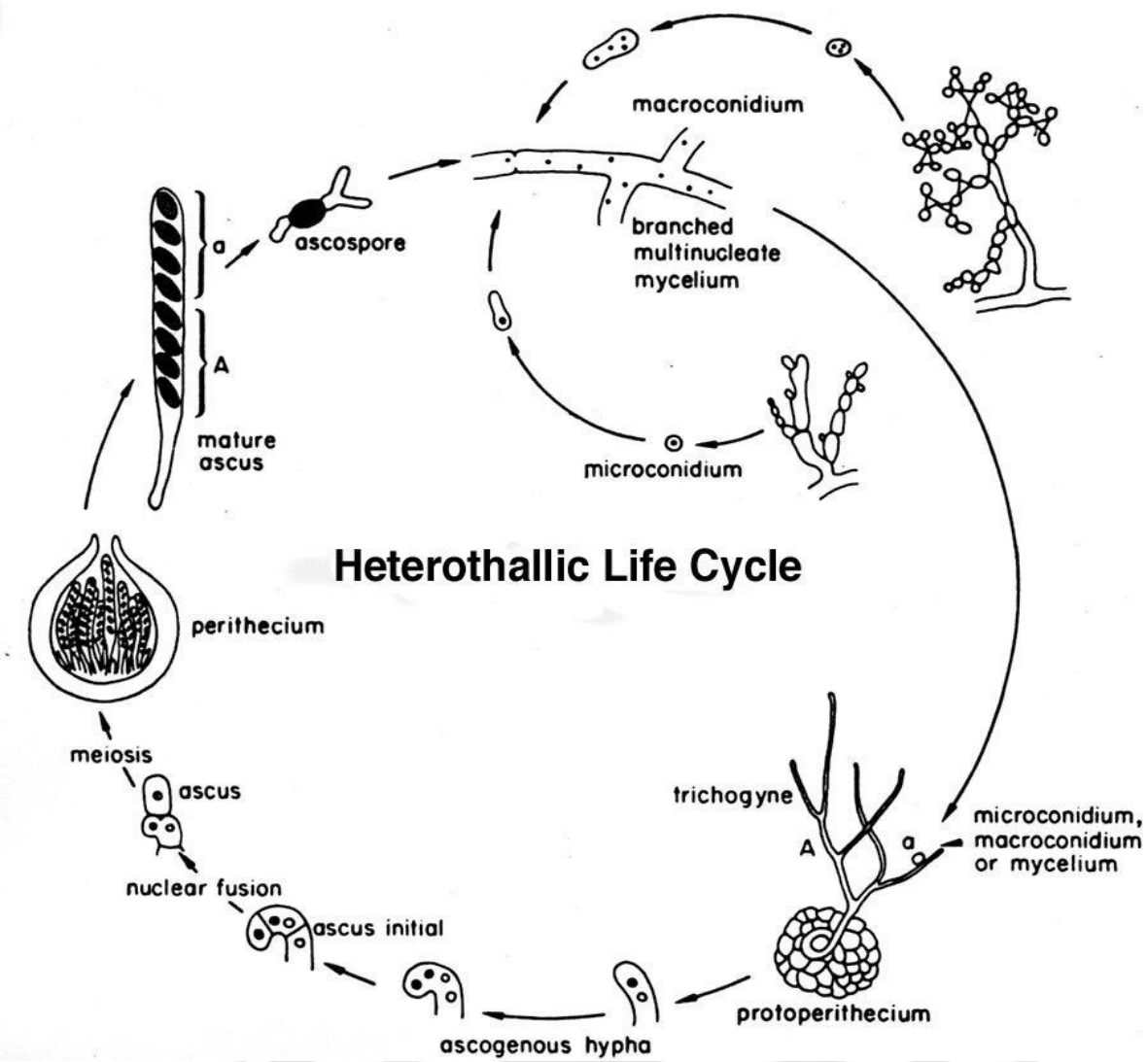

Figure 1.7 The Life cycle of *N. crassa*. The multinucleate and branching vegetative mycelium undergoes an asexual cycle in which it develops into aerial hyphae and asexual spores, either multinucleate macroconidium or uninucleate microconidium, which then disperse and repeats the asexual cycle when landing on suitable substrates. The sexual cycle is initiated by nitrogen starvation and low temperatures. Colonies of either mating type, *mat A* or *mat a*, generate a female sexual structure known as the protoperithecium, which is fertilized by conidia of the opposite mating type. This structure matures into the perithecium, where a dikaryon undergoes a series of mitosis and meiosis, ultimately forming eight linearly arranged ascospores within an ascus sac. Upon heat

activation, these mature, pigmented, multinucleate ascospores develop into new hyphae, completing the asexual cycle or serving as male or female parents for another sexual cycle**.** Adapted from FGSC (https://www.fgsc.net//Neurospora/sectionB2.htm).

1.5.3 Zinc signaling in *Neurospora crassa*

A comparative analysis of metal ion transportomes in *N. crassa* reveals the presence of seven putative members belonging to the ZIP transporter family (Table 1.2) (Kiranmayi and Mohan 2006). Among the seven ZIP transporters, the zinc-regulated transporters *tzn-1* (NCU07621.3) and *tzn-2* (NCU11414.3) have been studied (Kiranmayi et al., 2009). The TZN-1 exhibits similarities to the high-affinity zinc transporter Zrt1p in *S. cerevisiae* and the deletion of *tzn-1* gene causes aconidiation phenotype in *N. crassa* (Kiranmayi et al. 2009). In the *N. crassa* genome, there are nine putative members of the CDF transporters, within these, *trm-25/ zrc-1* (NCU03145) and *trm-29/msc-2* (NCU07262), show structural similarities to the established zinc-CDF transporters found in other species (Table 1.2) (Montanini et al. 2007; Kiranmayi et al. 2009). The *zrg-17* (NCU01254) was not listed in the metal transportome (Kiranmayi and Mohan 2006); however, the *zrg-17* transporter clusters appear to be specific for Ascomycota (Montanini et al. 2007) and only the *zrg-17* has been extensively studied among the CDF transporters. The Δ*zrg-17* mutant exhibited various zinc-suppressible phenotypes, including reduced growth rate, shorter aerial hyphae, and early and enhanced conidiation (Tiwari et al. 2018). Additionally, ZRG-17 plays a vital role in mitigating ER stress and facilitating cellulose degradation in low zinc conditions, and the expression of *zrg-17* gene was increased under low zinc conditions in a Zap-1-dependent manner (Tiwari et al. 2018).

[a]Table 1.2 Zinc transporter proteins in *N. crassa*

Sl. No.	NCU No.	Gene name	Linkage group	Family	Metals	[b]Best overall (e-value; organism; protein name; accession number)
1.	00860.2	*trm-37*	I	ZIP	Zn^{2+}	3e-158; *Chaetomium globosum*; Zinc/iron permease; KAH6651372.1
2.	02879.2	*trm-38*	I	ZIP	Zn^{2+}/ Fe^{3+}	1e-168; *Schizothecium vesticola*; ZIP zinc transporter; KAK0745595.1
3.	04819.2	*trm-39*	VI	ZIP	Zn^{2+}/ Fe^{2+}	0; *Cercophora newfieldiana*; Zinc/iron permease; KAK0641065.1
4.	07621.2	*tzn-1*	IV	ZIP	Zn^{2+}/Fe^{3+}	6e-144; *Cercophora caudata*; zinc-regulated transporter 1; KAK0620679.1
5.	[c] 11414	*tzn-2*	IV	ZIP	Zn^{2+}	3e-162; *Dactylonectria estremocensis*; ZIP zinc transporter; KAH7155761.1
6.	06380.2	*yke-4*	IV	ZIP	Zn^{2+}/Fe^{3+}	0; *Schizothecium vesticola*; zinc transporter; KAK0750960.1
7.	06473.2	*trm-43*	III	ZIP	Zn^{2+}/Fe^{3+}	2e-121; *Bombardia bombarda*; ZIP zinc

						transporter- protein; KAK0630830.1
8.	03145.2	*trm-25/ zrc-1*	I	CDF	$Cd^{2+}/Zn^{+2}+/Co^{2+}$	7e-163; *Madurella mycetomatis*; Zinc/ cadmium resistance protein; KXX78170.1
9.	04818.2	*trm-26*	VI	CDF	Me^{2+}	0; *Coniochaeta hoffmannii*; Cation efflux family protein; KAJ9165607.1
10.	05157.2	*trm-27*	VI	CDF	Me^{2+}	0; *Polychaeton citri*; Cation efflux family protein; KAF2722091.1
11.	06699.2	*trm-28*	V	CDF	Me^{2+}	0; *Cercophora caudata*; Cation efflux family protein; KAK0626599.1
12.	07262.2	*trm-29/ msc-2*	IV	CDF	Me^{2+}	0; *Echria macrotheca*; Cation efflux family protein; KAK1752177.1
13.	07879.2	*trm-30*	III	CDF	Me^{2+}	0; *Cercophora caudata*; Cation efflux family protein; KAK0623462.1
14.	09368.2	*trm-31*	I	CDF	Me^{2+}	0; Pleurostoma richardsiae; Cation efflux family protein; KAJ9157382.1
15.	07709.2	*trm-32*	IV	CDF	Cd^{2+}/Zn^{2+}	3e-78; *Lasiosphaeria miniovina*; Cation efflux protein; KAK0722187.1

16.	00029.2	*trm-33*	III	CDF	Cd^{2+}/Zn^{2+}	1e-149; *Lasiosphaeria miniovina*; Zinc/iron permease; KAK0709114.1

[a]Adapted from (Kiranmayi and Mohan 2006)

[b]BLASTP search was performed for both the ZIP and CDF zinc transporters using the default parameters in NCBI-BLASTP (https://blast.ncbi.nlm.nih.gov/Blast.cgi) seraches (Altschul et al. 1990, 1997).

[c]NCU11414 (was indicated as NCU009655.2 in Kiranmayi and Mohan 2006)

1.6 Objectives of this study

Zinc transporters in *N. crassa* remained largely unexplored. The cellular mechanisms regulating zinc homeostasis, and the cellular roles and functions of zinc transporter genes in various cellular processes such as growth, sexual development, and stress response in *N. crassa* are not fully known yet. A preliminary study regarding CDF zinc transporter *zrg-17* demonstrated its involvement in vegetative growth and development as well as asexual sporulation in *N. crassa* (Tiwari et al. 2018). However, the cellular roles of other CDF zinc transporters such as *zrc-1* and *msc-2*, and their interactions remained unknown in *N. crasa*. Therefore, additional studies are needed to fully understand the intricate mechanisms governing zinc transport and regulatory processes in *N. crassa*. To address this gap in knowledge and unravel the cellular roles of *zrc-1* and *msc-2*, as well as the regulation of CDF zinc transporter genes by ZAP-1 transcription fcator, this thesis work is structured around the following three broad objectives:

1. To investigate the cellular roles of the CDF family of zinc transporters *zrc-1* and *msc-2* in *Neurospora crassa*,
2. To study the genetic interaction of *zrc-1*, *msc-2*, and *zrg-17* in *Neurospora crassa*, and

3. To investigate the role of ZAP-1 transcription factor in regulating CDF zinc transporters in *Neurospora crassa*.

2

MATERIALS AND METHODS

2.1 Materials

2.1.1 Chemicals and other materials

The chemicals and reagents used in this study are listed in the table 2.1. Glassware and plasticware materials used in this study were obtained from Borosil (Mumbai, India), and Jain scientific glassworks (Ambala, India). Plasticwares were acquired from Genaxy (New Delhi, India) and Tarsons (Kolkata, India).

Table 2.1 Chemicals and reagents used in this study

Sl. No.	Chemical/ Reagent	Chemical formula	Make	Catalogue No.
1.	Absolute ethanol	C_2H_5OH	MERCK	1.00983.0511
2.	Agarose	N/A	Invitrogen	16500-500
3.	Ammonium iron (II) sulphate hexahydrate	$Fe(NH_4)_2(SO_4)_2.6H_2O$	MERCK	103792
4.	Ammonium molybdate tetrahydrate	$(NH_4)_6Mo_7O_{24}.4H_2O$	SRL	014892
5.	Ammonium nitrate	NH_4NO_3	Fisher Scientific	21445
6.	Ammonium per sulphate (APS)	$(NH_4)_2S_2O_8$	SRL	0148134
7.	Ampicillin sodium salt	$C_{16}H_{18}N_3NaO_4S$	HIMEDIA	MB104-5G
8.	L-Arginine	$C_6H_{14}N_4O_2$	HIMEDIA	PCT0302-25G
9.	Avicel R PH-101	N/A	SIGMA-ALDRICH	11365
10.	Bacto-agar	N/A	HIMEDIA	GRM026-500G
11.	D-Biotin	$C_{10}H_{16}N_2O_3S$	SRL	0248120
12.	Boric acid	H_3BO_3	SRL	0244112
13.	Bradford reagent	N/A	HIMEDIA	ML106-500ML
14.	Bromophenol blue	$C_{19}H_{10}Br_4O_5S$	SRL	0240168
15.	Cadmium chloride	$CdCl_2$	HIMEDIA	GRM8016-100G
16.	Calcium chloride dihydrate	$CaCl_2.2H_2O$	SRL	0349152
17.	Calcium D-pantothenate	$C_{18}H_{32}CaN_2O_{10}$	HIMEDIA	CMS178-100G
18.	Calcofluor White Stain	N/A	SIGMA-ALDRICH	18909-100ML-F
19.	Cetyltrimethyl ammonium bromide (CTAB)	$C_{19}H_{42}BrN$	aMResco	0833-500G
20.	Chloroform	$CHCl_3$	SRL	0328101
21.	Citric acid monohydrate	$C_6H_8O_7.H_2O$	SRL	0348216

22.	Copper sulphate pentahydrate	$CuSO_4.5H_2O$	SRL	0347102
23.	Copper(II) chloride dihydrate	$CuCl_2.2H_2O$	MERCK	QJ5Q652270
24.	Diethyl pyrocarbonate (DEPC)	$C_6H_{10}O_5$	SRL	46791
25.	Dimethyl sulphoxide (DMSO)	C_2H_6OS	MERCK	109678
26.	3,5-Dinitrosalicylic acid (DNSA)	$C_7H_4N_2O_7$	SRL	13313(0420304)
27.	Dithiothreitol (DTT)	$C_4H_{10}O_2S_2$	SRL	17315
28.	Ethidium bromide (EtBr)	$C_{21}H_{20}BrN_3$	SRL	054817
29.	EDTA	$C_{10}H_{16}N_2O_8$	SRL	18240
30.	EGTA	$C_{14}H_{24}N_2O_{10}$	HIMEDIA	MB130-10G
31.	Ferrous sulphate heptahydrate	$FeSO_4.7H_2O$	RANKEM	F0044
32.	Formaldehyde	CH_2O	SRL	AS017-500ML
33.	D-Fructose	$C_6H_{12}O_6$	SRL	064855
34.	Glacial acetic acid	CH_3COOH	MERCK	1.93402.0521
35.	D-Glucose	$C_6H_{12}O_6$	SRL	42738
36.	L-Glutamine	$C_5H_{10}N_2O_3$	HIMEDIA	PCT0308-100G
37.	Glycerol (glycerin) anhydrous	$C_3H_8O_3$	SRL	072929
38.	Glycine	$C_2H_5NO_2$	SRL	69422
39.	Herring sperm DNA	N/A	Promega	D181B
40.	Hydrochloric acid	HCl	HIMEDIA	AS003-500ML
41.	Hydrogen peroxide	H_2O_2	MERCK	61765305001730
42.	Hygromycin B	N/A	HIMEDIA	PCT1503-20ML
43.	HEPES buffer	$C_8H_{18}N_2O_4S$	SRL	084023
44.	Isopropanol	C_3H_7OH	SRL	092956
45.	Lithium chloride	LiCl	SRL	124919
46.	Luria Bertani Agar	N/A	HIMEDIA	M1151-500G
47.	Luria Bertani Broth	N/A	HIMEDIA	M1245-500G
48.	Magnesium chloride hexahydrate	$MgCl_2.6H_20$	HIMEDIA	GRM3922-500G
49.	Magnesium sulphate heptahydrate	$MgSO_4.7H_2O$	Qualigens	18955
50.	Manganous chloride tetrahydrate	$MnCl_2.4H_2O$	SRL	1348152
51.	Manganous sulphate monohydrate	$MnSO_4.H_2O$	Qualigens	25255
52.	Methanol	CH_3OH	HIMEDIA	AS058-500ML

53.	*N,N'*-Methylenebisacrylamide	$C_7H_{10}N_2O_2$	SRL	38516
54.	*β*-Mercaptoethanol	C_2H_6OS	SRL	1324196
55.	MOPS buffer	$C_7H_{15}NO_4S$	HIMEDIA	RM660-100G
56.	Nickel(II) chloride hexahydrate	$NiCl_2.6H_2O$	MERCK	QH5Q652267
57.	Peptone	N/A	HIMEDIA	RM001-500G
58.	Phenol: Chloroform: Isoamyl alcohol (25:24:1)	N/A	SRL	69031
59.	Phusion® High-Fidelity DNA Polymerase	N/A	NEB	M0530S
60.	Piperazine-N,N' bis(2-ethanesulphonic acid)	$C_8H_{18}N_2O_6S_2$	HIMEDIA	RM659-25G
61.	Polyethyleneglycol 4000	N/A	SRL	1647131
62.	Potassium acetate	$C_2H_3O_2K$	HIMEDIA	GRM3930-500G
63.	Potassium hydroxide	KOH	RANKEM	P0390
64.	Potassium nitrate	KNO_3	TITAN	761
65.	Potassium phosphate dibasic	K_2HPO_4	HIMEDIA	GRM1045-500G
66.	Potassium phosphate monobasic	KH_2PO_4	HIMEDIA	GRM249-500G
67.	SD growth media w/o URA	N/A	HIMEDIA	G067
68.	Silica gel (6-12 mesh)	N/A	SIGMA-ALDRICH	214426-1KG
69.	Skimmed milk powder	N/A	HIMEDIA	M530-500G
70.	Sodium acetate anhydrous	$C_2H_3NaO_2$	HIMEDIA	TCO23-500G
71.	Sodium arsenate dibasic heptahydrate	$Na_2HAsO_4.7H_2O$	HIMEDIA	10048-95-0
72.	Sodium bicarbonate dihydrate	$Na_3C_6H_5O_7.2H_2O$	SRL	89399
73.	Sodium carbonate anhydrous	Na_2CO_3	SRL	64079
74.	Sodium citrate dihydrate	$Na_3C_6H_5O_7.2H_2O$	HIMEDIA	GRM255-500G
75.	Sodium dodecyl sulphate (SDS)	$NaC_{12}H_{25}SO_4$	SRL	194821
76.	Sodium hydroxide	NaOH	TITAN	439
77.	Sodium molybdate dihydrate	$Na_2MoO_4.2H_2O$	SRL	1947166
78.	Sodium nitrate	$NaNO_3$	HIMEDIA	GRM416-500G

79.	Sodium potassium tartrate tetrahydrate	$C_4H_4O_6KNa{\cdot}4H_2O$	SRL	18241
80.	Sodium sulphate anhydrous	Na_2SO_4	SRL	59977
81.	D-Sorbitol	$C_6H_{14}O_6$	SRL	14281
82.	Sorbose	$C_6H_{12}O_6$	LOBA Chemie	0607700025
83.	Sucrose	$C_{12}H_{22}O_{11}$	MERCK	61839805001730
84.	Sulphuric acid	H_2SO_4	HIMEDIA	AS015-500ML
85.	SYBR Green Real-Time PCR Mix	N/A	Life Technologies	4472903
86.	Taq DNA Polymerase	N/A	NEB	M0273S
87.	Tris base	$C_4H_{11}NO_3$	RANKEM	T0350
88.	Triton X-100	N/A	SRL	64518
89.	TRIzol™ reagent	N/A	Invitrogen	15596026
90.	D-Xylose	$C_5H_{10}O_5$	SRL	84974
91.	Yeast extract	N/A	SRL	34266
92.	Zinc sulphate heptahydrate	$ZnSO_4.7H_2O$	SRL	264745
93.	Plasmid DNA Isolation Kit	N/A	Qiagen	12123
94.	PCR Purification Kit	N/A	Qiagen	28104
95.	Verso cDNA Synthesis Kit	N/A	Thermo Scientific	AB-1453/A

Not Applicable (N/A): Chemical formula doesn't exist.

2.1.2 Organisms and strains

2.1.2.1 *Neurospora crassa* strains

The *N. crassa* strains used in this study were either obtained from the Fungal Genetics Stock Center (FGSC, University of Missouri, Kansas City, MO 64110; McCluskey 2003; McCluskey et al. 2010) or generated in our laboratory (Table 2.2).

Table 2.2 *N. crassa* strains used in this study

Sl. No.	Strain	Strain type or NCU No.	Genotype	Reference
1.	74-OR23-IVA	Wild Type	wild type *mat A*	FGSC 2489
2.	ORS-SL6a	Wild Type	wild type *mat a*	FGSC 4200
3.	1858	Homokaryotic	*ras-1*^{bd}; *mat A*	FGSC 1858

4.	1859	Homokaryotic	*ras-1*^{bd}; *mat a*	FGSC 1859
5.	*his-3*	Histidine auxotroph	*his-3*; *mat A*	FGSC 6032
6.	Δ*zrc-1*	NCU03145	Δ*zrc-1*:: *hph*; *mat A*	FGSC 12277
7.	Δ*zrc-1*	NCU03145	Δ*zrc-1*:: *hph*; *mat a*	Our Laboratory (This study)
8.	Δ*msc-2*	NCU07262	Δ*msc-2*:: *hph*; *mat a*	FGSC 11540
9.	Δ*msc-2*	NCU07262	Δ*msc-2*:: *hph*; *mat A*	Our Laboratory (This study)
10.	Δ*zrg-17*	NCU01254	Δ*zrg-17*:: *hph*; *mat A*	FGSC 18312
11.	Δ*zrg-17*	NCU01254	Δ*zrg-17*:: *hph*; *mat a*	Our Laboratory
12.	Δ*zap-1*	NCU02699	Δ*zap-1*:: *hph*; *mat a*	FGSC 11347
13.	Δ*zap-1*	NCU02699	Δ*zap-1*:: *hph*; *mat A*	Our Laboratory (This study)
14.	Δ*zrc-1*; *ras-1*^{bd}	Homokaryotic	Δ*zrc-1*; *ras-1*^{bd}	Our Laboratory (This study)
15.	Δ*msc-2*; *ras-1*^{bd}	Homokaryotic	Δ*msc-2*; *ras-1*^{bd}	Our Laboratory (This study)
16.	Δ*zrc-1*; Δ*msc-2*	Double mutant	Δ*zrc-1*: Δ*msc-2*; *mat A*	Our Laboratory (This study)
17.	Δ*zrc-1*; Δ*zrg-17*	Double mutant	Δ*zrc-1*: Δ*zrg-17*; *mat a*	Our Laboratory (This study)
18.	Δ*msc-2*; Δ*zrg-17*	Double mutant	Δ*msc-2*: Δ*zrg-17*; *mat a*	Our Laboratory (This study)
19.	Δ*zap-1*; Δ*zrc-1*	Double mutant	Δ*zap-1*: Δ*zrc-1*; *mat A*	Our Laboratory (This study)
20.	Δ*zap-1*; Δ*msc-2*	Double mutant	Δ*zap-1*: Δ*msc-2*; *mat a*	Our Laboratory (This study)
21.	Δ*zap-1*; Δ*zrg-17*	Double mutant	Δ*zap-1*: Δ*zrg-17*; *mat a*	Our Laboratory (This study)
22.	$P_{ccg\text{-}1}$*::zap-1::gfp*	Homokaryotic	Δ*zap-1::hph::Pccg-1::zap-1::gfp A*	Our Laboratory (This study)

2.1.2.2 Bacterial strains

The *Escherichia coli* DH5α strain with genotype *SupE*44 Δ*lac*U169 (φ80*lacZ* ΔM15) *hsdR*17 *recA*1 *end A*1 *gyrA*96 *thi*-1 *relA*1 was used for regular bacterial cloning, transformations, plasmid growth, and isolation (Sambrook and Russell 2001).

2.1.2.3 Plasmid vectors

(i) pMF272

The plasmid vector pMF272 is 8.4 kb in size (Figure 2.1), contains the GFP variant gene (*sgfp*), the lacZ′ sequence that includes both the T7 and SP6 promoters, ampicillin resistance gene as the bacterial selectable marker, and a multiple cloning site (MCS) enabling the translational fusing of *N. crassa* genes to *sgfp* (https://www.fgsc.net//plasmid/image/609.jpg). The *sgfp* gene is a variant of GFP, where a serine to threonine substitution at position 65 (S65T) leads to more brightness, thus, this GFP variant is a suitable choice for studies in *N. crassa*, additionally, the mutation makes the codon bias similar to that found in humans and *N. crassa* (Freitag et al. 2004). The *sgfp* as well as the transgene is regulated by the inducible *ccg-1* promoter, which is significantly activated by stress or glucose deprivation in *N. crassa* (Arpaia et al. 1995). Using the pBM60 backbone the $P_{ccg\text{-}1}$::*sgfp* cassette was constructed, thereby, allowing gene replacement of the transgene by targeting to the *his-3* gene locus (Margolin et al. 1997).

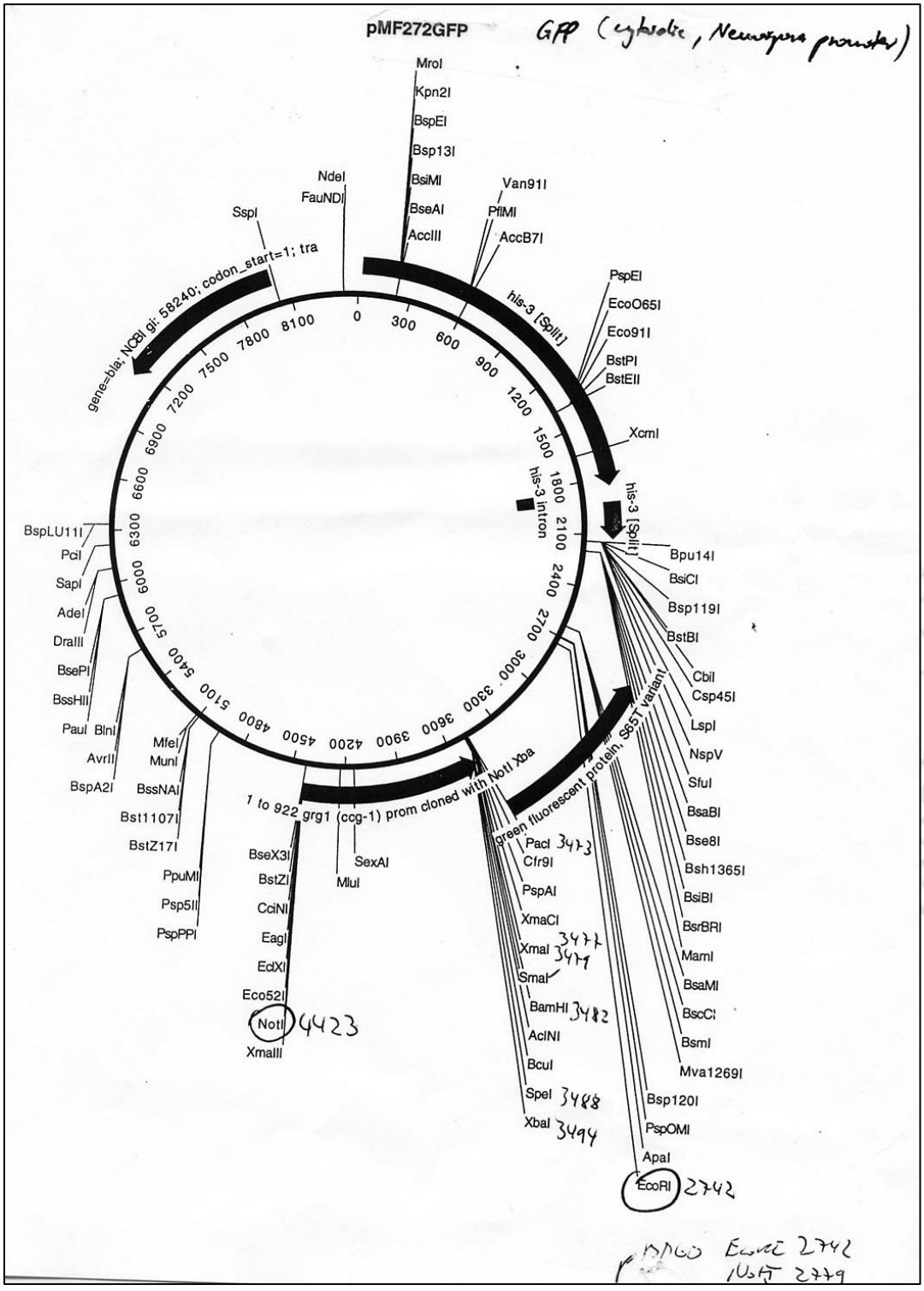

Figure 2.1 Schematic representation of pMF272 vector. The pMF272 vector is 8.4 kb in size, it consists of unique restriction sites at the MCS region. The plasmid vector pMF272 is available at https://www.fgsc.net//plasmid/image/609.jpg.

(ii) pRS426

The plasmid vector pRS426 is 11.116 kb in size (Figure 2.2) and consists of the backbone from the yeast/*E. coli* shuttle vector pRS426PVG (Ouyang et al. 2015). The vector pRS426 contains ampicillin resistance (ApR) as the bacterial selectable marker and yeast auxotrophic marker URA3 as the yeast selectable marker. The vector also contains a multiple cloning site (MCS), a 5xGlycine linker, a V5 peptide tag and the *gfp* gene tag to the promoter $P_{nit\text{-}6}$. The *nit-6* gene encodes for nitrite reductase, and $P_{nit\text{-}6}$ is induced by nitrate and repressed by glutamine (Ouyang et al. 2015). The vector also carries the 5′ and 3′ flanking regions for the *N. crassa pan-2* and the *nit-6* promoter fragments. Moreover, pRS426 also contains *bar* gene as the selection marker for *N. crassa*, which confer resistance to Phosphinothricin (glufosinate ammonium) commonly known as Basta® or Ignite® (Pall 1993; Ouyang et al. 2015).

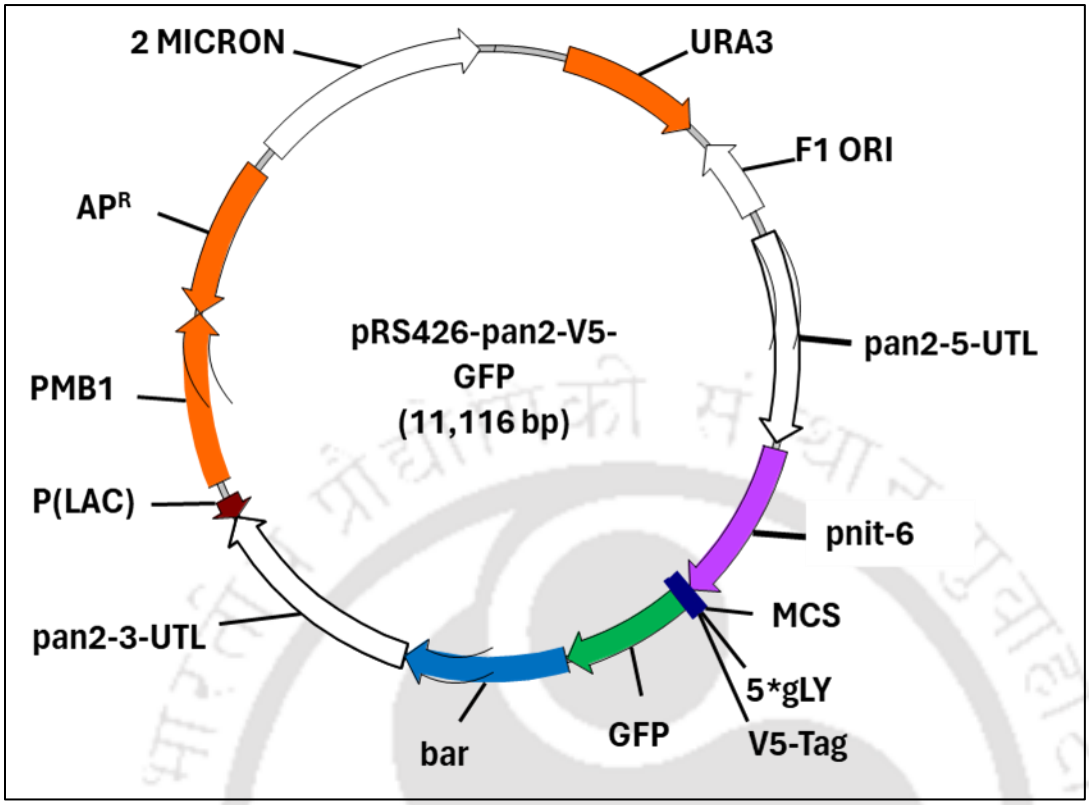

Figure 2.2 Schematic representation of pRS426 vector. The Yeast/ *E. coli* shuttle vector pRS426 vector is 11,116 bp in size. The figure is adapted from Ouyang *et al.* (2015).

2.1.2.4 *Saccharomyces cerevisiae* strains

The yeast strains BY4742 (wild type) and YJL056C (*ZAP1*Δ) were a gift from Dr. Shirisha Nagotu of Organelle Biology and Cellular Ageing Laboratory (OBCAL), BSBE department, IIT Guwahati, India.

2.1.3 Growth media, Antibiotics, and other commonly used solutions

1. **Bacterial media:** The bacterial growth media Luria Bertani (LB) broth, LB agar, terrific broth, and SOC (Super optimal broth with Catabolite repression) medium were purchased from Himedia (Mumbai, India). These media were prepared and further sterilized by autoclaving using the manufacturer's protocol.

2. **Yeast media:** The yeast growth media YPD (Yeast Extract-Peptone-Dextrose) was prepared with 1 % Yeast extract, 2% Peptone, and 1% Glucose. For YPD agar, 2 % agar was added to the media. SD (Synthetic Defined) growth media without URA was used for the selection of yeast transformants, 2.7 g of SD growth media without URA powder and 2 % agar were dissolved in 100 ml water.
3. **Ampicillin:** 100 mg/ml stock solution of Ampicillin was prepared by dissolving 200 mg of ampicillin powder in 2 ml sterile autoclaved water and aliquots of 500 µl were stored at -20 °C.
4. **Azole agents:** Itraconazole and fluconazole were prepared as described previously (Pereira and Said 2009)**.**
   i) **Itraconazole (50 mg/ml):** Itraconazole tablet Itrasig (Signova Pharmaceuticals Pvt. Ltd.) was taken as the source for Itraconazole. The capsule was pulverized and 50 mg of the powder was dissolved in 1 ml DMSO.
   ii) **Fluconazole (50 mg/ml):** Fluconazole tablet OneCan^{TM} (Wallace Pharmaceuticals Pvt. Ltd.) was taken as the source for fluconazole. The capsule was pulverized and 50 mg of the powder was dissolved in 1 ml DMSO.
5. **0.5 M EDTA (pH 8.0):** To prepare 0.5 M EDTA, 18.61g of EDTA was dissolved in 50 ml of distilled water, the pH was adjusted to 8.0 using NaOH, further the final volume was adjusted to 100 ml and sterilized by autoclaving and stored at room temperature.
6. **Diethylpyrocarbonate (DEPC):** To prepare 0.1% DEPC solution, 1 ml of DEPC was added to 999 ml sterile distilled water and was sterilized by autoclaving.
7. **Ethidium bromide (EtBr):** To prepare a stock solution of EtBr (10 mg/ml), 20 mg EtBr was dissolved in 2 ml distilled water.

8. **Hygromycin B:** A 50 mg/ml Hygromycin B, which is a ready-to-use solution, was procured from Himedia (Mumbai, India) and used at a working concentration of 220 µg/ml.
9. **1 M LiCl:** To prepare 1 M LiCl, 0.4239 g of LiCl was dissolved in 5 ml of sterile distilled water, further the final volume was adjusted to 10 ml, and sterilized by autoclaving.
10. **8 M LiCl:** To prepare 8 M LiCl, 33.9 g of LiCl was dissolved in 50 ml of DEPC-treated sterile distilled water, further the final volume was adjusted to 100 ml, and sterilized by autoclaving.
11. **5 M NaCl:** To prepare 5 M NaCl, 29.22 g of NaCl was dissolved in 80 ml of distilled water, then the final volume was adjusted to 100 ml, and sterilized by autoclaving.
12. **2 N NaOH:** To prepare 2 N NaOH, 8 g of NaOH pellet was dissolved in 50 ml of DEPC-treated water, further the final volume was adjusted to 100 ml and sterilized by autoclaving.
13. **10 N NaOH:** 10 N NaOH was prepared in a plastic beaker placed on ice by slowly dissolving 40 g of NaOH pellet in 80 ml of distilled water while stirring, further, the final volume was 100 ml and stored at room temperature.
14. **3 M Na-acetate (pH 5.2):** To prepare 3 M Na-acetate (pH 5.2), 24.61 g Na-acetate was dissolved in 70 ml DEPC-treated water, and pH was adjusted to 5.2 with glacial acetic acid. The final volume was adjusted to 100 ml by adding DEPC treat water and sterilized by autoclaving.
15. **50% PEG (Polyethylene Glycol):** To prepare 50% PEG, 5 g of PEG was dissolved in 5 ml of distilled water, further, the final volume was to 10 ml and sterilized by autoclaving.
16. **10% SDS:** To prepare 10 % SDS, 1 g of SDS was dissolved in 5 ml sterile double-distilled water, while stirring and heating at 65 °C, the final volume was adjusted to 10 ml and stored at room temperature.

17. **Skimmed Milk:** To prepare skimmed milk 2.1 g of skimmed milk powder was dissolved in 30 ml of sterile distilled water, sterilized by autoclaving, and stored at 4 °C.
18. **1 M Sorbitol:** To prepare 1 M sorbitol, 18.21 g of sorbitol was dissolved in 70 ml distilled water, further the volume was adjusted to 100 ml, and was sterilized by autoclaving.
19. **1 M Tris-HCl (pH 7.5):** To prepare 1 M Tris-HCl (pH 7.5), 12.11 g of Tris base was dissolved in 70 ml distilled water and the pH was adjusted to 7.5 by adding HCl, the final volume was adjusted to 100 ml and sterilized by autoclaving.
20. **1 M Tris-HCl (pH 8.0):** To prepare 1 M Tris-HCl (pH 8.0), 12.11 g of Tris base was dissolved in 70 ml of DEPC-treated water and the pH was adjusted to 8.0 by adding HCl, further the final volume was adjusted to 100 ml and sterilized by autoclaving.
21. **1 M $ZnSO_4.7H_2O$:** To prepare 1 M $ZnSO_4.7H_2O$ solution, 28.754 g of $ZnSO_4.7H_2O$ was dissolved in 50 ml distilled water while stirring, then the final volume was adjusted to 100 ml, sterilized by autoclaving, and stored at 4 °C.
22. **0.5 M $ZnSO_4.7H_2O$:** To prepare 0.5 M $ZnSO_4.7H_2O$ solution, 14.377 g of $ZnSO_4.7H_2O$ was dissolved in 50 ml distilled water while stirring, the final volume was adjusted to 100 ml, autoclaved, and stored at 4 °C.
23. **6X Gel-loading Buffer (Type III):** To prepare 6X Gel-loading Buffer (Type III), a solution of 0.25% (w/v) bromophenol blue, 0.25% (w/v) xylene cyanol FF, and 30% glycerol (v/v) was added in sterile distilled water, and stored in aliquots of 500 µl at 4 °C.
24. **50X TAE:** To prepare 50X TAE stock solution, 24.2 g of Tris base was dissolved in 50 ml distilled water, 5.71 ml of glacial acetic acid, and 10 ml of 0.5 M EDTA (pH 8.0) were added, further the final volume was adjusted to 100 ml. The solution was stored at 4 °C.

25. **1X TE:** To prepare 1X TE, 10 mM Tris-HCl (pH 8.0) and 1 mM EDTA (pH 8.0) were taken from their respective stocks, mixed and the solution was stored at 4 °C.
26. **10X MOPS electrophoresis buffer:** To prepare 10X MOPS stock solution, 4.18 g of MOPS was dissolved in 40 ml of DEPC-treated water, the pH was adjusted to 7.0 with 2 N NaOH, then 2 ml of 1 M sodium acetate solution (20 mM) and 2 ml of 0.5 M EDTA pH 8.0 (10 mM) were added. The final volume was then adjusted to 100 ml with DEPC-treated water. The solution was filter sterilized using a 0.45 µm syringe filter (HIMEDIA, SF182E) and stored in the dark at room temperature.
27. **0.5 M PIPES buffer (pH 6.7):** To prepare 0.5 M PIPES buffer (pH 6.7), 1.5 g PIPES was dissolved in 5 ml sterile distilled water, pH was adjusted to 6.7 by adding 10 N NaOH solution, the final volume was adjusted to 10 ml. The solution was sterilized using 0.45 µm syringe filter (HIMEDIA, SF182E), and stored at −20 °C.
28. **Alkaline lysis Solution I:** Alkaline lysis solution I contains 50 mM glucose, 25 mM Tris-Cl (pH 8.0), and 10 mM EDTA (pH 8.0), the solution was sterilized by autoclaving and stored at 4 ºC.
29. **Alkaline lysis Solution II:** Alkaline lysis Solution II contains 0.2 N NaOH and 1% SDS, and this solution was freshly prepared before use.
30. **Alkaline lysis Solution III:** Alkaline lysis Solution III was prepared by adding 60 ml of 5 M potassium acetate, and 11.5 ml of glacial acetic acid, the final volume was adjusted to 100 ml by adding distilled water. The solution was sterilized by autoclaving and stored at 4 ºC.
31. **Inoue transformation buffer:** The Inoue transformation buffer (Inoue et al. 1990) contains 55 mM $MnCl_2$, 15 mM $CaCl_2$, 250 mM KCl, and 10 mM PIPES buffer (pH 6.7).

32. **Yeast transformation buffer:** The yeast transformation buffer contains 1 M LiCl, 50% PEG, 100 mM Tris HCl (pH 7.5), and 10 mM EDTA (pH 8.0).
33. **Lysis buffer for *N. crassa* genomic DNA isolation:** The lysis buffer for the isolation of genomic DNA of *N. crassa* contains 10 mM Tris HCl (pH 7.5), 0.5 M NaCl, 10 mM EDTA, 1% SDS, and 1% CTAB, these components are sequentially added and mixed thoroughly using a vortex mixture.
34. **Lysis buffer for *N. crassa* RNA isolation:** The lysis buffer for isolation of RNA of *N. crassa* contains 100 mM Tris HCl (pH 8.0), 0.6 M NaCl, 10 mM EDTA (pH 8.0), 4.5 % SDS, and 2 % β-mercaptoethanol, this solution is freshly prepared before use.

2.1.4 Solutions for growth, maintenance, and crossing of *N. crassa* strains

i. **Biotin solution:** Biotin solution was prepared by dissolving 5 mg biotin in 100 ml 50% (v/v) ethanol and stored at 4 °C.

ii. **L-Histidine:** From a stock of 50 mg/ml, 2 ml per 100 ml medium is added. The stock solution of L-Histidine was autoclaved and stored at 4 °C.

iii. **Trace element solution:** To prepare trace element solution the following chemicals are sequentially dissolved in 80 ml of distilled water while stirring, further the final volume was adjusted to 100 ml. To the solution, 1 ml of chloroform was added as a preservative and stored at 4 °C.

	Trace element solution	**Trace element solution without zinc**
$C_6H_8O_7.H_2O$	5.00 g	5.00 g
$ZnSO_4.7H_2O$	5.00 g	0
$Fe(NH_4)_2(SO_4)_2.6H_2O$	1.00 g	1.00 g
$CuSO_4.5H_2O$	0.25 g	0.25 g

$MnSO_4.H_2O$	0.05 g	0.05 g
H_3BO_3	0.05 g	0.05 g
$Na_2MoO_4.2H_20$	0.05 g	0.05 g

iv. **Vogel's Medium N (VGN):** A 50X stock solution of Vogel's Medium N (Vogel 1956, 1964) with zinc and without zinc was prepared by sequentially adding the following chemicals in 50 ml distilled water while stirring, further the final volume was adjusted to 100 ml. Chloroform was added as a preservatives and stored at 4 °C.

	50X Vogel's medium N (VGN)	**50X Vogel's medium N without Zinc***
$Na_3C_6H_5O_7.2H_2O$	12.5 g	12.5 g
KH_2PO_4	25 g	25 g
NH_4NO_3	10 g	10 g
$MgSO_4.7H_2O$	1 g	1 g
$CaCl_2.7H_2O$ (pre-dissolve in 5 ml H_2O)	0.5 g	0.5 g
Biotin Solution	500 µl	500 µl
Trace Element Solution*	500 µl	500 µl
Chloroform	300 µl	300 µl

***** The Trace element solution without zinc (discussed in section 2.1.4: iii) was added in the 50X Vogel's medium N without Zinc.

VG

Vogel's Medium N	1X
Glucose	1.5% (w/v)

VG agar

Vogel's Medium N	1X
Glucose	1.5% (w/v)
Agar	2 % (w/v)

v. **Low zinc media (LZM):** Low zinc media comprising different zinc concentrations (LZVG, LZVG1, LZVG100, LZVG1000) were prepared using 100 µM EDTA as the zinc chelator (Zhao and Eide 1996a), and sterilized by autoclaving.

LZVG

Composition	**Concentration**	**Amount to be added for 100 ml media**
50X Vogel's medium N without Zinc	1X	2 ml
Glucose	1.5% (w/v)	1.5 g
Agar *	2 % (w/v)	2 g
ETDA	100 µM	20 µl (From 0.5 M EDTA stock solution)

* For liquid medium, agar is not added.

LZVG1

Composition	Concentration	Amount to be added for 100 ml media
50X Vogel's medium N without Zinc	1X	2 ml
Glucose	1.5% (w/v)	1.5 g
Agar *	2 % (w/v)	2 g
ETDA	100 µM	20 µl (From 0.5 M EDTA stock solution)
$ZnSO_4.7H_2O$	1 µM	0.2 µl (From 0.5 M $ZnSO_4.7H_2O$ stock solution)

* For liquid medium, agar is not added.

LZVG100

Composition	Concentration	Amount to be added for 100 ml media
50X Vogel's medium N without Zinc	1X	2 ml
Glucose	1.5% (w/v)	1.5 g
Agar *	2 % (w/v)	2 g
ETDA	100 µM	20 µl (From 0.5 M EDTA stock solution)
ZnSO4.7H2O	100 µM	20 µl (From 0.5 M ZnSO4.7H2O stock solution)

* For liquid medium agar is not added.

LZVG1000

Composition	Concentration	Amount to be added for 100 ml media
50X Vogel's medium N without Zinc	1X	2 ml
Glucose	1.5% (w/v)	1.5 g
Agar *	2 % (w/v)	2 g
ETDA	100 µM	20 µl (From 0.5 M EDTA stock solution)
ZnSO4.7H2O	1 µM	200 µl (From 0.5 M ZnSO4.7H2O stock solution)

***** For liquid medium agar is not added.

vi. **4X Synthetic Crossing Medium (SCM):** 4X Synthetic Crossing Medium (Westergaard and Mitchell 1947) was prepared by sequentially adding the following chemicals in 80 ml of distilled water while stirring, the final volume was adjusted to 100 ml and sterilized by autoclaving and stored at 4 °C.

4X Synthetic Crossing Medium (SCM)

KNO_3	0.4 g
K_2HPO_4	0.28 g
KH_2PO_4	0.2 g
$MgSO_4.7H_2O$	0.2 g
$CaCl_2.2H_2O$	40 mg
NaCl	40 mg

Biotin Solution	20 µl
Trace Element Solution	20 µl

SCM Agar

SCM	1X
Glucose	1.5% (w/v)
Agar	1.5% (w/v)

vii. **10X FGS (Fructose, Glucose, and Sorbose) Stock:** The stock solution of 10X FGS was prepared by dissolving the following chemicals in 50 ml of distilled water. The final volume of the solution was adjusted to 100 ml, sterilized by autoclaving, and stored at 4 °C.

10X FGS Stock

Fructose	5% (w/v)
Glucose	5% (w/v)
Sorbose	20% (w/v)

FGS Agar

FGS	1X
Vogel's Medium N	1X
Agar	1.5% (w/v)

Top Agar

FGS	1X
Vogel's Medium N	1X
Agar	2.8% (w/v)

viii. **Medium for Circadian Clock Study:** For the study of the circadian clock in a race tube, the medium was prepared by dissolving the following chemicals in 100 ml distilled water, and sterilized by autoclaving before use.

Circadian Clock Medium (Park and Lee 2004)

Vogel's Medium N	1X
Glucose	0.1% (w/v)
L-Arginine	0.17% (w/v)
Biotin	50 ng/ml
Agar	1.5% (w/v)

2.1.5 Primers used in this study

Custom oligonucleotide primers that are used in this study were purchased from Bioserve Biotechnologies (India) Pvt. Ltd. (Hyderabad, India) as well as from Integrated DNA Technologies (Iowa, USA). List of primers used in this study are enlisted in Table 2.3.

Table 2.3 List of primers used in this study

Sl. No.	Primers	Sequence (5′-3′)	Source
1.	5HPHR	ATCCACTTAACGTTACTGAAATC	(Deka et al. 2011)

2.	HI-ZRC-1 SN	GGGAGGTGGTTCTTATGCTC	Our Laboratory (This study)
3.	HI-MSC-2 SN	CGCCAGTCCTGTAAGGACCA	Our Laboratory (This study)
4.	Zrg-17-KOC-F	GGAAACCGAGACAACAGTCC	Our Laboratory (This study)
5.	RT-NCU03145Fw	TCCAAGTGATGCTGGCGATC	Our Laboratory (This study)
6.	RT-NCU03145Rv	CGTAGGAGAACTGATCTGTTG	Our Laboratory (This study)
7.	RT-NCU07262Fw	CCAAGTTCACTGthCGTTTCTG	Our Laboratory (This study)
8.	RT-NCU07262Rv	AGGAGACCGAGGGAATCTG	Our Laboratory (This study)
9.	RT-ZRG-17Fw	CCTTTGCAATGGCGAGCCA	Our Laboratory (This study)
10.	RT-ZRG-17Rv	GGGGTTCCTGAAAGAAGGAA	Our Laboratory (This study)
11.	HI-NCU02699Fw	CCGTTCAGGTTTCCATTGGG	Our Laboratory (This study)
12.	NCU02699 Fw	ATGCGCCCTGACCATTACGAT	Our Laboratory (This study)
13.	NCU02699 Rv	ATGGCTCCCCTCATCACCAAT	Our Laboratory (This study)
14.	Pccg-1 Fw	CCATCATCAGCCAACAAAGC	Ananya Barman Thesis (TH-1649/11610630; http://gyan.iitg.ernet.in/handle/123456789/899)

15.	Pnit-6 Fw	CTAGTCTTTCTGTCGTCAGC	(Gohain and Tamuli 2019)
16.	GFP Rv	AACTTGTGGCCGTTTACGTC	(Gohain and Tamuli 2019)
17.	RT-NCU02699Fw	GGAATTATGGGTTTCTCTGCG	Our Laboratory (This study)
18.	RT-NCU02699Rv	GGATGTACATGTGCTGCGTC	Our Laboratory (This study)

2.2 Methods

2.2.1 Growth condition of *N. crassa*

The *N. crassa* strains were cultured and maintained essentially as described previously (Davis and de Serres 1970). The *N. crassa* strains were cultivated on Vogel's media (VG and VG agar) (Vogel 1956, 1964) for vegetative growth, and on synthetic crossing medium (SCM) (Westergaard and Mitchell 1947) for crossing and sexual development. Germination of ascospores was performed on FGS media (Davis and de Serres 1970). The FGS agar medium was supplemented with hygromycin at a concentration of 220 µg/ml for screening of the *N. crassa* knockout mutants containing the *hph* cassette (Colot et al. 2006).

2.2.2 Growth condition of *S. cerevisiae*

The *S. cerevisiae* were grown and maintained essentially as described previously (Sherman 2002). *S. cerevisiae* cells were routinely grown on YPD media, and colonies from the plates were inoculated in YPD liquid (without agar) media and cultured for overnight. The cells that were grown till the stationary phase, then pre-cultured twice and then transferred to fresh media for further experiments.

2.2.3 Setting up crosses and harvesting ascospores

The *N. crassa* strains of opposing mating types were crossed using the previously described protocol (Westergaard and Mitchell 1947; Davis and de Serres 1970). Briefly, the agar plugs of opposite mating type were inoculated ~2 cm apart on 55 mm diameter Petri dishes containing SCM agar and incubated for 18 to 21 days at 22 °C in a BOD incubator. After 14 days, the plates are flipped over and the ascospores begin to shoot on the lid within 16-18 days. Further, the lid was washed with 1 ml sterile distilled water to harvest the ascospores. Thus, the harvested ascospores were plated on FGS agar plates and germinated by heat activation at 55−65 °C for 30−60 min and incubated at 30 °C for vegetative growth. The germinated ascospores were picked under a dissecting microscope, transferred to VG agar slants, and incubated at 30 °C.

2.2.4 Maintenance of stocks

The silica and glycerol stocks of the *N. crassa* strains were prepared for long-term preservation. The strains were first cultivated in VG agar slants for three days at 30 °C in complete darkness, followed by four days at room temperature in complete light. The silica gels (6-12 Mesh, Grade 40) are sterilized by autoclaving and kept for drying at 60 °C before use. The cryotubes (4.5 ml) were filled with the dried sterilized silica and cooled on ice for 30 min. Then, 1 ml of autoclaved skimmed milk (5 %) was added to each culture tube and vortexed vigorously. The spore suspension was aliquoted using Pasteur pipettes, and then dispensed to the cryo tube containing the pre-chilled silica gel. The tubes were vigorously vortexed for 5 min to break up any clumps. The tubes were vortexed regularly for eight to ten days and then the stocks were stored at -20 °C until further use. For making a glycerol stock, the conidia of each strain are suspended in 1 ml of sterile water and transferred to an Eppendorf tube. An

equal volume of 40 % sterile glycerol was then added, mixed thoroughly, and then kept at -80 °C until further use.

To prepare glycerol stocks of *S. cerevisiae* strains, the cells were grown in YPD and incubated overnight at 30 °C with shaking at 180 rpm, and then transferred to a fresh YPD medium. These cells were further pre-cultured twice and allowed to reach an exponential growth phase, then 600 µl of the cell culture were taken in an Eppendorf tube, and 400 µl of sterilized 87 % glycerol was added and then kept at -80 °C until further use. The cells stored as glycerol stocks are revived by streaking them into YPD agar plates.

2.2.5 Colony morphology and growth rate analysis

To study the colony morphology, the *N. crassa* strains were inoculated in 50 ml of VG media, containing various amounts of zinc (VG, LZVG, LZVG1, LZVG100, and LZVG1000), in a 250 ml flask. The cultures were incubated for three days at 30 °C followed by 4 days under light at room temperature. For radial growth, the mycelial plug of *N. crassa* strains was inoculated at the center of a 90-mm Petri dish and incubated at 30 °C. The colony growth was recorded at every three hours interval from 12 to 18 hour to determine the radial growth rate. For apical growth, the conventional race tube method was used (Ryan et al. 1943). The race tubes were partially filled with 13 ml media, and the mycelial plugs of *N. crassa* strains were inoculated at one end of the tube. The cultures were incubated at 30 °C, and the growth front was recorded every 12 h for 3 days. The distance of the hyphal growth front from the inoculation point was measured and plotted against time to determine the apical growth rate of *N. crassa*. Radial and apical growth rates were calculated as cm/h and cm/day respectively.

2.2.6 Aerial Hyphae development analysis

To determine aerial hyphae height, test tubes containing VG medium were inoculated with $1x10^6$ conidia/ml and incubated for three days in the dark at 30 °C and four days in the light at room temperature. The aerial hyphae height was measured and photographed.

2.2.7 Hyphal morphology analysis

To determine the hyphal morphology, strains were cultivated for 12–16 h at 30 °C on a thin layer of VG agar medium on glass slides. And observed under the microscope, microscope (Leica S9i Stereomiroscope, Leica Microsystems, Wetzlar, Germany).

2.2.8 Conidial cell count

For quantification of conidia production, the mycelial plugs of *N. crassa* strains were inoculated in a 55-mm Petri dish containing VG agar medium and incubated in the dark at 30 °C for three days and under light at 22 °C for four days. The conidia were scraped off from the agar surface using 1 ml sterile distilled water, the conidial suspensions were collected in Eppendorf tubes, and were briefly agitated for thorough resuspension of conidia. The conidial suspension was diluted appropriately, and the number of conidia was counted with a hemocytometer under a trinocular microscope (Nikon ECLIPSE E200, Japan).

2.2.9 Carotenoid accumulation estimation

To estimate carotenoid accumulation, conidia (~1×10^6 conidia/ml) were inoculated in sterile 90-mm Petri dishes containing VG medium supplemented with 0.2 % tween 80 (Zalokar 1954). The cultures were initially incubated at 30 °C for 48 hours in the dark and subsequently incubated at 8 °C, 22 °C, and 30 °C for additional 24 h under white light. The mycelia were extracted from these cultures,

lyophilized, and pulverized into a fine powder using mortar and pestle. Carotenoid was extracted from a 50 mg dry-weight powder sample using acetone and hexane. Briefly, 50 mg of mycelial powder and 1 ml of acetone were mixed in microcentrifuge tube and kept in a rotating mixer for 5 hours. The solution was centrifuged at 12,000 x g for 10 min at room temperature, and the supernatant was collected in a fresh microcentrifuge tube and solution was kept at -80 °C for two h. The solution was then left at room temperature for overnight with the tube lids open. In the following day, 1 ml of hexane was added to the microcentrifuge tube and carotenoid accumulation was extracted. The maximum absorbance value at 470 nm was used to calculate the total carotenoid content using the following formula:

Total carotenoid content (µg/g) = [Total absorbance × Total volume of extract (1 ml) × 10^4] / [Absorption coefficient (2500) × sample weight (g)] as previously described (Rodriguez-Amaya and Kimura 2004).

2.2.10 Circadian regulated conidiation assay

To perform the circadian-regulated conidiation assay, *N. crassa* strains were inoculated at one end of a race tube containing 13 ml of circadian agar media. The race tubes were incubated at 20 °C for 24 h under constant light and the growth front was recorded at 24. The tubes were then inverted and incubated at 20 °C, under constant darkness for 5−7 days, and the growth front was marked every day for one week under a red safe light. The period length was then determined by multiplying the distance between conidial bands by the inverse slope (https://www.fgsc.net//teaching/circad.htm). Additionally, the experiment was conducted at 30 °C to observe the effects under various temperature ranges.

2.2.11 Fertility assay

The fertility assay was performed to determine the female and male fertility of *N. crassa* mutant strains. Taking the opposite mating type strains were used as a male and a female parent in the crosses that were set using 55-mm Petri dishes containing SCM. Agar plugs of one of the two strains were firstly inoculated as a female parent and incubated at 22 °C for 7 days, then the conidial suspension of the opposite mating type was inoculated as the male parent and incubated at 22 °C for additional 7 days. After seven days following fertilization, perithecia development was observed under a microscope (Leica S9i Stereomicroscope, Leica Microsystems, Wetzlar, Germany) and photographed.

2.2.12 Visualization of Internal Septation

To visualize internal septation, the strains were grown on a thin layer of VG agar medium on glass slides and incubated for 12–16 h at 30 °C. The developing hyphae were stained for 10-15 min in the dark with calcofluor white (CFW; 0.1% in 0.05 M PBS). Further, the samples were examined with DAPI filters with an exposure time of 300–400 ms under a trinocular inverted fluorescence microscope (Olympus CKX53, Japan).

2.2.13 Fluorescence microscopy for localization

To visualize GFP expression using inverted fluorescent microscope (Olympus CKX53, Japan), sample was prepared as described previously (Raju 1982). The mycelium from the freshly grown culture was placed on a glass slide with 3:1 ethanol: acetic acid for 10 mins, and washed with distilled water. The 4′,6-diamidino-2-phenylindole dye (DAPI nucleic acid stain; D1306, Invitrogen Ltd., USA) dye was diluted to 0.1 µg/ml and the cells were suspended for 10 mins at room temperature. The cells were washed in water twice. Finally, the cells were suspended in 25% glycerol solution and squashed under a cover glass, and observed using a trinocular Inverted microscope (Olympus CKX53, Japan). A pE-

300 white CoolLED light source was used to illuminate the samples, and they were then visualized using a green fluorescence filter and DAPI filter.

2.2.14 Septation study using Field Emission Scanning Electron Microscopy (FESEM)

For visualization under FESEM, the strains were freshly grown in VG liquid medium for 18 h. The mycelium was incorporated on a thin glass slide and dried at 40 ˚C for 8 hours to 10 until dried. After drying, the glass slide was mounted onto the stub, coated with gold, and observed (10K X magnification) under a FESEM (Gemini 300, Carl Zeiss).

2.2.15 Time course quantification of conidia

For the time course conidia study, strains (~10^3 conidia) were grown on 55-mm Petri dishes containing VG agar medium and incubated at 30 °C in complete darkness. At 12-hour intervals over 72 hours, the conidia were harvested by scraping the agar surface using sterile distilled water and counted with a hemocytometer under a trinocular microscope (Nikon ECLIPSE E200, Japan).

2.2.16 Submerged culture conidiation assay

For conidiation in submerged cultures, conidial suspensions (10^6 conidia/ml) were inoculated in VG liquid medium supplemented with or without 2% peptone (w/v) in 250 ml flasks, and incubated at 30 °C with shaking at 180 rpm for 16 h. To observe the development of conidiophores, aliquots of these cultures were examined under a microscope (20X magnification; Nikon Eclipse Ti-S inverted microscope, model DS-Fi2-U3, Japan).

2.2.17 Endoplasmic reticulum (ER) stress assay

For ER stress assay, dithiothreitol (DTT) was used as the ER stress-inducing agent. The ability of the *N. crassa* strains to produce aerial hyphae under different concentrations of DTT was examined.

Conidial suspension (10^6 conidia/ml) was inoculated in sterile test tubes containing VG liquid supplemented with different concentrations of DTT (0.5 mM, 1 mM, and 2 mM) and incubated at 30 °C for three days in the dark, followed by two days under the light, and the aerial hyphae height of the strains were measured.

2.2.18 Cellulose degradation assay

For degradation of cellulose under different concentrations of zinc, ~10^6 conidia/ml conidial suspension was inoculated in a sterile 250 ml flask containing 50 ml of 1X Vogel's Medium with 2% microcrystalline cellulose (VC) supplemented with different concentrations of zinc (LZVC1; 1 µM $ZnSO_4$, LZVC100; 100 µM $ZnSO_4$, LZVC1000; 1000 µM $ZnSO_4$) and incubated at 30 °C with shaking at 180 rpm for seven days in complete darkness and photographed. The ability of the strains for cellulose breakdown was assessed by their growth on microcrystalline cellulose.

2.2.19 Glucose concentration estimation by DNSA

The glucose released in the VC medium (as discussed in section 2.2.17) under varying zinc concentrations was measured as described previously (Miller 1959; Shao and Lin 2018). The concentrations of reducing sugar in samples were measured using the 3, 5-Dinitrosalicylic acid (DNSA) reagent and D-glucose as a reference. D-glucose solutions of varying concentrations were prepared to use as standard. In separate test tubes, 3 ml of the unknown sample and standard were collected, where 3 ml of DNSA reagent was added and the test tube was kept for 5 min in a boiling water bath (99-100 °C). The test tubes were allowed to cool down and the absorbance is recorded at 575 nm. The standard curve of absorbance vs. concentration of D-glucose with known concentration was plotted, which was used to determine the glucose concentration in the sample.

2.2.20 Estimation of protein concentration using Bradford Method

The proteins released in the VC medium (as discussed in section 2.2.17) under different zinc concentrations were measured as described previously (Bradford 1976). The concentrations of protein present in the sample are measured using Bovine serum albumin (BSA) as standard and Bradford reagent. BSA solutions of varying concentrations were prepared and use as the standard. In separate test tubes, 20 µl of the unknown sample and standard were collected and 180 µl of Bradford reagent was added, the test tube was then kept for 5−10 min in complete darkness and the absorbance was recorded at 595 nm. The standard curve of absorbance vs. concentration of BSA with known concentration was plotted, then this was used to determine the protein concentration in the sample.

2.2.21 Stress assay

2.2.21.1 Temperature sensitivity

For temperature sensitivity assay, ~1 cm diameter mycelial agar plugs from freshly grown strains were inoculated at the center of 90 mm Petri dishes containing VG agar and incubated at three different temperatures of 20, 30, and 40 °C. The colony diameter was measured at every 3 h interval starting from 12 to 24 h and the growth rates were calculated. The growth rate at 30 °C was regarded as 100%, the average percentage (%) of growth rates at 20 and 40 °C were calculated.

2.2.21.2 pH stress assay

For the pH stress assay, freshly harvested conidial (10^6 conidia/ml) suspension from 5-day-old cultures were inoculated in sterile test tubes with VG liquid with pH of 3.8, 5.8, and 7.8. The cultures were incubated for three days in the dark at 30 °C and subsequently for four days in the light at room temperature. The aerial hyphae heights were measured and photographed. Based on the growth rate at

pH 5.8 (control), which was regarded as 100%, the average percentage (%) of growth rates at pH 3.8 and 7.8 were calculated.

2.2.21.3 Osmotic stress assay

For osmotic stress assay, ~1 cm diameter mycelial agar plugs from freshly grown strains were inoculated at the center of 90 mm Petri dishes containing VG agar medium supplemented with hyperosmotic agents NaCl, KCl, and sorbitol at varying concentrations of 0 (control), 0.5, 1, and 1.5 M. Then the cultures were and incubated at 30 °C in complete darkness, the colony diameter was measured at every 3 h interval starting from 12 to 24 h, and the growth rates were calculated. Based on the growth rate in the control condition, which was considered as 100%, the average percentage (%) of growth rates at different concentrations of the salts were calculated

2.2.21.4 Azole stress assay

For the azole stress assay, ~1 cm diameter mycelial agar plugs from freshly grown strains were inoculated at the center of 90 mm Petri dishes containing VG agar medium supplemented with the azole drugs fluconazole and itraconazole at concentrations of 0 (control) and 0.5 mg/ml. The cultures were incubated at 30 °C in complete darkness, the colony diameter was measured at every 3 h interval starting from 12 to 24 h, and the average growth rates were calculated. The sensitivity of the strains to the drugs was determined by the following formula (Zhou et al. 2022):

$$\text{The relative inhibitory rates} = \left(1 - \frac{Diameter\ of\ the\ colony\ plate\ with\ drug}{Growth\ time} \Big/ \frac{Diameter\ of\ the\ colony\ plate\ without\ drug}{Growth\ time}\right) * 100\%.$$

2.2.22 Preparation of ultracompetent bacterial cells

The preparation of ultracompetent cells for cloning was essentially prepared as described previously (Inoue et al. 1990). A single colony of *E. coli* DH5α was picked from a fresh streaked LB agar plate inoculated into 10 ml of LB broth, and incubated at 37 °C with shaking at 180 rpm overnight. Then 1% of the overnight culture was inoculated in 50 ml of fresh LB broth and incubated at 37 °C with shaking at 180 rpm till it reached the log phase. The absorbance OD_{600} was measured, and once the OD_{600} reached 0.450−0.600, the culture was chilled on ice. The cells were harvested by centrifuging at 3000 x g for 10 min at 4 °C. The supernatant/media was discarded and the cells pellet was resuspended in 16 ml of ice-cold Inoue transformation buffer (10 mM PIPES pH 6.7, 15 mM $CaCl_2$, 250 mM KCl, 55 mM $MnCl_2$; Inoue et al. 1990) and kept on ice for 10 min. The centrifugation process was repeated and the cells were resuspended in 4 ml of ice-cold Inoue transformation buffer containing 7% DMSO. The cell suspension was distributed into 100 µl aliquots, frozen in liquid nitrogen, and stored at -80 °C for further use.

2.2.23 Small-scale isolation of plasmid DNA from bacterial culture

The isolation of plasmid DNA in small-scale or mini-preparation was performed by the alkaline lysis method (Sambrook and Russell 2001). Overnight bacterial culture ~5 ml, was briefly centrifuged in a fresh 1.5 ml microcentrifuge tube for 60 sec at 12,000 x g at 4 °C and the supernatant was discarded. The pellets were suspended in 100 µl alkaline lysis solution I with vigorous vortexing. Then 200 µl of freshly made alkaline lysis solution II was added to the mixture and immediately mixed by inverting the tube. After that, 150 µl of Alkaline Lysis Solution III was added, mixed by inverting the tube, and incubated on ice for 5 min. The tube was centrifuged at 12,000 x g for 10 min at 4 °C. The supernatant was transferred to fresh microfuge tubes and an equal volume of phenol: chloroform: isoamyl alcohol

mixture (25:24:1) was added, and centrifuged for 10 min at 12,000 x g at 4 °C. The supernatant was carefully transferred to a fresh 1.5 ml microcentrifuge tube and 1 ml of absolute ethanol was added to precipitate the plasmid DNA. The tube was gently inverted for few times and the plasmid DNA was pelleted by centrifugation at 12,000 x g for 10 min at 4 °C. The supernatant was discarded and the pellet was washed with 70% ethanol by centrifuging at 12,000 x g for 5 min at 4 °C. The pellet was air-dried at room temperature and the pellet was dissolved in 20 µl of 1X TE buffer (pH 8.0) and stored at 4 °C.

2.2.24 Digestion of plasmid DNA with restriction endonuclease

The plasmid DNA was subjected to restriction digestion following the manufacturer's guidelines for the particular restriction endonucleases used (New England Biolabs, USA). For restriction digestion, 1 µl (10 units) of restriction endonuclease was added in a final reaction volume of 50 µl containing an aliquot of ~1 µg of plasmid DNA, and the reaction was performed at the conditions recommended by the manufacturer. The digested DNA fragments was analyzed using agarose gel electrophoresis.

2.2.25 Ligation of digested vectors and inserts

The ligation reactions were performed using the Quick LigationTM Kit (Cat. no. M2200S, New England Biolabs, USA). A 20 µl ligation reaction mixture was prepared by mixing 50 ng of linearized DNA vector, a 3-fold molar excess of insert DNA, 10 µl of 2X ligation buffer, 1 µl of quick T4 DNA ligase enzyme, and nuclease-free water to make up the remaining volume. The ligation reaction was carried out in a circulating water bath (MRC Scientific Instruments, Israel) for 15–30 min at 25 °C.

2.2.26 Transformation of ultracompetent *E. coli* cells by heat shock

The competent cells were either freshly prepared or taken from the -80 °C freezer and incubated on ice for thawing. A sample of ligated DNA ~100 ng was added to the competent cell and gently mixed, then incubated on ice for 20−30 min. The cells were then subjected to heat shock at 42 °C in a water bath for 90 sec and immediately placed on ice for 10–20 seconds. Further, the cells were recovered by adding 600 µl of pre-warmed SOC medium and incubating for 1 hour at 37 °C and 180 rpm. Then, four LB agar plates (90 mm) supplemented with 100 µg/ml of ampicillin were plated with 150−200 µl of each cell culture, and incubated at 37 °C overnight.

2.2.27 Transformation of the *N. crassa* strain by electroporation

The protocol for the transformation of the *N. crassa* strain by electroporation was based on the method described previously (Margolin et al. 1997; Bhat et al. 2004). The recipient strain was grown for 7 days at 30 °C in 250 ml conical flasks containing VG agar medium. The conidia were harvested in sterile water and isolated from the mycelium by running the suspension through cheesecloth attached to a 250 ml conical flask (the mouth of the flask had been wrapped in cheesecloth and previously autoclaved to ensure its sterilization). The conidial suspension was collected in a falcon tube and centrifuged at 1500 rpm for 5 min at 4 °C. The conidial mass was washed twice with 25 ml of sterile water and resuspended in ice-cold 1 M sorbitol at a concentration of $3x10^9$ spores/ml. Then 40 µl of the conidial suspension was mixed with the plasmid construct and placed in a pre-chilled 2 mm sterile electroporation cuvette (Biorad Laboratories, Hercules, CA). The electroporation of conidia was done in the BioRad gene pulsar apparatus (Biorad Laboratories, Hercules, CA). The electroporation conditions were 1.5 kV (voltage gradient), 25 µF (capacitance), and 600 Ω (resistance). The time constant varies from 13 to 15 ms. Immediately following the electric pulse, 1 ml of chilled 1 M sorbitol

was added to the cuvette and incubated on ice for 3−5 min. The transformant conidial suspension was mixed with top agar and plated on an FGS agar plate and incubated at 30 °C. After 2-3 days, about 5-10 transformants were usually obtained per plate. To eliminate the possibility of any contamination, a control transformation was done with conidial suspension without adding a plasmid construct.

2.2.28 Isolation of genomic DNA of *N. crassa*

For isolation of genomic DNA, the *N. crassa* strains were grown in VG liquid at 30 °C at 180 rpm for three days. Then the mycelial mass was harvested, cut into small size, and lyophilized. The dried mycelia mass was pulverized into fine powder. In fresh 2 ml microcentrifuge tubes, ~150 mg mycelial powder was taken and 1 ml of DNA lysis buffer (10 mM Tris-HCl at pH 7.5, 0.5 M NaCl, 10 mM EDTA, 1% SDS, and 1% CTAB) was added and mixed thoroughly using toothpick or pipette tips. The microcentrifuge tubes were incubated at 65 °C for 45 min, followed by centrifugation at 12,000 rpm for 10 min. The supernatant was transferred to a fresh microcentrifuge tube and 600 µl of phenol: chloroform: isoamyl alcohol mixture (25:24:1) was added. The microcentrifuge tubes were kept in a rotating mixer for 15−20 min and centrifuged at 12,000 x g for 10 min. The aqueous phase was carefully pipetted to a fresh tube and 600 µl of chloroform was added to remove the last traces of phenol and then centrifuged at 12,000 x g for 10 min. The aqueous phase was carefully pipetted to a fresh 1.5-ml microcentrifuge tube. To the aqueous phase, 1 ml of pre-chilled absolute alcohol was added the precipitate the DNA and was mixed gently by inverting for few times and allowed to stand for 30 min. To pellet down the DNA, the tubes were then centrifuged at 12,000 x g for 10 min. The supernatant was discarded and the pellet was washed with 70% ethanol by centrifuging at 12,000 x g for 10 min. To remove the traces of ethanol, the tubes were air-dried to at room temperature for 20−30 min. Then 30 µl of 1 X TE buffer (pH 8.0) was added to dissolve the pellets and stored at 4 °C. All the centrifugation was carried out at room temperature.

2.2.29 Isolation RNA from *N. crassa* strain

The protocol for the isolation of RNA from *N. crassa* strains was based on a previously described method (https://www.fgsc.net//fgn37/sokol.html). The conidia of the strain were grown in sterile 250 ml flasks containing 50 ml VG medium at 30°C with shaking at 180 rpm for 12 to 16 h. The mycelial mass was harvested, cut into thin pieces, and collected in a 2 ml microcentrifuge tube, and the masses were immediately frozen using liquid nitrogen. The frozen tissue was pulverized to a fine powder using a sterilized glass rod and 400 µl of TRIzol reagent (Invitrogen, CA) was added. Subsequently. 750 µl lysis buffer (0.6 M NaCl, 10 mM EDTA, 100 mM Tris HCl, pH 8.0, 4% SDS) and 750 µl of phenol: chloroform: isoamyl alcohol (PCI; 25:24:1) were added. The tubes were kept on rotating mixer for 20 min, and centrifuged at 10,000 x g, for 10 min. In a fresh 2 ml microcentrifuge tube, the upper aqueous phase was collected and 750 µl of phenol: chloroform: isoamyl alcohol mixture (25:24:1) was added. The solutions were briefly vortexed and centrifuged at 10,000 x g for 10 min. Further, the aqueous phase was collected in a fresh 2 ml microcentrifuge tube and 750 µl of 8 M LiCl was added. The mixture was stored at 4 °C for 20−24 hours. The following day the tubes were briefly vortexed and centrifuged at 10,000 x g for 10 min. The supernatant was discarded and the pellet was suspended in 300 µl double distilled DEPC treated water, 30 µl of 3 M Na-acetate (pH 5.2), and 750 µl of absolute ethanol, and mixed by inverting the tubes gently. The tubes were stored at -80 °C for 1 h or -20 °C for 2 h and then centrifuged at 10,000 x g, for 10 min. The precipitate (pellet) was washed with 70% ethanol by centrifuging at 10,000 x g, for 10 min. The pellets were dried for 10−30 min at room temperature and finally dissolved in 20−30 µl DEPC treated water. The RNA was stored at -80 °C. All the centrifugation was carried out at room temperature.

2.2.30 Quantification of nucleic acids

For quantification of nucleic acids, the OD the samples were measured at 260 nm using a NanoPhotometer® (IMPLEN, Germany). The following empirical relationships were used to calculate the concentrations: an OD_{260} of 1 corresponds to ~50 µg/ml of double-stranded DNA, 40 µg/ml of single-stranded DNA and RNA, and ~20 µg/ml of single-stranded oligonucleotides. By calculating the OD_{260}/OD_{280} ratio, the purity of nucleic acids was determined. Pure DNA and RNA preparations have OD_{260}/OD_{280} ratios of 1.8 and 2.0, respectively.

2.2.31 Polymerase chain reaction (PCR)

The routine polymerase chain reaction (PCR) reaction was performed using Taq DNA polymerase (Cat. No. M0273S, New England Biolabs, USA), which is isolated from *Thermus aquaticus* (Chien et al. 1976; Saiki et al. 1988), or Dynazyme II DNA polymerase (Cat. No. F-501 250U, Thermo Scientific), isolated from *Thermus brockianus*. Phusion® High-Fidelity DNA Polymerase (Cat. no. M0530S, New England Biolabs, USA) was used for cloning since it has both 3'→5' exonuclease proofreading activity and 5'→3' polymerase activity. The novel Pyrococcus-like enzyme is combined with a processivity-enhancing domain, increasing fidelity and speed with an error rate that is > 50 times lower than Taq DNA polymerase. The PCR conditions differ depending on the size of the PCR product and the annealing temperature of the primers. All PCRs were carried out following the manufacturer's instructions using a thermal cycler (Arktik Thermal Cycler, Thermo Fisher Scientific, USA).

2.2.32 Reverse transcription PCR for cDNA synthesis

For reverse transcription PCR (RT-PCR) based gene expression study, the RNA extracted from the mycelial mass (discussed in the section 2.2.27) was used for cDNA synthesis using Verso cDNA Synthesis Kit (Cat. no. AB-1453/A, Thermo Fisher Scientific, USA). Following this, 2 µg of total RNA was used as a template for a 20 µl reaction. The cDNA synthesis process was performed only for a single cycle under the following conditions: 42 °C for 30 minutes, followed by 95 °C for 2 minutes. To examine the expression of the target gene, the synthesized cDNA templates were subjected to quantitative real-time PCR cycling with gene-specific primers.

2.2.33 Quantitative Real-time PCR (qRT-PCR)

The cDNA synthesized from the total RNA (discussed in the section 2.2.30) was further used to perform Quantitative Real-Time PCR (qRT PCR) analysis. The qRT-PCR was carried out on a real-time PCR machine (ABI 7500 Fast, Applied Biosystems, USA and AriaMx Real-Time PCR System, Agilent, India). In general, RT-PCR reaction mix consist of 4.5 µl of cDNA (~100 ng), 0.25 µl of forward primer, 0.25 µl of reverse primer, and 5 µl of SYBR® Select Master Mix (Cat. No. 4472903, Life Technologies, USA) in a 10 µl reaction mixture. For the negative control, sterile DEPC-treated distilled water was used, instead of the cDNA as the template. The PCR parameter used was as follows: 95 °C for 10 min followed by 40 cycles of 95 °C for 15 s and 60 °C for 1 min. The fold change in the relative expression of the target genes was determined using the $2^{-\Delta\Delta C_T}$ approach (Livak and Schmittgen 2001), *β-tubulin* gene expression level as the reference control, and the expression in the wild type as the calibrator.

2.2.34 Agarose gel electrophoresis

The DNA samples were loaded with 1 µl of 6X DNA loading dye (0.25% bromophenol blue, 0.25% xylene cyanol, 30% glycerol). Depending on the size of the fragments to be resolved, the samples were loaded on 0.7% −1.5% agarose gels cast on 1X TAE containing 0.5 g/ml ethidium bromide (EtBr). Electrophoresis was performed at 80−100 V in 1X TAE buffer. To estimate DNA fragment sizes, standard DNA size markers (1 kb DNA ladder; cat No. NEB #B7025, NEB; Ipswich, MA, USA) were used alongside the sample. The EtBr-stained DNA samples were visualized using a gel doc (Image 4.1, Bio-Rad, USA; or Mega Bio print, Vilbert Lormat, France). Likewise, the RNA samples were resolved in a 1.5% agarose gel with 2.2 M formaldehyde, 1X MOPS buffer, and 0.5 g/ml EtBr.

2.2.35 Preparation of yeast-competent cells by lithium acetate (LiAc) method

For yeast-competent cell preparation, the yeast cells were grown in 10 ml YPD to stationary phase as previously described (2.2.2; Altherr et al. 1983). From this culture, 0.1 % was inoculated into a fresh 50 ml YPD and incubated at 30 °C with shaking at 180 rpm. The absorbance OD_{600} was measured, until it reaches OD_{600} = 0.4 − 0.6. The cells were harvested by centrifuging at 1,500 g for 5 min at 22 °C. The supernatant was discarded and cell pellet washed twice with 15 ml of 1X TE buffer by centrifuging at 1,500 g for 5 min. Then, the pellet was resuspended with 5 ml of 0.1 M LiAc, and the cell suspension was incubated at 22 °C for 30 min. The competent cells were harvested by centrifugation at 1,500 g for 5 min. The supernatant was discarded and the cells were resuspended in 5 ml of 0.1 M LiAc and 15% glycerol. The cell suspension was distributed into 200 µl aliquots and stored at -80 °C for further use.

2.2.36 Yeast transformation by lithium acetate (LiAc) method

Yeast transformation was performed using the competent cells prepared (as described above 2.2.33) by the lithium acetate (LiAc) method (Altherr et al. 1983; Gietz and Akio 1988). In a microcentrifuge tube, 200 µl of yeast-competent cells was taken from -80 °C and thawed on ice. Then, 360 µl of transformation mix [250 µl of 50% PEG4000, 36 µl of 1 M LiAc, 50 µl of 2 mg/ml denatured herring sperm DNA and ~100 ng of plasmid DNA (or PCR product), final volume adjusted by sterile distilled water] was added to the yeast-competent cells. The cell and the transformation mixture were mixed gently by pipetting then incubated for 60−120 min at 30 °C with shaking. This was followed by giving heat shock at 42 °C for 30 min in a water bath, and then the cells were incubated on ice for 1−2 min. The cells were then harvested by centrifugation at 3000 rpm for 2 min. The supernatant was discarded and cell pellet was finally suspended in 200 µl of YPD liquid and the complete suspension was plated on selective plates. After incubation at 30 °C for 2−3 days, the transformant colonies were visible on the plates.

2.2.37 Isolation of yeast genomic DNA (gDNA)

For isolation of yeast genomic DNA (gDNA), the cells were grown on YPD media, and the freshly grown colonies from the plates were inoculated in YPD agar media and cultured overnight. Subsequently, cells from a freshly streaked plate were picked and mixed with 50 µl of 0.2% sodium dodecyl sulphate (SDS) in 0.5 ml microcentrifuge tube. The mixture was then vigorously vortexed for 15−30 s and incubated at 70 °C for 5−10 min. The cells were then centrifuged at 12,000 x g for 1 min. The supernatant containing the genomic DNA was transferred to a new tube and used for PCR or stored at -20 °C for further use.

2.2.38 Yeast spot assay

Spot assay for yeast strains, was performed based on a previously described method (Zubko and Zubko 2014). The cells were grown on YPD agar media, and the freshly grown colonies from the plates were inoculated in YPD liquid media and cultured at 30 °C with shaking at 180 rpm overnight. Then the cells were grown till the stationary phase and then transferred to fresh media and grown at 30 °C with shaking at 180 rpm until OD_{600} = 1. Then, serial dilutions of each strain (four to six 10-fold dilutions) were plated (2 µl) onto YPD agar plates. The YPD agar plates were incubated at 30 °C for 24 −48 h to visualize cell growth.

2.2.39 Statistical Analysis

In this study, every quantitative experiment was run at least three times (n = 3). Statistical analysis was performed using one-way or two-way analysis of variance (ANOVA) (with multiple comparisons) and Tukey's post hoc analysis (Nanda et al. 2021) using GraphPad Prism 8.2.4 (https://www.graphpad.com/). The error bar indicates mean ± standard deviation. Stars (*) indicate significantly different values at significant, $p<0.05$ (one stars), very significant, $P < 0.01$ (two stars), and extremely significant, $P < 0.001$ (three stars).

2.3 Databases and software programs used in this study

1. **Basic Local Alignment Search Tool (BLAST):** The BLAST program (Altschul et al. 1990, 1997) was used to compare nucleotide or protein sequences to the reference sequence databases. This is available at http://blast.ncbi.nlm.nih.gov/Blast.cgi.
2. **Clustal X:** The Clustal X software (Thompson et al. 1997) was used for aligning multiple sequences of DNA and protein sequences. This is available online at http://www.clustal.org/clustal2/.

3. **Conserved Domain Database (CDD):** The CDD online program (Yang et al. 2020) was used to identify conserved domains in the proteins. This is available online at https://www.ncbi.nlm.nih.gov/cdd/.
4. **Dali Webserver:** The Dali protein structure comparison server (Holm 2022) is a network service for comparing protein structures in 3D. This is available online at http://ekhidna2.biocenter.helsinki.fi/dali/.
5. **ExPasy Translate tool:** The ExPasy Translate tool was used for translating DNA/RNA sequences to protein sequences This is available online at https://web.expasy.org/translate/.
6. **GalaxyWEB (GalaxyRefine):** The GalaxyWEB (Ko et al. 2012) web server was used for protein structure prediction and refinement. This is available online at https://galaxy.seoklab.org/cgi-bin/submit.cgi?type=REFINE.
7. **GeneDoc:** The GeneDoc software (Nicholas et al. 1997) was used for editing and annotating multiple sequence alignments. This is available online at http://nrbsc.org/gfx/genedoc.
8. **ImageJ/Fiji**: The ImageJ/Fiji (Schindelin et al. 2012) is an open-source platform for biological-image analysis and processing. This is available online at https://imagej.net/software/fiji/.
9. **Interpro:** The Interpro web server (Paysan-Lafosse et al. 2023) enables protein functional analysis by categorizing proteins into families, predicting domains, and identifying key locations. This is available online at https://www.ebi.ac.uk/interpro/.
10. **I-TASSER:** The Iterative Threading ASSEmbly Refinement (I-TASSER) is an online approach to protein structure prediction and structure-based function identification (Yang and Zhang 2015; Zheng et al. 2021). This is available online at https://zhanggroup.org/I-TASSER/.

11. **MatInspector:** The MatInspector software (Cartharius et al. 2005) enables the identification of transcription factor binding site in a DNA sequence by utilizing a large library of matrix. This is available online at https://www.genomatix.de/matinspector/.

12. **MEGA11:** The Molecular Evolutionary Genetics Analysis v11 (MEGA11) software (Tamura et al. 2021) was used for constructing phylogenetic trees and sequence alignment. This is available online at http://www.megasoftware.net/.

13. ***N. crassa* genome databases**: Genome resource for Neurospora is available at http://fungidb.org. The web site for Fungal Genetics Stock Center is http://www.fgsc.net/.

14. **NCBI/EMBL:** The online servers of the National Center for Biotechnology Information (NCBI) and European Molecular Biology Laboratory (EMBL)) were used to retrieve the primary sequence of proteins or nucleic acid. These are available online, NCBI at http://www.ncbi.nlm.nih.gov/, and EMBL at http://embl.org/.

15. **PyMol:** The PyMOL v2.5 software enables visualization of the proteins predicted three-dimensional structures. This is available online at https://pymol.org/2.

16. **STRING:** The Search Tool for The Retrieval of Interacting Genes/Proteins (STRING) version 10.0 (Szklarczyk et al. 2019) is an online tool used to predict functional protein association networks. This is available online at https://string-db.org/

17. **Site for reverse-complement:** The sequence manipulation suite (SMS) software was used for analyzing and formatting DNA and protein sequences as well as to convert a DNA sequence into reverse-complement sequence. This is available online at http://www.bioinformatics.org/sms/index.html.

18. **Structural Analysis and Verification Server (SAVES):** SAVES is a web server used for protein structure analysis and validation. The PROCHECK, ERRAT, and VERIFY 3D

programs from this server were used for protein structure validation. This is available online at https://saves.mbi.ucla.edu/.

19. **SWISS-MODEL:** SWISS-MODEL web server (Bienert et al. 2017) is an online tool for protein structure homology-modelling. This is available online at https://swissmodel.expasy.org/.

20. **DeepTMHMM:** The Deep learning TransMembrane prediction using Hidden Markov Models (DeepTMHMM) software (Hallgren et al. 2022) was used for the prediction of the membrane topology of transmembrane proteins. This is available online at https://dtu.biolib.com/DeepTMHMM.

21. **UCSF ChimeraX:** UCSF ChimeraX program (Pettersen et al. 2004) used for the interactive visualization and analysis of molecular structures (protein structures). This is available online at https://www.cgl.ucsf.edu/chimera/.

22. **UniProt:** UniProt sever was used to retrieve the primary sequence of proteins. This is available online at https://www.uniprot.org

23. **VMD:** Visual Molecular Dynamics v1.9.4 (VMD) is a molecular visualization program for displaying and analyzing large biomolecular systems using 3-D graphics and built-in scripting. This is available online at https://www.ks.uiuc.edu/Research/vmd/.

3

INVESTIGATING THE CELLULAR ROLES OF THE CDF FAMILY ZINC TRANSPORTERS *ZRC-1* AND *MSC-2* IN *NEUROSPORA CRASSA*

3.1 Introduction

The CDF family of zinc transporters plays a role in zinc homeostasis in a variety of taxa, ranging from prokaryotes to eukaryotes. The CDF family of zinc transporters are characterized by their ability to transport metal ions, including zinc, from the cytoplasm to the lumen of intracellular organelles or outside the cell (Paulsen and Saier 1997; Gaither and Eide 2001a; Nies 2003; Kambe et al. 2004; Cousins et al. 2006). The CDF family transports zinc inside the cell via a Zn^{2+}/ K^{+} and Zn^{2+}/ H^{+} antiport mechanism (Guffanti et al. 2002; Chao and Fu 2004a). The majority of CDF family members of zinc transporters are predicted to have six or more transmembrane domains (TMDs), a C-terminal domain (CTD) having histidine-rich motifs that protrude into the cytoplasm (Kolaj-Robin et al. 2015). This histidine-rich motif is typically in the cytoplasmic loop between TMD 4 and TMD 5 with the sequence $(HX)_n$, where X=G/C and n = 3−6 (Paulsen and Saier 1997). The histidine-rich motif possibly binds to zinc ion and involves in functional and regulatory roles (Paulsen and Saier 1997; Harris 2002; Fukue et al. 2018).

The CDF proteins closely regulate the export and import of zinc into the cellular compartments to maintain cellular functions and prevent zinc toxicity. In *S. cerevisiae*, the Msc2p and Zrg17p transmembrane proteins form a heteromeric complex in the ER and mediate zinc transport into the ER under low zinc conditions (Ellis et al. 2005). Furthermore, the ZAP-1 transcription factor activates the plasma membrane-based high-affinity zinc transporters, causing a sudden influx of zinc (Zhao and Eide 1997). Zrc1p imports the extra zinc into vacuoles for storage and thereby serves as a suppressor of zinc toxicity (Miyabe et al. 2001).

In *N. crassa* the regulations of zinc transporters and maintenance of zinc homeostasis are still not clear. Previous studies showed the presence of nine putative CDF family proteins in *N. crassa*

(Kiranmayi and Mohan 2006; Montanini et al. 2007). Excluding ZRG-17, cellular roles of the remaining CDF proteins are remained unknown. The *N. crassa* Δ*zrg-17* mutant showed several zinc suppressible phenotypes such as slow growth rate, short aerial hyphae, and defects in asexual sporulation (Tiwari et al. 2018). In addition, the expression of *zrg-17* was upregulated under low zinc, and the ZRG-17 protein is crucial for ER stress tolerance and cellulose degradation under low zinc conditions in *N. crassa* (Tiwari et al. 2018).

We obtained the knockout mutants for two CDF zinc transporter genes NCU03145 and NCU07262, which are the *S. cerevisiae* orthologs of the Zrc1p and Msc2p of, respectively, from the FGSC (Table 2.2). In this study, I investigated the role of ZRC-1 and MSC-2 in vegetative growth, asexual and sexual developments in of *N. crassa*.

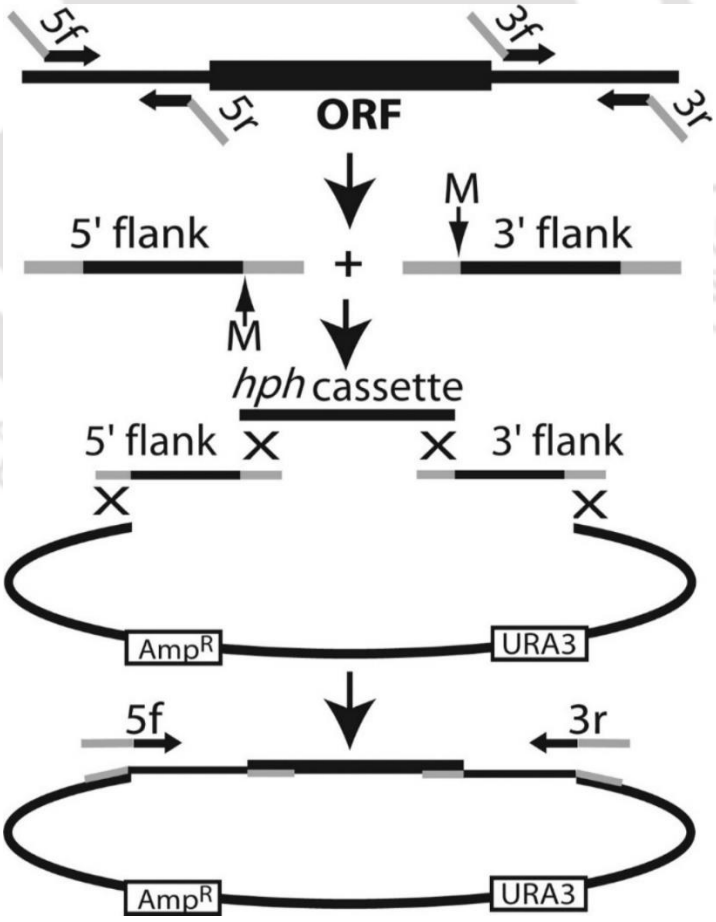

Figure 3.1 Schematic diagram of generating knockout mutants in *N. crassa*. The 5′ and 3′ flank fragments of the target genes were PCR amplified from the wild type using the primer pairs 5f and 5r and 3f and 3r, respectively. The 5′ tails of primer 5r and 3f contain MmeI sites (M) and are homologous to the *hph* cassette that confers resistance to the antibiotic hygromycin B, whereas, the 5′ tails of primers 5f and 3r are homologous to the yeast shuttle vector pRS426 (Christianson et al. 1992; Colot et al. 2006). The two flanks (5′ and 3′ flanks) along with the *hph* cassette and PRS426 vector are co-transformed into yeast. Homologous recombination produces the formation of a circular construct, and primers 5f and 3r are used to amplify the final linear deletion cassette from the yeast DNA. The *hph* is transcribed in the antisense direction relative to the transcription of the target gene. Adapted from Colot *et al.* (2006).

3.2. Results

3.2.1 Identification of the *N. crassa* ZRC-1 and MSC-2 homologs

3.2.1.1 Sequence analysis revealed that the NCU03145 and NCU07262 genes encode the zinc resistance-conferring (ZRC-1) and meiotic sister-chromatid recombination (MSC-2) proteins, respectively, in *N. crassa*

The NCU03145 and NCU07262 genes contain an open reading frame (ORF) of 1,566 and 1,812 base pairs, respectively. Sequence analysis of NCU03145 and NCU07262 was performed using the sequences retrieved from the Fungal & Oomycete informatics resources (https://fungidb.org/fungidb). The NCU03145 gene is genetically mapped in the supercontig one, from the nucleotide position 4719127 – 4721704 (+ strand), located at the right arm of linkage group one (LG IR; Figure 3.2 A). The NCU03145 ORF contains three exons and two introns (Figure 3.3 A). The NCU07262 gene is genetically mapped in the supercontig four, from the nucleotide position 4586141 − 4589012 (-

strand), and located at the right arm of linkage group four (LG IVR; Figure 3.2 B). The NCU07262 ORF contains two exons and one intron (Figure 3.3 B).

The NCU03145 (*trm-25*; GenBank accession no. XP_964194.1; https://www.ncbi.nlm.nih.gov/protein/XP_964194.1/) and NCU07262 (*trm-29*; GenBank accession no. XP_962116.1; https://www.ncbi.nlm.nih.gov/protein/XP_962116.1/) was used as the query sequence in a BLASTP analysis (Altschul et al. 1990, 1997) to identify its homologues. Based on the E value, percent identities, and gaps, the proteins were chosen and aligned accordingly using CLUSTAL X (Thompson et al. 1997) and GeneDoc (Nicholas et al. 1997) for visualization of the aligned proteins (Figure 3.4). The sequence analysis revealed that the NCU03145 and NCU07262 encode a cation efflux protein, showing sequences similar to members of the CDF family of zinc transporters, zinc resistance-conferring (Zrc1p) and meiotic sister chromatid (Msc2p) of *S. cerevisiae*, respectively (Figure 3.4). Further, the various conserved domains present within ZRC-1 and MSC-2 proteins were found using the InterPro webserver (https://www.ebi.ac.uk/interpro/) and both ZRC-1 and MSC-2 proteins contain cation efflux transmembrane domains and cation efflux C-terminal domains that are found in almost every member of the CDF family of zinc transporters (Figure 3.5 A, B; Persans *et al.* 2001; Kolaj-Robin *et al.* 2015). Moreover, the transmembrane helices present within were predicted using the DeepTMHMM (Hallgren *et al.* 2022; https://dtu.biolib.com/DeepTMHMM). The transmembrane prediction revealed that both ZRC-1 and MSC-2 of *N. crassa* contain six transmembrane domains (TMD I - TMD VI) and both ZRC-1 and MSC-2 possess a histidine-rich region, suggesting that these regions within the membrane may be involved in zinc transport or sensing the level of zinc, and it may cause the domains to change conformation once it reaches a certain level of zinc inside the membrane-enveloped organelle (Figure 3.5; Table 3.1). Additionally, phylogenetic analysis of ZRC-1 and MSC-2 was performed using MEGA11 software (Rzhetsky and Nei 1993;

Tamura et al. 2021), using the minimum evolution method, the aligned homologous sequences were then utilized to construct a phylogenetic tree. In a phylogenetic analysis, the ZRC-1 and MSC-2 protein was found to be closely grouped among Sordariomycetes (Figure 3.6). Taken together, the NCU03145 and NCU07262 genes encode the *N. crassa* ZRC-1 and MSC-2 proteins, which are the *S. cerevisiae* orthologs of Zrc1p and Msc2p, respectively.

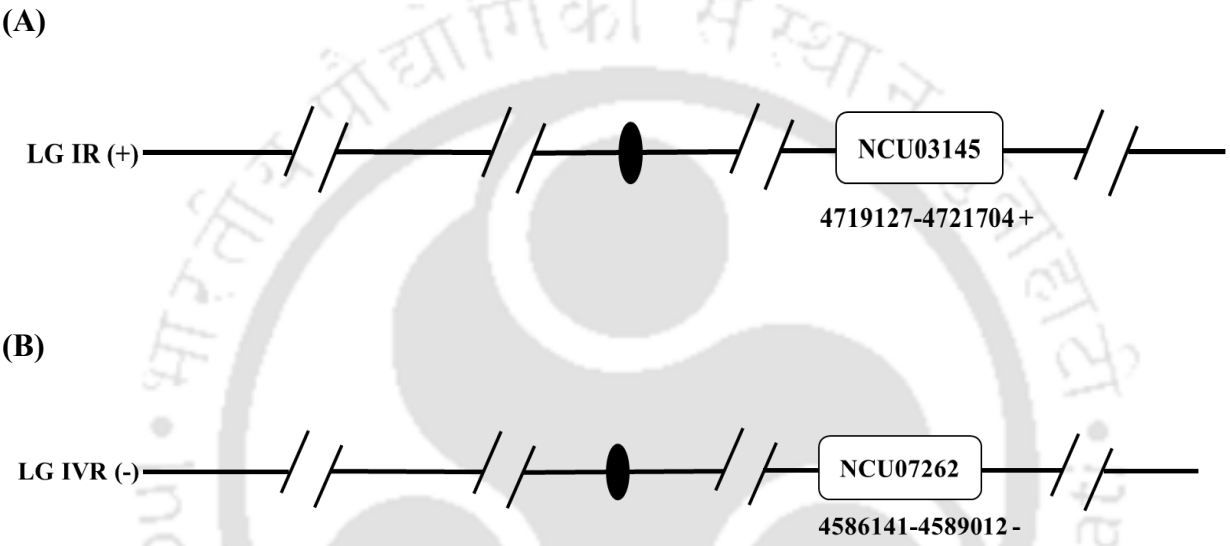

Figure 3.2 Genomic organization of NCU03145 and NCU07262 in *N. crassa*. (A) Position of the NCU03145 gene on the LG IR. The NCU03145 gene is localized at the right arm of supercontigs one from position 4719127 – 4721704 (+ strand). **(B)** Position of the NCU07262 gene on LG IVR. The NCU07262 gene is localized at the right arm of supercontig four from position 4586141 – 4589012 (- strand). The solid black circle indicates the centromere in each line.

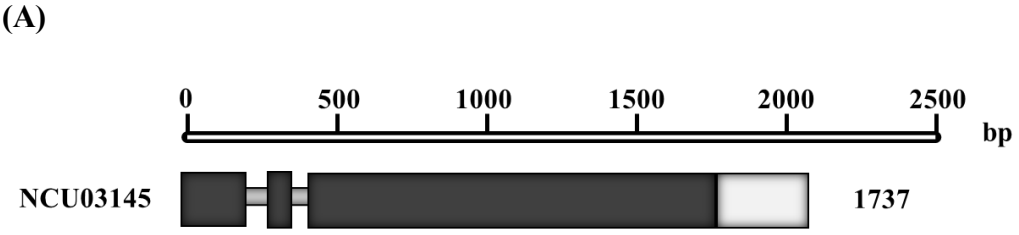

(B)

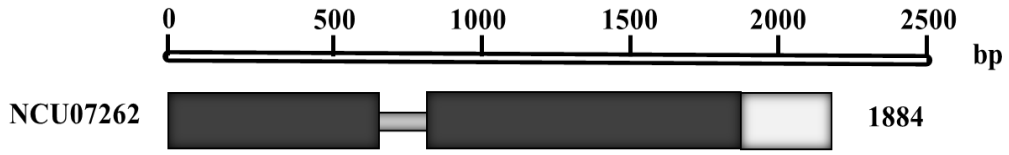

Figure 3.3 Gene organization of NCU03145 and NCU07262 in *N. crassa*. (A) The NCU03145 gene possesses three exons (black bar), two introns (grey bar), and Untranslated region (UTR; white bar). **(B)** The NCU07262 gene possesses two exons (black bar), one intron (grey bar), and untranslated region (UTR; white bar).

(A)

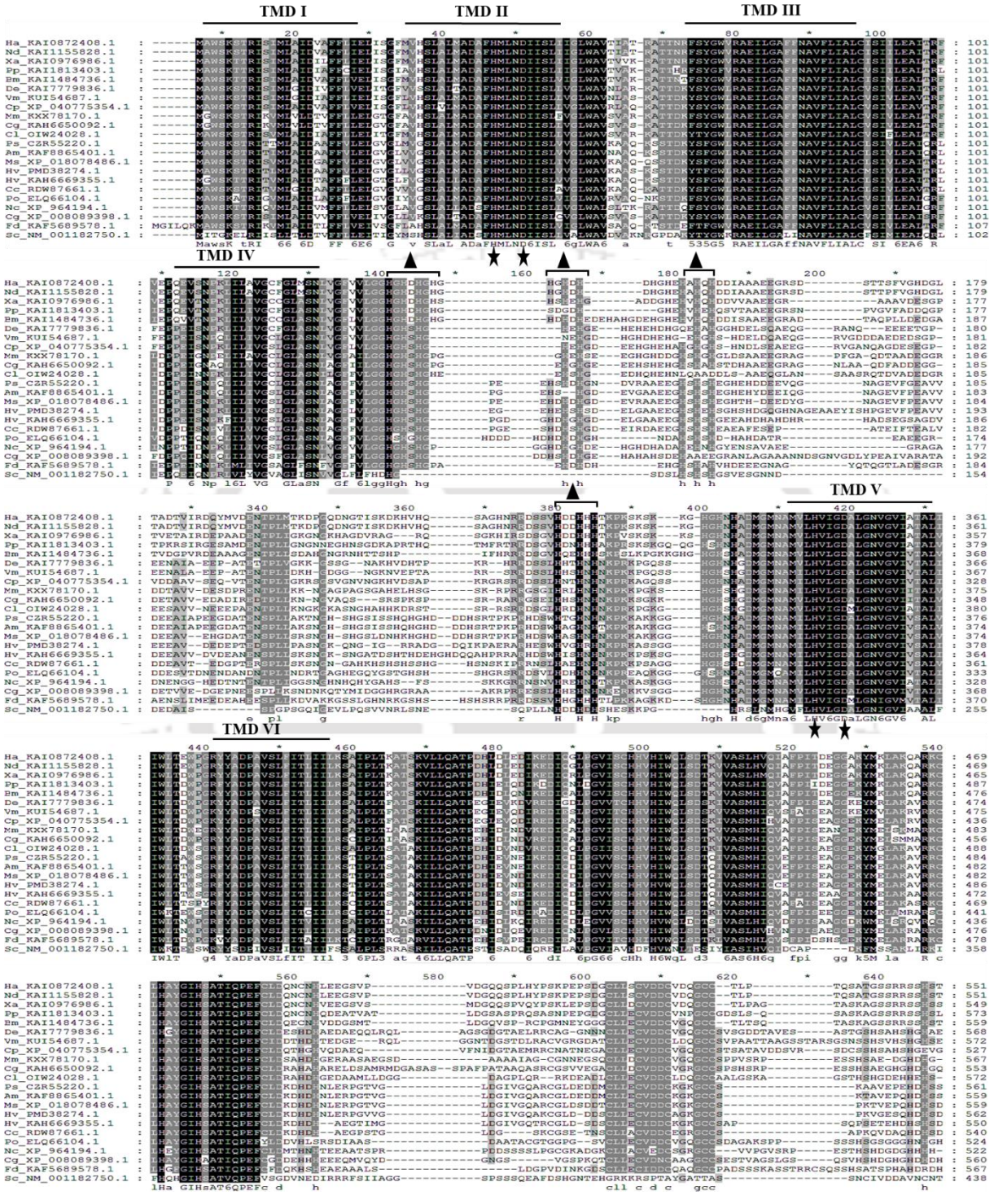

(B)

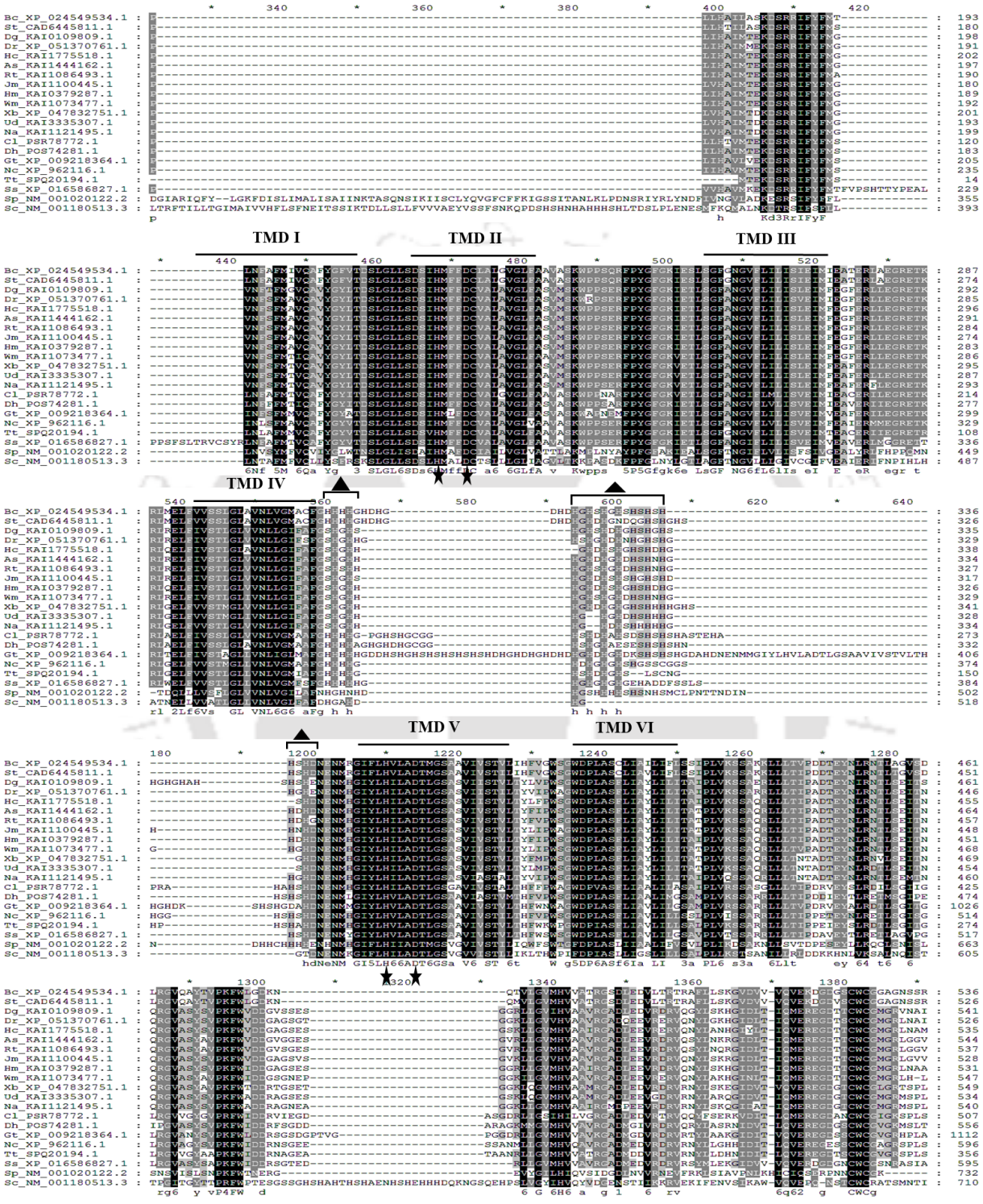

Figure 3.4 Sequence analysis of NCU03145 and NCU07262 of *N. crassa*. Conserved amino acids are indicated in black (100%), dark grey (>80%), and light grey (>60%) in the alignment. The

predicted transmembrane domains (I- VI) obtained from DeepTMHMM are shown. The black triangle (▲) between TMD IV and TMD V indicates the histidine-rich region predicted to be involved in metal binding (Paulsen and Saier 1997). The black star (★) indicates the zinc-binding motif (HD-HD) of TMD II and TMD V (Hoch et al. 2012). **(A)** Multiple sequence alignment of NCU03145 and its homologs. The sequences used in this analysis are *Hypoxylon argillaceum* (Ha), *Nemania diffusa* (Nd), *Xylaria arbuscula* (Xa), *Poronia punctata* (Pp), *Biscogniauxia mediterranea* (Bm), *Diaporthe eres* (De), *Valsa mali* (Vm), *Cryphonectria parasitica* (Cp), *Madurella mycetomatis* (Mm), *Chaetomium globosum* (Cg), Coniochaeta ligniaria (Cl), *Phialocephala subalpine* (Ps), *Acephala macrosclerotiorum* (Am), *Mollisia scopiformis* (Ms), *Hyaloscypha variabilis* (Hv), *Halenospora varia* (Hv), *Coleophoma crateriformis* (Cc), *Pyricularia oryza* (Po), *Neurospora crassa* (Nc), *Colletotrichum graminicola* (Cg), *Fusarium denticulatum* (Fd), *Saccharomyces cerevisiae* (Sc). **(B)** Multiple suence alignemnt of NCU07262 and its homologs. The sequences used in this analysis are *Botrytis cinerea* (Bc), *Sclerotinia trifoliorum* (St), *Daldinia grandis* (Dg), *Durotheca rogersii* (Dr), *Hypoxylon cercidicola* (Hc), *Annulohypoxylon stygium* (As), *Rostrohypoxylon terebratum* (Rt), *Jackrogersella minutella* (Jm), *Hypomontagnella monticulosa* (Hm), *Whalleya microplaca* (Wm), *Ustulina deusta* (Ud), *Nemania abortiva* (Na), *Coniella lustricola* (Cl), *Diaporthe helianthin* (Dh), *Gaeumannomyces tritici* (Gt), *Neurospora crassa* (Nc), *Thermothielavioides terrestris* (Tt), *Sporothrix schenckii* (Ss), *Schizosaccharomyces pombe* (Sp), *Saccharomyces cerevisiae* (Sc).

(A)

(B)

(C)

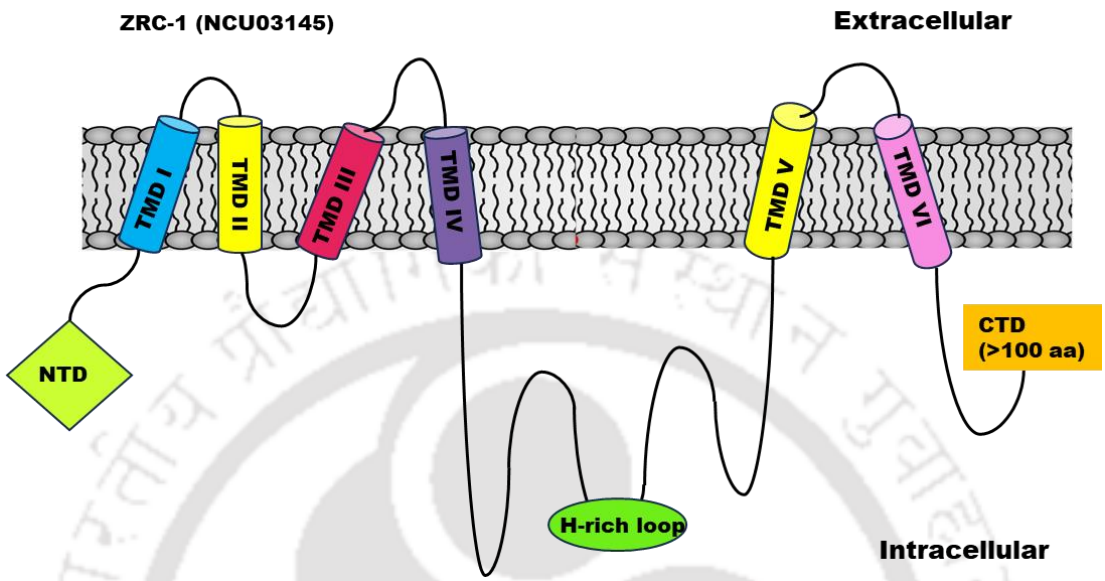

(D)

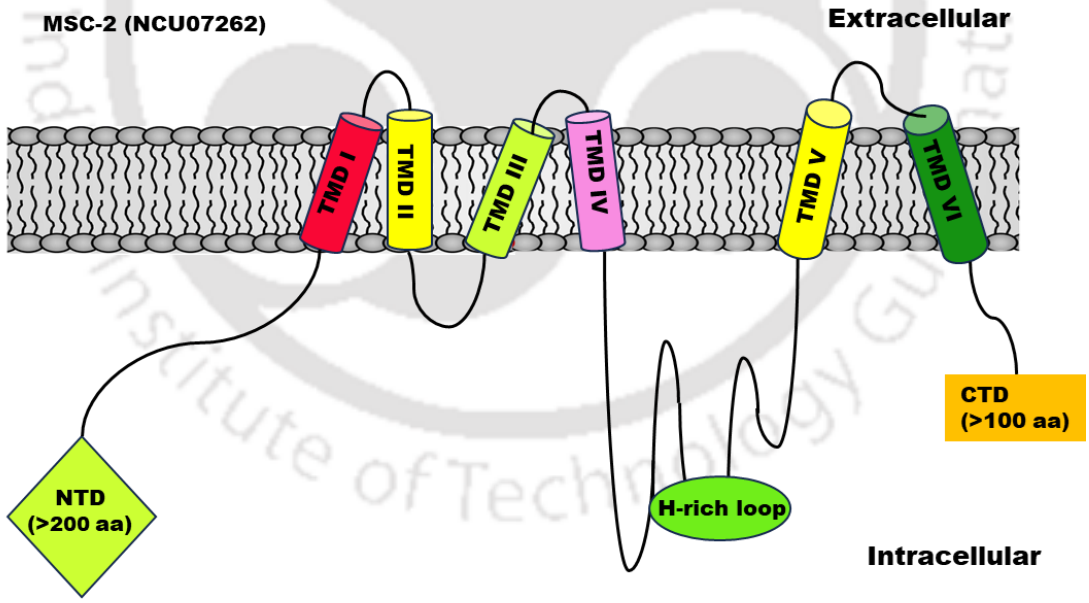

Figure 3.5 Domain organization of ZRC-1 and MSC-2 of *N. crassa*. (A) Conserved domain organization of ZRC-1 of *N. crassa*. The ZRC-1 of *N. crassa* encodes a 522 amino acid in length. **(B)**

Conserved domain organization of MSC-2 of *N. crassa*. The MSC-2 of *N. crassa* encodes a 604 amino acid in length. The conserved domain organization of ZRC-1 and MSC-2 of *N. crassa* was drawn using Illustrator for Biological Sequences (IBS) webserver (http://ibs.biocuckoo.org/online.php). Both ZRC-1 and MSC-2 contain a cation efflux transmembrane domain (TMD), and a cation efflux C-terminal domain (CTD) (Kolaj-Robin et al. 2015). **(C)** Putative membrane topology of ZRC-1. **(D)** Putative membrane topology of MSC-2. The transmembrane domains are represented as TMD I- TMD VI. The N-terminal domain (NTD) is represented in lime diamond. The histidine-rich motifs in green oval, and the C-terminal domain (CTD) in orange rectangle. The position of the transmembrane helices is given in Table 3.1.

Table 3.1 Transmembrane domain prediction of ZRC-1 and MSC-2 of *N. crassa*.

Region	ZRC-1	MSC-2
Intracellular	1 – 8	1 – 230
TM helix 1	9 – 29	231 – 251
Extracellular	30 – 35	252 – 260
TM helix 2	36 – 56	261 – 276
Intracellular	57 – 75	277 – 297
TM helix 3	76 – 98	298 – 316
Extracellular	99 – 111	317 – 334
TM helix 4	112 – 132	335 – 352
Intracellular	133 – 311	353 – 436

TM helix 5	312 – 332	437 – 457
Extracellular	333 – 342	458 – 465
TM helix 6	343 – 358	466 – 487
Intracellular	359 – 522	488 – 604

(A)

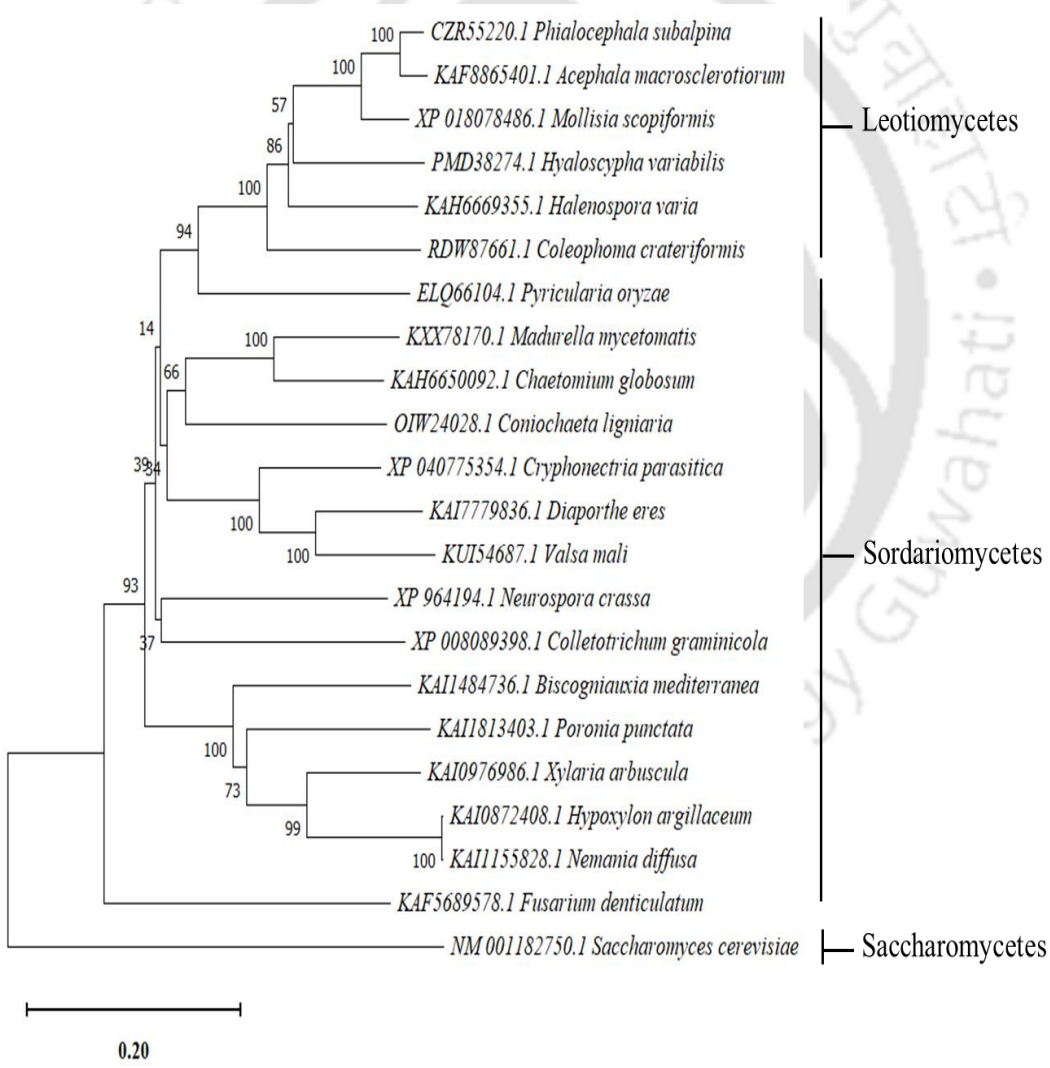

(B)

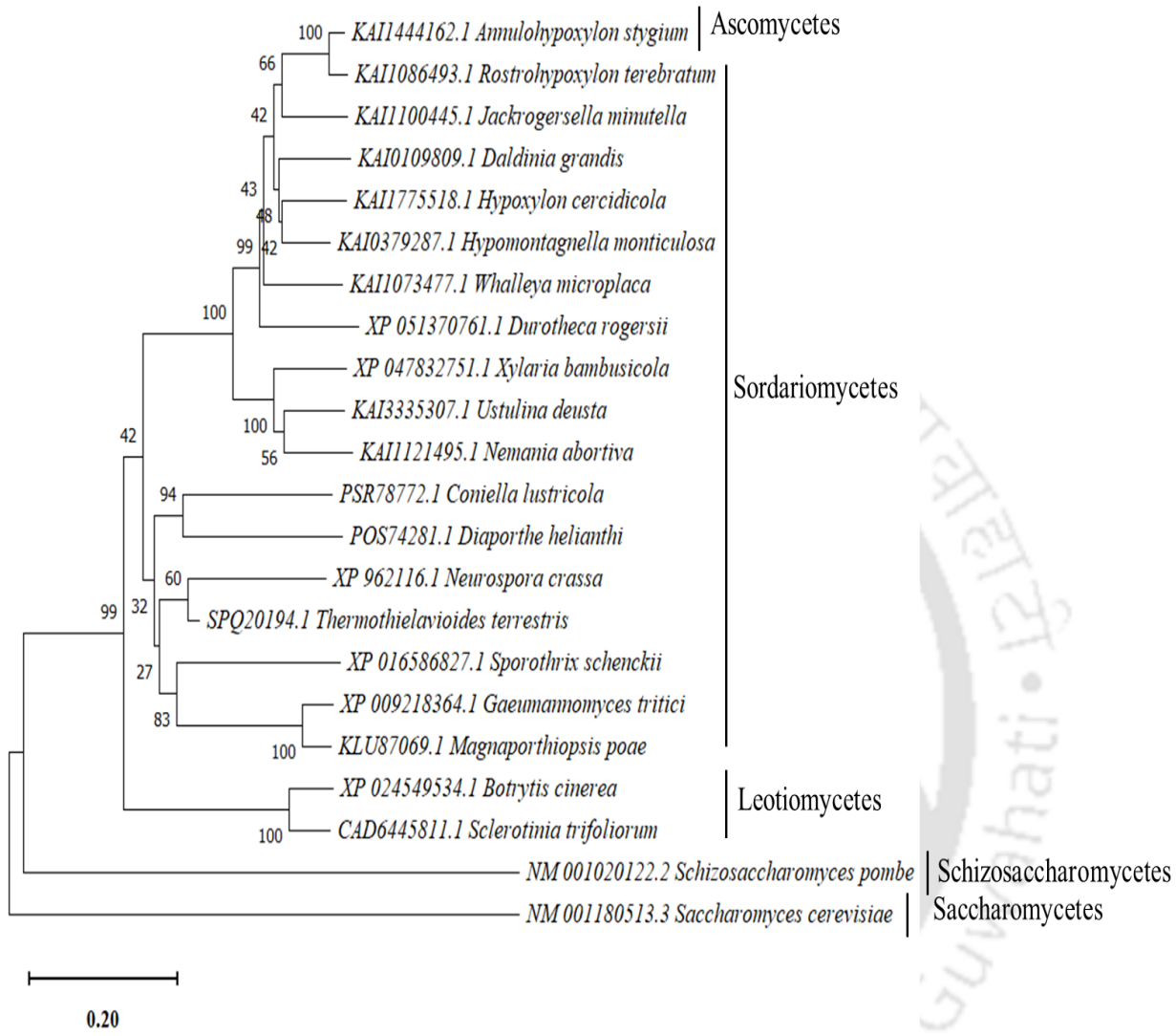

Figure 3.6 Phylogenetic analysis of ZRC-1 and MSC-2 of *N. crassa*. The phylogenetic analysis was performed using the MEGA11 program using the minimal evolution technique and 1000 bootstrap replications (the bootstrap values are shown as nodes in the phylogram). The scale at the bottom represents the genetic distance corresponding to the number of amino acid substitutions per site. **(A)** Phylogenetic analysis of ZRC-1 of *N. crassa* and its orthologs throughout the fungal kingdom. **(B)** Phylogenetic analysis of MSC-2 of *N. crassa* and its orthologs throughout the fungal kingdom.

3.2.1.2 Prediction of interacting partners of ZRC-1 and MSC-2 using the STRING analysis

The probable interacting partners of ZRC-1 and MSC-2 proteins were identified using the Search Tool for the Retrieval of Interaction Genes/Proteins (STRING 11.5) database (https://string-db.org/). The STRING analysis could predict both direct (physical) and indirect (functional) interactions, and assist to understand the cellular processes at the system level, including the structural, functional, and evolutionary characteristics of proteins (Szklarczyk et al. 2019)

The Protein-protein interacting network of ZRC-1 revealed a network with 11 nodes (ZRC-1 and 10 additional proteins) and 39 edges. This network has a PPI enrichment p-value of 1.05e-11, an average node degree of 7.09, an average local clustering coefficient of 0.874, and a network with an average node degree of 7.09 (Figure 3.6 A; Table 3.2). ZRC-1 has also been shown to interact with CLN-3, a vacuolar protein known to play a role in cellular pH regulation in *S. cerevisiae* (Padilla-López and DA 2006). The Protein-protein interacting network of MSC-2 reveals 11 nodes (MSC-2 and 10 additional proteins) and 34 edges. This network has a PPI enrichment p-value of 8.32e-09, an average node degree of 6.18, an average local clustering coefficient of 0.855, and a network with an average node degree of 6.18 (Figure 3.6 B; Table 3.2). MSC-2 also showed interaction with MCD-4 which has mannose-ethanolamine phosphotransferase activity and is implicated in ATP transport and the formation of glycosylphosphatidylinositol (GPI) (Bowman et al. 2006) and ACW-1, a GPI anchored cell wall protein in *N. crassa* (Maddi et al. 2009). This interaction of MSC-2 with cell wall was reported in *S. pombe*, where *cis4* mutant showed severe sensitivity to micafungin (1,3-β-d-glucan synthase inhibitor) (Fang et al. 2008). Additionally, STRING data analysis revealed that ZRC-1 and MSC-2 interact with one another, as well as with some common interaction partners, some of which are ZIP and CDF family protein (Kiranmayi et al. 2009), such as ZRG-17 (Tiwari et al. 2018) and YKe4 (Kumánovics et al. 2006). Thus, SPRING analysis predicted several interacting partners of

ZRC-1 and MSC-2, including proteins involved in zinc and other signaling pathways, and suggest an interaction between zinc and other signaling proteins for proper coordination of physiological responses in *N. crassa*.

(A)

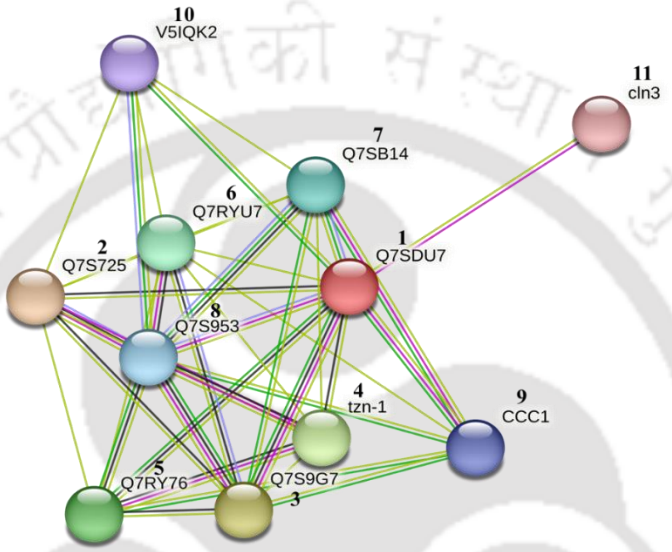

(B)

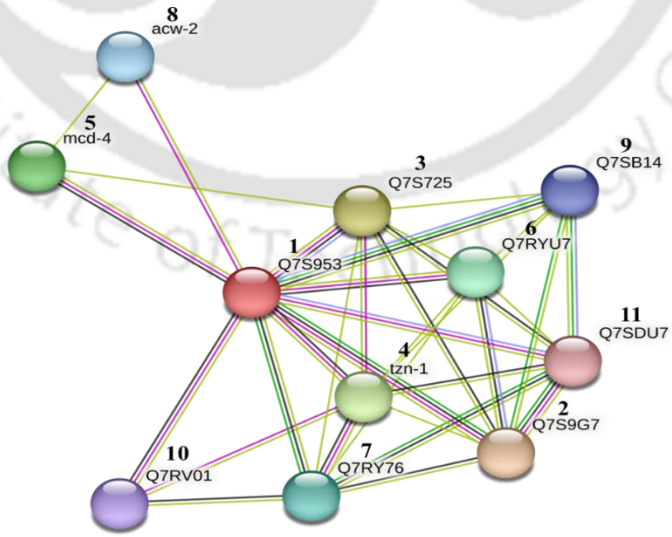

Figure 3.7 Schematic of interacting network of the *N. crassa* ZRC-1 and MSC-2 proteins predicted using STRING. (A) Analysis of the ZRC-1 protein interaction partners using STRING. Details of these numerous interacting proteins are listed in Table 3.3. **(B)** Analysis of the MSC-2 protein interaction partners using STRING. Details of these numerous interacting proteins are listed in Table 3.2. The edges in the network show a distinct and significant protein-protein interaction, demonstrating that proteins cooperate to carry out a common function. Pink-line: experimentally determined; Green-line: gene neighborhood; Red-line: gene fusions; Blue-line: gene co-occurrence; Yellow line: text mining; Black line: co-expression.

Table 3.2 Probable interacting partners of ZRC-1 and MSC-2 predicted by STRING

	Sl No.	Gene name or Protein ID	NCU No.	Name of Protein
ZRC-1	1	Q7SDU7	NCU03145	Zinc transporter ZRC-1
	2	Q7S725	NCU01254	Zinc transporter ZRG-17
	3	Q7S9G7	NCU06380	Zinc transporter YKE4
	4	*tzn-1*	NCU07621	Zinc-regulated transporter 1
	5	Q7RY76	NCU00029	ZIP metal ion transporter
	6	Q7RYU7	NCU06473	ZIP metal ion transporter
	7	Q7SB14	NCU07879	Mitochondrial metal transporter 2
	8	Q7S953	NCU07262	Zinc transporter MSC-2
	9	CCC-1	NCU11307	cation chloride co-transporter-1 CCC-1
	10	V5IQK2	NCU09368	Cation diffusion facilitator 10
	11	*cln-3*	NCU08408	Protein BTN-1
	1	Q7S953	NCU07262	Zinc transporter MSC-2

MSC-2	2	Q7S9G7	NCU06380	Zinc transporter YKE4
	3	Q7S725	NCU01254	Zinc transporter ZRG-17
	4	*tzn-1*	NCU07621	Zinc-regulated transporter 1
	5	*mcd-4*	NCU07999	GPI ethanolamine phosphate transferase GPIP-2
	6	Q7RYU7	NCU06473	ZIP metal ion transporter
	7	Q7RY76	NCU00029	ZIP metal ion transporter
	8	*acw-2*	NCU00957	Anchored cell wall protein 2
	9	Q7SB14	NCU07879	Mitochondrial metal transporter 3
	10	Q7RV01	NCU03947	E3 ubiquitin-protein ligase
	11	Q7SDU7	NCU03145	Zinc transporter ZRC-1

3.2.1.3 The ZRC-1 and MSC-2 showed structural similarities with the YiiP of *E coli*.

I used the only zinc transporter with the available X-ray crystallography of YiiP of *E. coli* (Lu and Fu 2007) as a template to predict the structures of ZRC-1 and MSC-2. The only zinc transporter with the available X-ray crystallography structure is the *E. coli* YiiP. YiiP is a ferrous-iron efflux pump (FieF: P69380) with 300 amino acid residues, belonging to CDF metal transporter located on the plasma membrane (Chao and Fu 2004b). In YiiP, the transmembrane residues Asp45 and Asp49 of TM helix 2 and His153 and Asp157 of TM helix 5 form a "DD-HD" motif, that is involved in the binding of zinc (Lu and Fu 2007). Protein structure prediction was performed using the standard homology modeling steps (Figure 3.7).

To predict the stricture, I used the Iterative Threading ASSEmbly Refinement (I-TASSER, https://zhanggroup.org/I-TASSER/), suite that uses threading and ab initio methods (Yang and Zhang 2015; Zheng et al. 2021). To improve the structural quality, the best-predicted structures of ZRC-1

and MSC-2 were refined using GalaxyWEB (https://galaxy.seoklab.org/index.html) (Ko et al. 2012). The resulting structure was then confirmed using the Ramachandran plot (Ramachandran and Sasisekharan 1968) obtained using PROCHECK v3.5 program, in SAVES v6.0 web server (https://saves.mbi.ucla.edu/), (Laskowski et al. 1993). After the refining procedure, residues in the most favored regions increased from 70.2% to 86.1% in ZRC-1 and from 62.7% to 82.2% in MSC-2. (Figure 3.9; Table 3.3). Using the Dali webserver (http://ekhidna2.biocenter.helsinki.fi/dali/) (Holm 2022), structural alignment between YiiP and the modeled structures of ZRC-1 and MSC-2 was carried out, resulting in RMSD values of 2.8 Å for ZRC-1 and 2.6 Å for MSC-2, indicating the significance of the structural similarity. Based on the structural alignment of YiiP with ZRC-1 and MSC-2, I found that the residue forming a "DD-HD" motif in YiiP was partially conserved as "HD-HD" in ZRC-1 and MSC-2 (Figures 3.8 and 3.10). The conservation of these zinc-binding motifs in ZRC-1 and MSC-2 indicated that these residues might play a role in zinc binding that is similar to YiiP. To further validate the results obtained from the structural alignment, the predicted ZRC-1 and MSC-2 structures were superimposed with YiiP and visualized using PyMOL (Figure 3.8). This analysis revealed that the *N. crassa* ZRC-1 and MSC-2 show structural similarities to the *E. coli* YiiP.

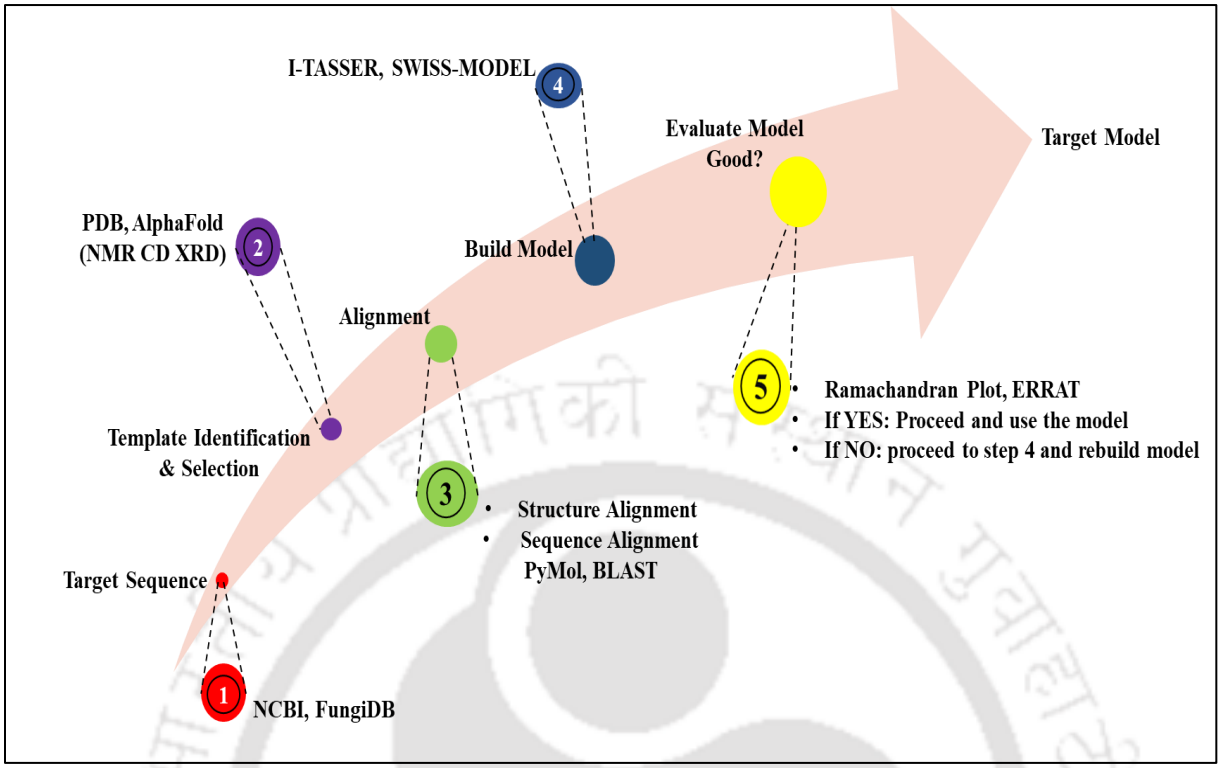

Figure 3.8 Schematic representation of the steps followed for homology modeling. The important events that influenced the homology modeling processes are shown in the figure. Firstly, the sequence of the query/target protein is obtained, using search tools like NCBI and FungiDB. Second, a structure that is similar to the target sequence is obtained using online search tools like PDB and Uniprot (AlphaFold), thereby selecting a suitable template. Third, the target sequence is realigned with the template, and alignment corrections are applied to ensure that the conserved or functionally significant residues/motifs are properly aligned. Fourth, the protein structure is predicted using tools such as I-TASSER, SWISS-MODEL, and AlphaFold. Fifth, validation of the model by verifying for stereochemical evaluation using tools like Ramachandran plot and the Dali web server. The predicted target model is visualized using PyMOL, VMD, and Chimera. The links to the software are added in materials and methods (Chapter 2).

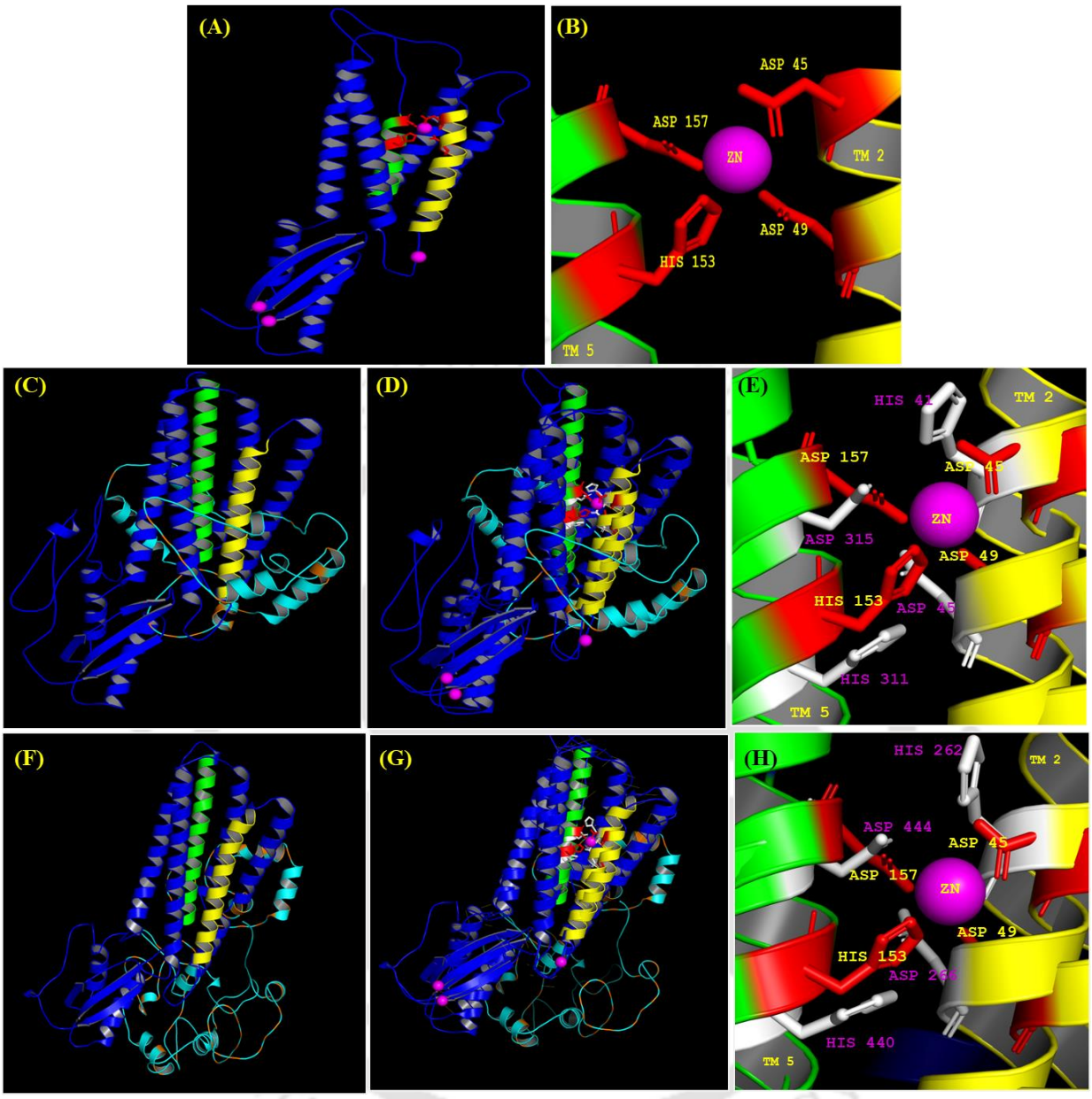

Figure 3.9 Visualization of the three-dimensional structures of the modeled ZRC-1 and MSC-2 structures in PyMOL. The protein is shown in blue, transmembrane domain (TM) 2 and 5 are shown in yellow and green, respectively, the regions that are structurally not aligned with YiiP are shown in cyan and the histidine-rich motifs are highlighted in orange. The amino acid residues interacting with zinc are shown in red (YiiP) and White (ZRC-1 and MSC-2), and zinc is shown as a purple sphere.

(A) X-ray crystallography structure of YiiP (FieF) obtained from PDB (ID: 3H90). **(B)** The zinc interacting site of YiiP shows the "DD-HD" motif present within the TM helix 2 and 5 of YiiP. The amino acid residues D45 and D49 in TM 2, and residues H153 and D157 in TM 5 interacting with zinc are shown. **(C)** The Modeled Structure of ZRC-1. **(D)** Super-imposed image of the modeled ZRC-1 and YiiP. Based on the alignment, zinc-interacting residues in ZRC-1 are shown in white (HD-HD), while YiiP (DD-HD) residues are shown in red. **(E)** The superimposed image of zinc interacting site of ZRC-1 with YiiP. The amino acid residues H41 and D45 of TM 2 and H311 and D315 of TM 5 of ZRC-1 that are aligned with the zinc interacting residues DD-HD of YiiP are shown in the figure. **(F)** The Modeled Structure of MSC-2. **(G)** Super-imposed image of the modeled MSC-2 and YiiP. Based on the alignment, the zinc interacting residues of MSC-2 are shown in white (HD-HD), while YiiP (DD-HD) residues are shown in red. **(H)** The superimposed image of the zinc ion interacting site of MSC-2 with YiiP. The amino residues H262 and D266 of TM 2 and H440 and D444 of TM 5 of MSC-2 that are aligned with the zinc interacting residues DD-HD of YiiP are shown in the figure.

(A)

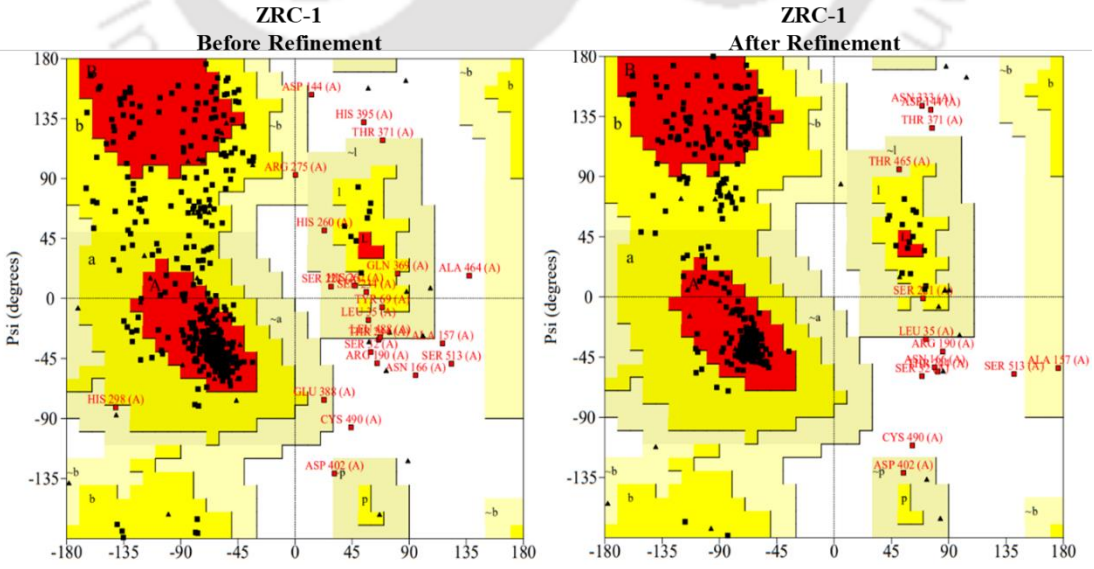

(B)

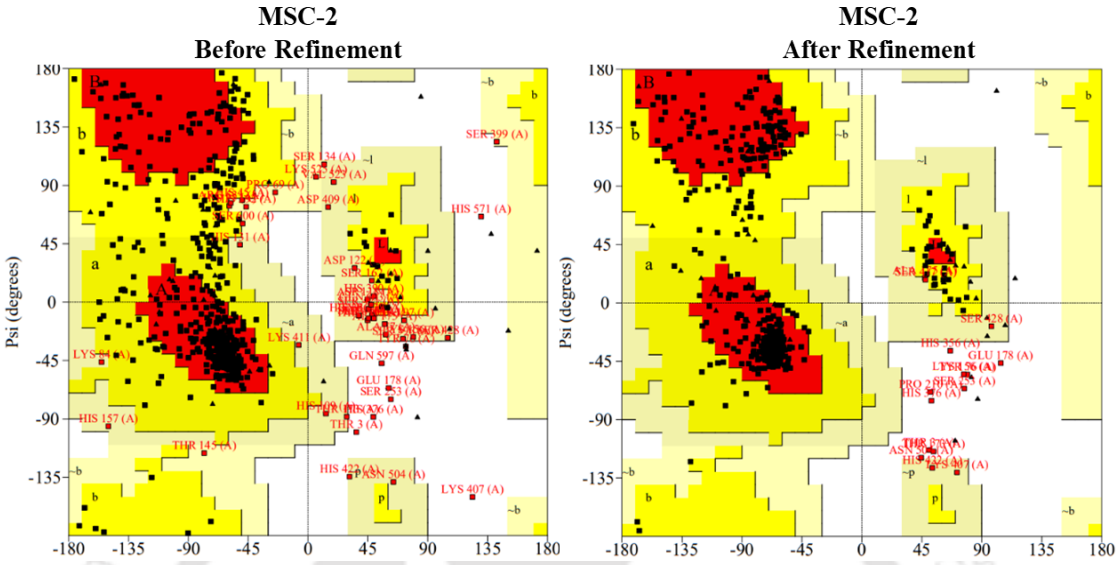

Figure 3.10 PROCHECK analysis for structure validation of modeled structure. Ramachandran plot of the modeled structures showing before and after refinement of **(A)** ZRC-1, and **(B)** MSC-2. The amino acid residues in the most favored regions are shown in red, residues in the allowed regions are shown in yellow, residues in the generously allowed regions are shown in pale yellow, and residues in the forbidden regions are shown in white.

Table 3.3 Percentage of residues in the Ramachandran plot before and after refinement of the structures of ZRC-1 and MSC-2 of *N. crassa*

	Plot statistics			
	ZRC-1		**MSC-2**	
	Before refinement	**After refinement**	**Before refinement**	**After refinement**
Residues in the most favored region	318 (70.2%)	390 (86.1%)	325 (62.7%)	426 (82.2%)

Residues in the additionally allowed region	112 (24.7%)	49 (10.8%)	149 (28.8%)	78 (15.1%)
Residues in the outlier region	23 (5.1%)	14 (3.1%)	44 (8.5%)	14 (2.7%)

(A)

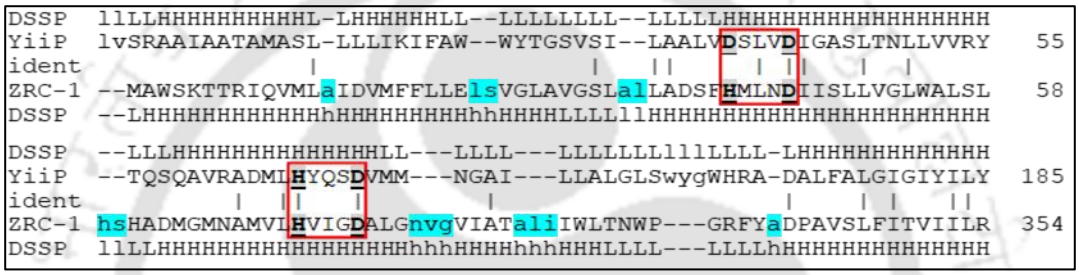

(B)

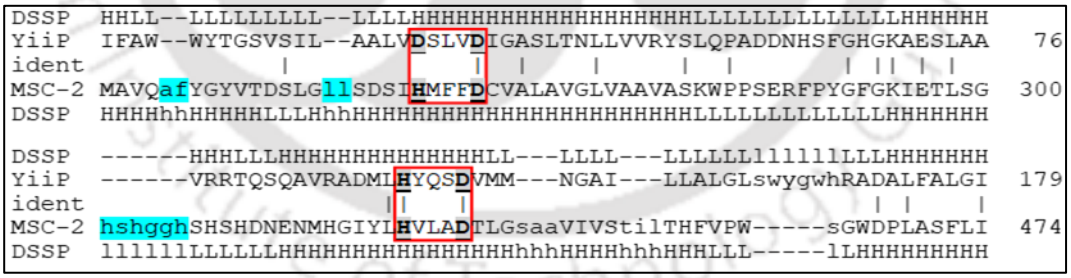

Figure 3.11 Structural alignment of the predicted protein models with YiiP of *E. coli*. The Conserved residues involved in zinc interaction which are the "DD-HD" motif of YiiP and the "HD-HD" motif of ZRC-1 and MSC-2, are aligned and highlighted within the red box. **(A)** Structural alignment between the predicted structure of ZRC-1 with YiiP. **(B)** Structural alignment between the

predicted structure of MSC-2 with YiiP. The unaligned residues are highlighted in cyan and the database of secondary structure (DSSP); H and h are helix and L and l are coil.

3.2.2 Role of *zrc-1* and *msc-2* on the growth and development of *N. crassa*

3.2.2.1 Confirmation of Δ*zrc-1* and Δ*msc-2* knockout mutants by PCR analysis

The Δ*zrc-1* and Δ*msc-2* knockout mutants were generated by the NIH Neurospora functional genomics project (http://geiselmed.dartmouth.edu/dunlaploros/genome/; Figure 3.1; Colot et al. 2006) and confirmed using Southern analysis (http://borkovichlims.ucr.edu/southern/). The Δ*zrc-1* and Δ*msc-2* knockout mutants were obtained from the Fungal Genetics Stock Center (FGSC; https://www.fgsc.net/) and were further verified using the HI-ZRC-1 SN and HI-MSC-2 SN forward primers specific for the region upstream of the 5′ flanks of the gene *zrc-1* and *msc-2*, respectively, and the 5HPHR reverse primer specific for the *hph* cassette used to generate the knockout mutants (Figure 3.11 A; Table 2.3, entries 1-3; Colot et al. 2006; Deka et al. 2011). These PCR-amplified products, with amplicons of ~1.47 and ~1.45 kb, respectively, confirmed the presence of the Δ*zrc-1* and Δ*msc-2* alleles in the respective mutant strains. (Figure 3.11 B).

(A)

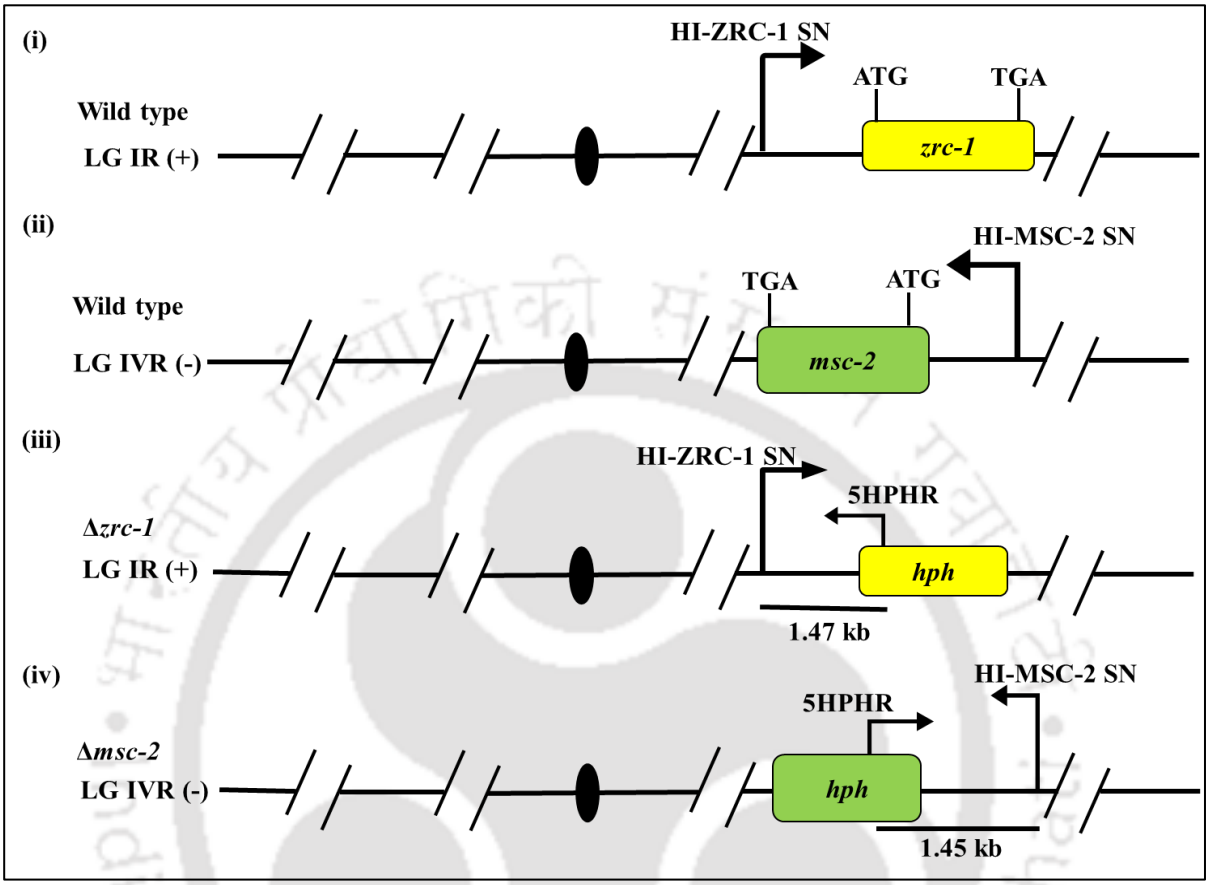

(B)

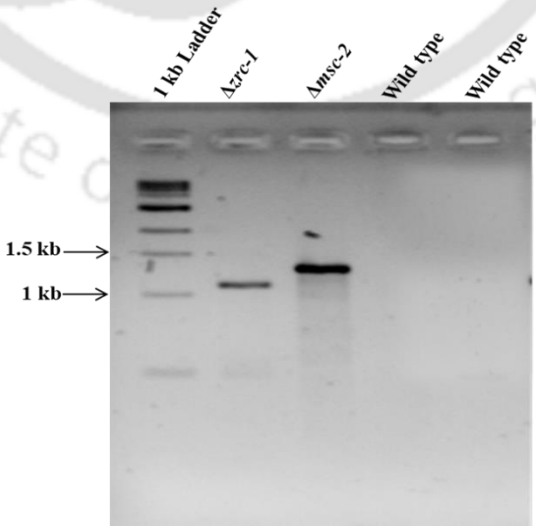

Figure 3.12 Confirmation of the Δ*zrc-1* and Δ*msc-2* knockout mutant strains. (A) Schematic representation for primers designed for confirming Δ*zrc-1* and Δ*msc-2* knockout mutants. The wild type containing *zrc-1* and *msc-2* genes and the location of the binding of the HI-ZRC-1 SN and HI-MSC-2 SN forward primers, respectively, are indicated by black arrows. The Δ*zrc-1* and Δ*msc-2* mutants containing the *hph* cassette and the binding of the primer pairs the HI-ZRC-1 SN and 5HPHR and HI-MSC-2 SN and 5HPHR are indicated by black arrows. The solid black circle indicates the centromere in each line. **(B)** PCR confirmation of Δ*zrc-1* and Δ*msc-2* knockout allele. The Δ*zrc-1* (Lane 2) and Δ*msc-2* (Lane 3) knockout mutants were confirmed using the forward primers HI-ZRC-1 SN and HI-MSC-2 SN and a common reverse primer, 5HPHR. The wild type was used as the control (lane 3 and lane 4). The PCR-amplified products were visualized in 0.8% agarose gel. (Lane 1: marker, 1 kb DNA ladder, NEB).

3.2.2.2 The Δ*zrc-1* showed shorter aerial hyphae in the low and high zinc conditions, and Δ*msc-2* mutants showed shorter aerial hyphae in zinc limiting condition

To explore the cell functions of *zrc-1* and *msc-2* in *N. crassa*, I studied the aerial hyphae of Δ*zrc-1* and Δ*msc-2* mutants under different zinc concentrations. In normal VG liquid media, both Δ*zrc-1* and Δ*msc-2* mutants were viable, indicating that *zrc-1* and *msc-2* are not essential for growth in *N. crassa* (Figure 3.12). In the zinc limiting condition (EDTA), both Δ*zrc-1* and Δ*msc-2* showed shorter aerial hyphae height compared to the wild type. Furthermore, zinc was supplemented to the medium to determine if the addition of zinc could restore growth. The Δ*zrc-1* and Δ*msc-2* mutants exhibited similar aerial hyphae height on the medium supplemented with 0.1 mM $ZnSO_4$, as in the normal medium (Figure 3.12 A and B). However, the Δ*zrc-1* mutant did not produce any aerial hyphae when the concentration of zinc was increased beyond 0.5 mM $ZnSO_4$, and the concentrations beyond 1 mM were lethal for Δ*zrc-1* mutant (Figure 3.12 A and B). The wild type and Δ*msc-2* showed aerial hyphae

growth even at high concentrations (1.5 mM) (Figure 3.12 A and B). These results suggested that *zrc-1* is critical for survival under high zinc conditions.

Furthermore, I determined the specific metal ions that inhibit the growth of Δ*zrc-1* and Δ*msc-2* mutants under metal-limiting conditions caused by the addition of EDTA (100 µM). The VG medium was supplemented with various metals, each at a concentration of 100 µM, including zinc (Zn), cadmium (Cd), cobalt (Co), copper (Cu), iron (Fe), manganese (Mn), and nickel (Ni). Among all the metals tested, only Zn^{2+} was able to restore the restricted growth observed due to the presence of EDTA (Figure 3.12 C). Therefore, EDTA at the concentration of 100 µM was binding to zinc effective enough to inhibit the fungal growth, which was rescued by the addition of zinc (100 µM) in the medium.

(A)

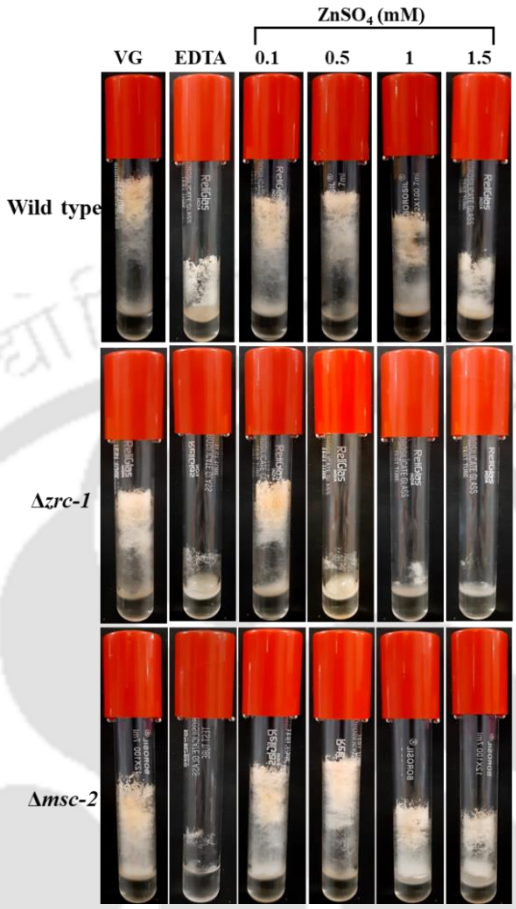

(B)

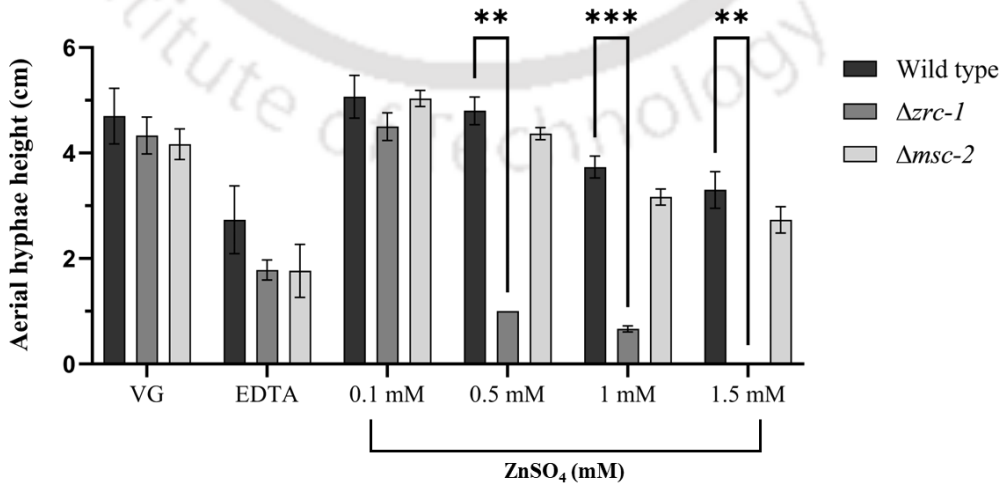

(C)

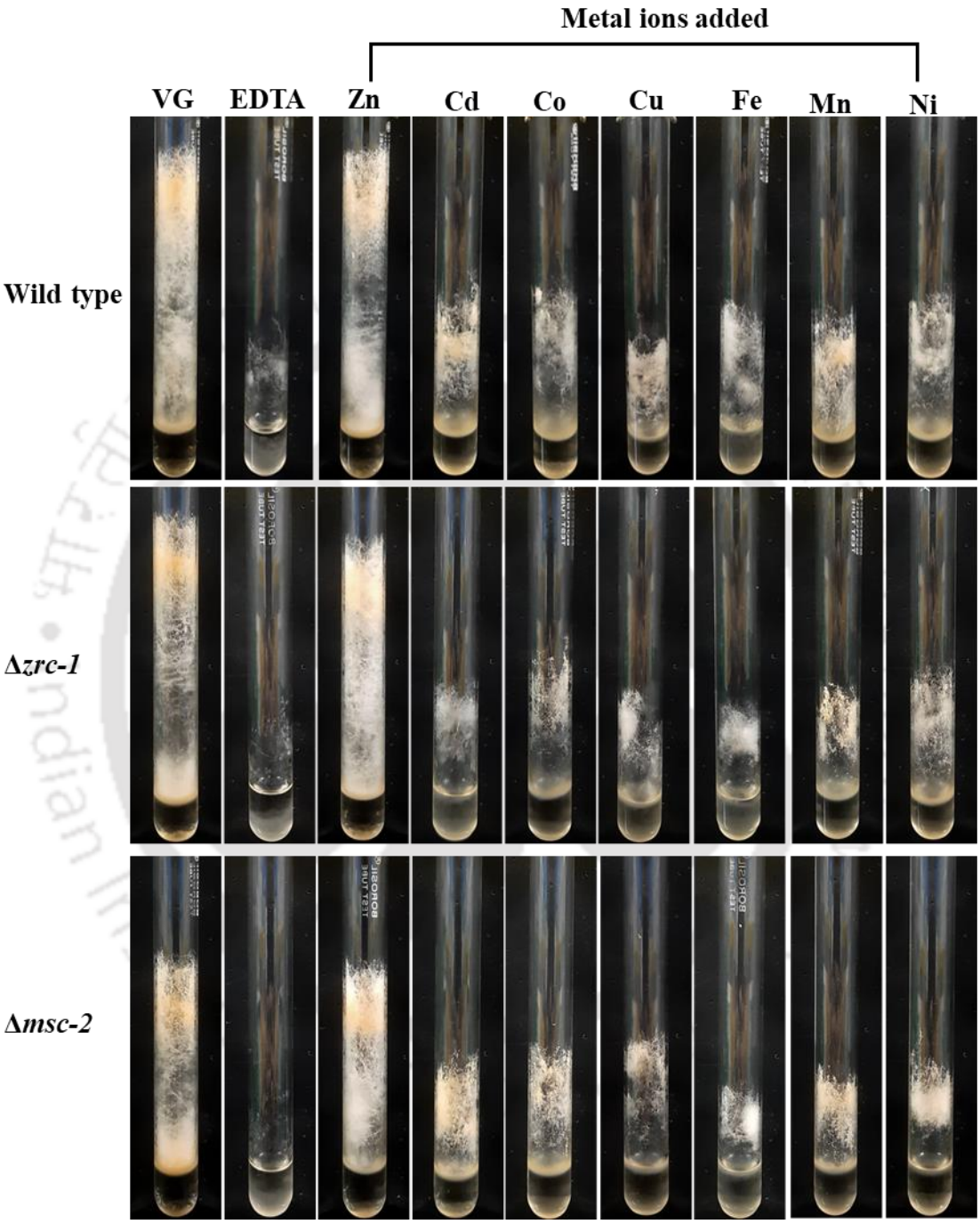

Figure 3.13 Aerial hyphae growth of wild type, Δ*zrc-1*, and Δ*msc-2* mutants under different zinc concentrations. (**A**) Aerial hyphae growth of wild type, Δ*zrc-1*, and Δ*msc-2* mutant strains under zinc

limiting conditions (EDTA) and different concentrations of zinc (0.1 mM, 0.5 mM, 1 mM, 1.5 mM). (**B**) Graphical representation of average aerial hyphae height of Δ*zrc-1* and Δ*msc-2* under different zinc concentrations. The error bars indicate the average standard deviation determined using data obtained from three separate experiments (n = 3). The asterisk represents a significant difference when comparing to the aerial hyphae of the wild type as measured by two-way ANOVA analysis with Tukey's *post hoc* test with P-values < 0.05 (*), < 0.01 (**), and < 0.001 (***). (**C**) Aerial hyphae of Δ*zrc-1* and Δ*msc-2* mutants under different metal conditions. An equal amount of conidia (10^6 conidia/ml) were inoculated into VG liquid media, containing different metal ions (100 µM). The cultures were incubated at 30 ˚C in the dark for three days and in light for two days and photographed.

3.2.2.3 The Δ*zrc-1* and Δ*msc-2* mutants exhibit distinct colony and hyphal morphology under different zinc conditions

To study the colony morphology of Δ*zrc-1* and Δ*msc-2*, mycelial plugs of the *N. crassa* strains were inoculated in VG agar medium containing different concentrations of zinc (0.1 mM, 0.5 mM, 1 mM, 1.5 mM) with 100 µM EDTA, and incubated at 30°C in the dark (Figure 3.13). The Δ*zrc-1* and Δ*msc-2* both displayed slower growth than wild type in the zinc limiting condition (EDTA), which was rescued by adding zinc into the medium. Similar to the aerial hyphae growth, the Δ*zrc-1* mutant exhibited distinct colony morphology at higher zinc concentrations (≥ 0.5 mM). The Δ*zrc-1* mutant showed 74 % and 18.75 % reduction in growth on the medium containing 0.5 and 1.5-mM zinc, respectively, compared to the growth in normal VG. Meanwhile, the wild type and Δ*msc-2* did not show comparable colony morphology on VG medium and VG containing 0.5 mM and 1.5 mM of zinc (Figure 3.13 A and B).

I also examined the hyphal morphology, frequency, and pattern of hyphal branching in the wild type, Δ*zrc-1,* and Δ*msc-2* under a microscope. The strains were inoculated in VG agar medium containing EDTA and various concentrations of zinc (0.1 mM, 0.5 mM, and 1.5 mM) and incubated at 30 °C in the dark for one day. The branching morphology of wild type, Δ*zrc-1,* and Δ*msc-2* strains remained mainly dichotomous in all the zinc concentrations tested (Figure 3.13 C). The Δ*zrc-1* mutant showed slow growth rate, defective branching patterns, lesser branches, and an overall sparse branching pattern at high zinc concentrations (≥ 0.5 mM) (Figure 3.13 C).

(A)

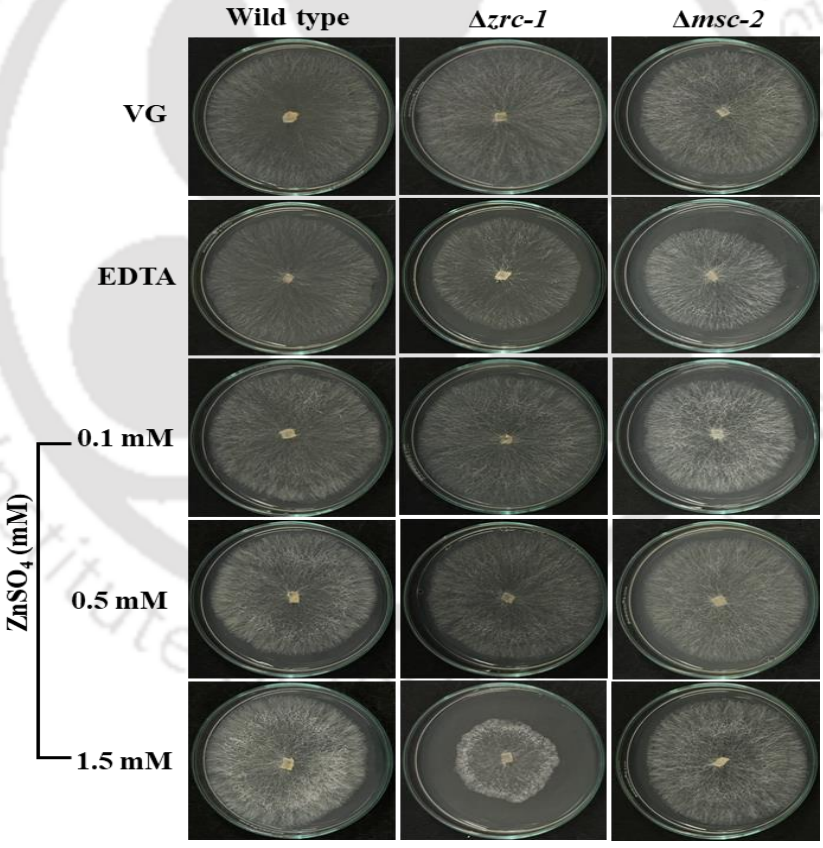

(B)

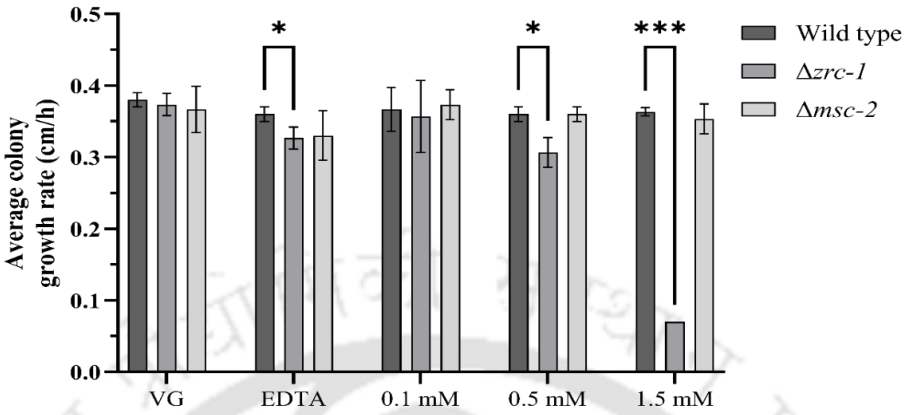

(C)

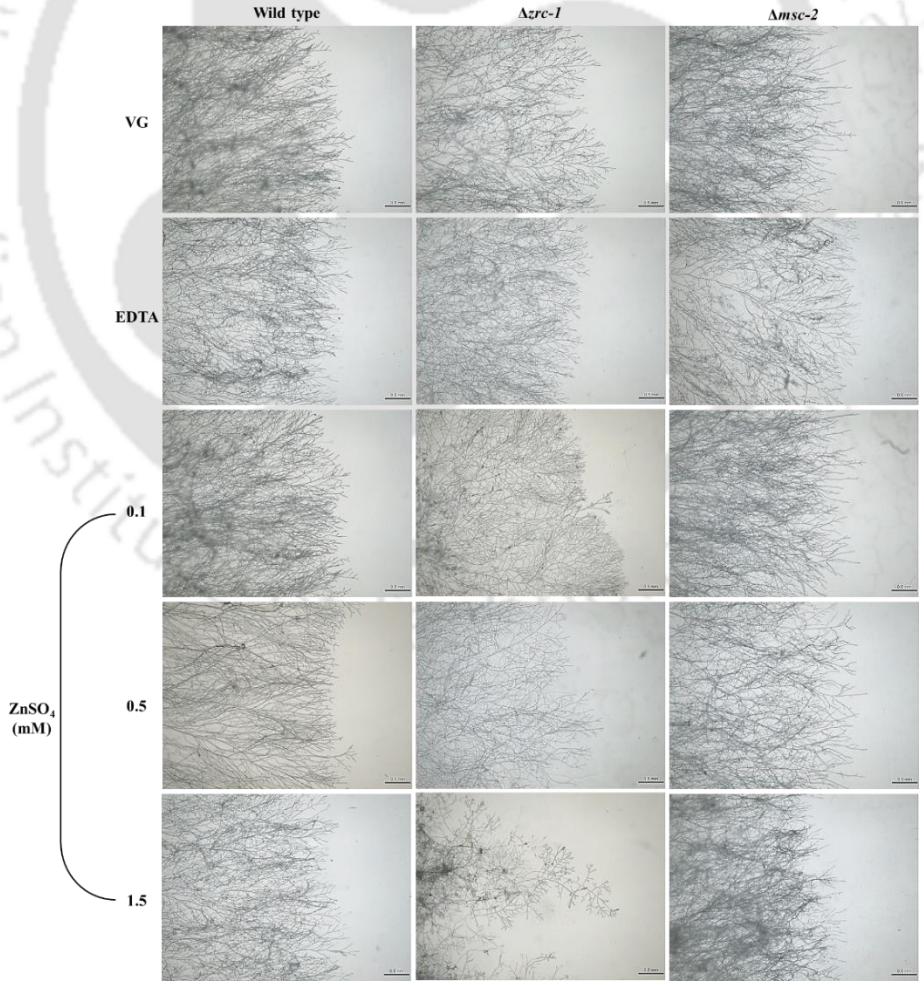

Figure 3.14 Colony and hyphal morphology of the wild type, Δ*zrc-1*, and Δ*msc-2* mutant strains in various amounts of zinc concentrations. **(A).** Colony morphology of *N. crassa* strain on 90 mm Petri dishes under various concentrations of zinc. The plates were incubated in the dark for 18 h and photographed. **(B).** Graphical representation of average colony growth rates of Δ*zrc-1* and Δ*msc-2* under various zinc concentrations. The error bars indicate the average standard deviation determined using data obtained from three separate experiments (n = 3). The asterisk represents a significant difference with respect to the aerial hyphae of the wild type, as measured by two-way ANOVA analysis with Tukey's *post hoc* test with P-values < 0.05 (*), < 0.01 (**), and < 0.001 (***). **(C).** Hyphal morphology of wild type, Δ*zrc-1*, and Δ*msc-2* in various concentrations of zinc observed under a microscope (Leica S9i, Germany). Scale bar = 0.5 mm.

3.2.3 Role of *zrc-1* and *msc-2* in the *N. crassa* asexual development

3.2.3.1 The Δ*zrc-1* and Δ*msc-2* mutants showed normal conidiation and carotenoid accumulation

In the life cycle of *N. crassa*, asexual sporulation or conidiation occurs during the asexual phase. Environmental stimuli, including nutrient deprivation, light, and circadian clock regulate conidiation (Springer and Yanofsky 1989; Ruger-Herreros and Corrochano 2020). The Zn_2Cys_6-type transcription factor ADA-6, which requires zinc for its proper structure and function, positively regulates several key asexual sporulation genes such as *aconidiate-3* (*acon-3*) and *fluffy* (*fl*) in *N. crassa* (Sun et al. 2019). Therefore, I investigated the effect of the *zrc-1* and *msc-2* deletions in conidiation and carotenoid accumulation (Figure 3.14). The Δ*zrc-1* and Δ*msc-2* mutants did not show a significant difference in the production of conidia compared to the wild type (Figure 3.14 A). Further, I measured the total amount of carotenoid present in the mycelia of Δ*zrc-1* and Δ*msc-2* mutants on exposure to light for one day at three different temperatures (8 ˚C, 22 ˚C, and 30 ˚C), because carotenogenesis is

known to be affected by light exposure time and temperature (Harding 1974). The Δ*zrc-1* and Δ*msc-2* mutants showed an equal amount of carotenoid accumulation as in the wild type in all the temperatures tested (Figure3.14 B).

(A)

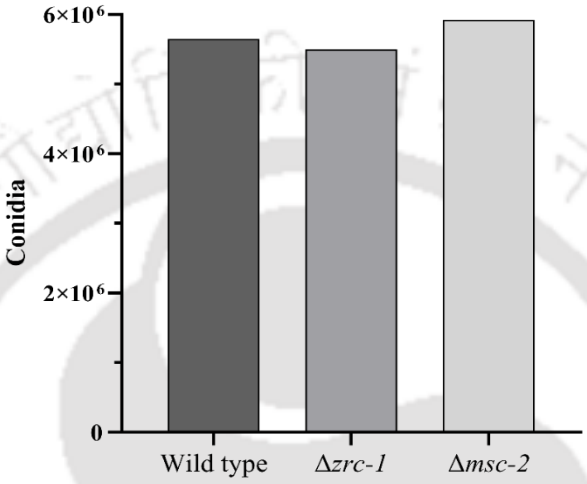

(B)

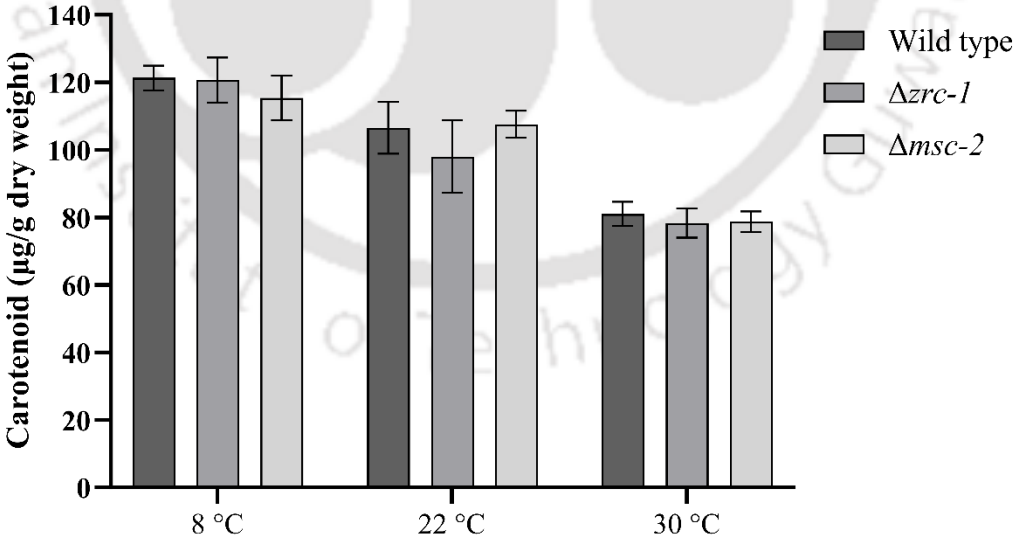

Figure 3.15 Conidiation and carotenoid accumulation in the wild type, Δ*zrc-1*, and Δ*msc-2* strains. (A). Quantification of conidia of the wild type, Δ*zrc-1*, and Δ*msc-2* mutants. The strains were grown in VG agar medium and incubated at 30 °C in the dark for two days, and then under the light at 30 °C for one day. The conidia were harvested and quantified. **(B).** Estimation of carotenoid accumulation in the wild type, Δ*zrc-1*, and Δ*msc-2* mutant strains. The carotenoid of the strains was extracted and expressed as µg carotenoid/g dry weight (Rodriguez-Amaya and Kimura 2004). The error bars indicate the average standard deviation determined using data obtained from three separate experiments (n = 3).

3.2.3.2 Circadian regulated conidiation in the Δ*zrc-1* and Δ*msc-2* mutants

The circadian clock is the only endogenous signal known to initiate conidiation in *N. crassa* (Dunlap and Loros 2004; Heintzen and Liu 2007). The *N. crassa* circadian clock regulates the *fluffy* (*fl*) gene, which is essential for conidiation (Correa and Bell-Pedersen 2002). To study the *N. crassa* circadian clock, the *ras-1*^{bd} mutant is used as a control strain. The *ras-1*^{bd} is a *band* (*bd*) mutant, which contains the T79I point mutation in the *Ras-1 GTPase* gene and as a result produces distinct rhythmic conidial bands even in the presence of high CO_2 levels unlike the wild type (Belden et al. 2007). To test a possible defect in circadian-regulated conidiation in the Δ*zrc-1* and Δ*msc-2* mutants, I generated double mutants, by crossing the Δ*zrc-1* and Δ*msc-2* knockout mutants with *ras-1*^{bd} mutant (Figure 3.15 A). Further, I measured the period length of *ras-1*^{bd}, Δ*zrc-1*; *ras-1*^{bd}, and Δ*msc-2*; *ras-1*^{bd} mutants, at different temperatures 20 °C and 30 °C. The period length of Δ*zrc-1*; *ras-1*^{bd}, and Δ*msc-2*; *ras-1*^{bd} was similar to *ras-1*^{bd}, indicating that deletion of *zrc-1* and *msc-2* did not affect the circadian clock in *N. crassa* (Figure 3.15 B and C).

(A)

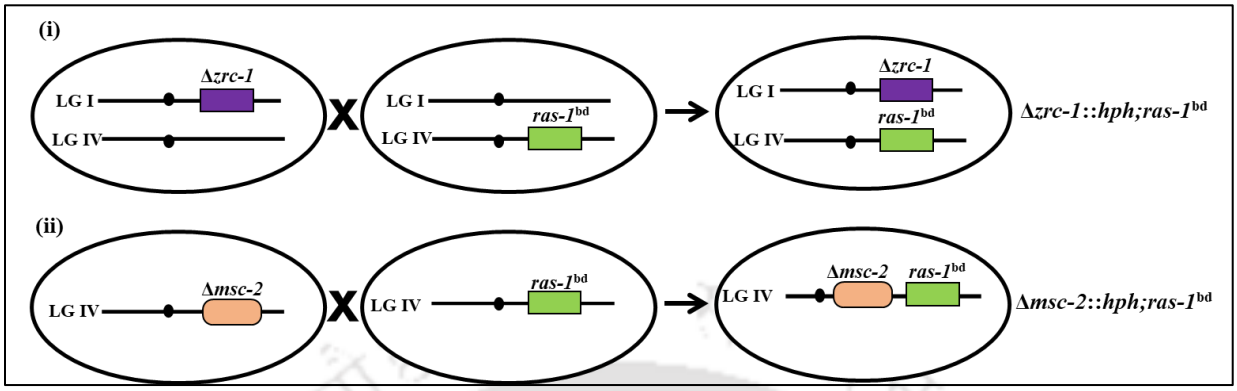

(B)

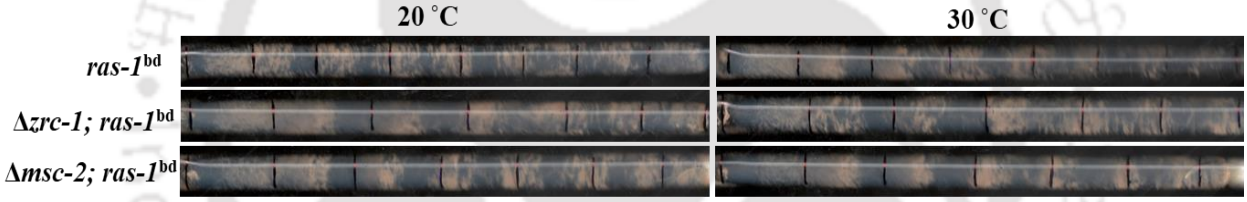

(C)

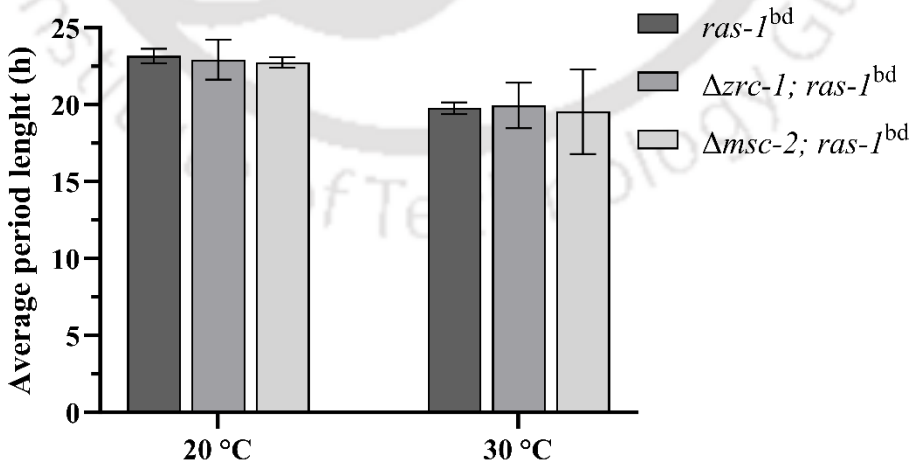

Figure 3.16 Circadian regulated conidiation of *ras-1*^{bd}, Δ*zrc-1*, and Δ*msc-2* strains. (A). Schematic representation of crosses to generate double mutants to study circadian rhythm. The Δ*zrc-1* (i), and Δ*msc-2* (ii) mutants are crossed with *ras-1*^{bd} of opposite mating types at 22 °C for 21 days, and ascospores from the crosses were harvested and germinated on the FGS medium and screened for the presence of *ras-1* ^{bd} allele for conidial banding phenotype and Δ*zrc-1* (i), and Δ*msc-2* (ii) alleles for the resistance to hygromycin B (Hyg^{R}). **(B).** Rhythmic conidiation pattern of *ras-1*^{bd}, Δ*zrc-1*, and Δ*msc-2* strains in inverted race tube. The mutant strains were grown under constant light at 20 °C, for 24 h, then they were shifted to constant darkness at 20 °C for 7 days. After transferring to darkness, the growth fronts were marked, under a safe red light, at every 12 h intervals. The experiment was also carried out at 30 °C and the tubes were photographed. **(C).** Period length of *ras-1*^{bd}, Δ*zrc-1*, and Δ*msc-2* strains. The period lengths were determined by multiplying the distances between the conidial bands by the inverse of the slope from the growth rate of each strain. The error bars indicate the average standard deviation determined using data obtained from three separate experiments (n = 3).

3.2.4 Role of *zrc-1* and *msc-2* on sexual reproduction in *N. crassa*.

3.2.4.1 The Δ*zrc-1* and Δ*msc-2* mutants exhibited both male and female fertile phenotypes in fertility assay

N. crassa contains two mating types (Idiomorphs) *mat a* and *mat A*, and undergoes complex sexual developmental stages involving a series of proteins, forming specialized cells for mating resulting in releases of nerve spores called ascospores. This process is triggered in response to light, nitrogen starvation, and low temperature (Perkins and Barry 1977; Raju 1992; Kim and Borkovich 2004). To understand the role of *zrc-1* and *msc-2* in sexual development, I performed the male-female fertility assay using the Δ*zrc-1 mat a/A*, and Δ*msc-2 mat a/A* knockout mutants and the wild type (OR a/A) control (Table 3.4). The Δ*zrc-1 mat a/A* and Δ*msc-2 mat a/A* knockout mutants exhibited male and

female fertile phenotypes and showed matured perithecia with abundant ascospores (Figure 3.17; Table 3.4).

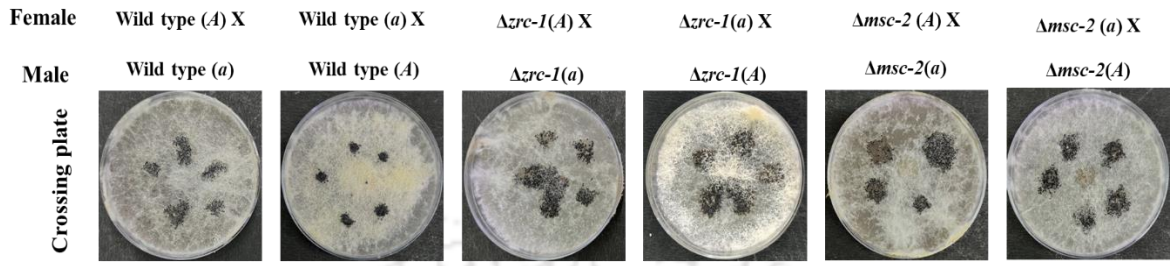

Figure 3.17 Perithecium formation in Δ*zrc-1* and Δ*msc-2* mutants. The wild type, Δ*zrc-1*, and Δ*msc-2* mutants were firstly grown as female parents on SCM, in complete darkness for 7 days at 22 ˚C. Then the opposite mating type of the strains, as male parent, was inoculated on the colony surface of the female parent and incubated in complete darkness for another 7 days at 22 ˚C. The formation of perithecia was examined and photographed.

Table 3.4 Sexual fertility assay on wild type, Δ*zrc-1*, and Δ*msc-2* strains

Sl No.	Female Parent	Male Parent	Perithecia formed	Ascospore Produced	Phenotype
1	OR A	OR a	Yes	Abundant	Fertile
2	OR a	OR A	Yes	Abundant	Fertile
3	Δ*zrc-1::hph;mat A*	Δ*zrc-1::hph;mat a*	Yes	Abundant	Fertile
4	Δ*zrc-1::hph;mat a*	Δ*zrc-1::hph;mat A*	Yes	Abundant	Fertile
5	Δ*msc-2::hph;mat A*	*Δmsc-2::hph;mat a*	Yes	Abundant	Fertile
6	Δ*msc-2::hph;mat a*	Δ*msc-2::hph;mat A*	Yes	Abundant	Fertile

3.2.5 Transcriptional analysis of *zrc-1* and *msc-2* genes in *N. crassa*

3.2.5.1 The *zrc-1* gene showed increased expression under low zinc condition

The Δ*zrc-1* and Δ*msc-2* mutants exhibited a slower growth rate in the zinc-limited conditions and Δ*zrc-1* mutant showed severe growth defects in zinc-rich conditions (≥ 1000 µM) (Figures. 3.13, 3.14). Therefore, I determined the expression of the *zrc-1* and *msc-2* in the wild type strain under various concentrations of zinc (VG, LZVG1, LZVG1000). Based on the phenotypic analysis, the expression of *zrc-1* was expected to be elevated under high zinc conditions. However, the expression of *zrc-1* in the low-zinc environment (LZVG1) was ~3-fold higher than in normal (VG) and high zinc conditions (LZVG1000) (Figure 3.18). In contrast, no significant difference was observed in the *msc-2* expression in VG, LZVG, and LZVG1000 medium (Figure 3.18). These results suggested that the zinc concentration regulates the expression of *zrc-1*, however, *msc-2* expression is independent of zinc concentration in the medium.

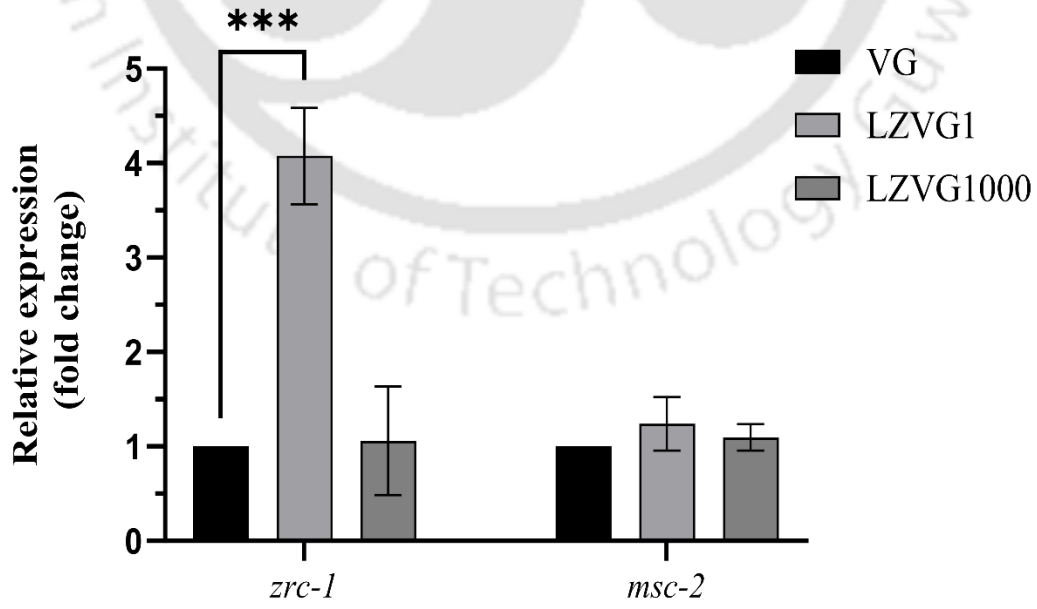

Figure 3.18 Expression analysis of *zrc-1* and *msc-2* in *N. crassa* under various zinc conditions. In the VG liquid medium, conidia (10^6 conidia/ml) were inoculated and the cultures were incubated for 16 h at 30 °C with shaking at 180 rpm in total darkness. The RNA was harvested, and the relative expression of *β-tubulin* gene of *N. crassa* was used to normalize the expression of the *zrc-1* and *msc-2* genes. The expression of the genes in low zinc (LZVG1) and high zinc (LZVG1000) medium was compared to the expression in normal zinc (VG) medium**.** The error bars indicate the average standard deviation determined using data obtained from three separate experiments (n = 3). The asterisk represents a significant difference as measured by two-way ANOVA analysis with Tukey's *post hoc* test with P-values < 0.05 (*), < 0.01 (**), and < 0.001 (***).

3.2.5.2 Promoter analysis of *zrc-1* and *msc-2* genes in *N. crassa*

A promoter is a crucial segment of DNA that initiates and regulates gene transcription. In a typical promoter, the key elements are represented by protein binding sites, and the corresponding proteins are referred to as transcription factors (TFs). By facilitating or inhibiting the transcription process, transcription factors play an important role in regulating the activity of the gene (Mitsis et al. 2020). I analyzed the promoter regions of the *zrc-1* and *msc-2* genes to identify putative transcriptional regulatory sequences using MatInspector (Cartharius et al. 2005).

The promoter region was analyzed by selecting ~2 kb sequences from upstream of the start codon of the ORF. In *zrc-1* and *msc*-2, several common transcriptional regulatory sequences, including Yeast stress response elements (Ruis and Schüller 1995), Yeast heat shock factors (Lorenz and Heitman 1998), and Carbon source-responsive elements (CSRE) (Schöler and Schüller 1994) were identified. The yeast zinc-responsive element sequence was found in the *zrc-1* promoter. The yeast zinc-responsive element sequence is the target region, where the zinc-responsive transcriptional

activator (Zap1p) binds in response to a low zinc condition (Zhao et al. 1998). However, the yeast zinc-responsive element sequence was not found in the *msc-2* gene promoter, but a copper inducible transcription factor (ACE-1) (Zhou and Thiele 1991) binding site is present in the *msc-2* promoter (Table 3.5).

Table 3.5 Putative transcriptional regulatory sequences in the promoter region of the *zrc-1* and *msc-2* genes

Gene	Transcription factor family	Function
zrc-1	Yeast GAL4 factor	DNA-binding zinc cluster transcription factor required for activation of GAL genes for metabolism of galactose (Breunig 2000)
	Yeast stress response elements	Transcriptional activator for genes in multi-stress response (Ruis and Schüller 1995)
	Yeast heat shock factors	Heat shock transcription factor Mga1 (Lorenz and Heitman 1998)
	Carbon source-responsive elements (CSRE)	The zinc cluster transcriptional activator binds to the CSRE (Schöler and Schüller 1994)
	Yeast zinc responsive element	Zinc-responsive transcriptional activator Zap1p (Zhao et al. 1998)
	Pleiotropic drug resistance responsive elements (PDREs)	Zinc cluster protein, a master regulator involved in recruiting other zinc cluster proteins to PDREs (Akache and Turcotte 2002)
	TEA/ATTS DNA binding domain factors	Candida developmental regulator (Schweizer et al. 2000)
	Regulator of Drug Sensitivity 1	Regulator of Drug Sensitivity 1, zinc cluster transcription factor involved in conferring resistance to cycloheximide (Akache and Turcotte 2002)
	Yeast stress response elements	Transcriptional activator for genes in multi stress response (Ruis and Schüller 1995)

msc-2	Carbon source-responsive elements (CSRE)	Zinc cluster transcriptional activator binds to the carbon source-responsive element (CSRE) of gluconeogenic genes (Vincent and Carlson 1998)
	Yeast heat shock factors	Heat shock transcription factor Mga1 (Lorenz and Heitman 1998)
	Pseudohyphal determinant 1	Transcription factors involved in the regulation of filamentous growth
	Metal regulatory element factors	Copper-signaling element, AMT1/ACE1 recognition sequence (Zhou and Thiele 1991)
	Pheromone response elements	Transcription factor activated by a MAP kinase signaling cascade activates genes involved in mating or pseudohyphal/invasive growth pathways (Zhu and Thiele 1996)
	Yeast metabolic regulator	Alcohol Dehydrogenase Regulator, carbon source-responsive zinc-finger transcription factor

3.3 Discussions

In this chapter, I described the sequence analysis that identified NCU03145 and NCU07262 as the homologs of ZRC-1 and MSC-2, respectively. Furthermore, I investigated the phenotypes of Δ*zrc-1* and Δ*msc-2* knockout mutants to identify the cellular roles of these genes in the vegetative growth, asexual development, and sexual development of *N. crassa*.

The sequences analysis revealed that NCU03145 and NCU07262 genes encode zinc transporters belonging to CDF family of proteins, showing similarity to homologs of Zrc1p and Msc2p of *S. cerevisiae*, respectively (Figure 3.4). Based on the sequence alignment, the *N. crassa* ZRC-1 and MSC-2 exhibited 39.14% and 44.93% sequence identities to the *S. Cerevisiae* Zrc1p and Msc2p, respectively. Further, both proteins exhibited some of the typical features of other classical CDF proteins such as the number of transmembrane helices (six), Histidine-rich cytoplasmic loop, and a long C-terminal domain (≥100 amino acid residues) (Figure 3.5; Kolaj-Robin *et al.* 2015). The Zrc1p is known to transport zinc between vacuoles and cytosol when the concentration of zinc is high in the

cytosol and Msc2p is localized to an internal membrane, functions in maintaining cellular zinc homeostasis (Li and Kaplant 1998; Miyabe et al. 2000). Similarly, in *S. pombe*, Zhf1 (zinc homeostasis factor) and Cis4 (chloride and immunosuppressant sensitive) are homologs of Zrc1p and Msc2p, which transport zinc into the ER and cis-Golgi, respectively (Clemens et al. 2002; Boch et al. 2008; Choi et al. 2018).

I also predicted the three-dimensional structure of the *N. crassa* ZRC-1 and MSC-2 using the X-ray crystallography structure of YiiP of *E. coli* as the template. The zinc-binding motif of YiiP, which is present in TM 2 and TM 5 as DD-HD (Lu and Fu 2007), is conserved as HD-HD in ZRC-1 and MSC-2 (Figure 3.8). This HD-HD motif is also conserved among the mammalian zinc transporters (ZnT1- ZnT8) (Hoch et al. 2012; Barber-Zucker et al. 2021). Due to the chemical similarities of Cd^{2+} and Zn^{2+}, there is a possibility that Cd^{2+} might access the Zn^{2+} transportation pathway to enter cells (He et al. 2006; Himeno et al. 2009), and it has been reported, that this hijacking of the zinc pathway is due to the ability of Cd^{2+} to bind to DD-HD, however, Cd^{2+} preferred to bind to DD-HD and not HD-HD (Hoch et al. 2012). While Zn^{2+} could effectively bind to both DD–HD (YiiP) and HD–HD (ZnT8) transport sites (Hoch et al. 2012). Therefore, the notable difference in the motif DD–HD in YiiP and HD–HD in ZRC-1 and MSC-2 (Figure 3.9), is the additional histidine residue that leads to metal specificity.

Further, I investigated the functions of ZRC-1 and MSC-2, in the vegetative growth, asexual, and sexual development of *N. crassa*. The Δ*zrc-1* and Δ*msc-2* mutants were viable and showed a growth rate similar to the wild type in the standard VG medium. However, the Δ*zrc-1* mutant was unable to produce aerial hyphae at zinc concentrations of 0.5 mM and above, whereas the wild type could grow at higher concentrations of zinc (1.5 mM) (Figure 3.13). In addition, the Δ*zrc-1* mutant showed a slow colony growth rate and sparse branching pattern under high zinc concentrations (≥ 0.5

mM) (Figure 3.14). The Δ*msc-2* mutant exhibited no significant differences in growth when compared to the wild type (Figure 3.14). Taken together, these results suggested that ZRC-1 is critical for survival under high zinc conditions in *N. crassa*. Similarly, an overproduction of Zrc1p caused a resistance to high zinc, and Zrc1p was important for zinc detoxification, while *MSC2* mutant showed growth similar to wild type in *S. cerevisiae* (Kamizono et al. 1989; Li and Kaplan 2001). Therefore, ZRC-1 and MSC-2 of *N. crassa* are functional orthologs of the *S. cerevisiae* zinc transporter proteins Zrc1p and Msc2p, respectively.

I also determined the expression analysis of *zrc-1* and *msc-2* under different concentrations of zinc. The Δ*zrc-1* mutant showed phenotypic defects under high zinc conditions (Figure 3.13 and 3.14); however, *zrc-1* expression was ~3-fold elevated in low zinc than in the high zinc conditions (Figure 3.17). Moreover, the promoter analysis identified putative ZRE consensus sequence (-ACCYYNAAGGT-) at the promoter region *of zrc-1* (Table 3.7), indicating that ZAP-1 might play a role in *zrc-1* regulation. In *S. cerevisiae* and *C. neoformans*, overexpression of Zrc1p exhibited tolerance to high zinc (Kamizono et al. 1989; Cho et al. 2018). The overexpression of *ZRC1* in *S. cerevisiae* and *C. neoformans* provides resistance to "zinc shock," which is the sudden influx of zinc into the cytosol caused by the activation of ZIP proteins in zinc deprived conditions (Zhao and Eide 1997; MacDiarmid et al. 2000; Cho et al. 2018). The ZAP-1 dependent regulations under low zinc conditions have also been reported in several other fungi, including *Aspergillus fumigatus* (Miyabe et al. 2000; MacDiarmid et al. 2003; Moreno et al. 2007; Amich and Calera 2014; Vicentefranqueira et al. 2018), *Candida albicans* (Kim et al. 2008; Nobile et al. 2009), and *Fusarium oxysporum* (López-Berges 2020). In addition, there was no significant difference in the expression of *msc-2* in all the zinc concentrations tested (VG, LZVG1, and LZVG1000). Similarly, the expression of *MSC-2* in *S. cerevisiae* was independent of zinc despite its crucial role in maintaining zinc homeostasis, by

transporting zinc to the ER (Lyons et al. 2000; Wu et al. 2008). These results suggested that the cell functions of MSC-2 and ZRC-1 are conserved in *S. cerevisiae* and *N. crassa*. In *S. cerevisiae*, MSc2p forms a heteromeric complex with another CDF zinc transporter protein Zrg17p, these two proteins localize in the ER membranes and help in transporting zinc into the secretory pathways, and the *S. pombe* homologs (Cis4 and Zrg17) of these proteins also show similar functional conservation (Li and Kaplant 1998; Ellis et al. 2005; Fang et al. 2008; Choi et al. 2018). Moreover, the deletion of *zrg-17* gene in *N. crassa* showed several zinc-suppressible phenotypes, such as slow growth rate, short aerial hyphae, and defects in asexual sporulation (Tiwari et al. 2018). Therefore, in the next chapter, I investigated the phenotypes of the double mutants, Δ*zrg-17;* Δ*msc-2*, Δ*zrg-17;* Δ*zrc-1* and Δ*zrc-1;* Δ*msc-2* to understand the genetic interactions among *zrc-1*, *msc-2,* and *zrg-17* genes.

I published results described in this chapter in Journal of Biosciences (Serena Ngiimei D and Ranjan Tamuli; 2024) and also presented as (i) Poster at XI International Conference on Biology of Yeast and Filamentous Fungi, held at University of Hyderabad, India, November 27-29, 2019; (ii) Oral presentation (online mode) at Molecular Intricacies of Plant Associated Microorganisms (MIPAM-2022) organized by Centre for DNA Fingerprinting and Diagnostics, Hyderabad, February 17-20, 2022; And (iii) Oral presentation (online mode) at Asian Mycological Congress 2021 (AMC2021), held at Thailand Science Park Convention Center, Pathum Thani, Thailand, August 3 - 5, 2022.

4

INVESTIGATING THE GENETIC INTERACTION OF *ZRC-1*, *MSC-2*, AND *ZRG-17* IN *NEUROSPORA CRASSA*

4.1 Introduction

Genetic interaction is a phenomenon in which the combined effects of mutations in two or more genes are different or more significant than what would be expected considering the individual effects of each mutation. Genetic interaction can be either negative or positive depending on how severe or mild the observed phenotype of a double mutant is when compared to the phenotypes of the single mutants. Double mutants with negative genetic interactions exhibit stronger-than-expected phenotypes, and double mutants with positive genetic interactions exhibit phenotypes that are less severe than expected based on single-mutant phenotypes (Baryshnikova et al. 2013). Genetic interactions can also occur between loci that regulate or influence the same phenotype, and they may exhibit either additive or multiplicative behavior, indicating the independent actions of the two loci (Morgan and Feldman 2001; Baryshnikova et al. 2013). Additionally, genetic interactions between two interdependent loci are epistatic, in which a mutation at one locus interacts with a mutation at another to affect the phenotype (Gavric and Griffiths 2003). A novel type of genetic interaction is an antagonistic interaction, which can be either synthetic sub-lethal or synthetic lethal, such interactions occur when the phenotype of the double mutant is significantly affected than the phenotype of individual single mutants (Morgan and Feldman 2001; Gavric and Griffiths 2003; Baryshnikova et al. 2013).

In Chapter 3, I described the roles of *zrc-1* and *msc-2* in fungal growth and development, the significance of zinc transportation, and zinc homeostasis. Further, I obtained the knockout of *zrg-17*, a member of CDF zinc transporter, from FGSC (https://www.fgsc.net/). The *N. crassa zrg-17* is encoded by NCU01254 and genetically mapped in the supercontig five from position 3383833 − 3386361 (+ strand), at the right arm of linkage group five (LG VR). The genomic sequence of NCU01254 contains two exons and one intron encoding 671 amino acid residues. In this Chapter, I generated the double mutants of zinc transporter *zrc-1*, *msc-2,* and *zrg-17* to understand the effect of

these mutations in fungal growth, development, mitigating stress such as ER stress, temperature sensitivity, pH stress, osmotic stress, and azole stress.

4.2 Results

4.2.1 Generation of the Δ*zrc-1*; Δ*msc-2*, Δ*msc-2*; Δ*zrg-17*, and Δ*zrc-1*; Δ*zrg-17* double mutants

The Δ*zrc-1*; Δ*msc-2*, Δ*msc-2*; Δ*zrg-17*, and Δ*zrc-1*; Δ*zrg-17* double mutants were generated by crossing the individual parental single mutant strains of opposite mating types (Table 2.2; Figure. 4.1). The ascospores from the 21 days-old crosses were harvested with ~1 ml of water and germinated on FGS medium by heat shock treatment at 60 °C for 45 min. The germinated progenies were picked and grown on VG agar medium, and incubated at 30 °C for two days in the dark and at room temperature for one day under light. The progenies were screened for hygromycin B resistance phenotype, and the presence of the respective knockout allele was confirmed by PCR analysis (Figure 4.2). The common reverse primer 5HPHR (Table 2.3) was used for all the double mutants in combination with the forward primers HI-ZRC-1 SN and HI-MSC-2 SN for the double mutant Δ*zrc-1*; Δ*msc-2*, HI-MSC-2 SN and Zrg-17-KOC-F for the double mutant Δ*msc-2*; Δ*zrg-17*, and HI-ZRC-1 SN and Zrg-17-KOC-F for the double mutant Δ*zrc-1*; Δ*zrg-17* (Table 2.3).

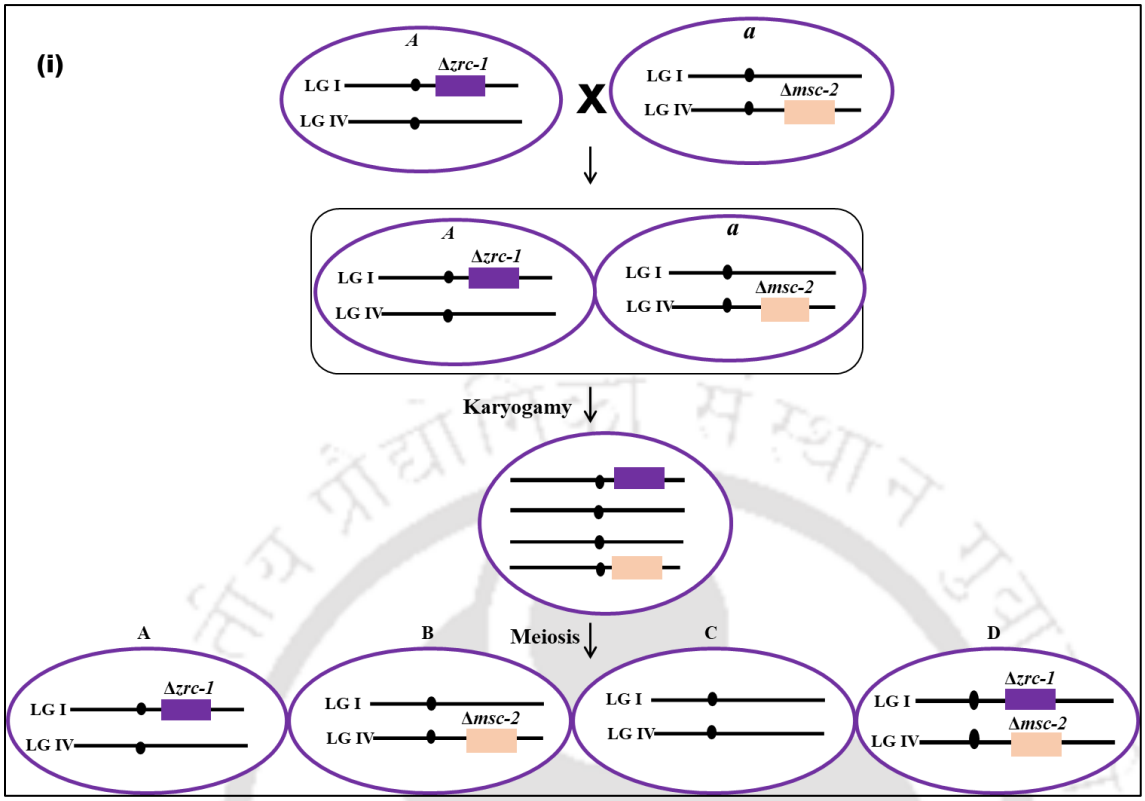

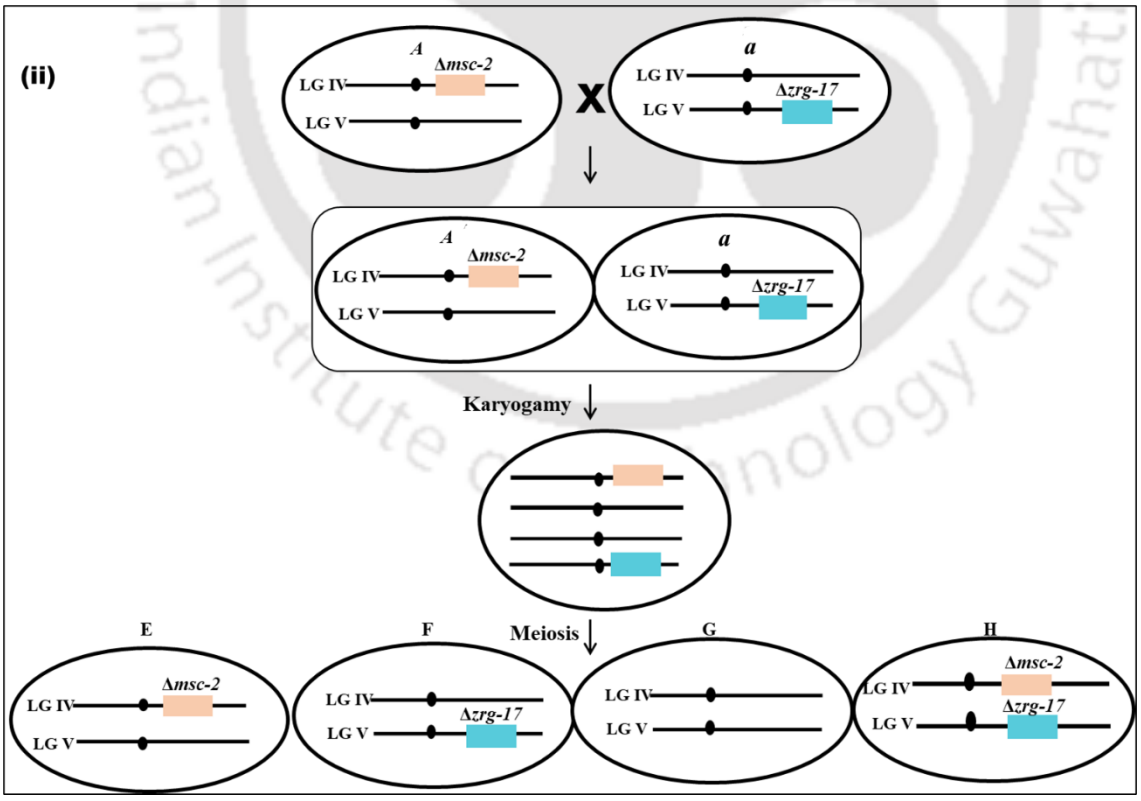

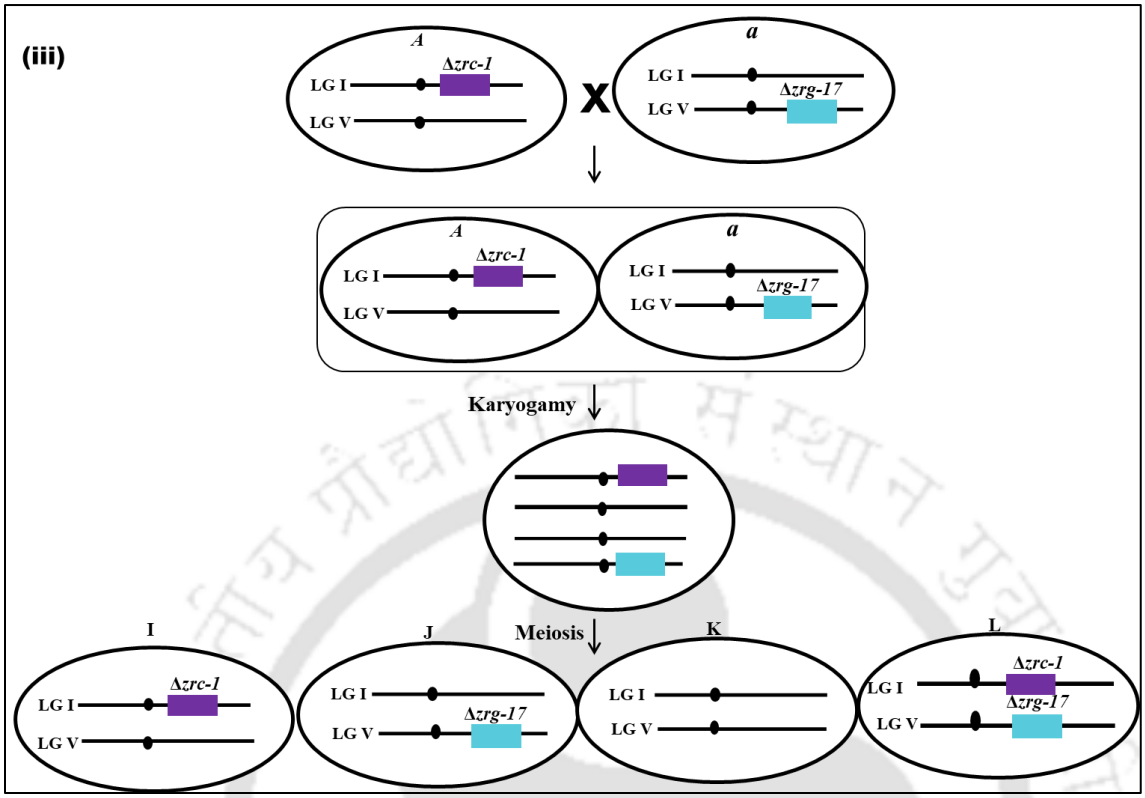

Figure 4.1 Generation of double mutants. Crosses to generate the double mutant are shown schematically in (i), (ii), and (iii). The single mutant Δ*zrc-1* was crossed with the opposite mating type of Δ*msc-2* to generate the double mutant Δ*zrc-1*; Δ*msc-2* (D). The single mutant Δ*msc-2* is crossed with the opposite mating type of Δ*zrg-17* to generate the double mutant Δ*msc-2*; Δ*zrg-17* (H). The single mutant Δ*zrc-1* is crossed with the opposite mating type of Δ*zrg-17* to generate the double mutant Δ*zrc-1*; Δ*zrg-17* (L).

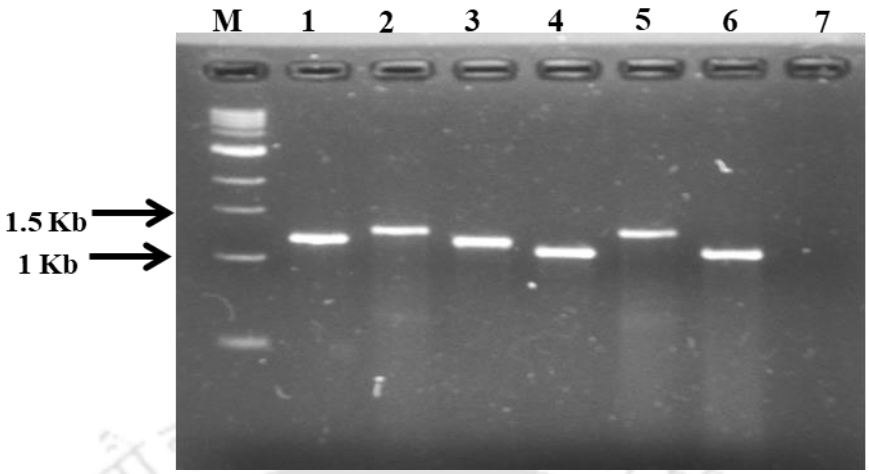

Figure 4.2 Confirmation of double mutants by PCR analysis. The double mutants Δ*zrc-1*; Δ*msc-2*, Δ*msc-2*; Δ*zrg-17*, and Δ*zrc-1*; Δ*zrg-17* were confirmed using the forward primers HI-ZRC-1 SN, HI-MSC-2 SN, and Zrg-17-KOC-F (Table 2.3), which are specific for the upstream of the genes *zrc-1*, *msc-2*, and *zrg-17*, respectively. A common reverse primer 5HPHR (Table 2.3) was used to confirm the *hph* cassette in all the double mutants (Colot et al. 2006; Deka et al. 2011). The presence of PCR-product of amplicon size ~1.47 kb, 1.45 kb, and 1.39 kb confirmed the Δ*zrc-1*, Δ*msc-2*, and Δ*zrg-17* alleles in the mutants. PCR amplified product of ~1.45 kb was observed for the Δ*msc-2* allele in the Δ*zrc-1*; Δ*msc-2* (lane 1) and Δ*msc-2*; Δ*zrg-17* (lane 3) double mutants. PCR amplified product of ~1.47 kb was observed for the Δ*zrc-1* allele in the Δ*zrc-1*; Δ*msc-2* (lane 2) and Δ*zrc-1*; Δ*zrg-17* (lane 5) double mutants. PCR amplified product of ~1.39 kb was observed for the Δ*zrg-17* allele in the Δ*msc-2*; Δ*zrg-17* (lane 4) and Δ*zrc-1*; Δ*zrg-17* (lane 6) double mutants. The wild type was used as the negative control for confirmation (lane 7). M: 1 kb DNA Ladder (NEB). The PCR products were visualized in a 0.8% agarose gel.

4.2.2 The *zrc-1*, *msc-2,* and *zrg-17* genetically interact for vegetative development under different zinc conditions

4.2.2.1 The double mutants Δ*zrc-1*; Δ*msc-2*, Δ*msc-2*; Δ*zrg-17*, and Δ*zrc-1*; Δ*zrg-17* showed distinct vegetative development under varying zinc concentrations

I studied the colony morphology, flask morphology, and hyphal extension of the double mutants Δ*zrc-1*; Δ*msc-2*, Δ*msc-2*; Δ*zrg-17*, and Δ*zrc-1*; Δ*zrg-17* under different concentrations of zinc (VG, LZVG1, LZVG100, LZVG1000) (Table 4.1; Figure 4.3). The phenotypes of all the *N. crassa* strains, including the wild-type, *zrc-1*, *msc-2*, and *zrg-17* single mutants, as well as the Δ*zrc-1*; Δ*msc-2*, Δ*msc-2*; Δ*zrg-17*, and Δ*zrc-1*; Δ*zrg-17* double mutants on the medium containing 100 µM (LZVG100) of zinc concentration were similar to VG (control) medium.

The Δ*zrc-1*; Δ*msc-2* double mutant exhibited phenotypes similar to parental strains, the Δ*zrc-1* mutant causes a decrease in the growth under the high zinc conditions (LZVG1000) (Table 4.1; Figure 4.3 A and B). Moreover, the hyphal extension rate of Δ*zrc-1*; Δ*msc-2* was slightly lower than that of the wild type under high zinc concentrations (Figure 4.3 C). The growth defect of the Δ*zrc-1*; Δ*msc-2* double mutant in LZVG1000 was more distinct in the flask morphology, which could be due to a longer period of incubation (7 days) (Figure 4.3 E). Intriguingly, the Δ*msc-2*; Δ*zrg-17* double mutant showed phenotypes similar to the wild type in all the concentrations of zinc, and the slow growth of the Δ*zrg-17* was masked by the Δ*msc-2* mutant, which suggested an epistatic interaction within *msc-2* and *zrg-17* (Figure 4.3). The Δ*zrc-1*; Δ*zrg-17* double mutant but not Δ*zrc-1*; Δ*msc-2* and Δ*msc-2*; Δ*zrg-17* double mutants showed severe growth defect in normal VG condition like the Δ*zrg-17* single mutant (Table 4.1, Figure 4.3). Additionally, the growth rate of Δ*zrc-1*; Δ*zrg-17* was significantly lower than the wild type in low and high zinc conditions (Figure 4.3). Taken together, these results suggested that *zrc-1*, *msc-2*, and *zrg-17* genetically interact and play key roles in vegetative development, tolerance to low and high zinc concentrations in *N. crassa*.

Table 4.1 Average colony growth rate of *N. crassa* strains

	Average growth rate (cm/h)[a]			
Strains	VG	LZVG1	LZVG100	LZVG1000
Wild type	0.38 ± 0.01	0.32 ± 0.01	0.36 ± 0.03	0.36 ± 0.01
Δ*zrc-1*	0.37 ± 0.01	0.36 ± 0.01 (*)	0.37 ± 0.02	0.30 ± 0.02
Δ*msc-2*	0.38 ± 0.04	0.34 ± 0.04	0.35 ± 0.05	0.36 ± 0.02
Δ*zrg-17*	0.20 ± 0.02 (*)	0.17 ± 0.01 (*)	0.20 ± 0.02 (*)	0.2 ± 0.02 (*)
Δ*zrc-1*; Δ*msc-2*	0.4 ± 0.02	0.32 ± 0.035	0.37 ± 0.05	0.32 ± 0.01
Δ*msc-2*; Δ*zrg-17*	0.37 ± 0.02	0.33 ± 0.02	0.36 ± 0.03	0.35 ± 0.01
Δ*zrc-1*; Δ*zrg-17*	0.20 ± 0.02 (*)	0.17 ± 0.01 (***)	0.20 ± 0.02 (*)	0.16 ± 0.02 (*)

[a] Results are shown as mean ± standard deviation for three independent experiments (n = 3) with *P-values* < 0.05 (*), < 0.01 (**), and < 0.001 (***) compared with the wild type strain as measured by two-way ANOVA with Tukey's *post hoc* test.

(A)

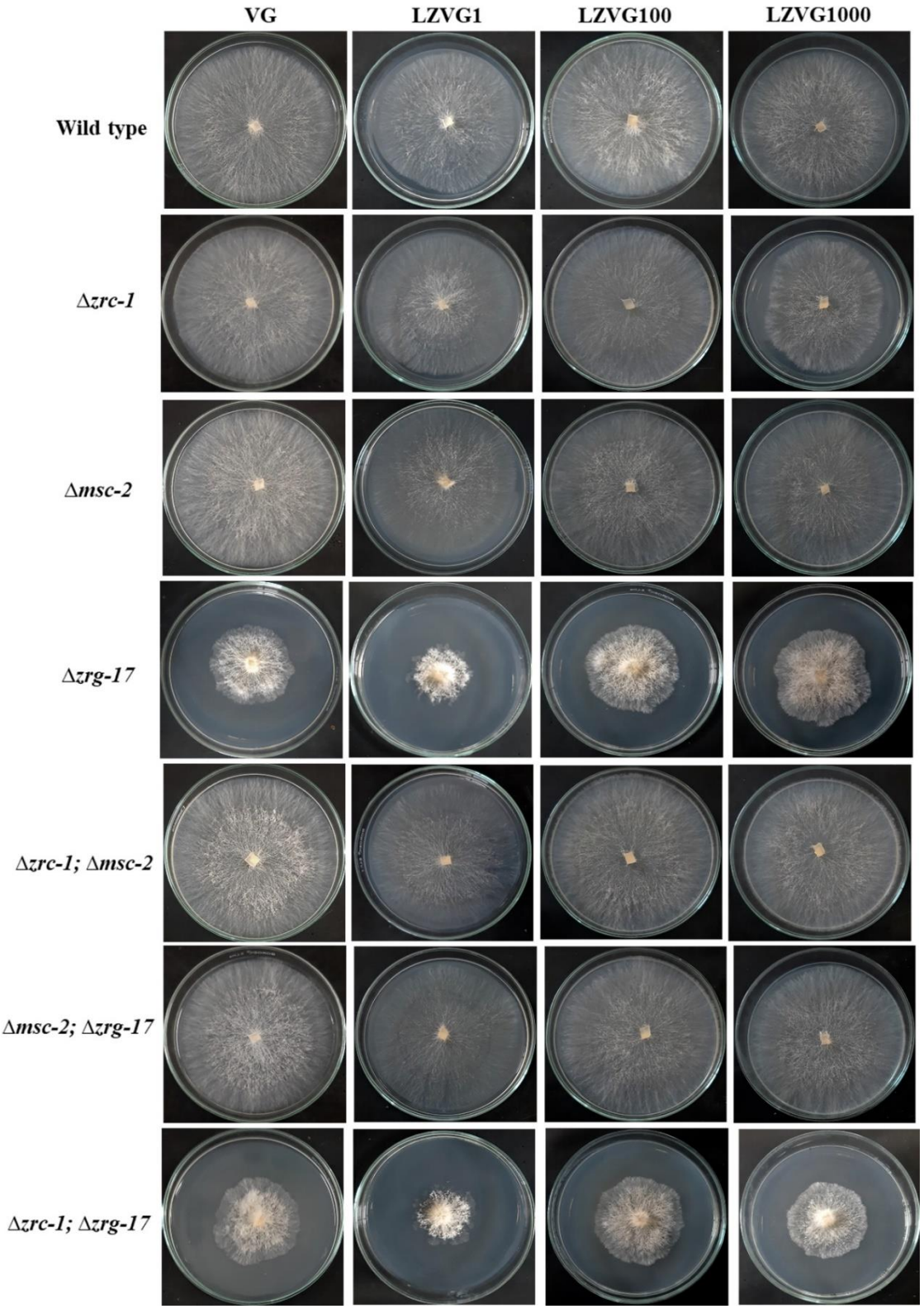

(B)

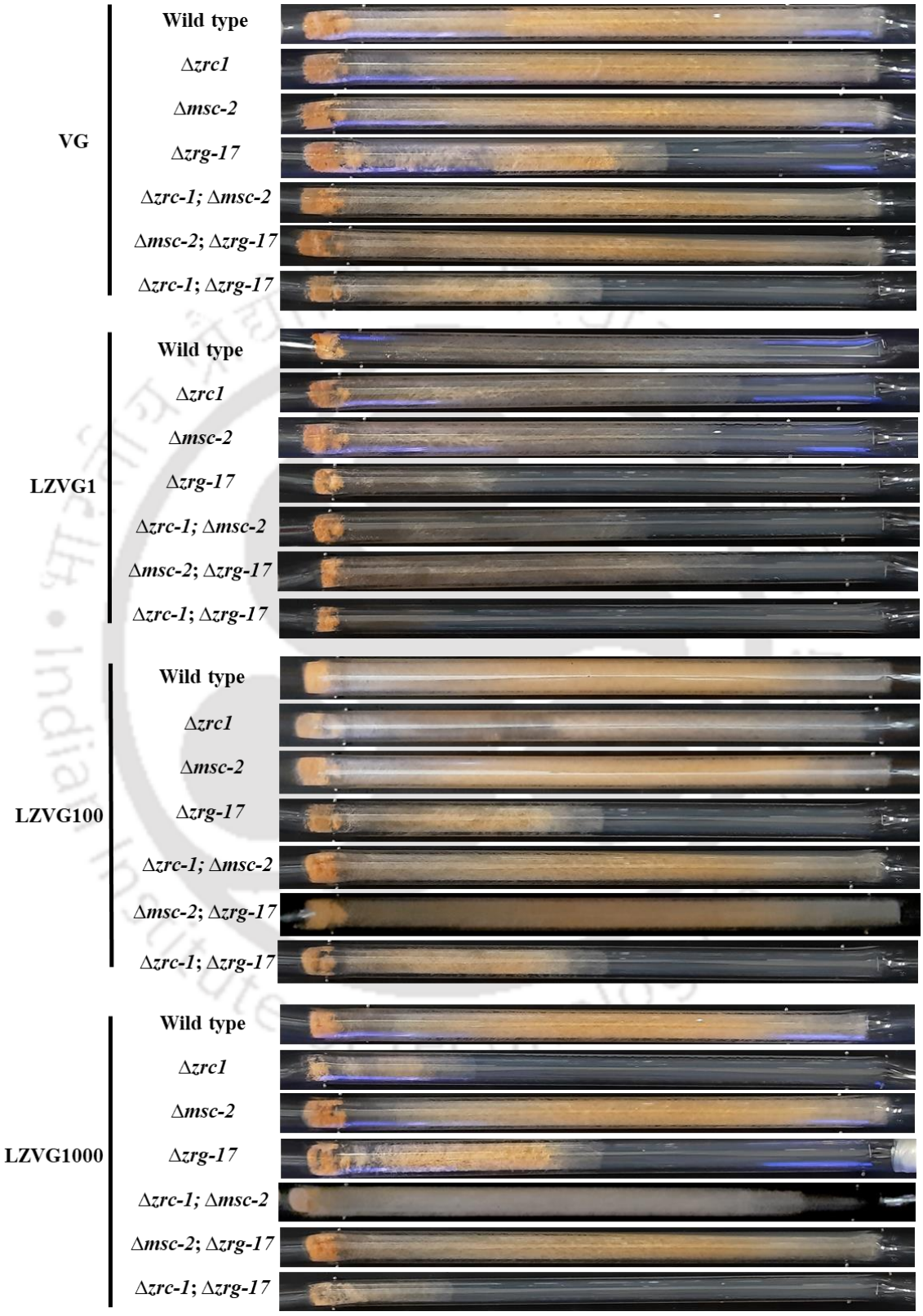

(C)

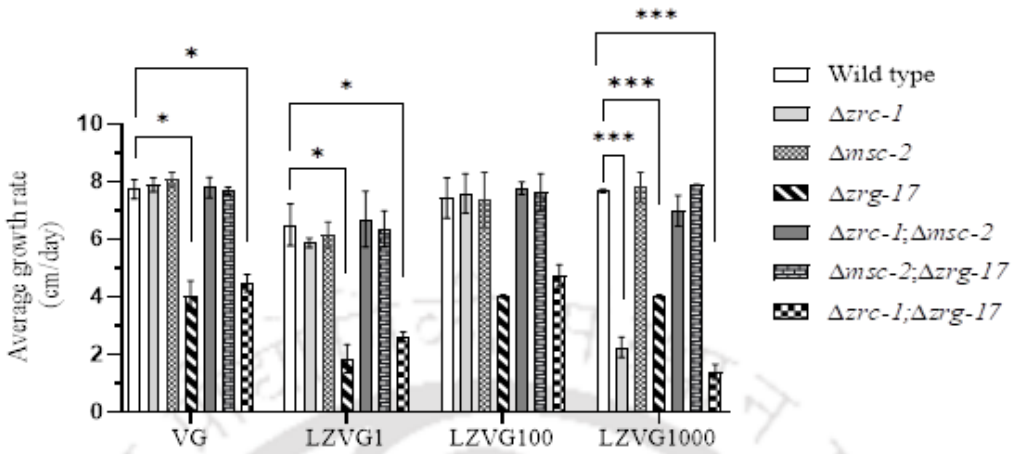

(D)

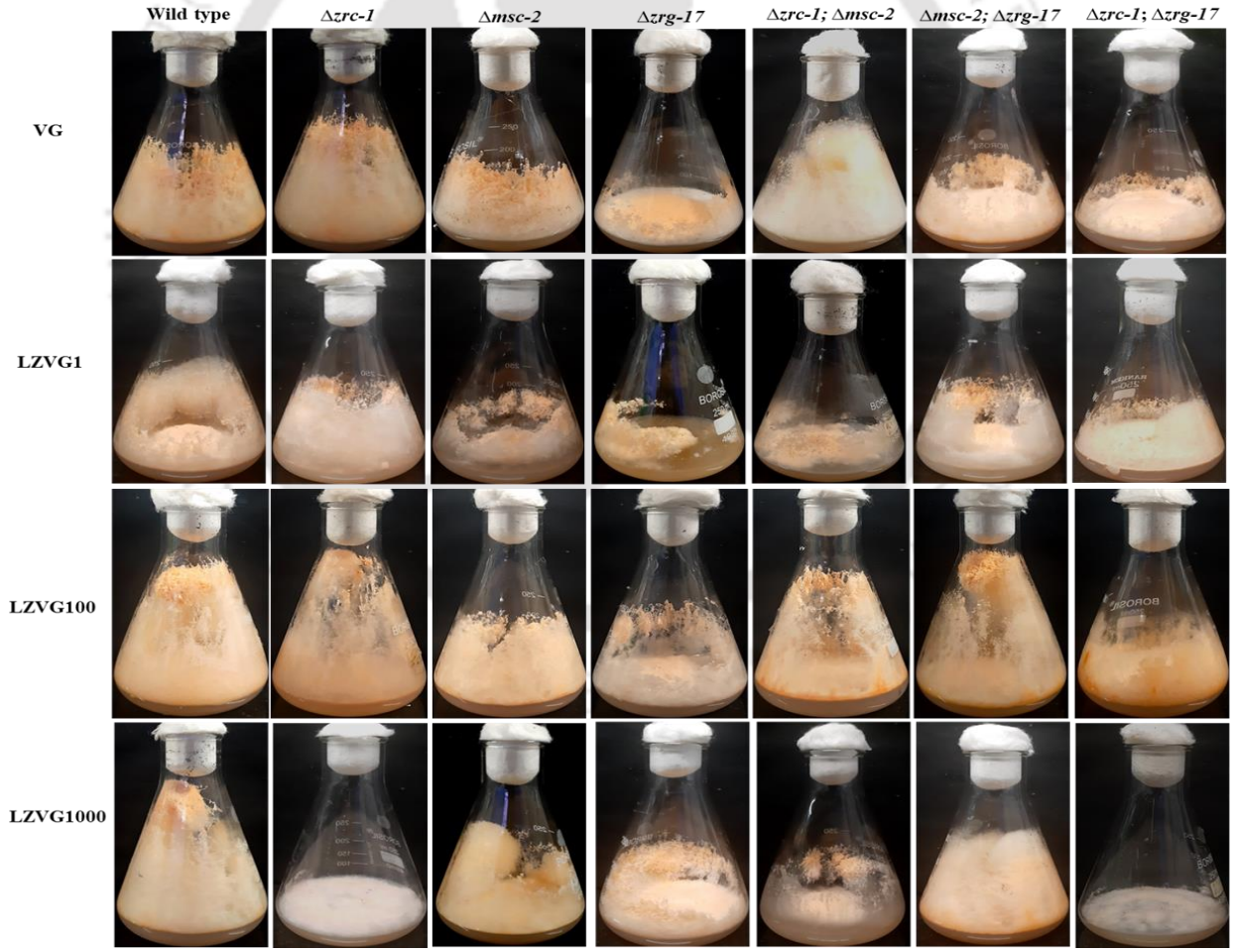

Figure 4.3 Growth phenotype of the wild type, Δ*zrc-1*, Δ*msc-2*, and Δ*zrg-17* single mutant and double mutant strains under different zinc concentrations. (A) Colony morphology of the mutant strains. The average colony growth rate of the strains under different concentrations of zinc was measured using 90 mm Petri dishes. The agar plugs of the strains were inoculated and incubated at 30 °C in the dark for 21 h and photographed. **(B)** Apical growth of the mutant strains. The apical growth was observed using race tubes. The strains were inoculated at one end of the tube containing VG agar media with different zinc concentrations and incubated at 30 °C in the dark for three days and photographed. **(C)** Average growth rate of the mutant strains. The growth rates were measured and average growth rates of each strain were calculated and the data expressed as cm/day were plotted on the graph. Error bars represent the standard deviations estimated from the data for three separate experiments (n = 3) with P-values < 0.05 (*), <0.01 (**), and <0.001 (***) compared with the wild type strain as measured by two-way ANOVA with Tukey's *post hoc* test. **(D)** The Flask morphology of mutant strains was examined under different concentrations of zinc. The agar plug of each mutant strain was inoculated in a 250 ml flask and incubated at 30 °C in the dark for 4 days in the dark and at room temperature for 3 days in the light and photographed.

4.2.2.2 The Δ*zrc-1*; Δ*msc-2*, Δ*msc-2*; Δ*zrg-17*, and Δ*zrc-1*; Δ*zrg-17* double mutants showed distinct aerial hyphae under different zinc conditions

In the asexual cycle, *N. crassa* produces aerial hyphae by apical extension under carbon source deprivation and in the presence of a water-air interface (Springer and Yanofsky 1989). The Δ*zrc-1*; Δ*msc-2*, Δ*msc-2*; Δ*zrg-17* and Δ*zrc-1*; Δ*zrg-17* double mutants showed distinct colony and flask morphology (Figure 4.3); therefore, I examined the aerial hyphae growth of the double mutants under different concentrations of zinc (Figure 4.4). The Δ*zrc-1*; Δ*msc-2* double mutant showed a mild decrease in aerial hyphae height when grown under high zinc (LZVG1000). The Δ*msc-2*; Δ*zrg-17*

double mutant did not show any significant difference in aerial hyphae height when compared to wild type in all the conditions tested. However, the Δ*zrc-1*; Δ*zrg-17* double mutant displayed severe aerial hyphae growth defect in all conditions, which was more pronounced in the LZVG1 or LZVG1000 medium with very short or absence of the hyphal extension (Figure 4.4).

(A)

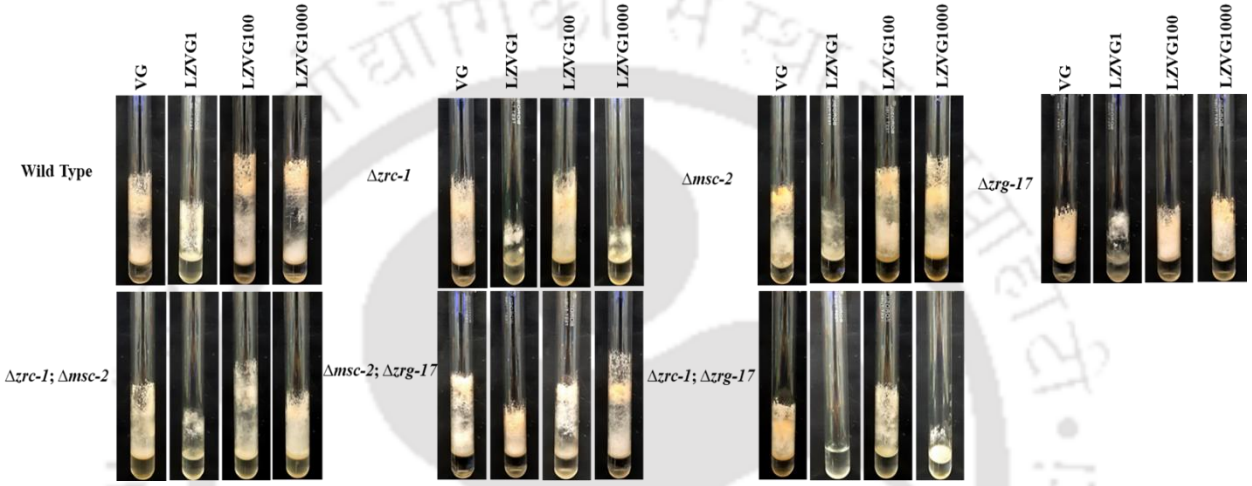

(B)

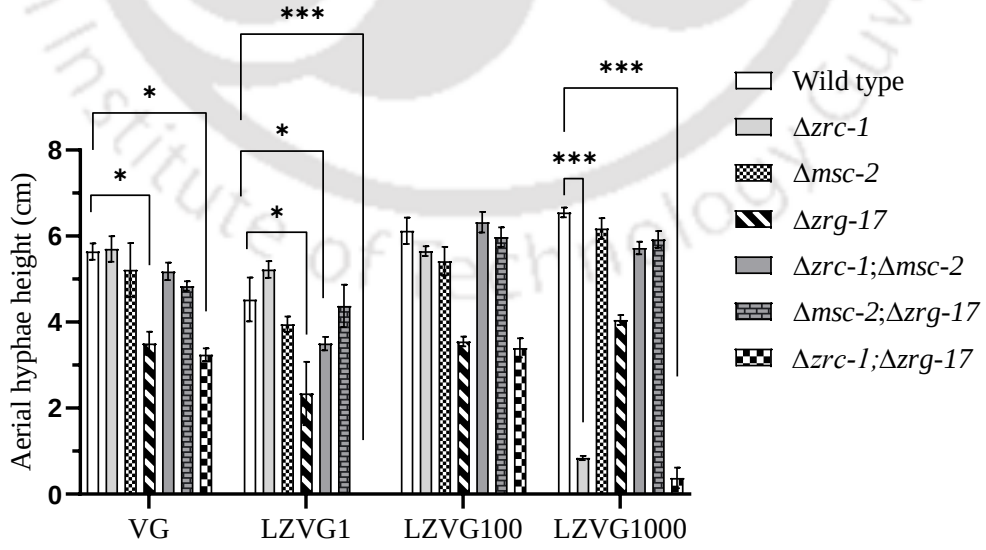

Figure 4.4 Aerial hyphae of wild type, Δ*zrc-1*, Δ*msc-2*, and Δ*zrg-17* single mutant and double mutant strains under different concentrations of zinc. (A) Aerial hyphae height of the mutant strains. The conidial suspensions (10^6 conidia/ml) were inoculated in VG liquid containing different concentrations of zinc and incubated at 30 °C in the dark for 3 days and at room temperature for 2 days in the light. **(B)** Graphical representation of aerial hyphae height of the mutant strains. The aerial hyphae heights of each mutant strain were measured and plotted on the graph. Error bars represent the standard deviations estimated from the data for three separate experiments (n = 3) with P-values < 0.05 (*), <0.01 (**), and <0.001 (***) compared with the wild type strain as measured by two-way ANOVA with Tukey's *post hoc* test.

4.2.2.3 Visualization and measurement of the inter-septal distance of *N. crassa* strains

The multinucleated cell hyphae of *N. crassa* contain septa or cross-walls, which serve as pores that allow intercompartmental exchange of nutrients and organelles, including nuclei. (Potapova and Golyshev 2016). These septations maintain the hyphal structural integrity and are essential for developmental processes, including asexual sporulation and protoperithecia formation (Rasmussen and Glass 2007; Mouriño-Pérez 2013). Therefore, I investigated if the slow growth phenotype of the Δ*zrg-17* and Δ*zrc-1*; Δ*zrg-17* mutants were due to defects in the septation using a fluorescent microscope and FESEM (Figure 4.5).

To visualize and estimate the inter-septal distance and hyphal width, I used the fluorescent blue dye calcofluor white (CFW), which binds to the cellulose and chitin of the cell wall (Seidel et al. 2013; Boyce et al. 2016). The Δ*zrc-1* and Δ*msc-2* single mutants, Δ*zrc-1*; Δ*msc-2* and Δ*msc-2*; Δ*zrg-17* double mutants had a larger hyphal compartment length at regular intervals and larger hyphal width similar to wild type. However, the Δ*zrg-17* and Δ*zrc-1*; Δ*zrg-17* mutant showed a distinctively decreased hyphal compartment length, resulting in a significant increase in the number of septa, and

shorter hyphal width (Table 4.2; Figure 4.5 A). In addition, using FESEM, I also examined for morphological variations at the septal region among the wild type and Δ*zrg-17* and Δ*zrc-1*; Δ*zrg-17* mutants (Figure 4.5 B). The strains were freshly grown in VG liquid medium for 18 h for visualization under FESEM. The mycelium was incorporated on a thin glass slide and dried at 40 °C for 8 h to 10 h. After drying, the glass slide was mounted onto the stub, coated with gold, and observed under a FESEM (Gemini 300, Carl Zeiss). The Δ*zrg-17* and Δ*zrc-1*; Δ*zrg-17* mutants showed a significant constriction in the septation site unlike to wild type (Figure 4.5 B).

(A)

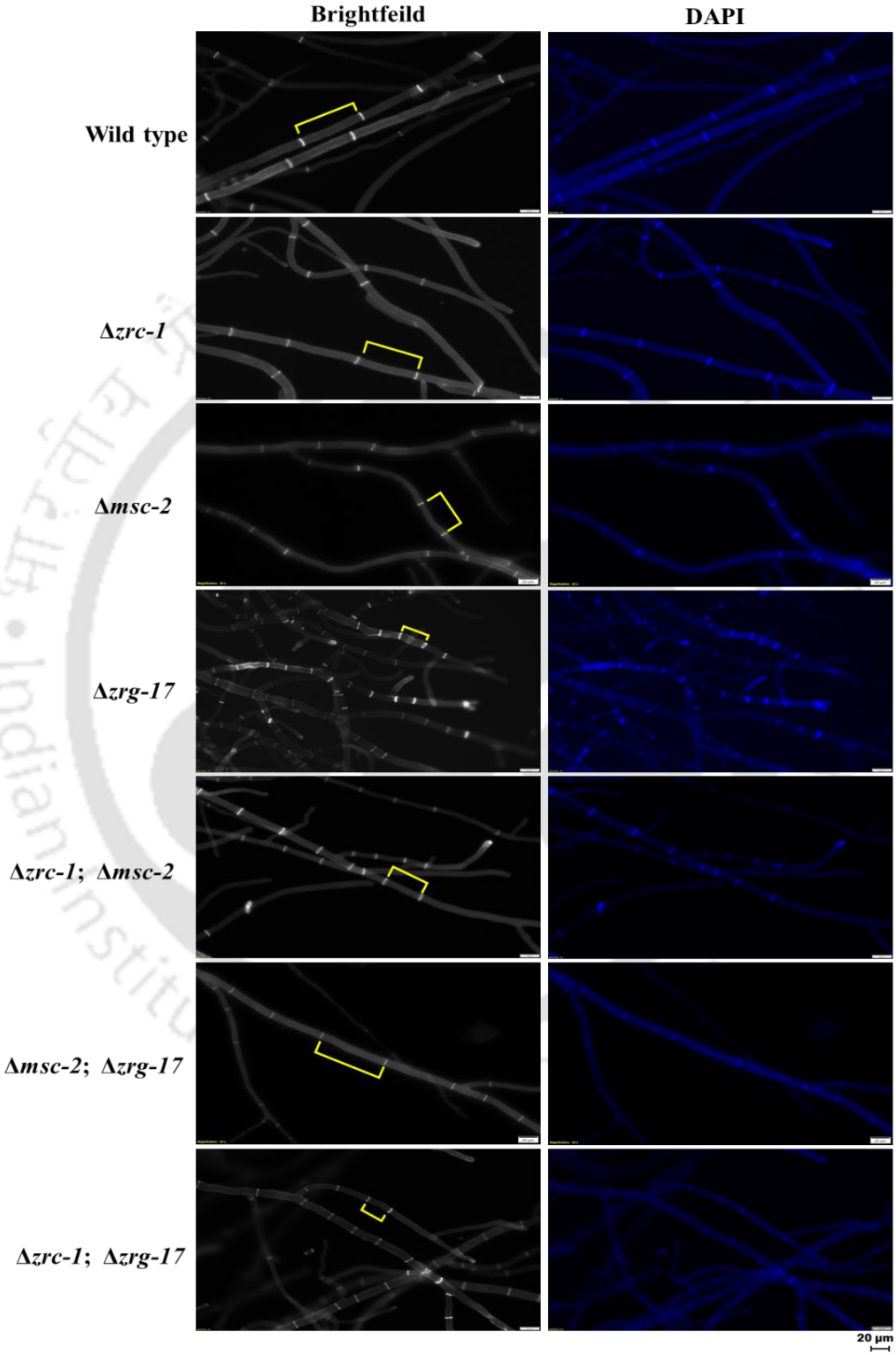

(B)

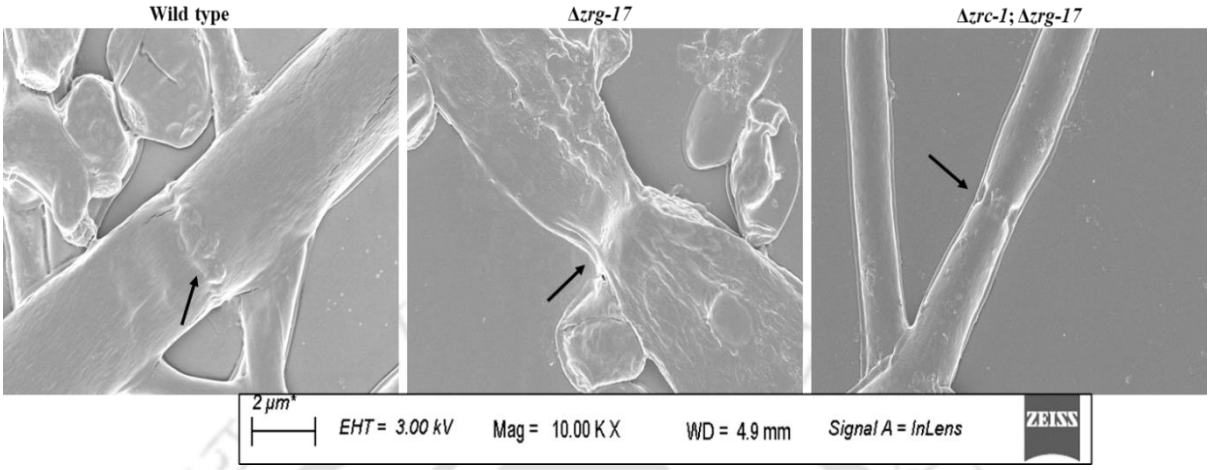

Figure 4.5 Visualization of internal septation of wild type, Δ*zrc-1*, Δ*msc-2*, and Δ*zrg-17* single and double mutant strains. (A) Visualization of septa of *N. crassa* strains using calcofluor (CFW) staining. The strains were grown on VG agar for 12 h at 30 °C, and visualized under a microscope using a DAPI filter (Olympus CKX53). Scale bar 20 µm. **(B)**. Analysis of septation of *N. crassa* strains using FESEM. The difference in structure in the area of septation of the wild type and the Δ*zrg-17* and Δ*zrc-1*; Δ*zrg-17* mutants are visible in the FESEM micrograph. Scale bar 2 µm.

Table 4.2 Hyphal compartment length and hyphal width of *N. crassa* strains

Strains	**Average length (µm)[a]**		**Septation length (µm)**	
	Hyphal width (n = 30)	**Septation length (n = 30)**	**Maximum**	**Minimum**
Wild type	10.4 ± 2.4	81 ± 26	135.99	32.85
Δ*zrc-1*	7.66 ± 2.66	81.33 ± 29.44	90.937	20
Δ*msc-2*	10.33 ± 4	80.33± 26.33	122.66	20
Δ*zrg-17*	7 ± 3 (**)	28.83 ± 10.53 (***)	57.937	16.68

Δ*zrc-1*; Δ*msc-2*	9.2 ± 4	84 ± 19	116	16
Δ*msc-2*; Δ*zrg-17*	8.66 ± 5	79.66 ± 25.16	127	20
Δ*zrc-1*; Δ*zrg-17*	7 ± 2.6 (**)	32 ± 10.75 (***)	52.66	19.06

[a]Results are shown as mean ± standard deviation for three independent experiments (n = 30) with *P-values* < 0.05 (*), < 0.01 (**), and < 0.001 (***) compared with the wild type strain as measured by one-way ANOVA.

4.2.3 The *zrc-1*, *msc-2,* and *zrg-17* genetically interact for asexual sporulation in *N. crassa*

4.2.3.1 The Δ*zrc-1*; Δ*zrg-17* double mutant showed early and enhanced conidiation

The zinc transporter Δ*zrg-17* mutant was previously reported to have short aerial hyphae, entering the program of conidiation prematurely, while producing a significant number of conidia (Tiwari *et al.* 2018). Likewise, the Δ*zrc-1*; Δ*zrg-17* double mutant exhibited short aerial hyphae (Figure 4.4). Therefore, I tested if the short aerial hyphae of the Δ*zrc-1*; Δ*zrg-17* double mutant was due to premature conidiation. I performed the time course conidiation assay and measured the number of conidia produced by the mutants (Figure 4.6). The analysis of conidia was conducted in a repressing condition which is glucose-rich medium (VG agar containing 1.5% glucose) and total darkness, the strains were inoculated (~10^3 conidia) and incubated at 30 °C. The conidia produced were harvested and counted every 12 h till 72 h. The wild type, Δ*zrc-1* and Δ*msc-2* single and Δ*zrc-1*; Δ*msc-2*, and Δ*msc-2*; Δ*zrg-17* double mutant strains were able to produce conidia only after 48 h of inoculation. However, the Δ*zrc-1*; Δ*zrg-17* double mutant produced premature conidia as early as 12 h, similar to the Δ*zrg-17* single mutant (Figure 4.6). Furthermore, even at 72 h after inoculation, the mutant strain produced more conidia than the wild type. This indicated that the Δ*zrc-1*; Δ*zrg-17* double mutant enters the program of conidiation earlier than wild type.

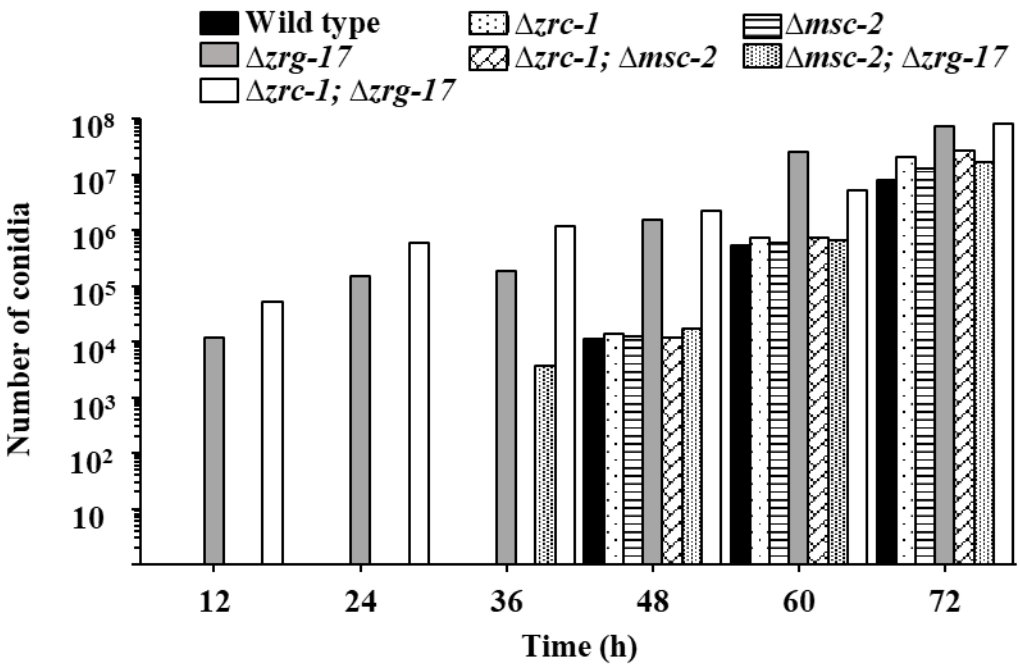

Figure 4.6 Time course conidiation of wild type, Δ*zrc-1*, Δ*msc-2*, and Δ*zrg-17* single and double mutant strains. The strains were inoculated in VG agar and incubated at 30 ˚C in complete darkness. After every 12 h interval till 72 h, the conidia of each strain were harvested and counted using a hemocytometer.

4.2.3.2 The Δ*zrc-1*; Δ*zrg-17* double mutant showed inappropriate conidiation under submerged culture and increased expression of conidiation-specific *con-10* gene

When *N. crassa* is under nutrient deprivation and the presence of an air-water interface, the aerial hyphae are formed followed by conidiation (Springer 1993). Conidiation does not generally occur in submerged culture, however, under carbon-nitrogen starvation or under cellular stress, conidiation in submerged culture has been reported in mutants of development and carotenogenesis control (*dcc-1*) (Barba-Ostria et al. 2011), and heterotrimeric guanine nucleotide binding Gα subunit (*gna-3*) (Kays and Borkovich 2004). Similarly, the Δ*zrc-1*; Δ*zrg-17* double mutant showed early and enhanced conidiation in a growth-repressing condition (Figure 4.6), therefore I examined if the double mutant

could conidiate in an unfavorable condition such as in a submerged condition. The wild-type strain produced long hyphae that interconnected to form a mycelium lacking conidiophores in a 16 h submerged culture. However, the Δ*zrg-17* and Δ*zrc-1*; Δ*zrg-17* mutants showed abundant conidiophores in submerged culture conditions corresponding to their short aerial hyphae (Figure 4.7 A). Previously, nutrient-rich peptone was added to the medium, to suppress inappropriate conidiation, which appears to have rescued the conidiation defects in submerged culture (Madi et al. 1997). Therefore, I tested if the addition of peptone in the medium can rescue the conidiation defects of Δ*zrg-17* and Δ*zrc-1*; Δ*zrg-17* mutants in submerged culture. The wild type strain remained unaffected and continued to form vegetative hyphae in the medium supplemented with 2 % peptone. Moreover, the Δ*zrg-17* and Δ*zrc-1*; Δ*zrg-17* mutants in the presence of nutrient-rich peptone in the medium were able to suppress the conidiophore formation resulting in the formation of vegetative hyphae, similar to wild type (Figure 4.7 A).

The conidiation-specific *con-10* gene is highly expressed during the conidiation process in the vegetative phase in *N. crassa* (Roberts et al. 1988; Navarro-Sampedro et al. 2008; Park and Yu 2012). Therefore, I examined the transcriptional level of the *con*-10 gene by qRT-PCR in the Δ*zrg-17* and Δ*zrc-1*; Δ*zrg-17* mutants. As expected, the *con-10* gene was overexpressed in the mutants in submerged culture, however, the expression was similar to the wild type when peptone was supplemented to the medium (Figure 4.7 B). Therefore, the inappropriate conidiation of the Δ*zrg-17* and Δ*zrc-1*; Δ*zrg-17* mutants in the submerged culture condition were consistent with the overexpression of *con-10*, indicating that ZRG-17 might play a role in regulating the expression of *con-10*.

(A)

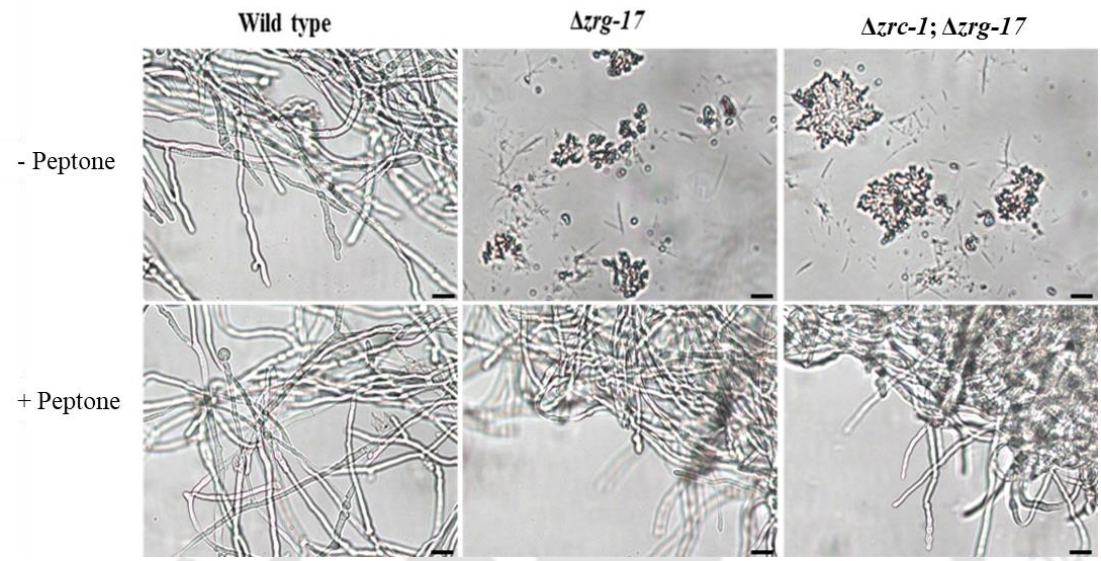

(B)

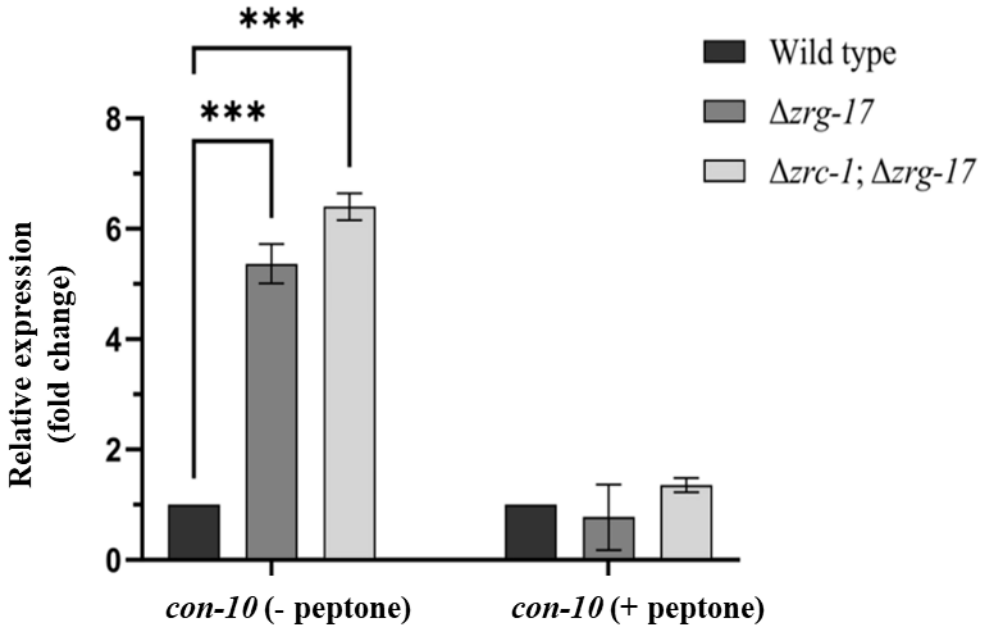

Figure 4.7 Conidiophore formation in submerged cultures of the wild type, Δ*zrg-17* and Δ*zrc-1*; Δ*zrg-17* mutant strains. (A) Visualization of conidiophore formation in the submerged condition.

Conidial suspensions (10^6 conidia/ml) were inoculated in VG liquid with and without peptone (2%) and the development of conidiophore and conidial germination into mycelium was observed under a microscope (Nikon Eclipse Ti-S inverted microscope, DS-Fi2-U3, Japan) after 16 h (Barman and Tamuli 2017). Scale bar 20 µm. **(B)** The *con-10* gene expression. The expression of the *con-10* gene was determined by qRT-PCR in three biological replicates. The relative expression of the *con-10* gene was normalized with the expression of *β-tubulin* and values were compared to that of wild type. Error bars indicate the standard deviation calculated from data of three independent experiments. The asterisk represents a significant difference when comparing the expressions with the wild type, as measured by two-way ANOVA analysis with Tukey's *post hoc* test with P-values < 0.05 (*), < 0.01 (**), and < 0.001 (***).

4.2.4 Endoplasmic Reticulum stress assay

4.2.4.1 The Δ*zrc-1*; Δ*msc-2* and Δ*zrc-1*; Δ*zrg-17* double mutants showed sensitivity to dithiothreitol (DTT)

In *S. cerevisiae*, zinc is transported from the cytoplasm into the ER by Msc2p, which is localized in the ER membrane. The deletion of *MSC2* causes ER stress under low zinc conditions and causes activation of the unfolded protein response (UPR) system (Ellis et al. 2004). In addition, the ZRG-17 in *N. crassa* plays a critical role in survival under the ER stress in low zinc conditions (Tiwari et al. 2018). In Chapter 3, I have concluded that the ZRC-1 and MSC-2 are *N. crassa* orthologs of the *S. cerevisiae* Zrc1p and Msc2p, respectively. Therefore, under various concentrations of dithiothreitol (DTT), I examined the fungal growth of the wild type, the Δ*zrc-1* and Δ*msc-2* single mutants, and the Δ*zrc-1*; Δ*msc-2*, Δ*msc-2*; Δ*zrg-17* and Δ*zrc-1*; Δ*zrg-17* double mutants. DTT is known to induce endoplasmic reticulum (ER) stress by inhibiting the formation of disulfide bonds and disrupting protein folding (Freedman 1995; Feige and Hendershot 2011). The Δ*zrc-1*, Δ*msc-2*, and Δ*msc*-2; Δ*zrg-*

17 mutants showed growth reduction similar to the wild type in the medium containing 2 mM DTT (Figure 4.8). However, the Δ*zrc-1*; Δ*msc-2* and Δ*zrc-1*; Δ*zrg-17* double mutants showed shorter aerial hyphae height, reduced growth rates of 29% and 24%, respectively, while the wild type showed reduced growth of 45% in the presence of 2 mM DTT (Figure 4.8). This suggested that CDF zinc transporters may be essential for ensuring the effective functioning of the ER in *N. crassa.*

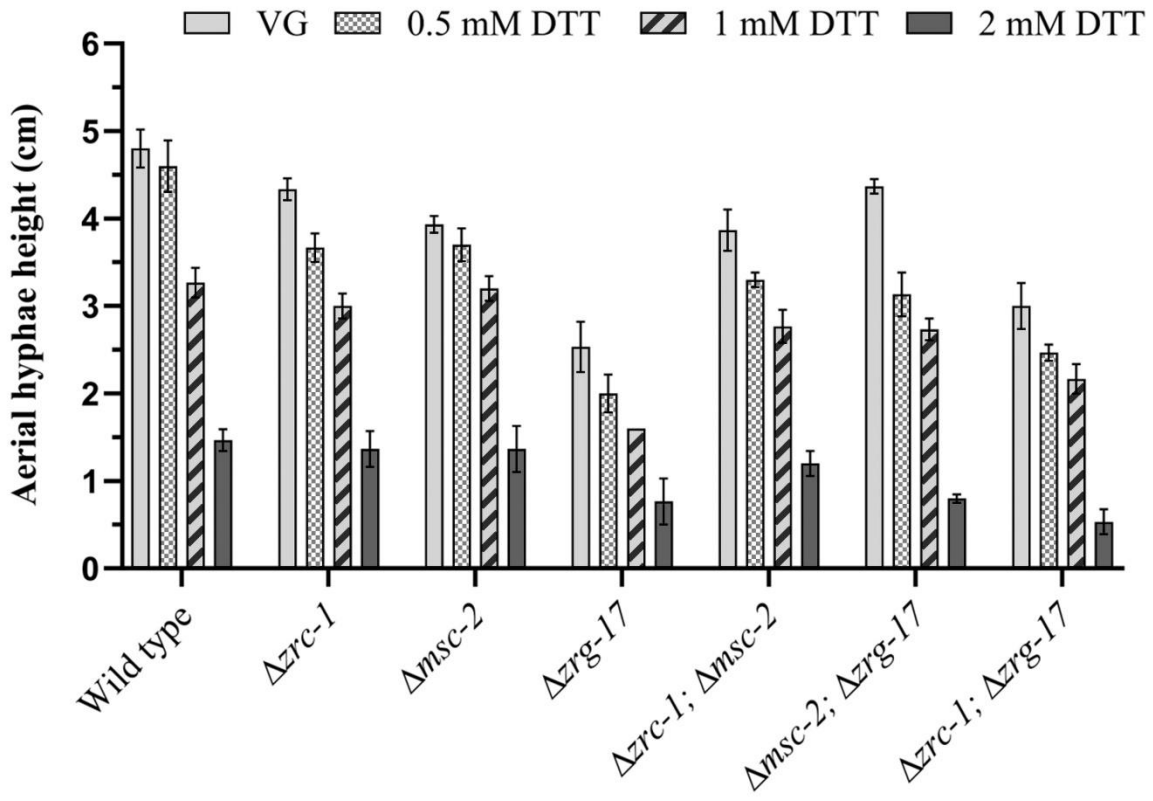

Figure 4.8 ER stress assay. DTT induced ER stress assay on wild type, Δ*zrc-1*, Δ*msc-2*, and Δ*zrg-17* single mutant and double mutant strains. The ability of the strains to produce aerial hyphae under different concentrations of DTT was examined. About 10^6 conidia/ml conidial suspension were inoculated in VG liquid media containing different concentrations of DTT (0.5 mM, 1 mM, and 2 mM) and incubated at 30 °C for 3 days in the dark and 2 days under the light, and the aerial hyphae

height of the strains were measured. Error bars indicate the standard deviations calculated from the data of three independent replicates.

4.2.4.2 The CDF zinc transporters of *N. crassa* are required for cellulose degradation under different zinc conditions

Glucose deprivation in the medium causes an environmental stress on the ER, which leads to interference with N-linked protein glycosylation (Scheuner et al. 2001). Therefore, glucose was replaced with cellulose in the medium causing a glucose-deprived environment to evaluate the effect of the glucose deprivation in the mutants. The CDF mutants were cultured in the liquid medium containing avicel (1.5% crystalline cellulose), with various concentrations of zinc. The cultures were incubated at 30 °C, in complete darkness for 7 days, with constant shaking at 180 rpm. After 7 days, the wild type, Δ*zrc-1*, Δ*msc*-2, and Δ*msc*-2; Δ*zrg-17* strains appeared to degrade cellulose (Figure 4.9 A). The Δ*zrc-1* was unable to grow and produce any mycelial mass at high zinc conditions (LZVG1000), however, the growth of the Δ*zrg-17*, Δ*msc-2*; Δ*zrc-1* and Δ*zrc-1*; Δ*zrg-17* mutants were severely impaired in all the concentrations of zinc tested (Figure 4.9 A). In addition, I measured the biomass produced from the growth culture simultaneously, and the growth of the strains in the liquid culture complemented their biomass weights (Table 4.3).

The strains showing growth defects under cellulose as the sole carbon source might secrete a reduced amount of cellulase enzyme, which could explain the inability of the mutant to grow and produce biomass in the cellulose medium. Therefore, I determined the concentrations of the secreted protein in the cultures and the glucose concentration to determine the cellulase activity (Mishra et al. 1984; Starr and Gonc 2018). The wild type, Δ*msc-2,* and Δ*msc-2*; Δ*zrg-17* mutant showed higher concentrations of protein and glucose in the supernatant (Figure 4.9 B, C). However, the Δ*zrc-1* showed a significant decrease in the concentration of protein and glucose in the high zinc condition.

Furthermore, Δ*zrg-17*, Δ*zrc-1*; Δ*msc-2* and Δ*zrc-1*; Δ*zrg-17* mutants secreted severely low protein and glucose in the supernatant, which was consistent with the growth and biomass accumulation of these mutants (Figure 4.9 B and C). These results demonstrated the significance of CDF zinc transporters in maintaining zinc homeostasis for degrading cellulose.

Table 4.3 Biomass accumulation in *N. crassa* strains

	Biomass weight (mg/ dry weight)[a]		
Strains	VC	LZVC1	LZVC1000
Wild type	714 ± 31.7	363 ± 55	868 ± 34
Δ*zrc-1*	676 ± 73.7	418 ± 40	-
Δ*msc-2*	662 ± 75.1	432 ± 44	637 ± 29
Δ*zrg-17*	-	-	118 ± 41 (***)
Δ*zrc-1*; Δ*msc-2*	-	-	-
Δ*msc-2*; Δ*zrg-17*	689 ± 35.8	342 ± 37	737 ± 22
Δ*zrg-17*; Δ*zrc-1*	-	-	-

[a]Results are shown as mean ± standard deviation for three independent experiments (n = 3) with *P-values* < 0.05 (*), < 0.01 (**), and < 0.001 (***) compared with the wild type strain as measured by two-way ANOVA with Tukey's *post hoc* test.

(A)

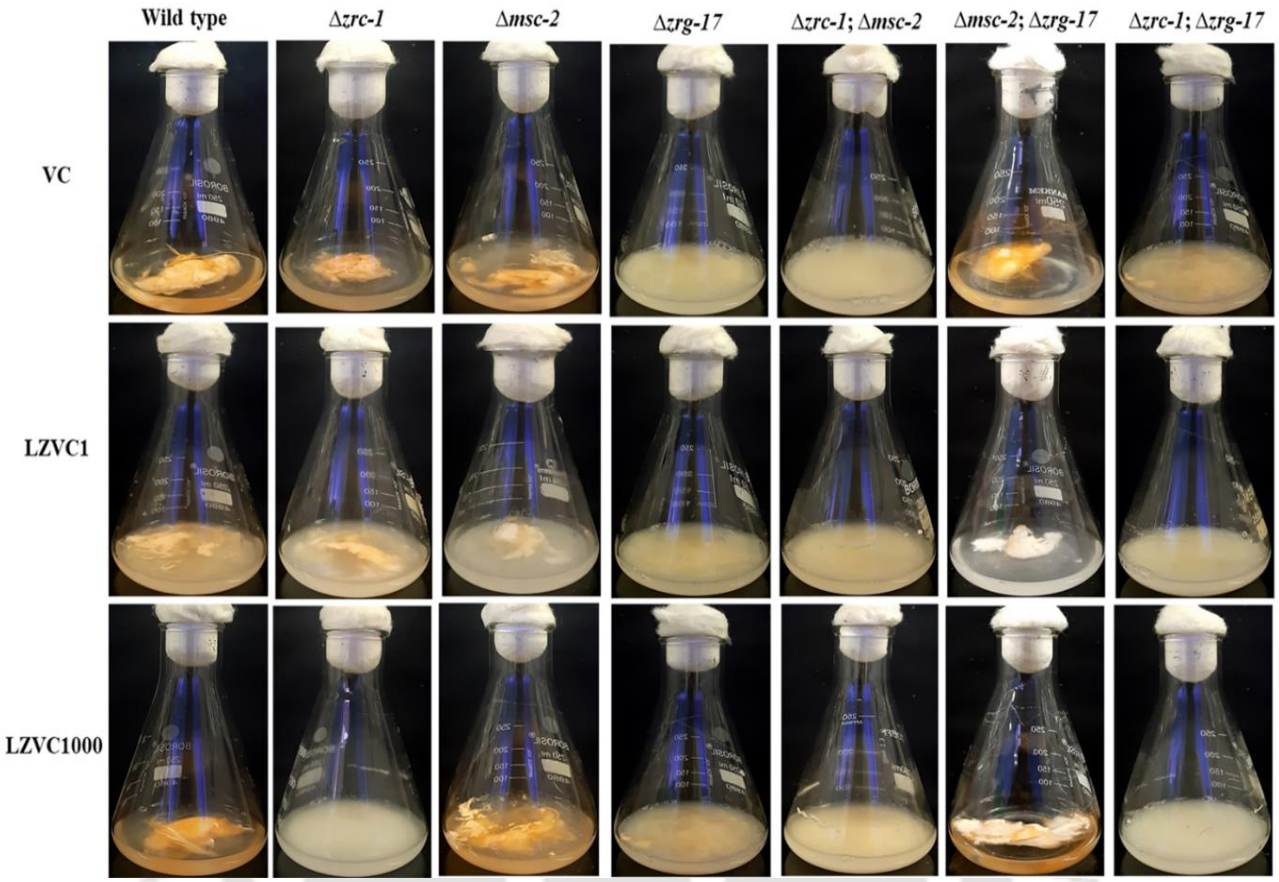

(B)

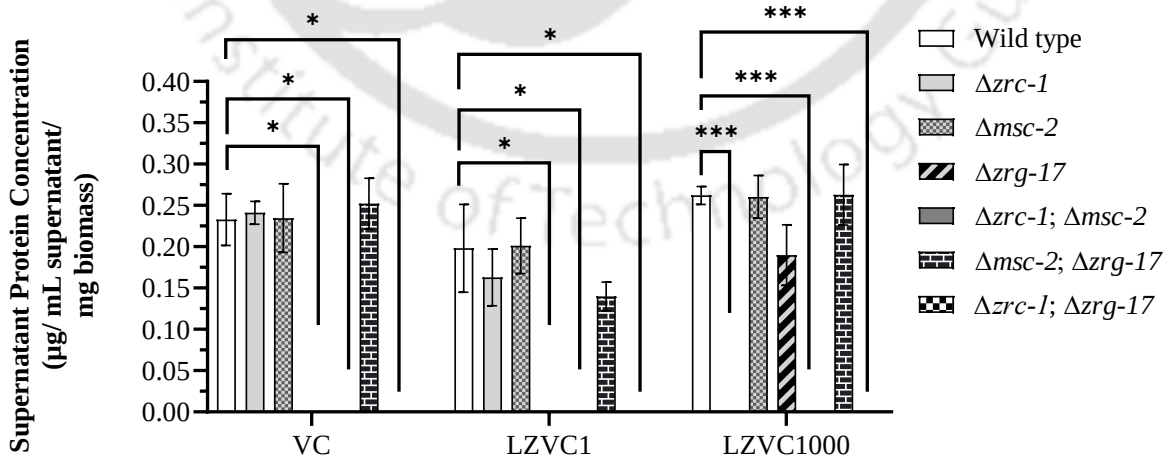

(C)

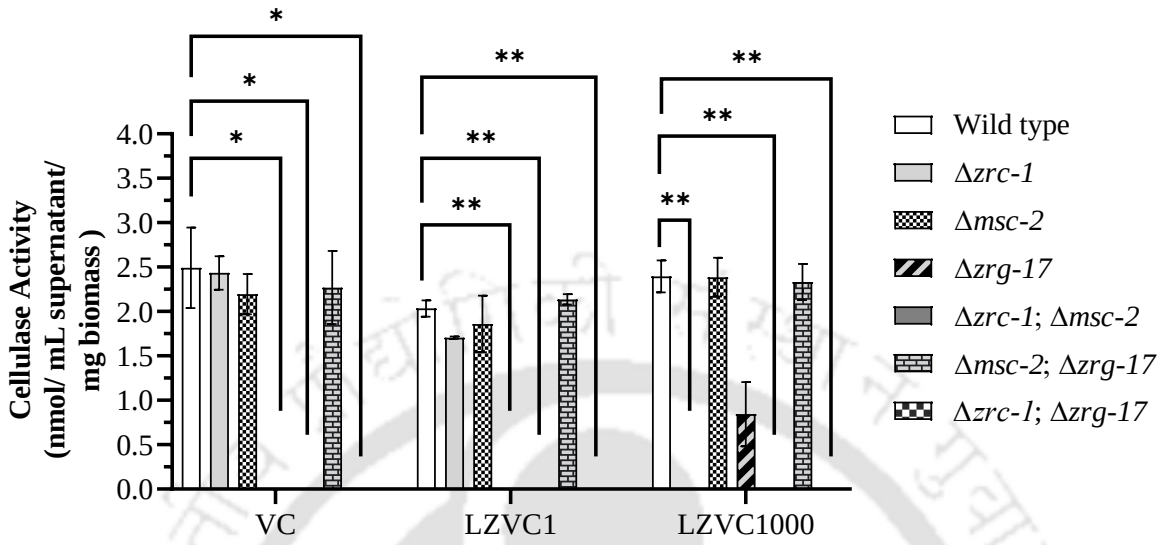

Figure 4.9 Cellulose degradation assay in the wild type, Δ*zrc-1*, Δ*msc-2*, and Δ*zrg-17* single mutant and double mutant strains under different concentrations of zinc. Degradation of cellulose in different concentrations of zinc. Approximately, 10^6 conidia/ml conidial suspension was inoculated in 50 ml Vogel's cellulose liquid media (VC, replacing glucose with 1.5% cellulose) containing different concentrations of zinc (LZVC1, LZVC100, LZVC1000) in 250 ml flask and incubated at 30 °C with shaking at 180 rpm for 7 days. **(A)** Flask morphology of the *N. crassa* strains. **(B)** Protein concentrations of each strain under different zinc concentrations. The concentrations of protein in the supernatant for each strain were measured by Bradford assay using Bovine serum albumin (BSA) as control (Bradford 1976). **(C)** Cellulase activity of the strains. The glucose released in the supernatant in the medium under different conditions of varying zinc concentrations was measured using D-glucose as standard by 3, 5-Dinitrosalicylic acid (DNSA), which is a reducing agent used to determine the reducing sugar present in samples. Results are shown as mean ± standard deviation for three independent experiments (n = 3). The asterisk represents a significant difference

when comparing with the wild type, as measured by two-way ANOVA analysis with Tukey's *post hoc* test with P-values < 0.05 (*), < 0.01 (**), and < 0.001 (***).

4.2.5 Temperature sensitivity assay

4.2.5.1 The Δ*zrc-1*, Δ*msc-2*, and Δ*zrg-17* single and double mutants showed insensitive to variation in temperature

In addition to nutritional conditions, temperature is another environmental aspect that has an important effect on the growth of *N. crassa*. When exposed to a temperature that is within the optimal range, an array of proteins are produced which has an impact on the growth of *N. crassa* (Plesofsky-Vig and Brambl 1985; Ivey et al. 2002). In the cellulose degradation assay (Figure 4.9), the amount of protein released by the mutants was significantly less than the wild type, which correspond to the growth of the CDF zinc transporter mutants. Therefore, I determined the growth rates of the CDF zinc transporter mutants under different temperatures (20 °C, 30 °C, and 40 °C). For each strain, the growth rates at 20 °C (low) and 40 °C (high) were compared to the ambient temperature 30 °C, where the growth was maximum. In the VG agar medium containing standard amounts of zinc, the Δ*zrc-1*, Δ*msc-2*, Δ*zrg-17* single mutants and the Δ*zrc-1*; Δ*msc-2*, Δ*msc-2*; Δ*zrg-17*, and Δ*zrc-1*; Δ*zrg-17* double mutants did not show any distinct significant difference in the growth rates compared to the wild type in all the temperatures tested (Figure 4.10).

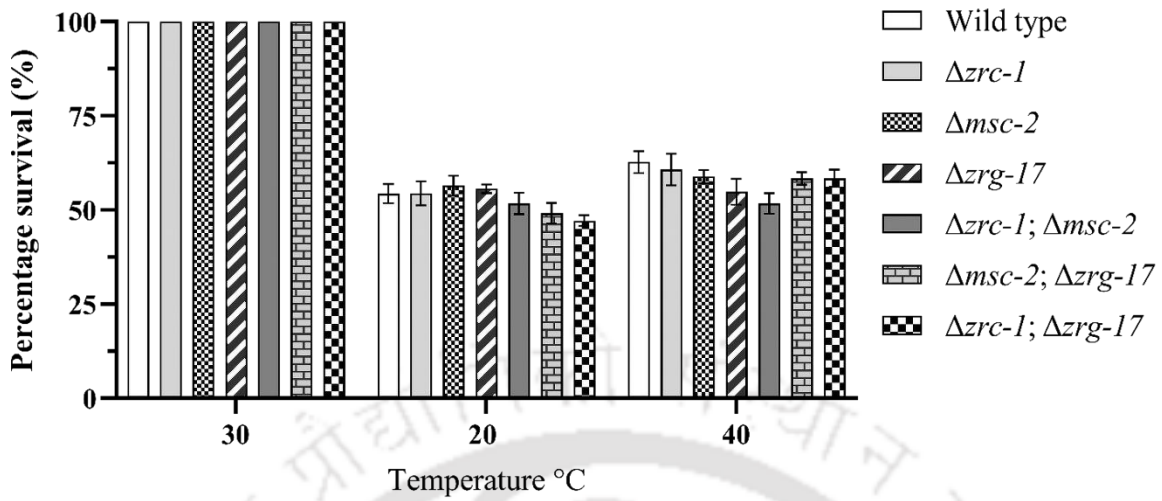

Figure 4.10 Assay for temperature sensitivity. Temperature sensitivity of the wild type, Δ*zrc-1*, Δ*msc-2*, and Δ*zrg-17* single and double mutant strains. The average growth of the strains was determined at low (20 °C) and high (40 °C) temperatures relative to the growth at the control temperature (30 °C). The error bars indicate the average standard deviation calculated from data from three independent experiments (n = 3).

4.2.6 pH-induced stress assay and Osmotic stress assay

4.2.6.1 The Δ*zrc-1*, Δ*msc-2*, and Δ*zrg-17* single and double mutant strains showed insensitivity to pH and Osmotic stress conditions

The extracellular pH and the salt concentrations are critical aspects of the environment to which organisms must adapt. The CDF zinc transporter mutants were grown under acidic (pH 3.8) and alkaline pH (7.8) medium and varying concentrations of NaCl (0.5 M and 1 M) and KCl (0.5 M and 1M). In the pH tolerance assay, I determined the ability of the strains to produce aerial hypha. The aerial hyphae height of each strain under pH 3.8 and pH 7.8 were measured and compared to the growth of the normal VG medium whose pH is 5.8 (Figure 4.11 A). Likewise, I measured the colony growth rates of the strains under increasing concentrations of NaCl and KCl (Figure 4.11 B). The Δ*zrc-*

1, Δ*msc-2*, and Δ*zrg-17* single mutants and Δ*zrc-1*; Δ*msc-2*, Δ*msc-2*; Δ*zrg-17*, and Δ*zrc-1*; Δ*zrg-17* double mutants did not show any distinct significant difference in the growth rates as compared to the wild type in all pH tested as well as in osmotic stress (Figure 4.11).

(A)

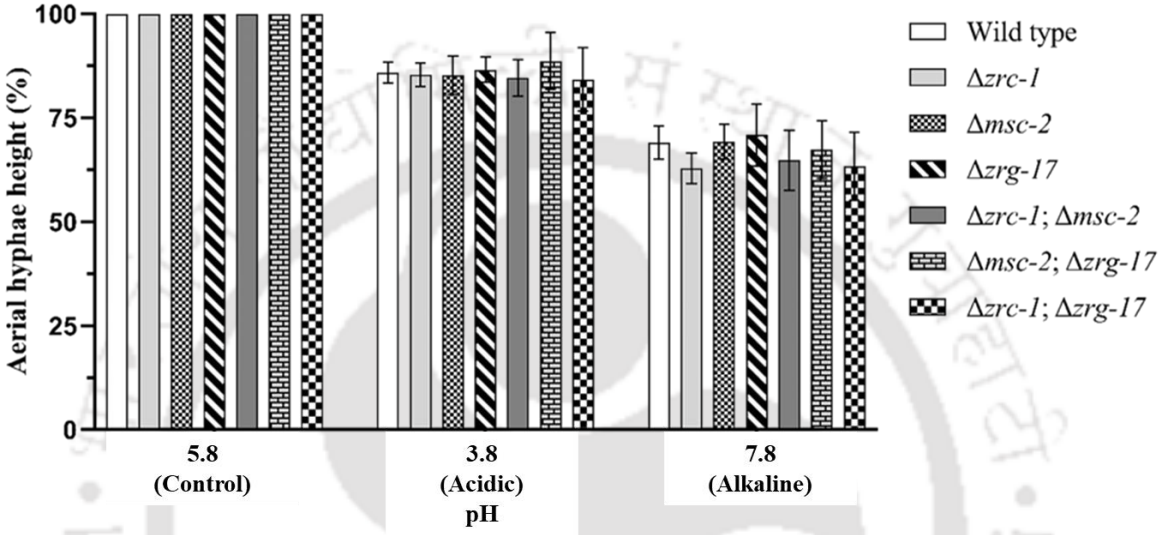

(B)

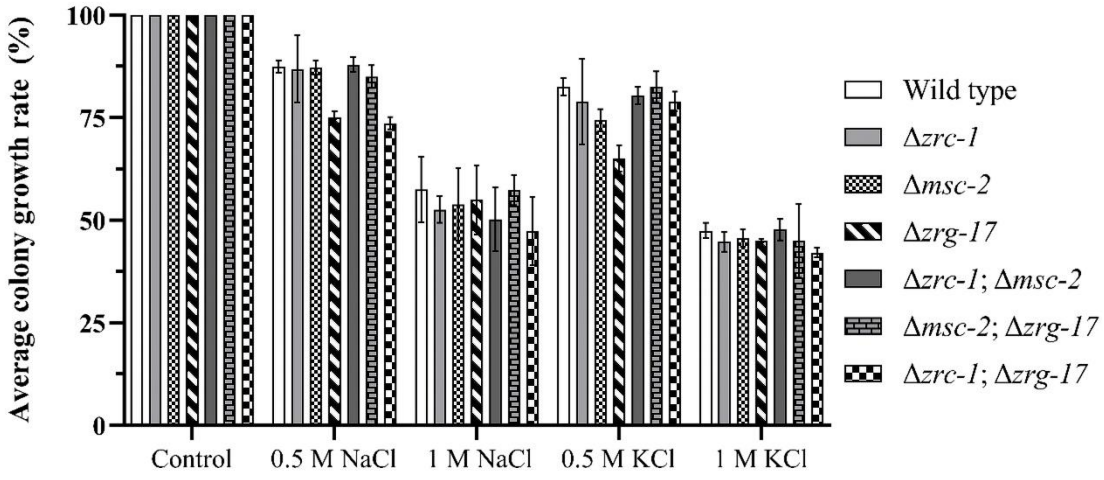

Figure 4.11 Average growth rate under the pH and osmotic stress conditions of wild type, Δ*zrc-1*, Δ*msc-2*, and Δ*zrg-17* single and double mutant strains. (A) pH sensitivity assay. The conidial suspension (10^6 conidia/ml) were inoculated in the medium containing different pH and the hyphal height was measured and compared to the aerial hyphae height at the standard VG medium. **(B)** Osmotic stress assay. The strains were cultures in the medium supplemented with various amounts of NaCl and KCl. The average colony growth rates were measured and compared to the growth rate in the standard VG medium. The error bars indicate the average standard deviation calculated from data from three independent experiments (n = 3).

4.2.7 Azole sensitivity assay

4.2.7.1 The Δ*zrc-1*, Δ*msc-2*, and Δ*zrg-17* single and double mutants were insensitive to azole stress

I examined the susceptibility of the Δ*zrc-1*, Δ*msc-2*, and Δ*zrg-17* single mutants and double mutants to antifungal azoles. The lanosterol 14-α-demethylase (ERG11) is targeted by azoles, thereby inhibiting ergosterol biosynthesis, which is the major component of the fungal cell wall (Shapiro et al. 2011). I used two azole drugs fluconazole (5 µg/ml) and ketoconazole (5 µg/ml) and the sensitivity of the strains to the drugs was determined by the relative inhibitory rates $= \left(1 - \frac{Diameter\ of\ the\ colony\ plate\ with\ drug}{Growth\ time} / \frac{Diameter\ of\ the\ colony\ plate\ without\ drug}{Growth\ time}\right) * 100\%$ (Zhou et al. 2022). The inhibitory rates of the drugs to the mutants were similar to the wild type strain (Figure 4.12).

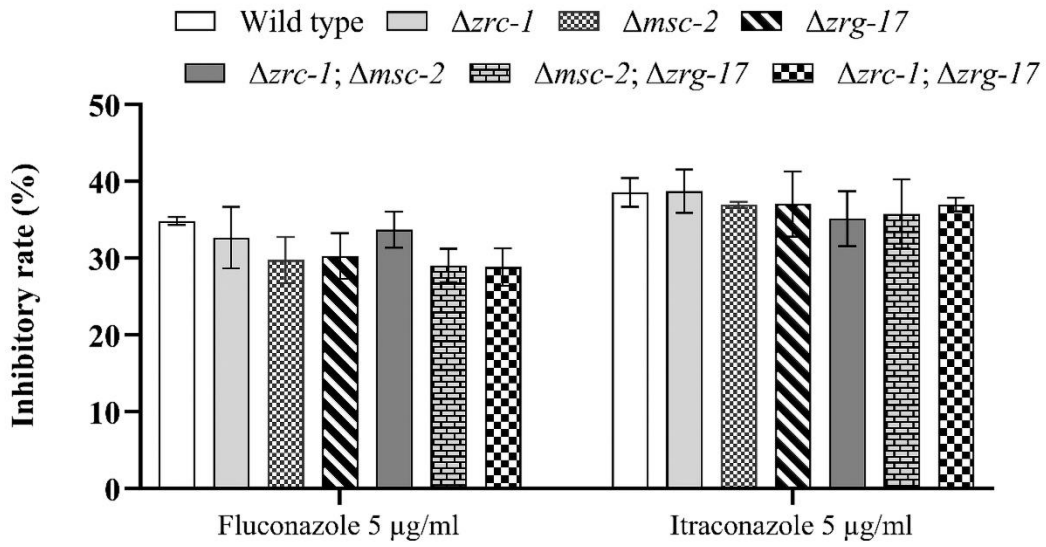

Figure 4.12 Susceptibility of the wild type, Δ*zrc-1*, Δ*msc-2*, and Δ*zrg-17* single and double mutant strains to fluconazole and itraconazole. The average colony growth rates of the strains cultured in the medium supplemented with fluconazole and itraconazole were measured and compared to the growth rate in the standard VG medium. Relative growth inhibition rates of the strains were determined based on colony diameters of the strains grown on plates with and without azole at indicated growth time. The error bars indicate the average standard deviation calculated from data from three independent experiments (n = 3).

4.2.8 Generation of the Δ*zrc-1*; Δ*msc-2*; Δ*zrg-17* triple mutant strain

To generate the Δ*zrc-1*; Δ*msc-2*; Δ*zrg-17* triple mutant, the Δ*zrc-1*; Δ*msc-2 mat A* double mutant was crossed with the opposite mating type of the Δ*zrg-17* single mutant (Table 2.2; Figure 4.13). The crosses were incubated at 22 °C in complete darkness and after 7 days of incubation, the plates were flipped upside down and incubated for another 14 days and the resulting ascospores from these crossings were harvested. Gemination of these ascospores were carried out on FGS medium by giving heat shock at the conditions described below.

1. 60 °C for 45 min (Set I, 114 progenies)
2. 58 °C for 45 min (Set II, 60 progenies) and
3. 65 °C for 30 min (Set III, 60 progenies).

The progenies of all the three sets (I, II and III) were picked, grown on VG agar medium, and incubated at 30 °C for two days in the dark and for one day at room temperature under light. The progenies were screened for hygromycin B resistance, and further analyzed by PCR to confirm the presence of the respective knockout allele. The common reverse primer 5HPHR (Table 2.3) was used in combination with the forward primers HI-ZRC-1 SN, HI-MSC-2 SN, and Zrg-17-KOC-F (Table 2.3), to confirm the Δ*zrc-1*, Δ*msc-2*, Δ*zrg-17* knockout alleles respectively. Despite screening >200 progenies, none of the progeny showed knockout allele for all the three genes, suggesting that the triple mutant might be inviable.

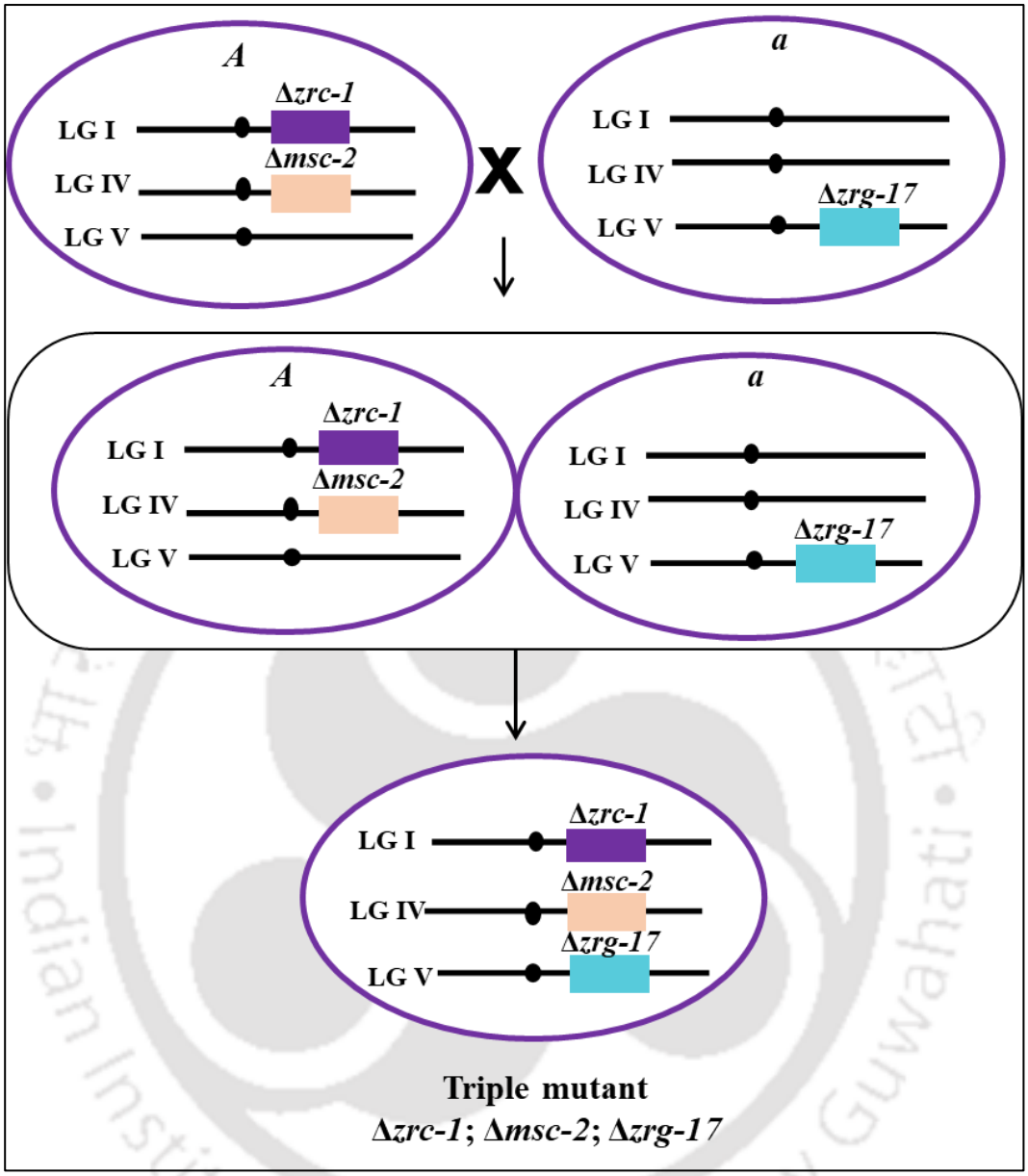

Figure 4.13 Schematic representation of generation of triple mutant. The Δ*zrc-1*; Δ*msc-2 mat A* was crossed with the Δ*zrg-17 mat a* on synthetic crossing media (Westergaard and Mitchell 1947) to generate Δ*zrc-1*; Δ*msc-2*; Δ*zrg-17*, triple mutant.

4.2.9 An overview derived from the study of the genetic interaction between the CDF zinc transporters in *N. crassa*

Analyzing double mutant phenotypes reveal gene interactions in a biological process, categorizing them as redundant, additive, or epistatic which is essential for interpreting genetic networks and understanding overall molecular and cellular mechanism (Gavric and Griffiths 2003; Baryshnikova et al. 2013). In *S. cerevisiae* the genetic interaction between *ZRC1* and *MSC2*, validates the redundancy of Zrc1p and Msc2p in facilitating zinc homeostasis in the ER (Ellis et al. 2004). Furthermore, the double mutations of *msc2Δzrg17Δ* provides genetic evidence for a functional complex, indicating that these two proteins are involved in the same ER pathway rather than in separate pathways in *S. cerevisiae* (Ellis et al. 2005). Likewise, the genetic interactions among CDF zinc transporters *zrc-1*, *msc-2*, and *zrg-17*, helps us understand how these genes work together and are responsible for the regulation of zinc within *N. crassa* (table 4.4).

Table 4.4 Impact of mutation of CDF zinc transporters *zrc-1*, *msc-2*, and *zrg-17* and their double mutants in *N. crassa*

Case no.	*zrc-1*	*msc-2*	*zrg-17*	Mutation	Strain viability	Phenotypic effect of mutation
1.	+	+	+	-	viable	Wild type
2.	+	+	KO	Single mutant	viable	Vegetative growth defects, Early & enhanced conidiation, Required for growth in low zinc (Tiwari et al. 2018)
3.	+	KO	+	Single mutant	viable	No phenotypic defects
4.	KO	+	+	Single mutant	viable	Unable to grow under high zinc concentration

5.	KO	KO	+	Double mutant	viable	Unable to utilize cellulose as sole carbon
6.	+	KO	KO	Double mutant	viable	Antagonistic effect: wild type like phenotype. The Δ*zrg-17* phenotypes are rescued by Δ*msc-2*.
7.	KO	+	KO	Double mutant	viable	Severe growth defects, irregular septation, defects in conidiation, and unable to utilize cellulose as sole carbon
8.	KO	KO	KO	Triple mutant	Unable to generate triple mutant (germinated > 200 spores)	

The presence of the gene is indicated by + (Present) and the absence of the gene is indicated by KO (Knockout).

4.3 Discussion

Genetic interactions are generally studied using double mutants in Saccharomyces, Neurospora, Chlamydomonas (Bruce 1974; Gavric and Griffiths 2003; Gerke et al. 2009). In this chapter, I described the genetic interactions among CDF zinc transporters *zrc-1*, *msc-2*, and *zrg-17.* The double mutants Δ*zrc-1;* Δ*msc-2*, Δ*msc-2*; Δ*zrg-17*, and Δ*zrc-1*; Δ*zrg-17* were generated by crossing their respective single mutants of opposite mating type (Figure 4.1). The double mutants were tested for vegetative developments on medium containing different concentrations of zinc. The Δ*zrc-1*; Δ*msc-2* double mutant showed slow growth (Figure 4.3) only under high zinc, this slow growth phenotype corresponds to the growth defect of parental single mutant Δ*zrc-1*. However, the Δ*msc-2*; Δ*zrg-17* double mutant showed a wild type like phenotype, whereby the double deletions of *msc-2* and *zrg-17*

resulted in the restoration of phenotypic defects of Δ*zrg-17* single mutant (Tiwari et al. 2018), including slow growth (Figure 4.3), asexual sporulation (Figure 4.6 and 4.7) and ability to grow under cellulose containing medium (Figure 4.9). Furthermore, the Δ*zrc-1*; Δ*zrg-17* double mutant showed additive phenotype that resulted in slow growth (Figure 4.3), defects in asexual sporulation (Figure 4.6), short intercompartmental septa and shorter hyphal width (Figure 4.5). Additionally, the Δ*zrc-1*; Δ*msc-2* and Δ*zrc-1*; Δ*zrg-17* double mutants were unable to grow under cellulose containing medium (Figure 4.9). Whereas, the *zrc-1*, *msc-2*, and *zrg-17* single mutants and double mutants showed no phenotypic defects to low (20 °C) and high temperatures (40 ˚C) (Figure 4.10), pH (pH 3.8 and 7.8) (Figure 4.11 A) and osmotic (NaCl and KCl) stress conditions (Figure 4.11 B), and azole drugs (Fluconazole and Itraconazole) (Figure 4.12).

The double deletion of *msc-2* and *zrg-17* rescued the phenotypic defects of the Δ*zrg-17* single mutant and displayed wild type like growth (Figures 4.3, 4.4, 4.5, 4.6, 4.8, and 4.9). These results suggested a potential antagonistic relationship between *msc-2* and *zrg-17*, that might correspond to a similar pathway of action. Previously, the *S. cerevisiae* Zrg17p and Msc2p and the *S. pombe* Zrg17 and Cis4 were shown to form a heteromeric complex and involved in transporting zinc into the secretory pathways, suggesting a similarity in the MSC-2 and ZRG-17 interactions in various organisms (Ellis et al. 2005; Fang et al. 2008; Choi et al. 2018).

The Δ*zrc-1;* Δ*zrg-17* double mutant showed distorted aerial hyphae (Figure 4.4 A), shorter inter-septal distance (Table 4.2), resulting in more septation (Figure 4.5 A). Similarly, in *N. crassa*, a Rho-type GTPase, *rho-4* is one of the key genes in septation, and Δ*rho-4* mutant exhibits retarded growth, defects in aerial hyphae, and conidiation (Rasmussen and Glass 2005). Moreover, Δ*zrc-1;* Δ*zrg-17* also showed conidiation defects, such as early and enhanced immature conidiation (Figure 4.6). Previously, it has been reported that the short aerial hyphae could be due to the strain entering the

program of conidiation prematurely leading to shorter aerial hyphae, and this correlation between short aerial hyphae and the release of immature conidia was seen in Δ*dcc-1* mutant (Barba-Ostria et al. 2011), and Δ*plc-1*; Δ*splA2* and Δ*plc-1*; Δ*cpe-1* double mutants (Barman and Tamuli 2017). Additionally, in submerged culture the Δ*zrc-1;* Δ*zrg-17* mutant produced inappropriate conidiation and was unable to form mycelial aggregates like the wild type (Figure 4.7 A). Previously, zinc homeostasis was shown necessary for grain formation in *M. mycetomatis* (du Pré et al. 2022), and the C_2H_2 zinc finger transcription factor MaNCP1 was found to control conidiation in *Metarhizium acridum* (Li et al. 2022). The inappropriate asexual sporulation under submerged culture was correlated with the increased expression of the *con-10* gene in the Δ*zrc-1;* Δ*zrg-17* mutant (Figure 4.7 B). The conidiation specific gene, *con-10* was shown to highly expressed during conidiation process in *N. crassa* (Roberts et al. 1988; Olmedo et al. 2010). These results suggested that *zrc-1* and *zrg-17* CDF zinc transporters and their interactions are necessary for normal septa development and proper conidiation in *N. crassa*.

In the eukaryotic cells, ER is the site for folding of proteins that are targeted for secretion or membrane-bound, and the initial stages of protein maturation in the ER are crucial for ensuring the proper folding of these proteins (Harding et al. 1999; Hetz 2012). The efficiency and accuracy of protein folding is constantly modified through the dynamic integration of multiple cellular and environmental signals, for example, protein synthesis is decreased in response to ER stress induced by DTT which inhibits disulfide bond formation (Sawyer et al. 1994; Simons et al. 1995; Rand and Grant 2006; Fan et al. 2015). Additionally, the insufficient supply of glucose caused by the use of cellulose as a substrate results in the production of an array of enzymes, which compromise the ER folding capacity and result in the ER stress (Montenegro-Montero et al. 2015; Starr and Gonc 2018; Collier et al. 2020). Additionally, zinc concentrations in the culture medium have a significant effect on the

fungal morphology and zinc ion functions as a metal cofactor in various proteins (Raulin 1869; Linke et al. 2003). Therefore, sub-optimal zinc concentrations can lead to protein misfolding, resulting in ER stress and affecting the functioning of the ER (Li et al. 2023). In *S. cerevisiae*, the ER function is regulated by zinc homeostasis, which is facilitated by the ER proteins Zrg17p and Msc2p along with the vacuolar proteins Zrc1p and Cot1p (Ellis et al. 2004, 2005). Likewise, in *N. crassa*, the Δ*zrg-17* mutant could not grow under ER stress induced by DTT and was unable to degrade cellulose (Tiwari et al. 2018). Therefore, to elucidate the roles of CDFs in ER function, the wild type, Δ*zrc-1*, Δ*msc-2* and Δ*zrg-17* single and double mutant strains were investigated for ER stress mediated by DTT (Figure 4.8) and on the medium supplemented with cellulose as a carbon source (Figure 5.9). In DTT-containing medium, the Δ*zrc-1*; Δ*msc-2* and Δ*zrc-1*; Δzrg-*17* double mutants produced retarded aerial hyphae (Figure 4.8), and these mutants were unable to utilize cellulose, producing negligible or no biomass (Figure 4.9; Table 4.3). Furthermore, I measured the glucose amount and the protein concentrations released in the supernatant of the mutant strains. The estimated glucose released along with protein concentration corresponds to the growth of the strains in the provided conditions (Figure 4.9 B, C). Taken together, these suggested that CDF zinc transporters and their genetic interactions are necessary for the normal growth in *N. crassa*.

Further, to generate the triple mutants lacking *zrc-1*, *msc-2*, and *zrg-17*, I screened progenies (>200 progenies) from a cross involving Δ*zrc-1*; Δ*msc-2 mat A* crossed with Δ*zrg-17 mat a* (Figure 4.13). I attempted the generation of a triple mutant, because information regarding the triple deletions of *zrc-1*, *msc-2*, and *zrg-17* was lacking in any organism. Obtaining a viable triple mutant would indicate the possibility of functional redundancy and the presence of other genes that can suppress their mutations; however, inability to obtain any viable progeny would indicate that these are key essential genes involved in transporting zinc in *N. crassa*. I could not obtain a single viable progeny

from the large numbers of progenies screened (>200 progenies), thus, indicate an essential role of the *zrc-1*, *msc-2*, and *zrg-17* genes in zinc transport in *N. crassa*.

The *S. cerevisiae* zinc responsive transcription factor Zap1p regulates the expression of genes such as *ZRT1* and *ZRT2* (Zhao and Eide 1997), *ZRT3* and *ZRC1* (Miyabe et al. 2000; MacDiarmid et al. 2003), and *ZRG17* (Wu et al. 2011), involved in zinc uptake and distribution. Similarly, Zap1 controls the expression of a large number of genes in response to low zinc levels in *A. fumigatus*, *C. albicans*, and *C. gattii* (Eide 2021). Therefore, in the next chapter I described the identification and characterization of *zap-1* and proposed a model depicting zinc transport in *N. crassa*.

I published results described in this chapter in Journal of Biosciences (Serena Ngiimei D and Ranjan Tamuli; 2024) and also presented as (i) Oral presentation (online mode) at Molecular Intricacies of Plant Associated Microorganisms (MIPAM-2022) organized by Centre for DNA Fingerprinting and Diagnostics, Hyderabad, February 17−20, 2022, and (ii) Oral presentation (online mode) at Asian Mycological Congress 2021 (AMC2021), held at Thailand Science Park Convention Center, Pathum Thani, Thailand, August 3 - 5, 2022.

5

INVESTIGATING THE ROLE OF ZAP-1 TRANSCRIPTION FACTOR IN REGULATING CDF ZINC TRANSPORTERS IN *NEUROSPORA CRASSA*

5.1 Introduction

All organisms must ensure metal homeostasis in response to constantly changing extracellular or dietary amounts of metal intake to avoid their over-accumulation. Zinc is an essential metal required for growth and development of various organisms. The amount of total zinc needed for the optimum growth of eukaryotic cells ranges from 0.1−1 mM (Palmiter and Findley 1995; Suhy et al. 1999; MacDiarmid et al. 2000; Outten and O'Halloran 2001). In the cell, various pathways coordinate to maintain zinc homeostasis and for adequate supply of this metal for signaling events.

In *S. cerevisiae*, regulation of zinc homeostasis and coping with zinc deficiency are accomplished by the Zap1p transcription factor (Zhao and Eide 1997). Previous studies showed that Zap1p upregulates the expression of ~80 genes (Lyons et al. 2000; Wu et al. 2008). Zap1p binds to an eleven-base pair consensus sequence known as zinc-responsive element (ZRE), which is found in one or more copies in the promoter region of the target genes, under the zinc-limiting conditions (Zhao et al. 1998). Zap1p upregulates the expression of genes involved in zinc uptake and distribution, such as *ZRT1* and *ZRT2* (Zhao and Eide 1997), *ZRT3* and *ZRC1* (Miyabe et al. 2000; MacDiarmid et al. 2003), and *ZRG17* (Wu et al. 2011). The Zap1p consists of seven C_2H_2 zinc-fingers (Znf1-Znf7), two activation domains (AD1 and AD2), and a DNA binding domain (DBD) (Bird et al. 2000a, 2003; Frey and Eide 2011). The AD1 and AD2 activation domains activate transcription and function independently of each other (Bird et al. 2000b). Moreover, Zap1p auto-regulates via a positive feedback loop by sensing zinc (Zhao and Eide 1997; Bird et al. 2000a; Yao et al. 2023). The *Aspergillus fumigatus* Zap1p ortholog ZafA regulates zinc homeostasis through transcriptional activation of *zrfA*, *zrfB*, *zrfC*, and *aspf2*, and crucial for the pathogenicity and virulence (Moreno et al. 2007; Amich and Calera 2014; Vicentefranqueira et al. 2018). In *Candida albicans*, candida suppressor of *ROK1* (CSR1), an ortholog of Zap1p, is essential for the formation of biofilms and

involved in transcriptional regulation of zinc homeostasis by regulating the expression of ~60 genes, including *ZRT1*, *ZRT2*, *ZRT3*, and *PRA1* (Kim et al. 2008; Nobile et al. 2009). *ROK1* gene encodes a DEAD-box ATP-dependent RNA helicase, which is essential for cell cycle progression (Song et al. 1995). Zap1 also regulates the expression of multiple zinc-binding proteins and transporters in *Cryptococcus gattii* (Schneider et al. 2015). *ZAP1* expression is elevated under the zinc-depleted conditions, and *ZAP1* knockout reduces virulence and impairs growth in *C. gattii* (Schneider et al. 2012). In soil-borne fungal pathogen *Fusarium oxysporum*, *zafA* expression is upregulated under zinc deprivation, and *zafA* deletions lead to impaired growth (López-Berges 2020). ZafA-mediated adaptation to zinc limitation is also vital for *F. oxysporum* to be fully virulent on plant and animal hosts, (López-Berges 2020).

In Chapters 3 and 4, I discussed the cellular roles of CDF zinc transporters ZRC-1 and MSC-2 and the genetic interactions among the CDF; *zrc-1*, *msc-2,* and *zrg-17*. The expression studies suggested that low zinc levels upregulated the expression of *zrc-1* and *zrg-17* in a ZAP-1-dependent manner (Tiwari et al. 2018; Chapter 3). In this Chapter, I describe the identification, characterization and the role of ZAP-1 transcription factor in regulating CDF zinc transporters in *N. crassa*.

5.2 Results

5.2.1 Identification of the Zinc-responsive Activator Protein-1 (ZAP-1) using *in silico* analysis

5.2.1.1 The NCU02699 encodes the Zinc-responsive Activator Protein-1 (ZAP-1) in *N. crassa*

The information regarding NCU02699 was obtained from Fungal & Oomycete informatics resources (https://fungidb.org/fungidb). The NCU02699 gene is genetically mapped in supercontig one from position 3239395 - 3243393 (+ strand), at the left arm of linkage group one (LG IL; Figure 5.1 A), with an open reading frame of 2,130 base pairs. The genomic sequence of NCU02699 contains four exons and three introns (Figure 5.1 B) and encodes for a 710 amino acid residues zinc finger protein

(ZNF-14; GenBank accession no. XP_965472.3; https://www.ncbi.nlm.nih.gov/protein/553139100), which was used as a query sequence in a BLASTP (Altschul et al. 1990, 1997) analysis. Based on the *E* value, % identities, and gaps, the proteins were selected and aligned using CLUSTAL X and GeneDoc (Nicholas et al. 1997; Thompson et al. 1997). The sequence alignment of this protein revealed sequence similarities to the Zinc-responsive Activator protein (Zap1p) of *S. cerevisiae* with the majority of the sequence identity at the C-terminal region of the homologous proteins (Figure 5.2 A). A distinct attribute of all Zap1 orthologues is of the presence of five or more C_2H_2-zinc fingers clustered at the C-terminus (du Pré et al. 2022). The ZAP-1 of *N. crassa* showed 46.31% sequence identity to the Zap1p of *S. cerevisiae* and it possesses seven C_2H_2-zinc fingers (ZF1-ZF7; Figure 5.2 B), where ZF1 is located at the center, and ZF2 to Zf7 are found at the C-terminus, predicted by InterPro (https://www.ebi.ac.uk/interpro/protein/UniProt/Q7SH30/) and UniProt (Id: Q7SH30; https://www.uniprot.org/uniprotkb/Q7SH30). The aligned homologous sequences were further used to create a phylogenetic tree using MEGA11 software by minimal evolution approach (Rzhetsky and Nei 1993; Tamura et al. 2021). The constructed phylogram revealed that NCU02699 protein is closely grouped within Sordariomycetes (Figure 5.3 C). Therefore, NCU02699 encodes the ZAP-1 zinc finger transcription factor in *N. crassa*.

(A)

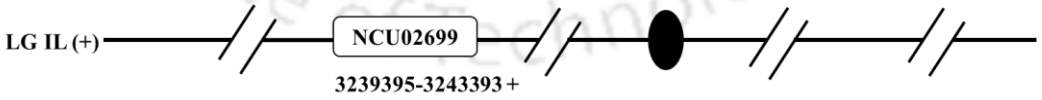

(B)

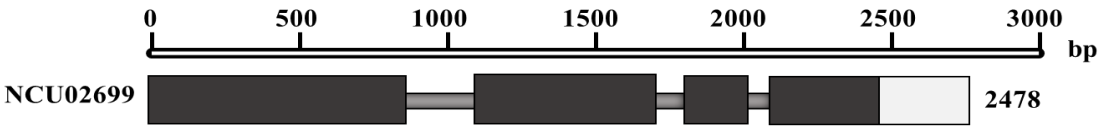

Figure 5.1 Genomic organization of NCU02699 in *N. crassa*. (A) Position of the NCU02699 gene on LG IL. The NCU02699 gene is localized at the left arm of supercontigs one from position 3239395 to 3243393 (+ strand). Solid circle indicates the centromere in each line. **(B)** Genetic organization of NCU02699. The NCU02699 gene possesses four exons (black colored bar), three introns (grey colored line), and untranslated region (UTR, light grey bar).

(A)

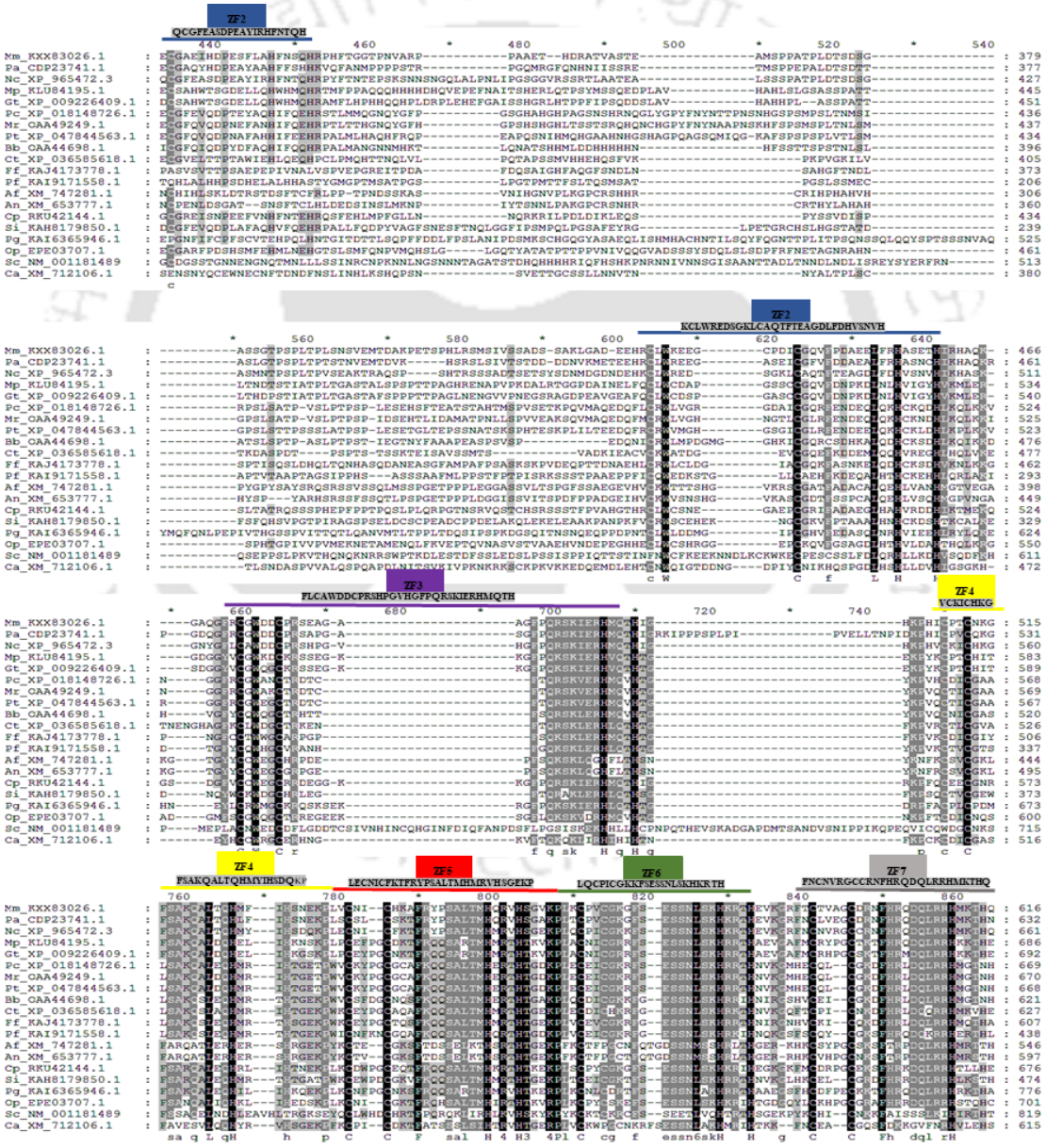

(B)

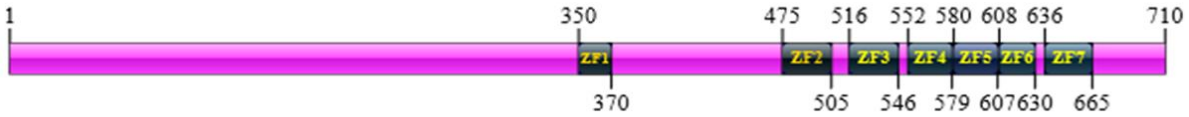

(C)

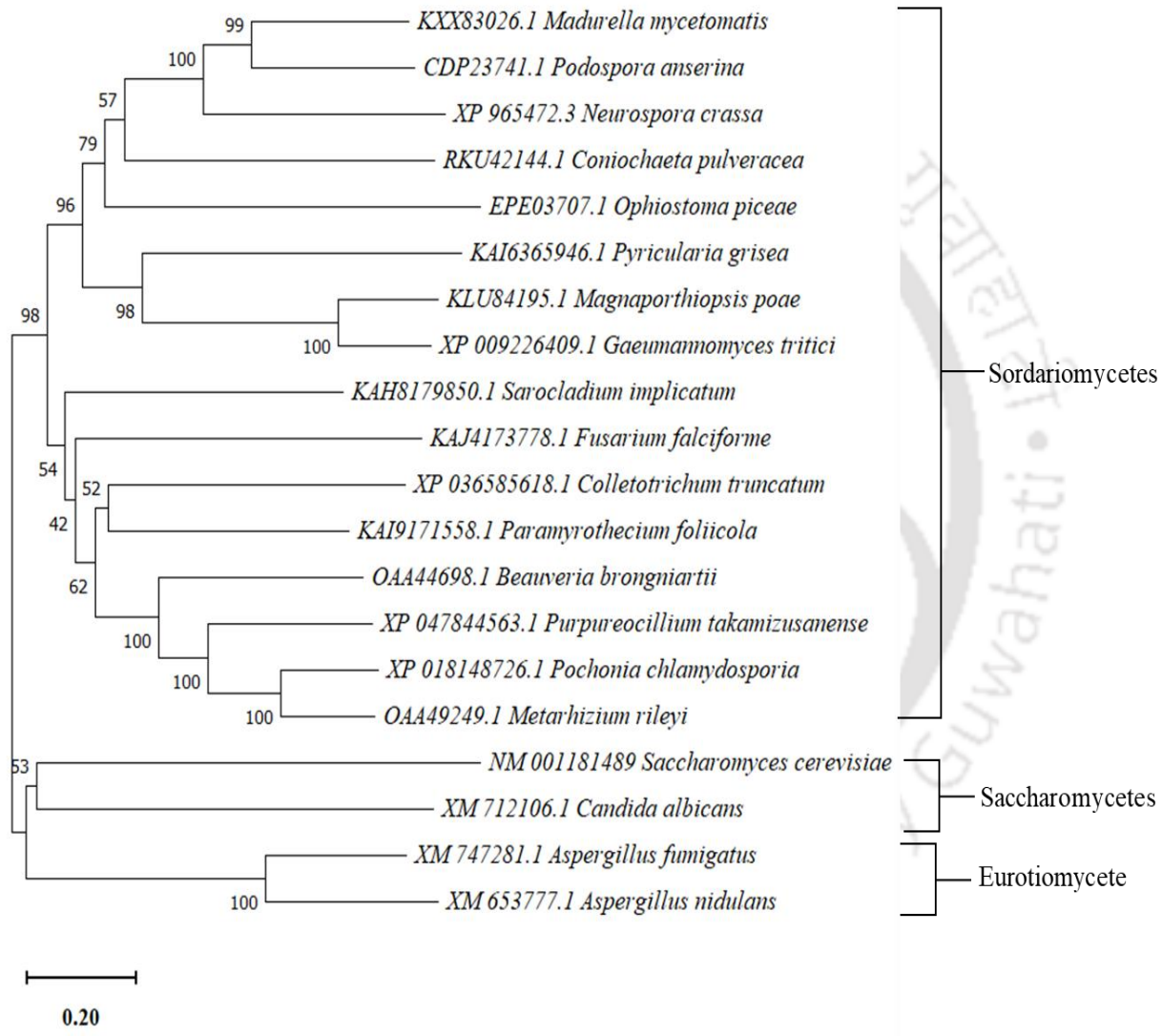

Figure 5.2 Sequence Analysis. (A) Sequence alignment of NCU02699 homologs. The positions of the C_2H_2-zinc finger domains predicted by SMART (Letunic et al. 2020; https://smart.embl.de/) protein structure analysis revealed that most C_2H_2-zinc finger domains concentrated at the C- terminus.

The sequences used in this analysis are *Madurella mycetomatis* (Mm), *Podospora anserina* (Pa), *Neurospora crassa* (Nc), *Magnaporthiopsis poae* (Mp), *Gaeumannomyces tritici* (Gt), *Pochonia chlamydosporia* (Pc), *Metarhizium rileyi* (Mr), *Purpureocillium takamizusanense* (Pt), *Beauveria brongniartii* (Bb), *Colletotrichum truncatum* (Ct), *Fusarium falciforme* (Ff), *Paramyrothecium foliicola* (Pf), *Aspergillus fumigatus* (Af), *Aspergillus nidulans* (An), *Coniochaeta pulveracea* (Cp), *Sarocladium implicatum* (Si), *Pyricularia grisea* (Pg), *Ophiostoma piceae* (Op), *Saccharomyces cerevisiae* (Sc), *Candida albicans* (Ca). Conserved amino acids are indicated in black (100%), dark grey (>80%), and light grey (>60%) in the alignment. **(B)** Domain organization of NCU02699. shows seven zinc finger domains, the domain structure was constructed using IBS 2.0 illustratorLow complexity regions (LCRs). **(C)** Phylogeny of NCU02699 and its orthologues throughout the fungal kingdom. The software MEGA11 was used to carry out the phylogenetic analysis using the minimal evolution approach and 1000 bootstrap replication (bootstrap values are indicated in the point as nodes in the phylogram).

5.2.1.2 Structural analysis of the ZAP-1 protein using the homology modeling approach

The NMR and CD structure of the AD2 domain in the *S. cerevisiae* Zap1p (Figure 5.3 A; 10.2210/pdb1ZW8/pdb; PDB ID:1ZW8; Wang et al. 2006) was used as the template for the homology modelling of ZAP-1 of *N. crassa*. The protein structure of ZAP-1 of *N. crassa* was predicted using the Iterative Threading ASSEmbly Refinement (I-TASSER) tool (https://zhanggroup.org/I-TASSER/; Yang and Zhang 2015; Zheng et al. 2021), SWISS-MODEL (https://swissmodel.expasy.org/; Waterhouse et al. 2018), and putative AlphaFold structure from UniProt database (https://www.uniprot.org/). To improve the structural quality, the best-predicted structures of ZAP-1 was refined using GalaxyWEB Refine (Ko et al. 2012; https://galaxy.seoklab.org/index.html) making the structure more stable (Figure 5.3 C). Furthermore, the Ramachandran plot was used to validate the

structures using PROCHECK (Laskowski et al. 1993) in Saves v6.0 web server (https://saves.mbi.ucla.edu/). In addition, the plot statistics of the structures indicating the percentage of residues in the most favored region before refinement was 54.7 %, which was increased to 87.8 % after refinement (Figure 5.3 C and Figure 5.4; Table 5.1). Additionally, structural alignment using the Dali webserver (http://ekhidna2.biocenter.helsinki.fi/dali/; Holm 2022), was also conducted, resulting in an RMSD value of 2.4 Å, and it was superimposed with the template model for visualization using PyMOL (Figure 5.3 B; https://pymol.org/2/). The structural alignment of the modeled ZAP-1 structure from *N. crassa* with the template AD2 structure of the Zap1p from *S. cerevisiae*, revealed that the ZF2 and ZF3 of ZAP-1 possess a similar zinc-binding pattern to that of AD2, where ZF1 and ZF2 interact via a hydrophobic surface to bind zinc and fold into a unique finger pair regulating AD2 (Figure 5.3 A; Wang et al. 2006; Eide 2009). This indicated that zinc might regulate the activity of ZAP-1 of *N. crassa* similar to that of Zap1p of *S. cerevisiae*.

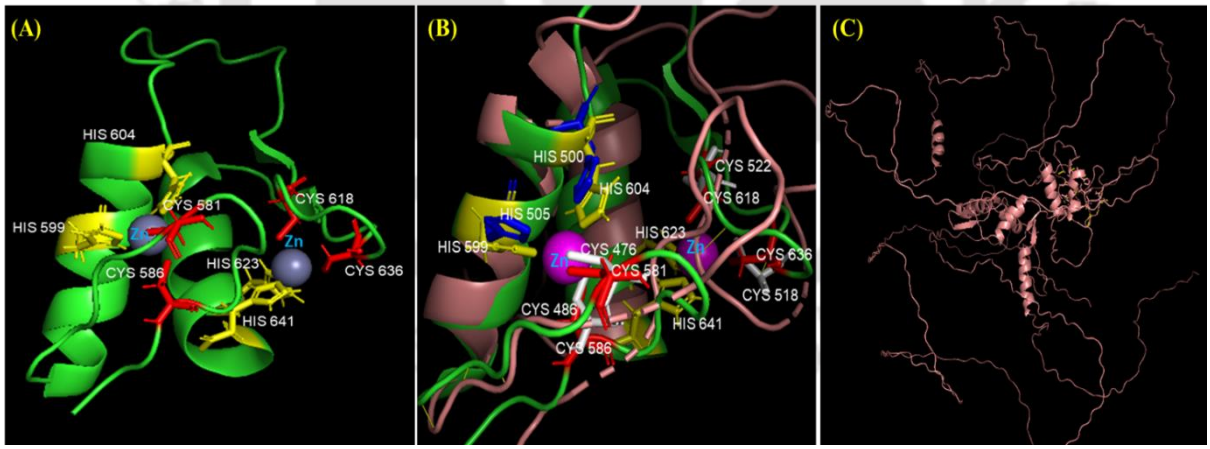

Figure 5.3 Homology model of ZAP-1 of *N. crassa*. (A) Modeled structure of AD2 of Zap1p in *S. cerevisiae* determined by solution NMR (PDB ID: 1ZW8). The C_2H_2 zinc fingers ZF1 and ZF2 interacting with zinc (grey sphere) are shown here, and the residues which are bound to zinc are

mentioned. **(B)** Superimposed image of the predicted modeled structure of ZAP-1 of *N. crassa* with AD2 of Zap1 of *S. cerevisiae*. The C_2H_2zinc fingers ZF1 and ZF2 of AD2 (green) of *S. cerevisiae* are superimposed with the ZF2 and ZF3 of ZAP-1 of *N. crassa* (pink) and residues bound to zinc (purple sphere) are mentioned. **(C)** Visualization of the modeled structure of ZAP-1 of *N. crassa*.

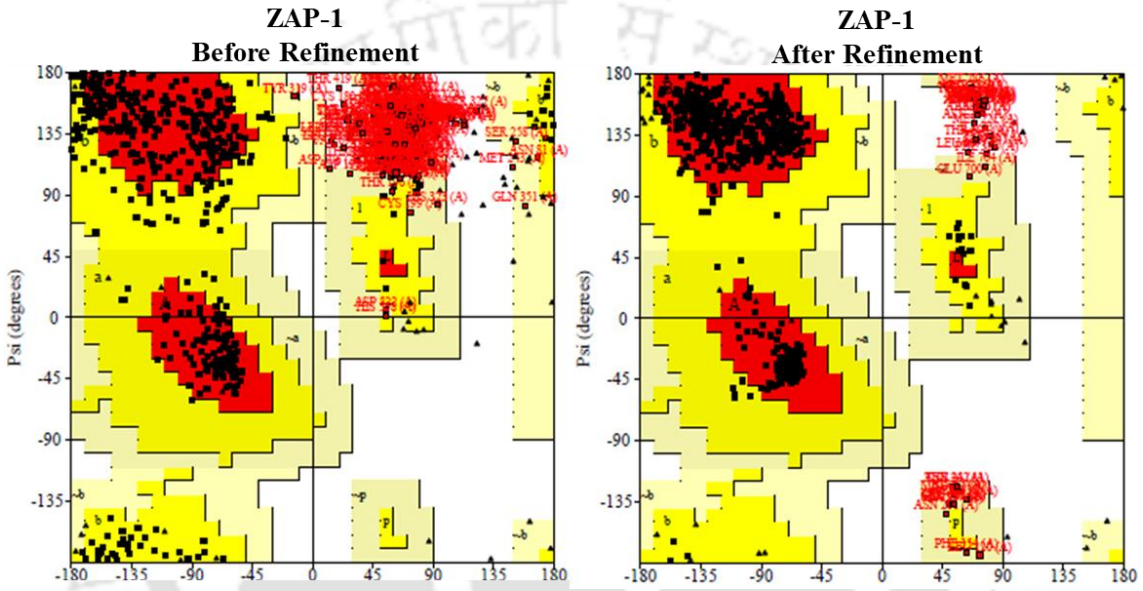

Figure 5.4 PROCHECK analysis for structure validation of modeled structure. Ramachandran plot of the modeled structure of ZAP-1 before and after refinement. The various color-coded regions stand for the most favored regions (red), allowed regions (yellow), generously allowed areas (pale yellow), and forbidden regions (white).

Table 5.1 Percentage of residues in the Ramachandran plot

Plot statistics	**Percentage (%)**	
Residues	**Before refinement**	**After refinement**
Residues in the most favored region [A, B, L]	336 (54.7 %)	539 (87.8 %)

Residues in the additionally allowed region [a, b, l, p]	112 (19.9 %)	37 (6 %)
Residues in the outlier region [~a, ~b, ~l, ~p]	114 (18.6 %)	23 (3.7 %)

5.2.2 Investigating the cellular roles of *zap-1* in *N. crassa*

5.2.2.1 Expression of *zap-1* gene is dependent on zinc concentrations

In *S. cerevisiae*, the expression of *ZAP1* was found to be elevated under low zinc conditions, which is critical for survival under this stress condition (Zhao and Eide 1997). Therefore, I studied the transcript level of *zap-1* gene in the wild type *N. crassa* using qRT-PCR under various amounts of zinc. The *zap-1* expression in low zinc was ~6.7-fold higher expression as compared to the expression in zinc-rich conditions (Figure 5.5). These results suggested that *zap-1* might play an important role in survival under low zinc conditions in *N. crassa*.

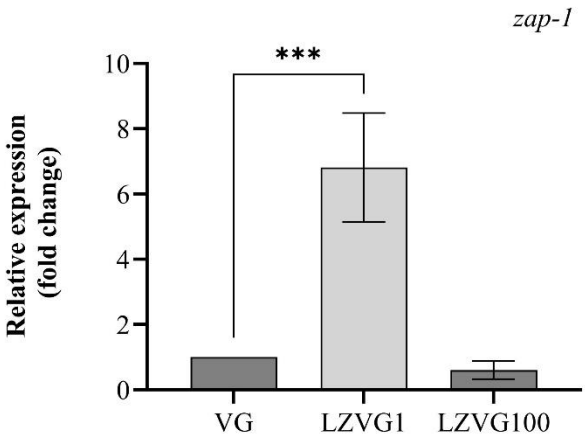

Figure 5.5 Expression analysis of *zap-1* gene in the wild type *N. crassa*. The RNA from wild type was extracted from media containing different zinc concentrations and the expression of *zap-1* was studied by qRT-PCR. The relative expression of the *zap-1* gene was normalized to the expression of *β-tubulin* gene and the fold changes of expression in low and high zinc conditions were compared to the expression in normal VG liquid medium. The error bars represent the standard deviations

calculated based on the results of three independent experiments (n = 3). In comparison to the expression of *zap-1* in normal VG liquid medium, the statistical significances were estimated by one-way ANOVA test and are represented by *P-values*< 0.05 (*), <0.01 (**), and < 0.001 (***).

5.2.2.2 Confirmation of Δ*zap-1* by PCR Analysis

The Δ*zap-1* knockout mutant was generated by the NIH Neurospora functional genomics project (http://geiselmed.dartmouth.edu/dunlaploros/genome/; Colot et al. 2006) and confirmed using Southern analysis (http://borkovichlims.ucr.edu/southern/). The Δ*zap-1* knockout mutant was obtained from the Fungal Genetics Stock Center (FGSC; https://www.fgsc.net/) and it was further verified using the HI-NCU02699Fw forward primer specific for the region upstream of the 5′flanks of the gene *zap-1* (Figure 5.7 A) and the 5HPHR reverse primer specific for the *hph* cassette used to generate the knock out mutants (Figure 5.6 B; entries 1 and 11, Table 2.3; Colot et al. 2006; Deka et al. 2011). This PCR-amplified product was confirmed by the presence of an amplicon size of ~1.41 kb, thereby confirming the presence of the Δ*zap-1* alleles in the mutant (Figure 5. 6 C).

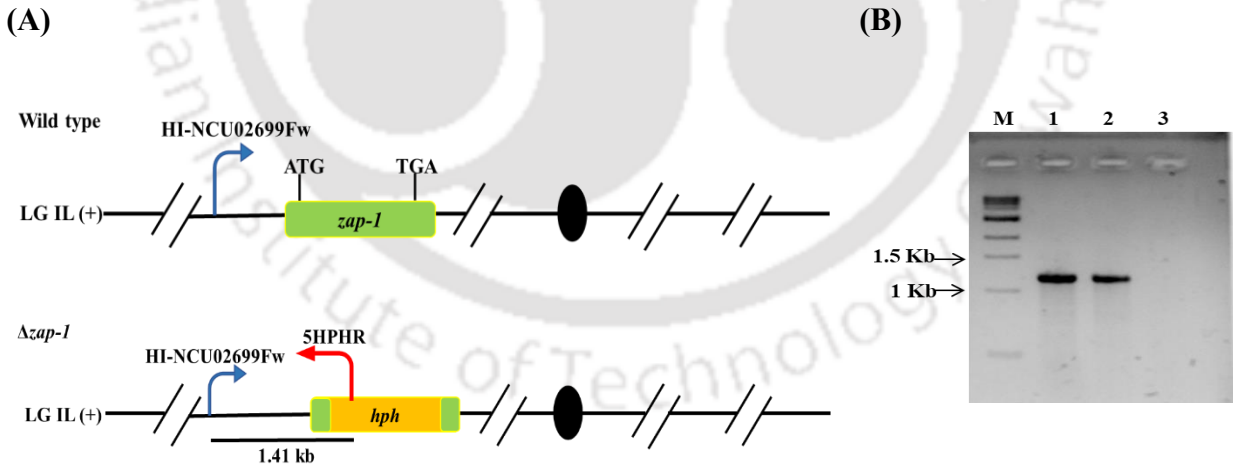

Figure 5.6 Confirmation of Δ*zap-1* knockout mutant. (A) Schematic representation for primer designing for confirming Δ*zap-1*. The wild type containing *zap-1* gene and the location of the binding

of the HI-NCU02699Fw primer is indicated by blue arrows. The Δ*zap-1* mutant containing the *hph* cassette and the binding of the primer pair the HI-NCU02699Fw and HPHR are indicated by blue and red arrows, respectively. Solid circle indicates the centromere in each line. **(B)** PCR confirmation of Δ*zap-1* knockout allele. The primer HI-NCU02699Fw as forward primer and HPHR as reverse primer for confirming Δ*zap-1 mat a* (lane 1) and Δ*zap-1 mat A* (lane 2) knockout mutants. The wild type was used as the control (lane 3) and M: 1 kb DNA ladder. The PCR amplified products of ~1.41 kb (Δ*zap-1 mat a/A*) were visualized in 0.8% agarose gel.

5.2.2.3 Δ*zap-1* knockout mutant showed short aerial hyphae under low zinc condition

To study the effect of Δ*zap-1* knockout mutant in *N. crassa*, the aerial hyphae heights under different concentrations of zinc were measured and compared to the wild type. The Δ*zap-1* mutant was not able to grow in medium containing a low zinc unlike the wild type (Figure 5.7 A). However, the short aerial hyphae in the Δ*zap-1* mutant were restored, when the medium was supplemented with increased amounts of zinc (Figure 5.7 B). This indicated that the *zap-1* gene is essential for survival under the low zinc condition in *N. crassa.*

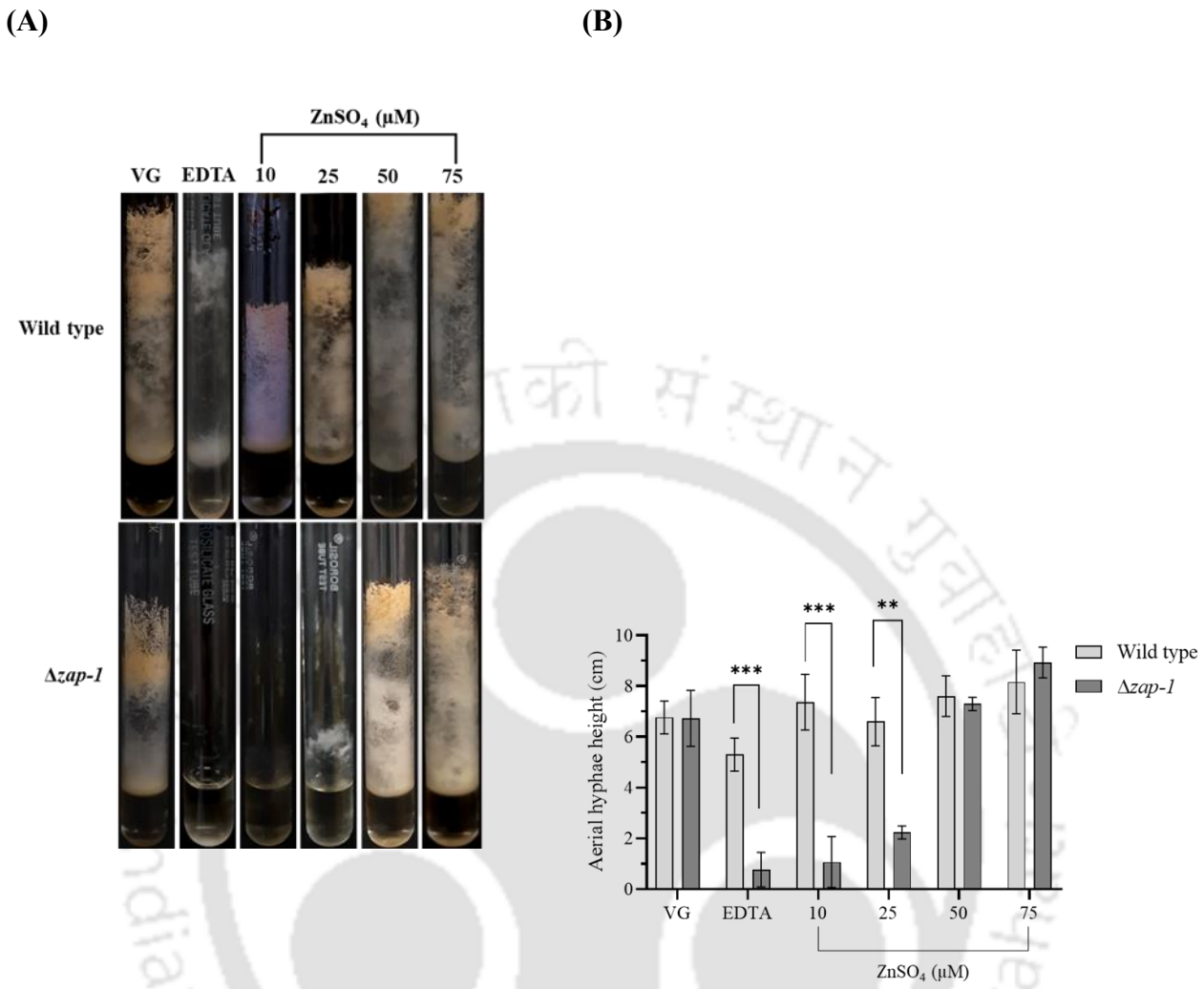

Figure 5.7 Aerial hyphae growth in the wild type and Δ*zap-1* mutant in the medium containing various amounts of zinc. (A) Aerial hyphae in the Δ*zap-1* mutant under different concentrations of zinc. An equal amount of conidia (10^6 conidia/ml) were inoculated in the VG liquid media containing different concentrations of zinc. The cultures were incubated at 30 °C in the dark for three days and in light for two days and photographed. **(B)** Graphical representation of aerial hyphae heights. The aerial hyphae heights were measured and compared to wild type. The error bars represent the standard deviations calculated based on the results of three independent experiments (n = 3). In comparison with the aerial hyphae heights of wild type under varying zinc concentrations, the statistical

significances were estimated two-way ANOVA analysis with Tukey's *post hoc* test with P-values < 0.05 (*), < 0.01 (**), and < 0.001 (***).

5.2.2.4 Cloning of the *zap-1* gene in the pMF272 vector

The *zap-1* gene was cloned in the pMF272 plasmid vector (Freitag et al. 2004) for the complementation analysis. The *zap-1* gene was PCR amplified from the wild type genomic DNA, using the NCU02699 Fw forward and NCU02699 Rv reverse primers (entries 12−13, Table 2.3; Figure 5.8 A), and gel purified (QIAquick PCR-Purification Kit, 28104, QIAGEN, Germany) the PCR product of size ~2.47 kb. The pMF272 vector was digested at the *Sma* I restriction site (R0141S, NEB, Ipswich, MA, USA) and gel purified. The *zap-1* product was then cloned into the *Sma* I site of the pMF272 plasmid vector (Figure 5.8 B). The ligated plasmid was transformed into ultra-competent *E. coli* DH5α cells, transformed colonies were selected based on ampicillin resistance, and one of the positive colonies, named as pSN-S64, was PCR verified using specific primer pairs (Table 2.3; Figure 5.8 C)

(A)

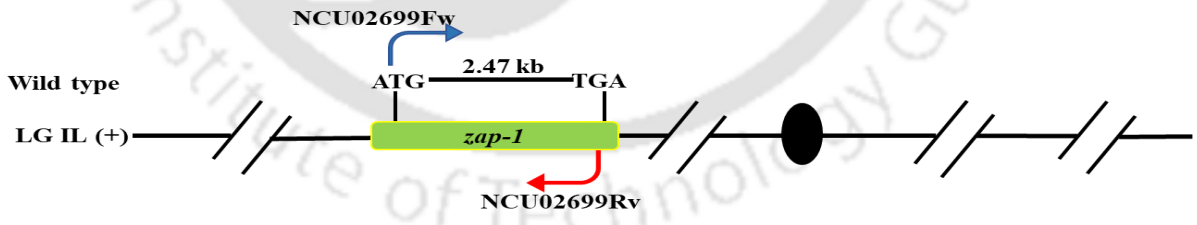

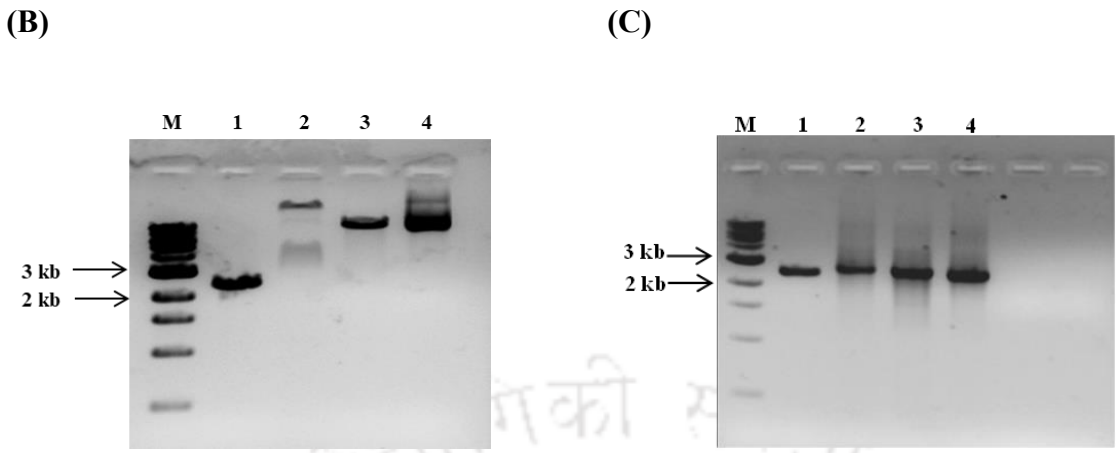

Figure 5.8 Cloning of the *zap-1* gene in the pMF272 vector. (A) Schematic representation of primers that are used to PCR amplify the *zap-1* gene from the wild type. The primer pair NCU02699Fw is used as the forward and NCU02699Rv as reverse primer, resulting in an amplicon of size ~2.47 kb. The binding region of the primers NCU02699Fw and NCU02699Rv are indicated by blue and red arrows, respectively. The relative positions of the start (ATG) and stop (TGA) codons are indicated. Solid circle indicates the centromere on each line. **(B)** Confirmation of ligation. The *zap-1* gene was PCR amplified from the wild type DNA using the sequence-specific primer pair (entries 12-13, Table 2.3; lane 1). The linearized vector displayed a shift in band as the size increased (~10.8 kb), indicating that the insert was ligated into the vector (lane 2). The vector pMF272 was linearized by digestion with *Sma* I restriction enzyme at multiple cloning site (MCS) of the vector (lane 3). The vector pMF272, size ~8.4 kb undigested (lane 4). M: The 1 kb DNA ladder (NEB, Ipswich, MA, USA) was loaded as the marker (M, lane 1). The PCR amplified product, ligated vector, digested vector, and undigested vector were resolved in an 0.8 % agarose gel. **(C)** PCR confirmation of pSN-S64 plasmid construct. The PCR products were resolved in an 0.8 % agarose gel. M: 1 kb DNA ladder (NEB), Lane 1: PCR amplified product of the *zap-1* gene using primer NCU02699 Fw forward primer and NCU02699 reverse primer (2,478 bp), lane 2: PCR amplified product for verification using Pccg-1Fw

forward and GFP Rv reverse primer (2,643 bp), lane 3: PCR-amplified product for verification of orientation of the insert using Pccg-1Fw as forward primer and NCU02699Rv as reverse primer (2,588 bp), lane 4: PCR-amplified product for verification of the orientation of the insert using NCU02699 Fw forward primer and GFP Rv reverse primer (2,553 bp).

5.2.2.5 Transformation of pSN-S64 construct into the *N. crassa* strain

The pSN-S64 plasmid construct carrying the *zap-1* gene was transformed into the *N. crassa his-3 mat A* strain (FGSC 6032) by electroporation, and selected based on the histidine prototrophy. One heterokaryotic strain was confirmed by PCR, and crossed with the Δ*zap-1 mat a* strain. Ascospores from this cross were harvested and germinated on a sorbose plate, and progenies were screened for the resistance to hygromycin (hyg^R) for the Δ*zap-1* allele and then confirmed by PCR analysis (Figure 5.9). This analysis identified a homokaryotic transformant $P_{ccg\text{-}1}$::*zap-1*::*gfp*, consisting of Δ*zap-1* mutant allele containing *zap-1*::*gfp* construct under the *ccg-1* promoter.

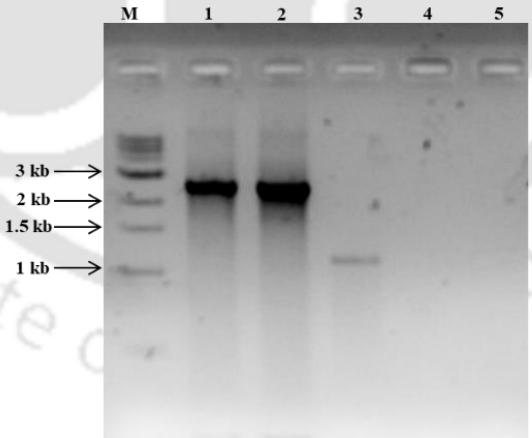

Figure 5.9 PCR verification of homokaryotic transformant. The confirmation of $P_{ccg\text{-}1}$::*zap-1*::*gfp* homokaryotic progeny by PCR. The PCR products were resolved in an 0.8 % agarose gel. M: 1 kb DNA ladder (NEB), Lane 1: PCR amplified product for verification using the Pccg-1Fw forward

primer and GFP Rv reverse primer (~2.6 kb), lane 2: PCR amplified product for verification using the NCU02699 Fw forward primer and GFP Rv reverse primer (~2.5 kb), lane 3: PCR-amplified product for confirmation of Δ*zap-1* knockout allele using the primer HI-NCU02699Fw forward primer and HPHR reverse primer (~1.4 kb), lane 4: the wild type was used as the control for verification using the Pccg-1Fw forward and GFP Rv reverse primer (no PCR product was obtained for the control, because binding sites for the primers are absent), lane 5: the Δ*zap-1* knockout was used as the control for verification using the NCU02699 Fw forward primer and GFP Rv reverse primer (no PCR product was obtained for the control, because binding site for the GFP Rv reverse primer is absent).

5.2.2.6 The *zap-1* gene is essential for vegetative development under low zinc conditions in *N. crassa*

In zinc-depleted conditions, the Δ*zap-1* mutant was not able to develop aerial hyphae (Figure 5.7; Figure 5.10). Similarly, the Δ*zap-1* mutant showed a significantly slower colony growth rate in the low zinc medium (LZVG1) compared to the wild type (Figure 5.11) and a severely retarded apical growth (Figure 5.12). However, zinc supplementation (LZVG100) could reverse these phenotypic defects. Additionally, colony growth rate, and apical growth in the homokaryotic transformant were similar to that of the wild type, suggesting that the wild type copy of the *zap-1* complements the Δ*zap-1* mutant. Therefore, the *N. crassa zap-1* gene is required for vegetative development in zinc-deficient conditions.

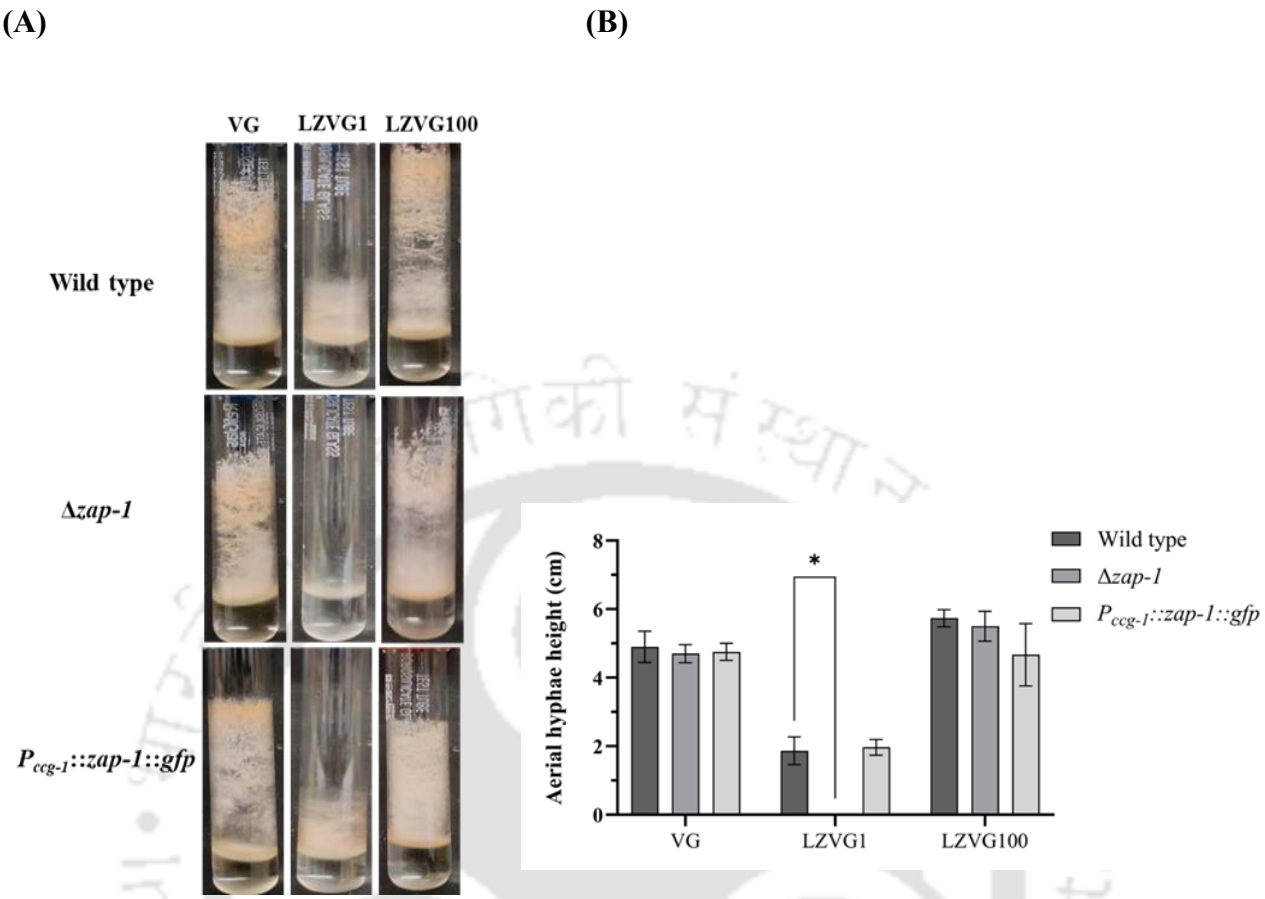

Figure 5.10 Significance of the *zap-1* gene for the development of aerial hyphae under zinc-deficient conditions in *N. crassa*. (A) Aerial hyphae of wild type, Δ*zap-1* and complemented strain P_{ccg-1}::*zap-1*::*gfp*. An equal amount of conidia (10^6 conidia/ml) were inoculated into VG liquid media, containing different concentrations of zinc (VG, LZVG1, LZVG100). The cultures were incubated at 30 °C in the dark for three days and in light for two days and photographed. **(B)** The average aerial hyphae heights of the strains. The Δ*zap-1* mutant showed no growth under low zinc LZVG1 condition. Error bars represent the standard deviations calculated based on the results of three independent experiments (n = 3). In comparison with the aerial hyphae heights of wild type, the statistical

significances were estimated by two-way ANOVA with Tukey's *post hoc* test and are represented by *P-values*< 0.05 (*).

(A)

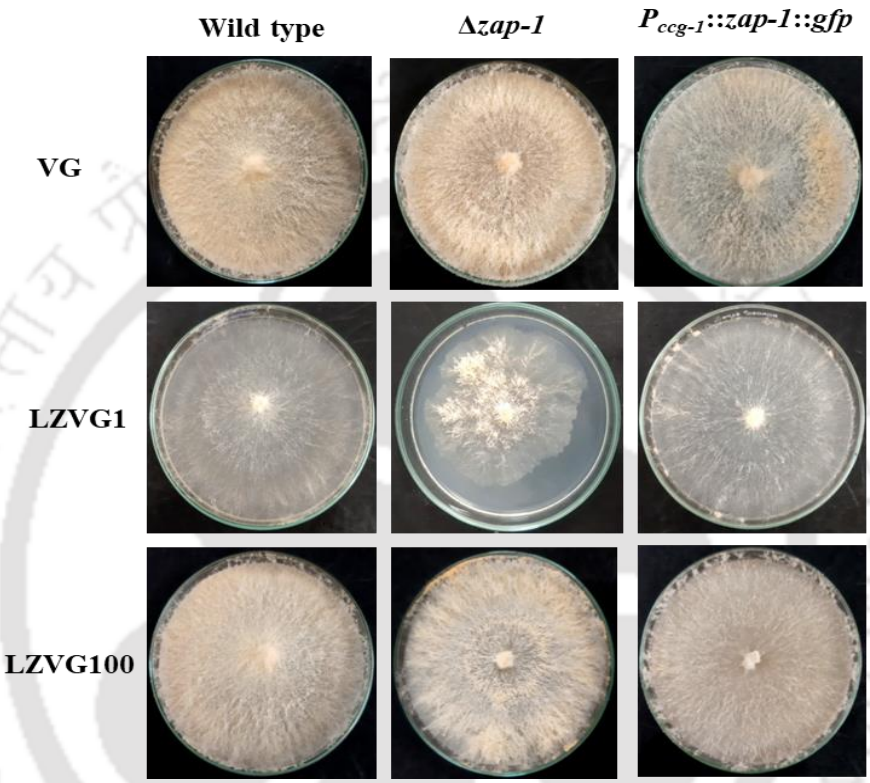

(B)

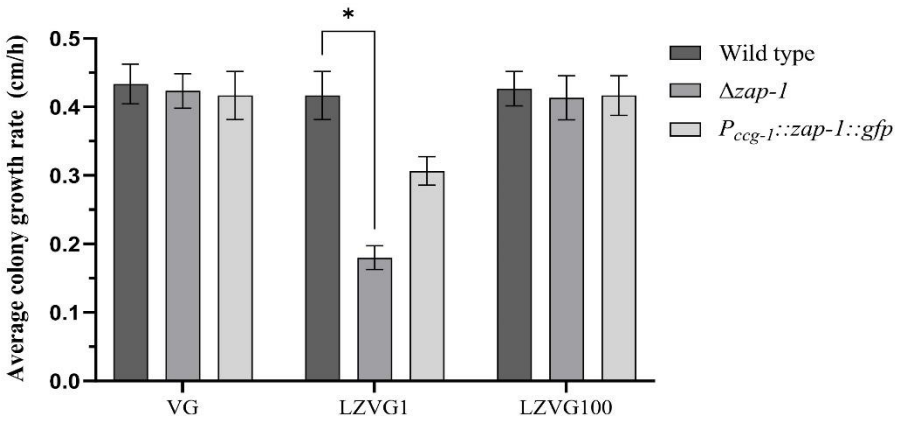

Figure 5.11 The *zap-1* gene is required for colony growth under zinc deficient condition in *N. crassa*. The strains were inoculated to VG agar medium containing different concentrations of zinc (VG, LZVG1, LZVG100) and incubated at 30 °C in complete darkness. **(A)** Colony morphology of wild type, Δ*zap-1* and complemented strain $P_{ccg\text{-}1}$::*zap-1*::*gfp*. **(B)** The average growth rates of *N. crassa* strains (cm h^{-1}). The colony growth rate of the strains under different conditions was determined. The error bars represent the standard deviations calculated based on the results of three independent experiments (n = 3). In comparison with the wild type, the statistical significances were estimated by two-way ANOVA test with Tukey's *post hoc* test and are represented by *P-values*< 0.05, < 0.01 (**), and < 0.001 (***)

(A)

(B)

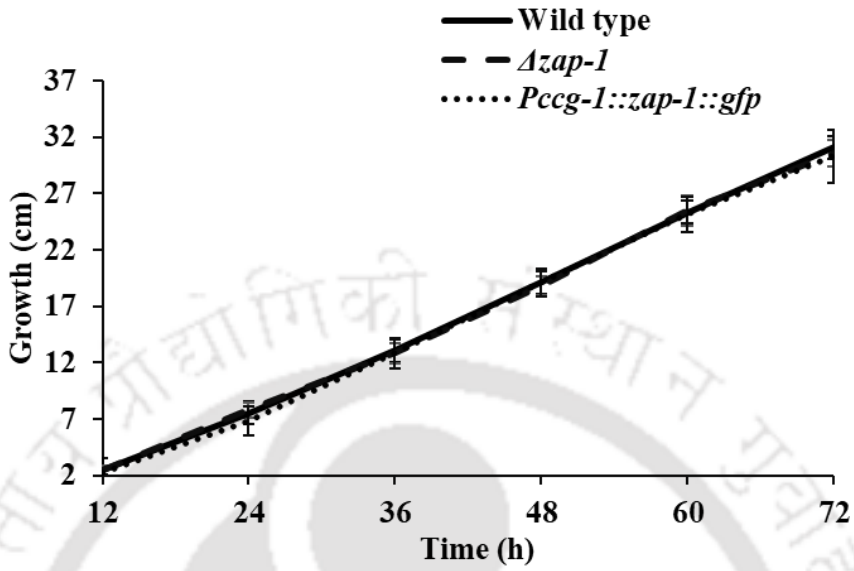

(C)

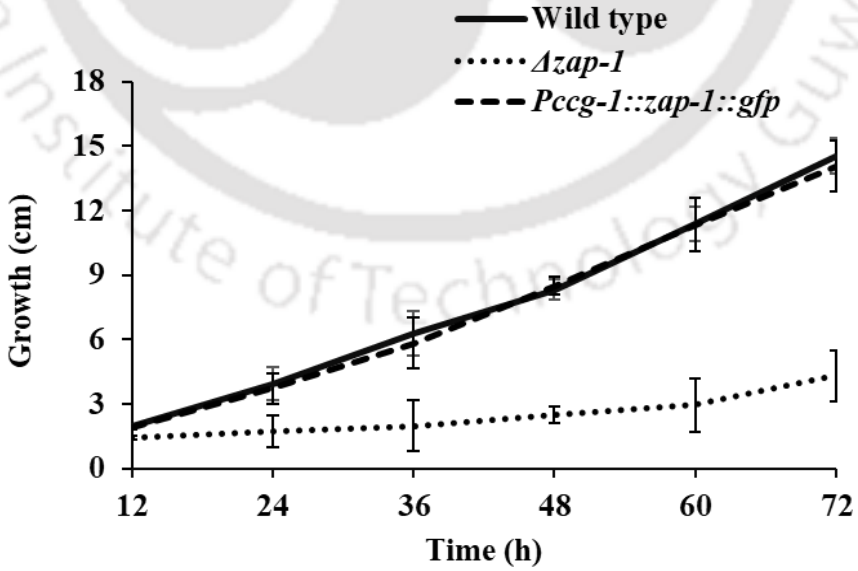

(D)

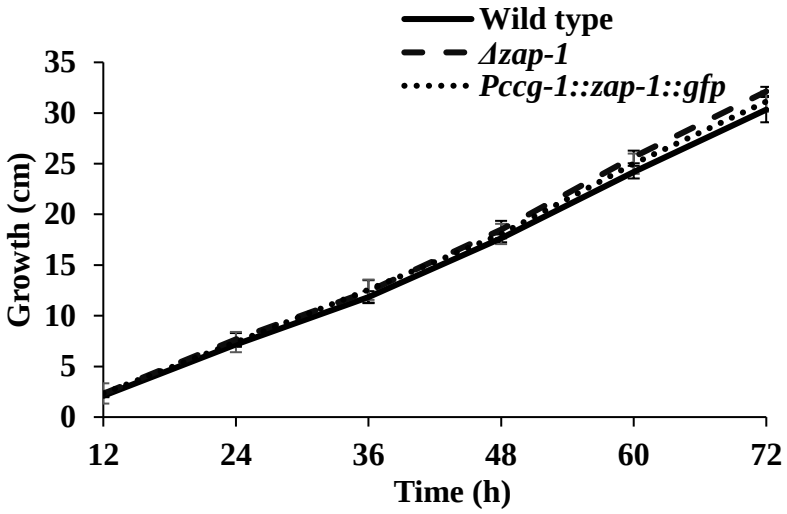

Figure 5.12 The *zap-1* gene is required for growth under zinc deficient conditions in *N. crassa*. **(A)** The apical growth rate of the strains was determined using race tubes. The strains were inoculated at one end of the tube and incubated at 30 °C and kept in the dark for three days and photographed. Growth rates of each strain at the various amounts of zinc containing medium, **(B)** VG, **(C)** LZVG1, and **(D)** LZVG100 were estimated at every 12 h interval till 72 h. The distances between the inoculation point and the hyphal growth front were determined and plotted against time. The error bars represent the standard deviations calculated based on the results of three independent experiments (n = 3).

5.2.2.7 Microscopy analysis showed that ZAP-1 is localized in the nucleus

The localization of ZAP-1 in *N. crassa* was analyzed using an inverted fluorescence microscope (Olympus CKX53, Japan). The $P_{ccg\text{-}1}$::*zap-1*::*gfp* homokaryotic strain was grown in the LZVG and LZVG100 liquid media and incubated at 30 °C for 8 h with shaking at 180 rpm. The 4′,6-diamidino-2-phenylindole dye (DAPI nucleic acid stain; D1306, Invitrogen Ltd., USA) was used to determine

the nuclear visualization as per the manufacturer's protocol. The images were captured in sequence, GFP image was obtained by excitation at 488 nm and emissions collected from 500−535 nm, nuclei stained with DAPI was excited at 358 nm with an exposure time of 300-400 ms, and emissions collected from 400−600 nm using a filter set for DAPI. These images were merged using ImageJ software (https://imagej.net/software/fiji/) to observe the localization. The microscopy analysis revealed that the *N. crassa* ZAP-1 is localized in the nucleus and the availability of zinc does not affect its localization (Figure 5.13). Similarly, the *S. cerevisiae* Zap1p was also shown localized in the nucleus and unaffected by zinc (Bird *et al.* 2000b).

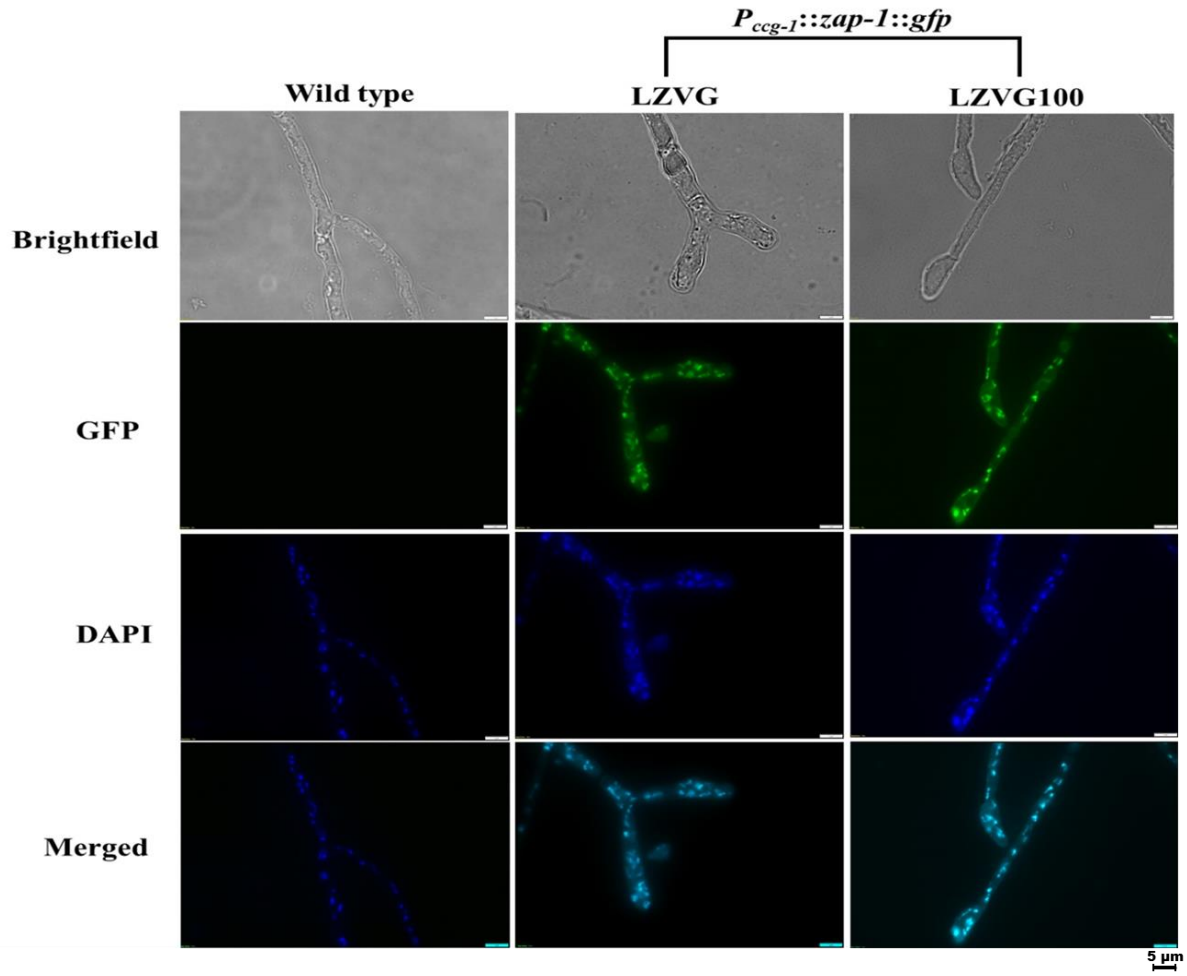

Figure 5.13 Microscopic analysis for subcellular localization of ZAP-1. Microscopy images of hypha of wild type and $P_{ccg\text{-}1}$::*zap-1*::*gfp* strains expressing GFP and stained with DAPI nucleic acid dye, were observed using an inverted fluorescence microscope (Magnification: 100X; Olympus CKX53, Japan). In the wild type, no GFP expression were observed, except for the DAPI-stained nuclei (wild type panel). In the $P_{ccg\text{-}1}$::*zap-1*::*gfp* strain, GFP expression was seen, and it was localized within the nucleus under both low and high zinc conditions, as indicated by the presence of DAPI-stained nuclei (Lower merged panel). Images were captured and for assembly ImageJ was used. Scale bar = 5 μm.

5.2.3 Interspecies complementation of the *S. cerevisiae zap1Δ* mutant using the *N. crassa zap-1* allele

5.2.3.1 Transformation of the *S. cerevisiae zap1Δ* mutant using the pSN-S5.1 construct

To test if the *N. crassa* ZAP-1 shares functional conservation with its Zap1p ortholog from *S. cerevisiae*, I performed an interspecies complementation analysis. I cloned the *N. crassa zap-1* gene in the pRS426 ($P_{nit\text{-}6}$::V5::GFP) (Ouyang et al. 2015) shuttle vector that contains selectable markers for amp^R for ampicillin resistance and *URA3* for uracil selection. The resulting transformants were screened based on ampicillin resistance, and a transformant (number 5, pSN-S5.1) was transformed into the *S. cerevisiae zap1Δ* (YJL056C) mutant by lithium acetate and heat shock method (Gietz and Akio 1988; Gietz and Schiestl 2007). The colonies were selected using URA3 as a selection marker; I screened the colonies using dropout growth media lacking uracil (SD Growth Medium w/o URA; G067, HiMedia, India). In the dropout growth media, only uracil prototrophic yeast strains can grow. I isolated a transformant *zap1Δ* + *Nczap-1* which was confirmed by PCR (Figure 5.14 A) for the *zap-1* gene and by inverted fluorescent microscope for the GFP expression (Figure 5.14 B).

(A)

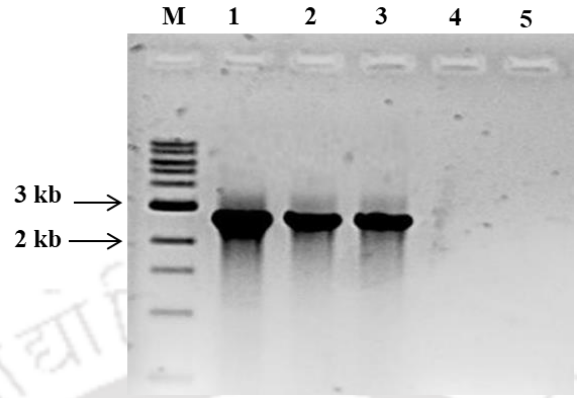

(B)

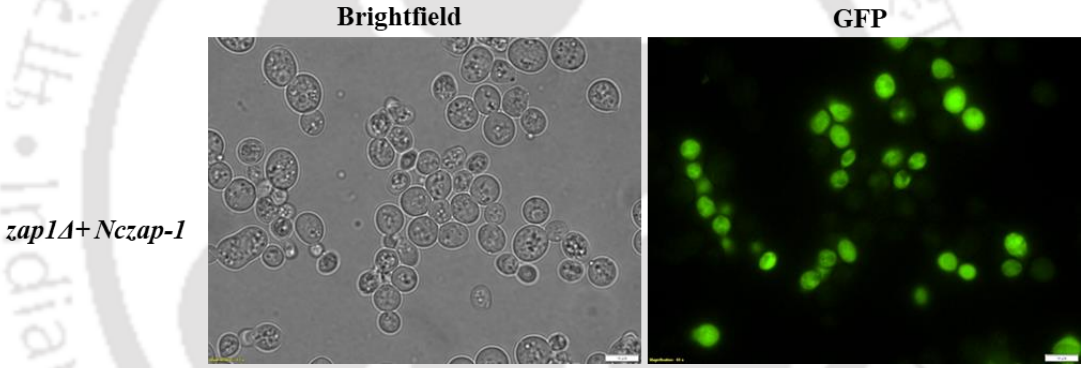

Figure 5.14 Transformation of the pSN-S5.1 into the *S. cerevisiae zap1Δ* mutant. (A) PCR confirmation of the *zap1Δ* + *Nczap-1* transformant colonies. The PCR products were resolved in an 0.8 % agarose gel; M, 1 kb DNA ladder (NEB, Ipswich, MA, USA); lane 1, PCR amplified product of the *zap-1* gene using the NCU02699 Fw forward and NCU02699 reverse primer pairs; lane 2, PCR amplified product for verification using the Pnit-6 Fw forward and GFP Rv reverse primer pairs, lane 3, PCR amplified product (positive control) of the pSN-S5.1 plasmid construct using the Pnit-6 Fw forward and GFP Rv reverse primers, lane 4, PCR amplified product (negative control) of wild type of *S. cereviseae* using the Pnit-6 Fw forward and GFP Rv reverse primer pairs. **(B)** Analysis of GFP

expression in transformant *zap1Δ* + *Nczap-1*, using an inverted microscope (Olympus IX83, Japan). The samples were illuminated with a pE-300 white CoolLED light source, and visualized using a green fluorescence filter set and images were captured. Scale bar =10 μM.

5.2.3.2 The *N. crassa zap-1* complements the slow growth phenotype of the *S. cerevisiae zap1Δ* mutant

The *S. cerevisiae zap1Δ* mutant exhibits slow growth phenotype in medium containing low zinc (Figure 5.15; Zhao and Eide 1997). Therefore, I investigated the complementation analysis using the *S. cerevisiae* transformant *zap1Δ* + *Nczap-1*. The cells were spotted on YPD agar media with (100 μM $ZnSO_4$) or without zinc (containing EDTA), and incubated at 30 °C for two days. In low zinc conditions, the *zap1Δ* mutant was not able to grow; however, this slow growth phenotype was rescued when zinc was added. Moreover, the *zap1Δ* + *Nczap-1* strain was able to partially complement the growth defect of *zap1Δ* mutant under low zinc conditions (Figure 5.15 A). I also performed a growth kinetics assay under different zinc concentrations. Similar to colony spot assay, the *zap1Δ* + *Nczap-1* strain did not show distinct growth and doubling time as compared to WT under the low zinc conditions, suggesting that the *zap1Δ* + *Nczap-1* transformant was able to complement the slow growth of *S. cerevisiae zap1Δ* mutant (Figure 5.15 B, C). Therefore, the ZAP-1 protein functions are conserved between *S. cerevisiae* and *N. crassa*.

(A)

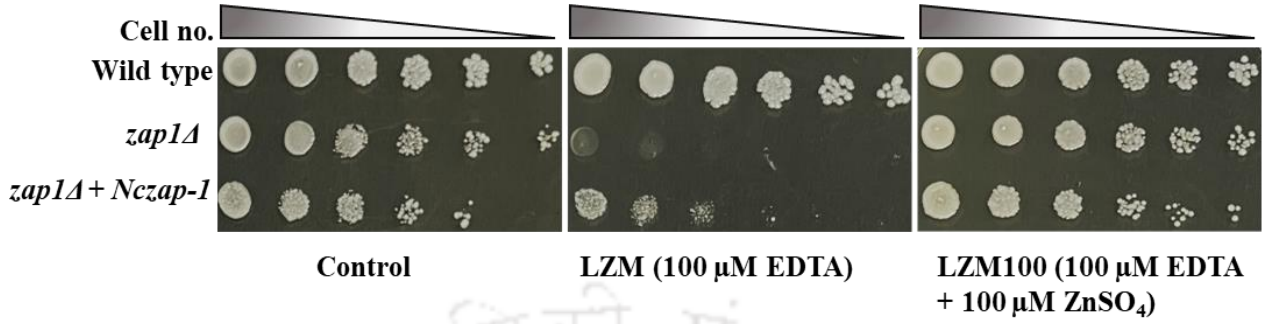

(B)

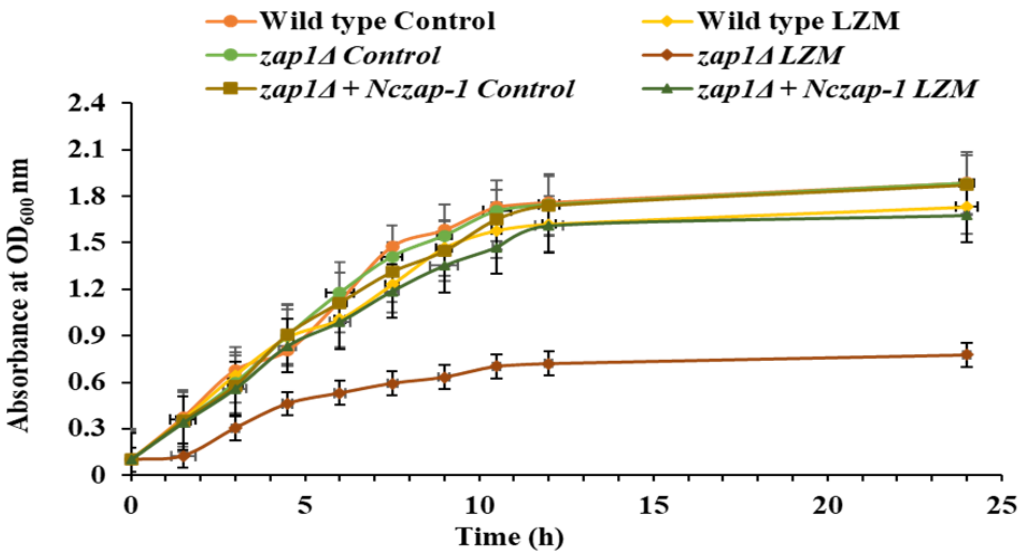

(C)

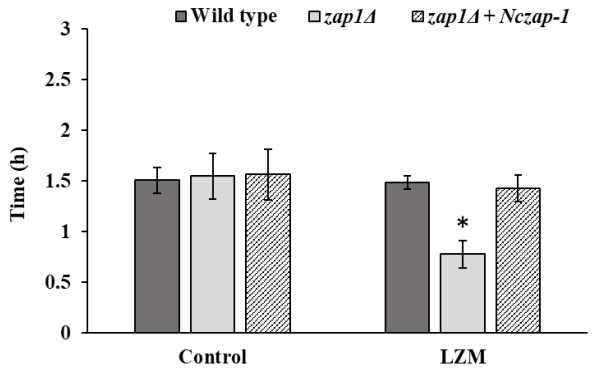

Figure 5.15 Complementation study of the *S. cerevisiae zap-1Δ* mutant. (A) Colony spot assay. The cells were resuspended in sterile water to obtain OD_{600} nm = 1, and serial dilutions (six 5-fold dilution; Zubko and Zubko 2014) of each strain were spotted onto YPD agar, Low Zinc Medium (LZM, YPD agar + 100 µM EDTA), and LZM100 (YPD agar + 100 µM EDTA + 100 µM $ZnSO_4$) plates. The plates were incubated h at 30 °C for two days to visualize cell growth. **(B)** Growth curve for *S. cerevisiae* strains. The cells were grown in control (YPD) and LZM (YPD + 100 µM EDTA). The cultures were incubated at 30 °C with shaking at 180 rpm and the OD_{600} was recorded at every 2 h interval till the 12 h, and the final OD_{600} was recorded at 24 h. The growth curve was plotted using OD_{600} against time. **(C)** The doubling time of the strains to represent the differences in growth rates during the exponential growth phase in control (YPD) and LZM (YPD + 100 µM EDTA). Error bars represent the standard deviations estimated from the data for three separate experiments (n = 3). In comparison with the wild type, the statistical significances were estimated by one-way ANOVA test and are represented by *P-values*< 0.05 (*), < 0.01 (**), and < 0.001 (***).

5.2.4 Genetic interaction of *zap-1* with *zrc-1*, *msc-2*, and *zrg-17* in *N. crassa*

5.2.4.1 Generation of the Δ*zap-1*; Δ*zrc-1*, Δ*zap-1*; Δ*msc-2*, Δ*zap-1*; Δ*zrg-17* double mutants

To generate Δ*zap-1*; Δ*zrc-1*, Δ*zap-1*; Δ*msc-2*, and Δ*zap-1*; Δ*zrg-17* double mutants, the individual parental single mutant strains were crossed (Figure 5.16 A). After 21 days, the ascospores from these crossings were harvested and germinated by heat shock at 60 °C for 45 min and plated on the FGS medium. The germinated progenies were picked on VG agar medium, and incubated at 30 °C for two days in the dark and at room temperature for one day under light. The progenies were screened for resistance to hygromycin B resistance phenotype, and the presence of the respective knockout allele was confirmed by PCR analysis. The common reverse primer 5HPHR was used in combination with

the forward primers HI-NCU02699Fw, HI-ZRC-1 SN, HI-MSC-2 SN, and Zrg-17-KOC-F, which are specific for the 5′ flanks of the *zap-1*, *zrc-1*, *msc-2*, and *zrg-17* genes, respectively (Figure 5.16 B).

(A)

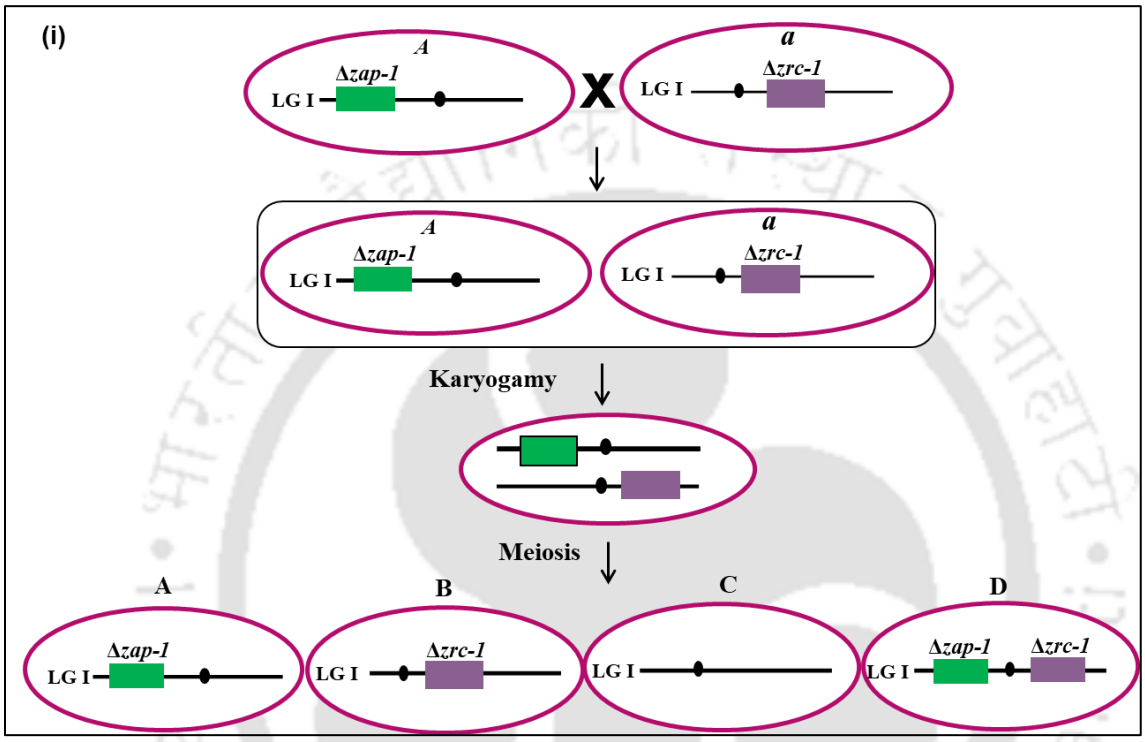

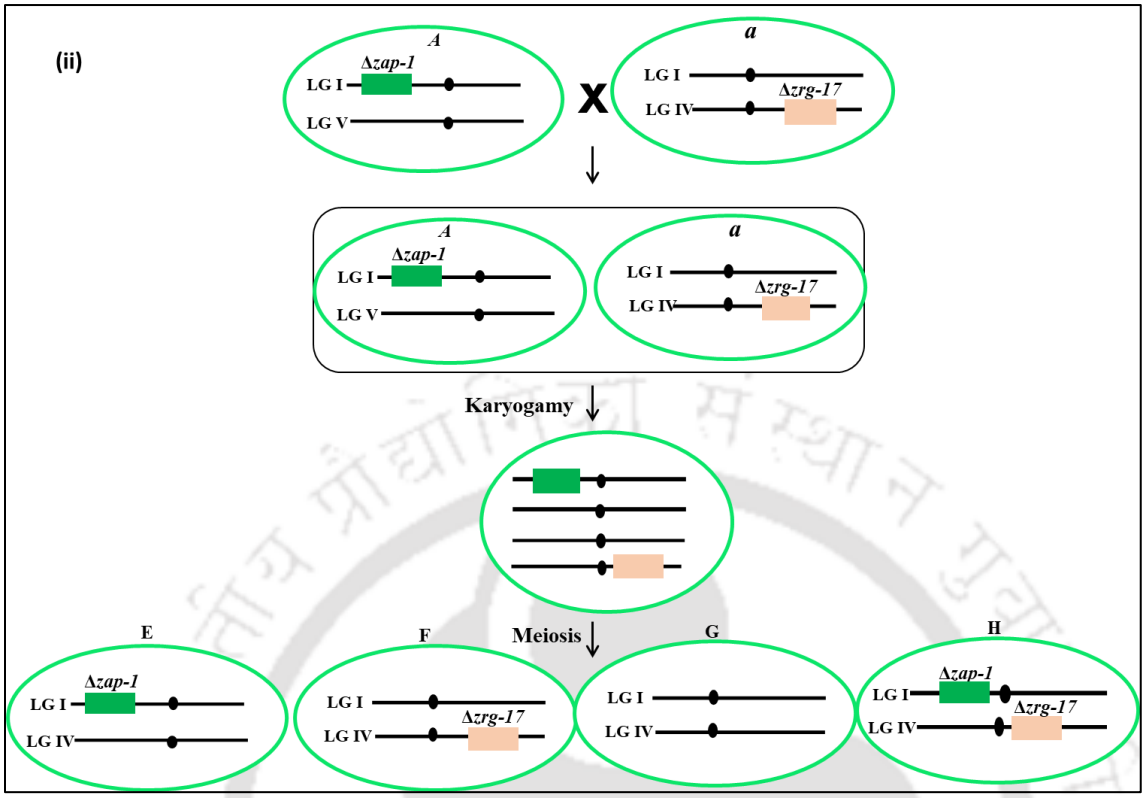

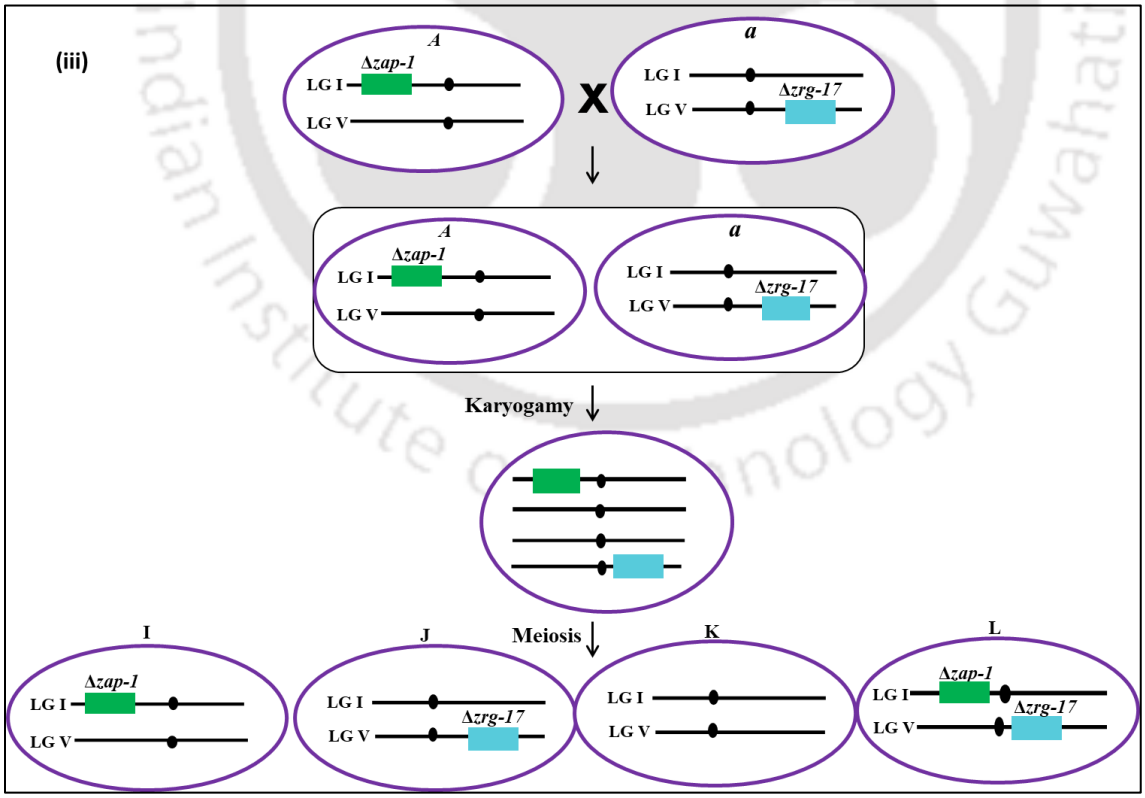

(B)

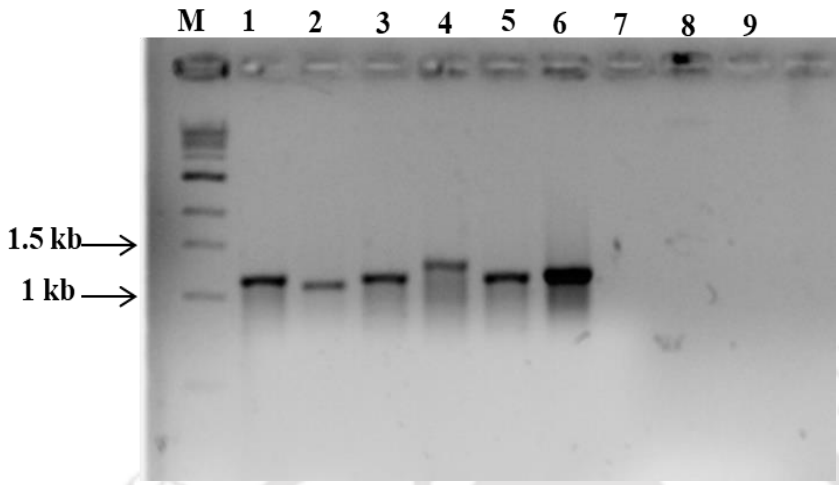

Figure 5.16 Generation of the double mutants and confirmation by PCR analysis. (A) Schematic of the crosses to generate the double mutants. The Δ*zap-1*, Δ*zrc-1*, Δ*msc-2*, and Δ*zrg-17* single mutants were crossed with the opposite mating type strains to generate Δ*zap-1*; Δ*zrc-1* (D), Δ*zap-1*; Δ*msc-2* (H), and Δ*zap-1*; Δ*zrg-17* (L) double mutants. **(B)** Confirmation of the Δ*zap-1*; Δ*zrc-1*, Δ*zap-1*; Δ*msc-2*, and Δ*zap-1*; Δ*zrg-17* double mutants by PCR. The PCR amplicon of size ~1.41 kb, 1.47 kb, 1.45 kb, and 1.39 kb confirmed the presence of Δ*zap-1*, Δ*zrc-1*, Δ*msc-2,* and Δ*zrg-17* alleles in the mutants. PCR amplified product of ~1.41 kb was observed for the Δ*zap-1* allele in the Δ*zap-1*; Δ*zrc-1* (lane 1), Δ*zap-1*; Δ*msc-2* (lane 3) and Δ*zap-1*; Δ*zrg-17* (lane 5) double mutants. PCR amplified product of ~1.39 kb was observed for the Δ*zrg-17* allele in the Δ*zap-1*; Δ*zrg-17* (lane 2) double mutants. PCR amplified product of ~1.47 kb was observed for the Δ*zrc-1* allele in the Δ*zap-1*; Δ*zrc-1* (lane 4). PCR amplified product of ~1.45 kb was observed for the Δ*msc-2* allele in the Δ*zap-1*; Δ*msc-2* (lane 6) double mutants. The wild type was used as the control (lanes 7, 8, and 9) in the PCR. The PCR products were visualized in a 0.8% agarose gel; M, 1 kb DNA Ladder (NEB, Ipswich, MA, USA).

5.2.4.2 The Δ*zap-1;* Δ*zrc-1*, Δ*zap-1*; Δ*msc-2,* and Δ*zap-1;* Δ*zrg-17* double mutants showed impaired vegetative development under low zinc condition

To study the colony morphology of the wild type, Δ*zap-1*, Δ*zrc-1*, Δ*msc-2*, Δ*zrg-17*, Δ*zap-1*; Δ*zrc-1,* Δ*zap-1*; Δ*msc-2*, and Δ*zap-1*; Δ*zrg-17* under different zinc conditions, agar plugs containing each of the strain were inoculated on VG agar medium supplemented with various amounts of zinc. The Δ*zap-1*; Δ*msc-2* and Δ*zap-1;* Δ*zrg-17* double mutants showed impaired growth in low zinc conditions, and Δ*zap-1;* Δ*zrc-1* showed slow growth phenotype in both low and high zinc conditions (Figure 5.17 A, B). Likewise, the apical growth of Δ*zap-1;* Δ*zrc-1*, Δ*zap-1*; Δ*msc-2,* and Δ*zap-1;* Δ*zrg-17* double mutants was halted after 24 h post-inoculation under the zinc-deprived conditions (Figure 5.18 C), suggesting that these mutants were able to adapt in the zinc depleted environment only in the beginning of stress condition. Similarly, the Δ*zap-1;* Δ*zrc-1*, Δ*zap-1*; Δ*msc-2,* and Δ*zap-1;* Δ*zrg-17* double mutants showed stunted aerial hyphae under low zinc conditions (Figure 5.18). These results indicated that *zap-1* interacts with *zrc-1*, *msc-2*, and *zrg-17* under low zinc conditions for proper vegetative development in *N. crassa*.

(A)

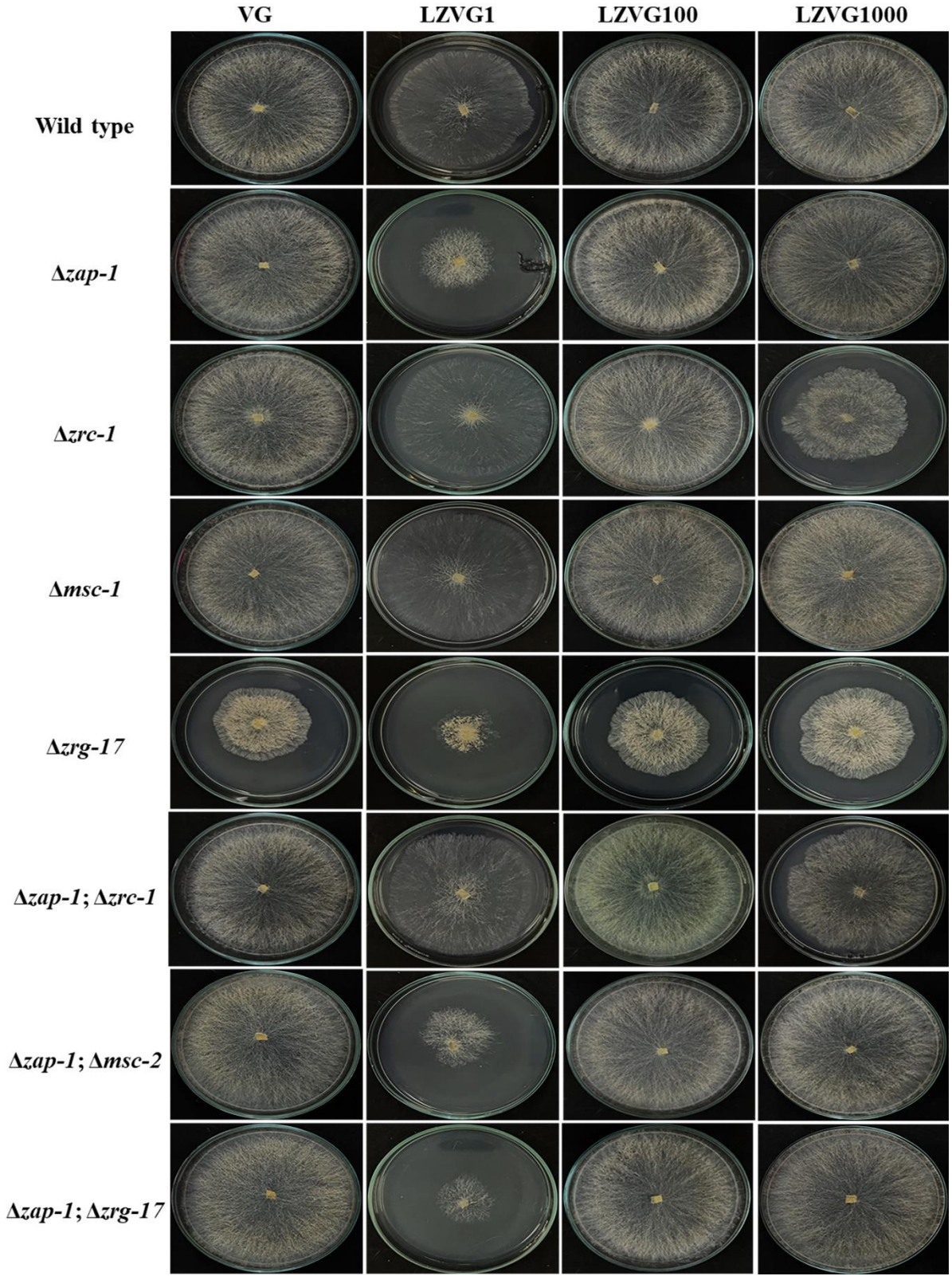

(B)

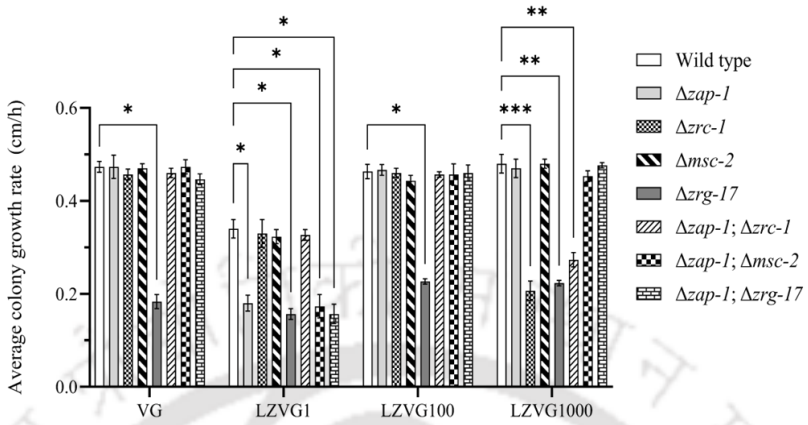

(C)

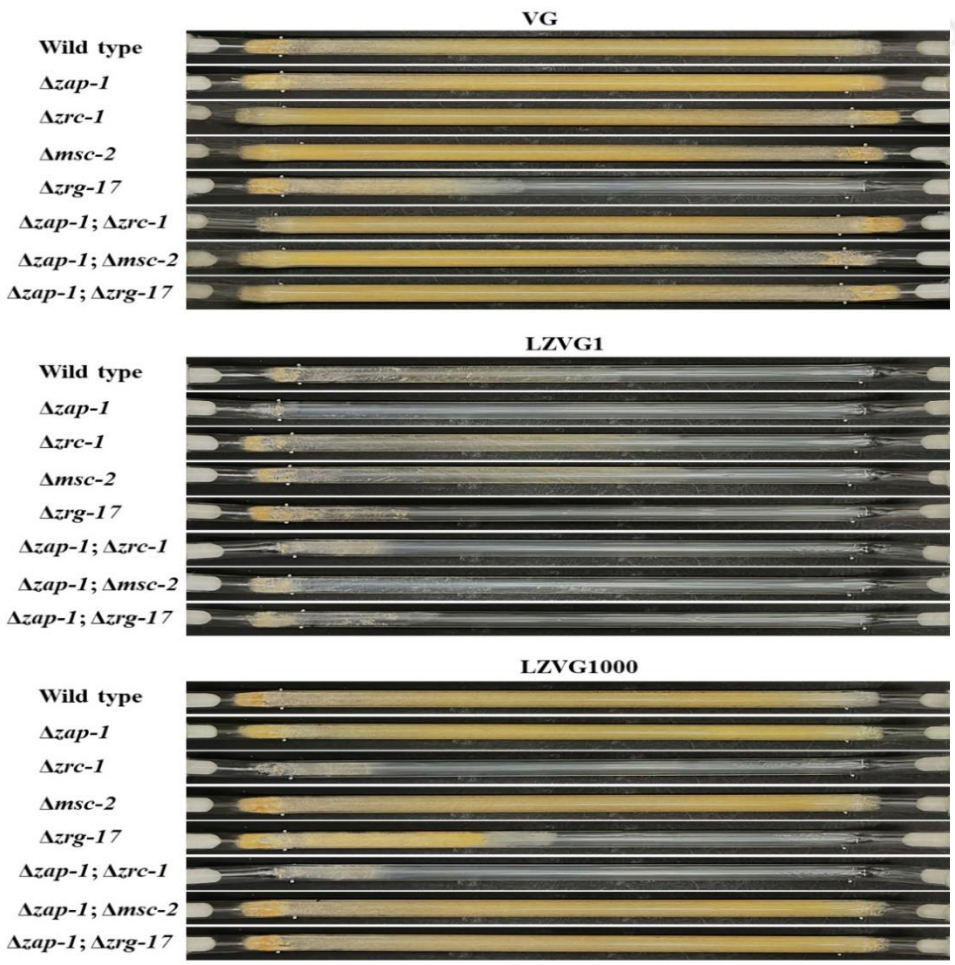

Figure 5.17 Growth phenotype of the wild type, Δ*zap-1*, Δ*zrc-1*, Δ*msc-2,* Δ*zrg-17* single and double mutant strains (A) Colony morphology. The agar pluck of *N. crassa* strains was inoculated at the center of the VG agar plates containing different concentrations of zinc and incubated at 30 °C in the dark for 24 h and photographed. **(B)** Average growth rate. The radial growths were measured and average growth rates of each strain were calculated and plotted on the graph. Error bars represent the standard deviations estimated from the data for three separate experiments (n = 3) with P-values < 0.05 (*), <0.01 (**), and <0.001 (***) compared with the wild type strain as measured by two-way ANOVA analysis with Tukey's *post hoc* test. **(C)** Apical growth of the double mutants in the race tubes. The strains were inoculated at one end of the tube containing VG agar media with various concentrations of zinc and incubated at 30 °C in the dark for three days and photographed.

(A)

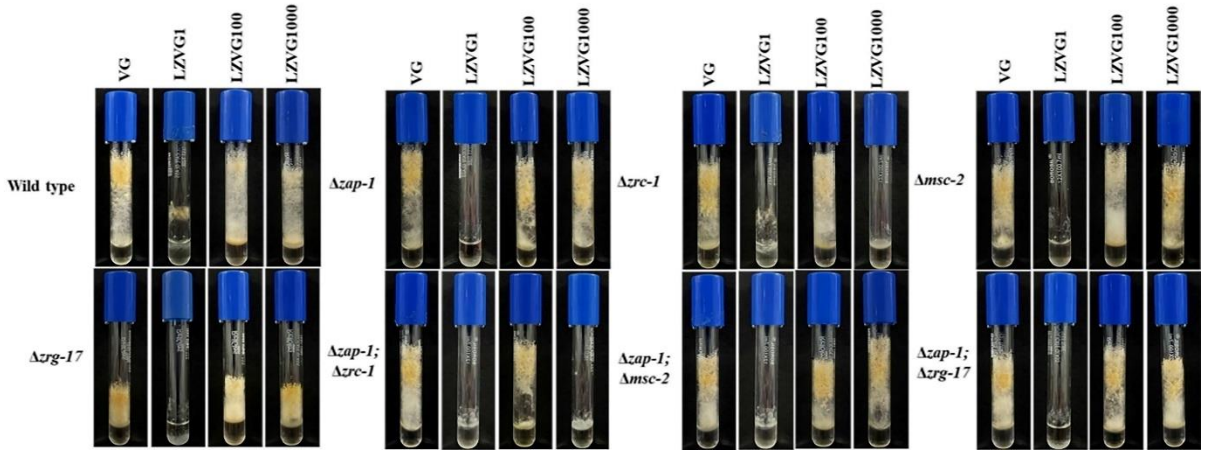

(B)

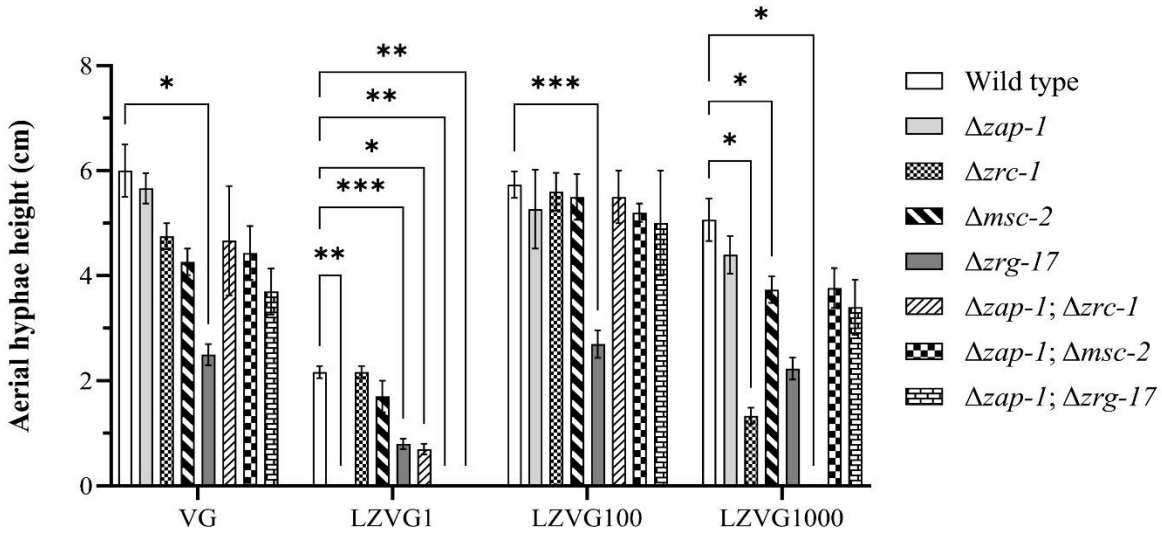

Figure 5.18 Aerial hyphae in the wild type, Δ*zap-1*, Δ*zrc-1*, Δ*msc-2,* Δ*zrg-17* single mutant and double mutant strains. **(A)** Development of the aerial hyphae. Conidial suspension (~ 1 × 10^6 cells/ml) of *N. crassa* strains was inoculated in test tubes containing VG liquid media with various concentrations of zinc and incubated at 30 °C in the dark for three days and in light for two days and photographed. **(B)** Average aerial hyphae height. The aerial hyphae heights of each strain were measured and plotted. Error bars represent the standard deviations estimated from the data for three separate experiments (n = 3) with P-values < 0.05 (*), <0.01 (**), and <0.001 (***) compared with the wild type strain as measured by one-way ANOVA test. two-way ANOVA analysis with Tukey's *post hoc* test with P-values < 0.05 (*), < 0.01 (**), and < 0.001 (***).

5.2.4.3 Temperature sensitivity analysis of the Δ*zap-1;* Δ*zrc-1*, Δ*zap-1*; Δ*msc-2,* and Δ*zap-1;* Δ*zrg-17* double mutants

Temperature is one of the main environmental elements that directly influences the structure and function of proteins, and consequently affect the growth and development in fungi (Suutari 1995;

Bakar et al. 2020; Zhao et al. 2020). In *N. crassa*, the temperature is a key environmental component for the regulation of vegetative development, including hyphal elongation, mycelium formation, regulation of the circadian rhythm, and carotenoid production, and entry to the sexual phase that yields ascospores (Colvin 1981; Springer and Yanofsky 1989; Diernfellner et al. 2005; Kronholm and Ketola 2018). the growth rates of Δ*zap-1*, Δ*zap-1;* Δ*zrc-1*, Δ*zap-1*; Δ*msc-2*, and Δ*zap-1;* Δ*zrg-17* mutants were comparable to wild type under standard zinc conditions at optimum temperature (30 °C) (Figure 5.18). Therefore, I determined the growth rate of the *N. crassa* strains at both a high (40 °C) and low (20 °C) temperatures. The Δ*zap-1*, Δ*zrc-1*, Δ*msc-2,* Δ*zrg-17* single mutants and Δ*zap-1;* Δ*zrc-1*, Δ*zap-1*; Δ*msc-2*, and Δ*zap-1;* Δ*zrg-17* double mutants did not show distinct growth differences at 20 °C and 40 °C in comparison to the wild type (Figure 5.19; Table 5.2).

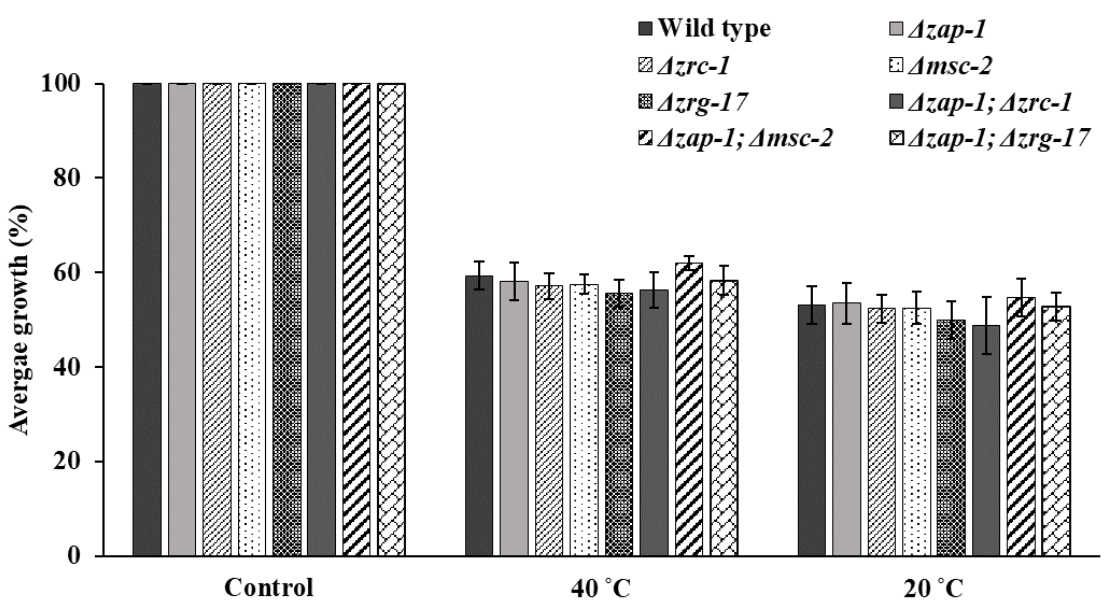

Figure 5.19 Temperature sensitivity assay in the double mutants. The *N. crassa* strains were inoculated on VG agar medium and incubated at low (20 °C), and high (40 °C) temperatures and the average growth rate was determined and compared to growth at the optimum temperature (30

°C). Error bars represent the standard deviations estimated from the data for three separate experiments (n = 3).

Table 5.2 Average colony growth rate of wild type, Δ*zap-1*, Δ*zrc-1*, Δ*msc-2,* Δ*zrg-17* single mutant and Δ*zap-1;* Δ*zrc-1*, Δ*zap-1*; Δ*msc-2,* and Δ*zap-1;* Δ*zrg-17* double mutants at 30 °C, 40 °C and 20 °C

Strains	Average colony growth rate (cm/h)[a]		
	30 °C	40 °C	20 °C
Wild type	0.42 ± 0.03	0.26 ± 0.01	0.24 ± 0.03
Δ*zap-1*	0.43 ± 0.03	0.25 ± 0.04	0.23 ± 0.03
Δ*zrc-1*	0.42 ± 0.04	0.24 ±0.015	0.22 ± 0.02
Δ*msc-2*	0.4 ± 0.01	0.23 ±0.019	0.21 ± 0.03
Δ*zrg-17*	0.16 ± 0.03	0.089 ± 0.04	0.08 ± 0.04
Δ*zap-1*; Δ*zrc-1*	0.39 ± 0.02	0.22 ± 0.08	0.19 ± 0.1
Δ*zap-1*; Δ*msc*-2	0.42 ± 0.04	0.26 ± 0.04	0.23 ± 0.034
Δ*zap-1*; Δ*zrg-17*	0.36 ± 0.05	0.21 ± 0.067	0.19 ± 0.02

[a] Results are shown as mean ± standard deviation for three independent experiments (n = 3).

5.2.4.4 ZAP-1 regulate expressions of *zrc-1*, *msc-2*, *zrg-17*, and *zrt3* genes under zinc deprivation in *N. crassa*

The *S. cerevisiae ZRT3*, a ZIP family member, , is Zap1p dependent and co-ordinates with Zrc1p in vacuoles to maintain zinc homeostasis (MacDiarmid et al. 2000). The closest homolog of Zrt3p in *N. crassa* is encoded by the NCU00029 gene (ZIP metal ion transporter, *trm-33*). There was no prior availability of reports on NCU00029 (also known as *zrt-3*); however, I determined the expression level in the Δ*zap-1* knockout mutant under the low-zinc conditions (Figure 5.20). Under low zinc conditions, the expression levels of *zrc-1* and *zrg-17* were elevated in a ZAP-1 dependent manner and *msc-2* expression was independent of zinc (Tiwari et al. 2018; Chapter 3). To confirm that ZAP-1 is the sole

transcriptional regulator active during low zinc conditions in *N. crassa*, I investigated the transcript levels of the zinc transporters *zrc-1*, *msc-2*, *zrg-17*, and *zrt3* (Figure 5.22). The *zrc-1*, *msc-2*, and *zrg-17* are members of the CDF family of zinc transporters and the genetic interactions amongst these genes are essential for maintaining zinc homeostasis for proper growth and development in *N. crassa* (Chapter 3 and 4). I also determined relative expression levels of *zrc-1*, *msc-2*, *zrg-17*, and *zrt3* in the wild type and Δ*zap-1* knockout mutants. The expression of the zinc transporters was significantly reduced in the absence of ZAP-1 (Figure 5.22). These results suggested that ZAP-1 might be the sole transcriptional activator under low zinc conditions.

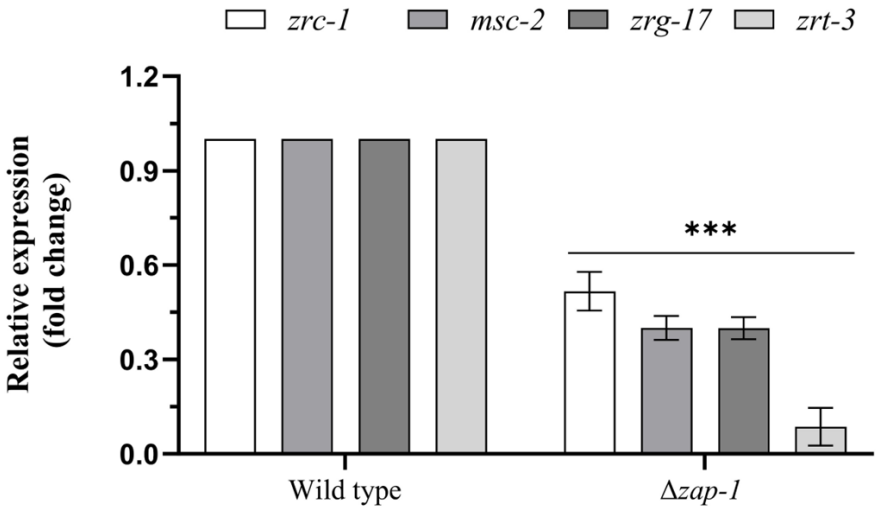

Figure 5.20 Expression analysis of the *zrc-1*, *msc-2*, *zrg-17*, and *zrt-3* genes. Conidia (10^6 conidia/ml) were inoculated in the VG liquid medium and the cultures were incubated for 16 h at 30°C with shaking at 180 rpm in total darkness. The RNA was harvested, and the relative expression of *β-tubulin* gene of *N. crassa* was used to normalize the expression of the *zrc-1*, *msc-2*, *zrg-17*, and *zrt-3* genes. The expression of the genes in the Δ*zap-1* mutant was compared to the expression in wild type. Error bars represent the standard deviations estimated from the data for three separate experiments (n

= 3) with P-value <0.05 (*), <0.01 (**), and <0.001 (***) two-way ANOVA analysis with Tukey's *post hoc* test.

5.2.5 A mechanistic model of zinc uptake, intracellular transport, and regulation in *N. crassa*

The process of zinc transport begins at the plasma membrane, where specialized ZIP family of zinc transporters (TZN1 and TZN2; Kiranmayi et al. 2009) facilitate the uptake of extracellular zinc ions into the cell when the concentration of zinc is low in the cell. In response to excess cytoplasmic zinc, the CDF transporter ZRC-1 protects the cells against zinc overload probably by transferring the excess zinc into vacuoles for storage (Figure 5.21). ZRG-17, an ER-localized CDF zinc transporter, plays a crucial role in ER function, vegetative growth, and asexual sporulation (Tiwari et al. 2018). In addition, genetic interaction between *msc-2* and *zrg-17* suggested their involvement in the same pathway. These zinc transporters are regulated by zinc concentrations in a ZAP-1 dependent manner. Furthermore, the ZAP-1 transcription factor, which is comprised of 710 amino acids and seven C2H2 zinc fingers, plays a critical role during low zinc conditions and is consequently upregulated under low zinc conditions. Additionally, ZAP-1 remains in the nucleus irrespective of the cytosolic zinc concentrations and possibly involves in the regulation of zinc transporter genes *zrc-1*, *zrg-17*, and *zrt3* by binding to the zinc responsive element (ZRE) within their promoter regions (Figure 5.21).

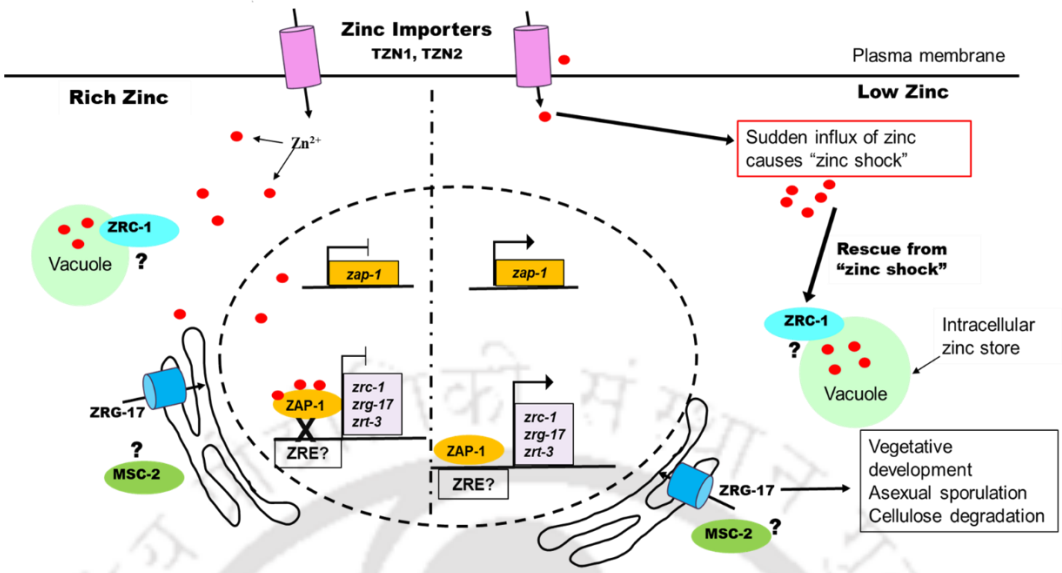

Figure 5.21 Mechanistic model depicting the role of zinc transporters *zrc-1*, *msc-2*, *zrg-17*, and *zap-1* in *N. crassa*. The CDF zinc transporters *zrc-1*, *zrg-17*, and *msc-2* functions in synchronization under the low and high zinc conditions to ensure optimum zinc concentrations for proper functioning of the cell. When cytosolic zinc concentration is low or depleted, the ZIP transporter proteins TZN1 and TZN2 transport zinc into cells through the plasma membrane (Kiranmayi et al. 2009). Alternatively, when zinc concentration is high or excessive, the ZnT/CDF transporter proteins ZRC-1, MSC-2, and ZRG-17 transport zinc into subcellular organelles. The zinc dependent transcriptional activator ZAP-1 is upregulated under low zinc conditions, and responsible for the up-regulation of several target genes such as *zrc-1*, *zrg-17* and *zrt3* under low zinc. TZN: zinc transporter; ZRC-1: zinc resistance conferring 1; MSC-2: meiotic sister chromatid 2; ZRG-17: zinc regulated gene 17; ZRT: zinc regulated transporter 3; ZAP-1: zinc activator protein 1; ZRE: zinc responsive element.

5.3 Discussion

The Zap1 transcriptional activator controls the expression of many genes in response to low zinc levels in *S. cerevisiae*, *A. fumigatus*, *C. albicans*, and *C. gattii* (Eide 2021). This helps the cell to maintain a constant intracellular environment for zinc even when the environment outside the cell changes and

also allows the cell adapt to zinc deficiency by changing the stress-related metabolic pathways. Hence, it is possible to hypothesize that ZAP-1 might play critical role in the maintenance of zinc homeostasis and the metabolic response to zinc deprivation in the filamentous fungus *N. crassa*.

In this chapter, I identified the closest homolog of Zap1p of *S. cerevisiae* in *N. crassa* using *in silico* approach. Further, I investigated the cell functions of *zap-1* gene in the development of *N. crassa* under different zinc conditions. In addition, I generated and analyzed the double mutant of *zap-1* with CDF zinc transporters *zrc-1*, *msc-2*, and *zrg-17* to understand the various phenotypic alterations that are regulated by their genetic interactions.

The sequence analysis revealed that the NCU02699 in *N. crassa* is the closest homolog to the Zap1p in *S. cerevisiae*. The sequence analysis of *N. crassa* ZAP-1 and its orthologs showed homology at the C-terminal, particularly at the zinc finger domains (Figure 5.2 A). The Zap1p of *S. cerevisiae* contains activation domains where zinc binds to activate (Bird et al. 2000b), and the DNA binding domain localized at the C-terminal comprising of C_2H_2 zinc-finger domains that binds to the promoter region of the target gene and control gene expression (Bird et al. 2000b, 2004). The Zap1p binding to the target gene is dependent on zinc concentrations and binding affinity is reduced in zinc-rich condition (Bird et al. 2000a; Frey and Eide 2011; Wilson and Bird 2016). Furthermore, phylogenetic analysis (Figure 5.2 C) revealed the closeness of ZAP-1 to the *Madurella mycetomatis* MmZafA, which is hypothesized to regulate the expression of genes involved in maintaining zinc homeostasis and is important for initiating the process of grains formation that results in mycetoma (du Pré et al. 2022).

I also predicted the three-dimensional protein structure of ZAP-1 using the structure of AD2 predicted by NMR and CD of Zap1p of *S. cerevisiae* as the template (Figure 5.3). The predicted modeled structure was validated by Ramachandran plot and structural alignment by Dali server and

modeled structure was superimposed with the template using PyMol. The predicted structure showed alignment in the region of ZF2 and ZF3 of ZAP-1 of *N. crassa* to the two zinc fingers of AD2 (ZF1 and ZF2), which is crucial for binding to zinc (Bird et al. 2000b), indicating the conservation of these activation domains in *S. cerevisiae* and *N. crassa* (Figure 5.3). In comparison to other zinc-binding sites, zinc bound to AD2 is extremely labile, which might be an important factor in their effectiveness in sensing zinc (Qiao et al. 2006). Therefore, these results suggested that the ZAP-1 in *N. crassa* is regulated by zinc in a manner similar to that of *S. cerevisiae*.

To understand the functional importance of ZAP-1 in *N. crassa*, I determined how zinc regulates *zap-1* expression using qRT-PCR. The overexpression of *zap-1* suggested that *zap-1* plays an important role under low zinc conditions (Figure 5.5). Moreover, the Δ*zap-1* knockout mutant was not able to grow in low zinc; however, this phenotype was rescued by increasing the concentrations of zinc (Figure 5.7). Similar growth defects under a zinc-deprived state were also reported in *S. cerevisiae* (Zhao and Eide 1997), *C. albicans* (Kim et al. 2008), *Candida dubliniensis* (Böttcher et al. 2015), and *Candida glabrata* (Gaspar-Cordeiro et al. 2022). Furthermore, I tested if the wild type ZAP-1 can complement the slow growth phenotype of Δ*zap-1* mutant under low zinc. To test this, I cloned the wild type *zap-1* under the *ccg-1* promoter in the vector pMF272, and transformed the plasmid construct into *N. crassa* recipient strain, and generated the $P_{ccg\text{-}1}$*::zap-1::gfp* homokaryotic strain. The $P_{ccg\text{-}1}$*::zap-1::gfp* strain was able to complement the slow growth phenotype of Δ*zap-1* mutant (Figures 5.10, 5.11, and 5.12). Therefore, the *zap*-1 gene is critical for survival under low zinc conditions in *N. crassa*.

Previous studies revealed that the zinc concentration in the medium does not affect the localization of Zap1p, which is localized in the nucleus of *S. cerevisiae* (Zhao and Eide 1997; Bird et al. 2000b). Similarly, the ZAP-1 of *N. crassa* was found to be localized in the nucleus under all zinc

conditions (Figure 5.13), suggesting that the function of ZAP-1 is also regulated by zinc. Additionally, ZAP-1 has two potential NLS (KHKR) and (RRHMKTHQK) in the ZF6 and ZF7 zinc finger regions, respectively, which are similar to the previously reported consensus of NLS sequences (Boulikas 1994).

Under zinc-limiting conditions, the *zap1Δ* knockout mutant of *S. cerevisiae* was not able to grow unless a significant amount of zinc is supplemented in the medium (Zhao and Eide 1997). Therefore, I investigated if the *N. crassa* ZAP-1 could rescue the slow growth phenotype of the *zap1Δ* knockout mutant of *S. cerevisiae*. I generated a *S. cerevisiae* transformant *zap1Δ* + *Nczap-1*, which was able to grow under zinc-limiting conditions (Figure 5.16). Interestingly, these results suggested that the ZAP-1 protein of *N. crassa* activates the promoter for zinc transporters in *S. cerevisiae*. In conclusion, despite the structural differences, the ability of the *N. crassa* ZAP-1 protein to rescue Zap1p function in the *S. cerevisiae zap1Δ* mutant suggested that, ZAP-1 potentially act as a transcriptional activator in *N. crassa*.

When two genes undergo mutations, sometimes the resulting phenotype is unexpected, considering the separate effects of each mutation. This phenomenon, which exhibits genetic interaction, can reveal how certain pathways and genes function (Mani et al. 2008). In Chapter 4, double mutants of the CDF zinc transporters *zrc-1*, *mzc-2*, and *zrg*-17 were investigated to study the genetic interactions among these genes. Likewise, to get a better understanding of the genetic interaction of the transcription factor *zap-1* with the CDF zinc transporters, double mutants Δ*zap-1*; Δ*zrc-1*, Δ*zap-1*; Δ*msc-2* and Δ*zap-1*; Δ*zrg-17* were generated (Figure 5.17). The phenotypes of the double mutants were studied under different concentrations of zinc. In normal conditions, the double mutants showed phenotypes similar to the wild type (Figure 5.17). However, the Δ*zap-1*; Δ*zrc-1*, Δ*zap-1*; Δ*msc-2*, and Δ*zap-1*; Δ*zrg-17* double mutants showed restricted growth similar to Δ*zap-1*

mutant under low zinc conditions, suggesting that *zap-1* is epistatic to *zrc-1*, *mzc-2*, and *zrg-17* (Figure 5.17 and Figure 5.18). This genetic interaction suggested that ZAP-1, like Zap1p of *S. cerevisiae* (Eide 2009, 2020) might be the only transcriptional activator functioning under low zinc conditions in *N. crassa*. The low expression levels of the *zrc-1*, *msc-2*, *zrg-17*, and *zrt-3* zinc transporters in the Δ*zap-1* mutant under low zinc provided additional evidence that ZAP-1 might be the only transcriptional regulator of these zinc transporters under these circumstances. This suggests that no other transcriptional activator can effectively activate these zinc transporters and sustain a consistent zinc supply because ZAP-1 is absent in the Δ*zap-1* knockout mutant. Therefore, ZAP-1 acts as the sole regulator of *zrc-1*, *msc-2*, *zrg-17*, and *zrt-3* zinc transporters under low zinc conditions in *N. crassa*.

A part of the results described in this chapter was presented as a poster at XI International Conference on Biology of Yeast and Filamentous Fungi, University of Hyderabad, India, November 27-29, 2019.

6

CONCLUSIONS AND FUTURE PERSPECTIVES

Major conclusions of this study

In this study, I investigated the cellular roles of *zrc-1* and *msc-2* members of zinc transporter belonging to the CDF family in *N. crassa*, using their knockout mutant strains. Sequence analysis has revealed that NCU03145 and NCU07262 show significant sequence similarities to the homologs of zinc resistance-conferring 1 (ZRC-1) and meiotic sister chromatid 2 (MSC-2), respectively, that are highly conserved among the members of fungal species. The ZRC-1 and MSC-2 of *N. crassa* exhibit the typical features of the other classical CDF proteins, including six transmembrane helices, a histidine-rich cytoplasmic loop, and a long C-terminal domain (≥100 aa). Moreover, the predicted structure of ZRC-1 and MSC-2 of *N. crassa* revealed that the zinc-binding motif DD-HD (Lu and Fu 2007) is partially conserved in ZRC-1 and MSC-2 as HD-HD motif, suggesting that they might be involved in zinc transportation. Additionally, the Δ*zrc-1* mutant exhibits a slow growth rate under high zinc (≥ 0.5 mM) conditions. However, the expression of *zrc-1* gene was elevated under low zinc conditions, suggesting the involvement of *zrc-1* in the growth and development of *N. crassa* under low zinc conditions.

I generated the Δ*zrc-1*; Δ*msc-2*, Δ*msc-2*; Δ*zrg-17*, and Δ*zrc-1*; Δ*zrg-17* double mutants to study their phenotypes for understanding genetic interactions of these genes. The Δ*msc-2;* Δ*zrg-17* double mutant showed antagonistic interaction and the Δ*zrc-1;* Δ*zrg-17* double mutant exhibited additive phenotype resulting in severe growth defects, irregular septation, defects in conidiation, and could not grow in the medium containing cellulose as carbon source. In addition, the Δ*zrc-1*; Δ*msc-2*, and Δ*zrc-1*; Δ*zrg-17* double mutants showed sensitivity to ER stress. Therefore, the *zrc-1*, *msc-2,* and *zrg-17* genes genetically interact to regulate several cell functions in *N. crassa*.

Furthermore, I identified the *N. crassa* homolog of the *S. cerevisiae* zinc activator protein (Zap1p). Sequence analysis revealed that the *N. crassa NCU02699* gene encodes ZAP-1 that displays

sequence homology with the *S. cerevisiae* Zap1p, particularly within the zinc finger domains in the C-terminal region. Moreover, the predicted protein structure of ZAP-1 demonstrates a resemblance in zinc binding characteristics between ZF2 and ZF3 in ZAP-1 of *N. crassa* and the ZF1 and ZF2 in Zap1p of *S. cerevisiae*. This similarity could potentially play a crucial role in their ability to effectively sense zinc. Additionally, the elevated gene expression of *zap-1* under low zinc conditions and localization of ZAP-1 in the nucleus under all zinc conditions demonstrated the functional significance of *zap-1* in *N. crassa*.

Interspecies complementation of the *S. cerevisiae zap1Δ* mutant by the *N. crassa zap-1* allele suggested functional conservation of the ZAP-1 transcriptional activator in these two organisms. In addition, I generated the Δ*zap-1*; Δ*zrc-1*, Δ*zap-1*; Δ*msc-2*, and Δ*zap-1*; Δ*zrg-17* double mutants to study the genetic interactions between *zap-1*, *zrc-1*, *msc-2* and *zrg-17* genes in *N. crassa*. The slow growth of Δ*zap-1*; Δ*zrc-1*, Δ*zap-1*; Δ*msc-2*, and Δ*zap-1*; Δ*zrg-17* double mutants under low zinc conditions suggested that *zap-1* might function upstream of *zrc-1*, *msc-2,* and *zrg-17*. Additionally, the low-level expression of *zrc-1*, *msc-2*, *zrg-17,* and *zrt-3* genes in the Δ*zap-1* mutant indicated that ZAP-1 might be the primary regulator of the zinc transporters under low zinc conditions in *N. crassa*.

Future perspectives of this research work

Further studies on the regulation and functional significance of these transporters will provide a deeper insight into their roles in *N. crassa*. The future directions of this research work are:

(i) Protein localization study of ZRC-1 and MSC-2 under varying zinc concentrations to understand the molecular mechanism of these transporters regulating the zinc level in *N. crassa*,

(ii) Protein-protein interaction study of MSC-2 and ZRG-17 by Co-Immunoprecipitation (CoIP) to validate the interaction of these two proteins,

(iii) Expression analysis of cellulose-degrading enzymes (cellobiose dehydrogenase) such as *cbh-1* (NCU07340), *gh6-2* (NCU09680), and *gh5-1* (NCU00762) in the Δ*zrc-1*; Δ*msc-2* and Δ*zrc-1*; Δ*zrg-17* double mutants to investigate the role of CDF zinc transporters in cellulose utilization, and

(iv) The protein-DNA interaction of the transcriptional factor ZAP-1 with the CDF zinc transporters genes, by chromatin immunoprecipitation (ChIP), followed by electrophoretic mobility shift assay (EMSA) to determine the specific binding sequence of ZAP-1 in the promoter of the target genes.

BIBLIOGRAPHY

Adlard PA, Parncutt JM, Finkelstein DI, Bush AI (2010) Cognitive loss in zinc transporter-3 knock-out mice: a phenocopy for the synaptic and memory deficits of Alzheimer's disease? J Neurosci 30:1631–1636

Akache B, Turcotte B (2002) New Regulators of Drug Sensitivity in the Family of Yeast Zinc Cluster Proteins*. J Biol Chem 277:21254–21260.

Alah V, Mahjen J, Sepehri M, Khatabi B (2021) Rhizosphere Alleviation of zinc deficiency in wheat inoculated with root endophytic fungus *Piriformospora indica* and rhizobacterium *Pseudomonas putida*. Rhizosphere 17:100311.

Alamir OF, Oladele RO, Ibe C (2021) Nutritional immunity: targeting fungal zinc homeostasis. Heliyon 7:e07805.

Altherr MR, Quinn LA, Kado CI, Rodroguez RL (1983) Transformation and Storage of Competent Yeast Cells. In: Lurquin PF, Kleinhofs A (eds) Genetic Engineering in Eukaryotes. Springer US, Boston, MA, pp 33–36

Altschul SF, Gish W, Miller W, et al (1990) Basic local alignment search tool. J Mol Biol 215:403–410.

Altschul SF, Madden TL, Schäffer AA, et al (1997) Gapped BLAST and PSI-BLAST: a new generation of protein database search programs. Nucleic Acids Res 25:3389–3402.

Amich J, Calera JA (2014) Zinc acquisition: a key aspect in *Aspergillus fumigatus* virulence. Mycopathologia 178:379–385

Amich J, Vicentefranqueira R, Mellado E, et al (2014) The ZrfC alkaline zinc transporter is required for *Aspergillus fumigatus* virulence and its growth in the presence of the Zn/Mn-chelating protein calprotectin. Cell Microbiol 16:548–564

Amico-Ruvio SA, Murthy SE, Smith TP, Popescu GK (2011) Zinc effects on NMDA receptor gating kinetics. Biophys J 100:1910–1918.

Andreini C, Bertini I, Cavallaro G, et al (2008) Metal ions in biological catalysis: from enzyme databases to general principles. JBIC J Biol Inorg Chem 13:1205–1218

Andrews GK, Wang H, Dey SK, Palmiter RD (2004) Mouse zinc transporter 1 gene provides an essential function during early embryonic development. genesis 40:74–81

Aramayo R, Selker EU (2013) *Neurospora crassa*, a model system for epigenetics research. Cold Spring Harb Perspect Biol 5:a017921

Arpaia G, Loros JJ, Dunlap JC, et al (1995) Light induction of the clock-controlled gene *ccg-1* is not

transduced through the circadian clock in *Neurospora crassa*. Mol Gen Genet 247:157–163.

Auld DS, Bergman T (2008) Medium- and short-chain dehydrogenase/reductase gene and protein families : The role of zinc for alcohol dehydrogenase structure and function. Cell Mol Life Sci 65:3961–3970.

Bafaro E, Liu Y, Xu Y, Dempski RE (2017) The emerging role of zinc transporters in cellular homeostasis and cancer. Signal Transduct Target Ther 2:17029.

Bakar NA, Karsani SA, Alias SA (2020) Fungal survival under temperature stress: a proteomic perspective. PeerJ 8:e10423

Baker CL, Loros JJ, Dunlap JC (2012) The circadian clock of *Neurospora crassa*. FEMS Microbiol Rev 36:95–110

Baltaci AK, Yuce K (2018) Zinc transporter proteins. Neurochem Res 43:517–530

Barba-Ostria C, Lledías F, Georgellis D (2011) The *Neurospora crassa* DCC-1 protein, a putative histidine kinase, is required for normal sexual and asexual development and carotenogenesis. Eukaryot Cell 10:1733–1739.

Barber-Zucker S, Moran A, Zarivach R (2021) Metal transport mechanism of the cation diffusion facilitator (CDF) protein family – a structural perspective on human CDF (ZnT)-related diseases. RSC Chem Biol 2:486–498.

Barman A, Tamuli R (2017) The pleiotropic vegetative and sexual development phenotypes of *Neurospora crassa* arise from double mutants of the calcium signaling genes *plc-1*, *splA2*, and *cpe-1*. Curr Genet 63:861–875.

Baryshnikova A, Costanzo M, Myers CL, et al (2013) Genetic interaction networks: toward an understanding of heritability. Annu Rev Genomics Hum Genet 14:111–133

Beadle GW, Tatum EL (1941) Genetic control of biochemical reactions in Neurospora. Proc Natl Acad Sci 27:499–506

Belden WJ, Larrondo LF, Froehlich AC, et al (2007) The band mutation in *Neurospora crassa* is a dominant allele of ras-1 implicating RAS signaling in circadian output. Genes Dev 21:1494–1505.

Berg JM, Shi Y (1996) The galvanization of biology: a growing appreciation for the roles of zinc. Science 271:1081–1085.

Bhat A, Tamuli R, Kasbekar DP (2004) Genetic transformation of *Neurospora tetrasperma,* demonstration of repeat-induced point mutation (RIP) in self-crosses and a screen for recessive

RIP-defective mutants. Genetics 167:1155–1164.

Bienert S, Waterhouse A, de Beer TAP, et al (2017) The SWISS-MODEL Repository-new features and functionality. Nucleic Acids Res 45:D313–D319.

Bird A, Evans-galea M V, Blankman E, et al (2000a) Mapping the DNA Binding Domain of the Zap1 Zinc-responsive Transcriptional Activator *. J Biol Chem 275:16160–16166.

Bird AJ, Blankman E, Stillman DJ, et al (2004) The Zap1 transcriptional activator also acts as a repressor by binding downstream of the TATA box in ZRT2. EMBO J 23:1123–1132.

Bird AJ, Gordon M, Eide DJ, Winge DR (2006) Repression of ADH1 and ADH3 during zinc deficiency by Zap1-induced intergenic RNA transcripts. EMBO J 25:5726–5734.

Bird AJ, McCall K, Kramer M, et al (2003) Zinc fingers can act as Zn2+ sensors to regulate transcriptional activation domain function. EMBO J 22:5137–5146.

Bird AJ, Zhao H, Luo H, et al (2000b) A dual role for zinc fingers in both DNA binding and zinc sensing by the Zap1 transcriptional activator. EMBO J 19:3704–3713.

Bistis GN (1981) Chemotropic interactions between trichogynes and conidia of opposite mating-type in *Neurospora crassa*. Mycologia 73:959–975

Bistis GN, Perkins DD, Read ND (2003) Different cell types in *Neurospora crassa*. Fungal Genet Rep 50:17–19

Boch A, Trampczynska A, Simm C, et al (2008) Loss of Zhf and the tightly regulated zinc-uptake system SpZrt1 in *Schizosaccharomyces pombe* reveals the delicacy of cellular zinc balance.

Bosomworth HJ, Adlard PA, Ford D, Valentine RA (2013) Altered expression of ZnT10 in Alzheimer's disease brain. PLoS One 8:e65475

Böttcher B, Palige K, Jacobsen ID, et al (2015) Csr1/zap1 maintains zinc homeostasis and influences virulence in *Candida dubliniensis* but is not coupled to morphogenesis. Eukaryot Cell 14:661–670.

Boulikas T (1994) Putative Nuclear Localization Signals (NLS) in Protein T ran scr i pt io n Factors. J Cell Biochem 55:32–58.

Bowman SM, Piwowar A, Al Dabbous M, et al (2006) Mutational analysis of the glycosylphosphatidylinositol (GPI) anchor pathway demonstrates that GPI-anchored proteins are required for cell wall biogenesis and normal hyphal growth in *Neurospora crassa*. Eukaryot Cell 5:587–600.

Boyce KJ, Cao C, Andrianopoulos A (2016) Two-Component Signaling Regulates Osmotic Stress

Adaptation via SskA and the High-Osmolarity Glycerol MAPK Pathway in the Human Pathogen *Talaromyces marneffei* . mSphere 1.

Bradford MM (1976) A rapid and sensitive method for the quantitation of microgram quantities of protein utilizing the principle of protein-dye binding. Anal Biochem 72:248–254.

Breunig KD (2000) Regulation of transcription activation by Gal4p. FOOD Technol Biotechnol 38:287–294

Brown GD, Denning DW, Gow NAR, et al (2012) Hidden killers: human fungal infections. Sci Transl Med 4:165rv13-165rv13

Bruce VG (1974) Recombinants between clock mutants of *Chlamydomonas reinhardi.* Genetics 77:221–230.

Cambareri EB, Jensen BC, Schabtach E, Selker EU (1989) Repeat-induced GC to AT mutations in Neurospora. Science (80-) 244:1571–1575

Cartharius K, Frech K, Grote K, et al (2005) MatInspector and beyond: promoter analysis based on transcription factor binding sites. Bioinformatics 21:2933–2942.

Cassandri M, Smirnov A, Novelli F, et al (2017) Zinc-finger proteins in health and disease. Cell Death Discov 3:17071.

Chaigne-Delalande B, Lenardo MJ (2014) Divalent cation signaling in immune cells. Trends Immunol 35:332–344

Chao Y, Fu D (2004a) Kinetic Study of the Antiport Mechanism of an *Escherichia coli* Zinc Transporter, ZitB*. J Biol Chem 279:12043–12050.

Chao Y, Fu D (2004b) Thermodynamic Studies of the Mechanism of Metal Binding to the *Escherichia coli* Zinc Transporter YiiP. J Biol Chem 279:17173–17180.

Chasapis CT, Loutsidou AC, Spiliopoulou CA, Stefanidou ME (2012) Zinc and human health: an update. Arch Toxicol 86:521–534

Chaturvedi V, Chaturvedi S (2011) *Cryptococcus gattii*: a resurgent fungal pathogen. Trends Microbiol 19:564–571

Chien A, Edgar DB, Trela JM (1976) Deoxyribonucleic acid polymerase from the extreme thermophile *Thermus aquaticu*s. J Bacteriol 127:1550–1557.

Chimienti F, Favier A, Seve M (2005) ZnT-8, a pancreatic beta-cell-specific zinc transporter. Biometals 18:313–317

Cho M, Hu G, Caza M, et al (2018) Vacuolar zinc transporter Zrc1 is required for detoxification of

excess intracellular zinc in the human fungal pathogen *Cryptococcus neoformans*. J Microbiol 56:65–71.

Choi S, Hu YM, Corkins ME, et al (2018) Zinc transporters belonging to the Cation Diffusion Facilitator (CDF) family have complementary roles in transporting zinc out of the cytosol. PLoS Genet 14.

Christianson TW, Sikorski RS, Dante M, et al (1992) Multifunctional yeast high-copy-number shuttle vectors. Gene 110:119–122.

Clemens S (2022) The cell biology of zinc. J Exp Bot 73:1688–1698.

Clemens S, Bloss T, Vess C, et al (2002) A Transporter in the Endoplasmic Reticulum of *Schizosaccharomyces pombe* Cells Mediates Zinc Storage and Differentially Affects Transition Metal Tolerance. J Biol Chem 277:18215–18221.

Cogoni C, Macino G (1999a) Posttranscriptional gene silencing in Neurospora by a RecQ DNA helicase. Science (80-) 286:2342–2344

Cogoni C, Macino G (1999b) Gene silencing in *Neurospora crassa* requires a protein homologous to RNA-dependent RNA polymerase. Nature 399:166–169

Coleman JE (1992) Zinc proteins: enzymes, storage proteins, transcription factors, and replication proteins. Annu Rev Biochem 61:897–946.

Collier LA, Ghosh A, Borkovich KA (2020) Heterotrimeric G-Protein Signaling Is Required for Cellulose Degradation in *Neurospora crassa*. MBio 11:e02419-20.

Colot H V., Park G, Turner GE, et al (2006) A high-throughput gene knockout procedure for Neurospora reveals functions for multiple transcription factors. Proc Natl Acad Sci U S A 103:10352–10357.

Colvin EW (1981) The β-effect. Silicon Org Synth 15–20.

Conklin DS, McMaster JA, Culbertson MR, Kung C (1992) COT1, a gene involved in cobalt accumulation in *Saccharomyces cerevisiae.* Mol Cell Biol 12:3678–3688.

Correa A, Bell-Pedersen D (2002) Distinct Signaling Pathways from the Circadian Clock Participate in Regulation of Rhythmic Conidiospore Development in *Neurospora crassa*. Eukaryot Cell 1:273–280.

Costello LC, Fenselau CC, Franklin RB (2011) Evidence for operation of the direct zinc ligand exchange mechanism for trafficking, transport, and reactivity of zinc in mammalian cells. J Inorg Biochem 105:589–599

Cotrim CA, Jarrott RJ, Martin JL, Drew D (2019) A structural overview of the zinc transporters in the cation diffusion facilitator family. Acta Crystallogr Sect D Struct Biol 75:357–367

Coudray N, Valvo S, Hu M, et al (2013) Inward-facing conformation of the zinc transporter YiiP revealed by cryoelectron microscopy. Proc Natl Acad Sci 110:2140–2145

Cousins RJ, Liuzzi JP, Lichten LA (2006) Mammalian zinc transport, trafficking, and signals. J. Biol. Chem. 281:24085–24089

Cuajungco MP, Lees GJ (1997) Zinc metabolism in the brain: Relevance to human neurodegenerative disorders. Neurobiol Dis 4:137–169.

Cuajungco MP, Ramirez MS, Tolmasky ME (2021) Zinc: Multidimensional Effects on Living Organisms. Biomedicines 9.

Davis RH, de Serres FJ (1970) Metabolism of Amino Acids and Amines Part A. Methods Enzymol 17:79–143

Davis RH, Perkins DD (2002) Neurospora: a model of model microbes. Nat Rev Genet 3:397–403

Deka R, Kumar R, Tamuli R (2011) *Neurospora crassa* homologue of Neuronal Calcium Sensor-1 has a role in growth, calcium stress tolerance, and ultraviolet survival. Genetica 139:885–894.

Dempski RE (2012) The cation selectivity of the ZIP transporters. Curr Top Membr 69:221–245

Diernfellner ACR, Schafmeier T, Merrow MW, Brunner M (2005) Molecular mechanism of temperature sensing by the circadian clock of *Neurospora crassa*. Genes Dev 19:1968–1973.

Dodge BO (1939) Some problems in the genetics of the fungi. Science (80-) 90:379–385

Dodson G, Steiner D (1998) The role of assembly in insulin's biosynthesis. Curr Opin Struct Biol 8:189–194.

Dogaris I, Mamma D, Kekos D (2013) Biotechnological production of ethanol from renewable resources by *Neurospora crassa*: an alternative to conventional yeast fermentations? Appl Microbiol Biotechnol 97:1457–1473

Drinker KR, Collier ES (1926) The Significance of Zinc in the Living Organism. J Ind Hyg 8:257–269

du Pré S, Dogra T, van de Sande WWJ (2022) The putative role of zinc homeostasis in grain formation by *Madurella mycetomatis* during mycetoma infection. Fungal Biol Rev 39:73–82.

Dunlap JC (1999) Molecular bases for circadian clocks. Cell 96:271–290

Dunlap JC, Loros JJ (2004) The Neurospora circadian system. J Biol Rhythms 19:414–424

Eide D, Broderius M, Fett J, Guerinot M Lou (1996) A novel iron-regulated metal transporter from

plants identified by functional expression in yeast. Proc Natl Acad Sci 93:5624–5628

Eide DJ (2006) Zinc transporters and the cellular trafficking of zinc. Biochim Biophys Acta - Mol Cell Res 1763:711–722.

Eide DJ (2009) Homeostatic and adaptive responses to zinc deficiency in *Saccharomyces cerevisiae.* J Biol Chem 284:18565–18568.

Eide DJ (2021) Homeostasis : Lessons Learned From Fungi. Crit Rev Biochem Mol Biol 55:88–110.

Eide DJ (2004) The SLC39 family of metal ion transporters. Pflügers Arch 447:796–800.

Eide DJ (1998) The molecular biology of metal ion transport in *Saccharomyces cerevisiae*. Annu Rev Nutr 18:441–469

Eide DJ (2020) Transcription factors and transporters in zinc homeostasis: lessons learned from fungi. Crit Rev Biochem Mol Biol 55:88–110.

Ellis CD, MacDiarmid CW, Eide DJ (2005) Heteromeric protein complexes mediate zinc transport into the secretory pathway of eukaryotic cells. J Biol Chem 280:28811–28818.

Ellis CD, Wang F, MacDiarmid CW, et al (2004) Zinc and the Msc2 zinc transporter protein are required for endoplasmic reticulum function. J Cell Biol 166:325–335.

Eng BH, Guerinot ML, Eide D, Saier MH (1998) Sequence analyses and phylogenetic characterization of the ZIP family of metal ion transport proteins. J Membr Biol 166:1–7

Fan F, Ma G, Li J, et al (2015) Genome-wide analysis of the endoplasmic reticulum stress response during lignocellulase production in *Neurospora crassa*. Biotechnol Biofuels 8:.

Fang Y, Sugiura R, Ma Y, et al (2008) Cation Diffusion Facilitator Cis4 Is Implicated in Golgi Membrane Trafficking via Regulating Zinc Homeostasis in Fission Yeast. Mol Biol Cell 19:1295–1303.

Feige MJ, Hendershot LM (2011) Disulfide bonds in ER protein folding and homeostasis. Curr Opin Cell Biol 23:167–175.

Frausto DAS (1991) The biological chemistry of the elements. Inorg Chem life 319–368

Freedman RB (1995) The formation of protein disulphide bonds. Curr Opin Struct Biol 5:85–91.

Freitag M, Hickey PC, Raju NB, et al (2004) GFP as a tool to analyze the organization, dynamics and function of nuclei and microtubules in *Neurospora crassa*. Fungal Genet Biol 41:897–910

Frey AG, Bird AJ, Evans-Galea M V, et al (2011) Zinc-regulated DNA binding of the yeast Zap1 zinc-responsive activator. PLoS One 6:e22535

Frey AG, Eide DJ (2012) Zinc-responsive coactivator recruitment by the yeast Zap1 transcription

factor. Microbiologyopen 1:105–114.

Frey AG, Eide DJ (2011) Roles of two activation domains in Zap1 in the response to zinc deficiency in *Saccharomyces cerevisiae*. J Biol Chem 286:6844–6854.

Fukada T, Kambe T (2011) Molecular and genetic features of zinc transporters in physiology and pathogenesis†. Metallomics 3:662–674.

Fukada T, Yamasaki S, Nishida K, et al (2011) Zinc homeostasis and signaling in health and diseases. J Biol Inorg Chem 16:1123–1134.

Fukue K, Itsumura N, Tsuji N, et al (2018) Evaluation of the roles of the cytosolic N-terminus and His-rich loop of ZNT proteins using ZNT2 and ZNT3 chimeric mutants. Sci Rep 8:14084.

Gaither LA, Eide DJ (2001a) Eukaryotic zinc transporters and their regulation. Biometals an Int J role Met ions Biol Biochem Med 14:251–270.

Gaither LA, Eide DJ (2001b) Eukaryotic zinc transporters and their regulation

Gaither LA, Eide DJ (2000) Functional expression of the human hZIP2 zinc transporter. J Biol Chem 275:5560–5564

Gaither LA, Eide DJ (2001c) The human ZIP1 transporter mediates zinc uptake in human K562 erythroleukemia cells. J Biol Chem 276:22258–22264

Galagan JE, Calvo SE, Borkovich KA, et al (2003) The genome sequence of the filamentous fungus *Neurospora crassa*. Nature 422:859–868

Gaspar-Cordeiro A, Afonso G, Amaral C, et al (2022) Zap1 is required for *Candida glabrata* response to fluconazole. FEMS Yeast Res 22:1–11.

Gavric O, Griffiths AJ (2003) Interaction of mutations affecting tip growth and branching in Neurospora. Fungal Genet Biol 40:261–270.

Gerke J, Lorenz K, Cohen B (2009) Genetic interactions between transcription factors cause natural variation in yeast. Science 323:498–501.

Gietz RD, Akio S (1988) New yeast-Escherichia coli shuttle vectors constructed with in vitro mutagenized yeast genes lacking six-base pair restriction sites. Gene 74:527–534.

Gietz RD, Schiestl RH (2007) Quick and easy yeast transformation using the LiAc/SS carrier DNA/PEG method. Nat Protoc 2:35–37.

Gohain D, Tamuli R (2019) Calcineurin responsive zinc-finger-1 binds to a unique promoter sequence to upregulate neuronal calcium sensor-1, whose interaction with MID-1 increases tolerance to calcium stress in *Neurospora crassa*. Mol Microbiol 111:1510–1528.

Grass G, Otto M, Fricke B, et al (2005) FieF (YiiP) from *Escherichia coli* mediates decreased cellular accumulation of iron and relieves iron stress. Arch Microbiol 183:9–18.

Guerinot ML (2000) The ZIP family of metal transporters. Biochim Biophys Acta 1465:190–198.

Guffanti AA, Wei Y, Rood S V, Krulwich TA (2002) An antiport mechanism for a member of the cation diffusion facilitator family: divalent cations efflux in exchange for K+ and H+. Mol Microbiol 45:145–153.

Gustin JL, Zanis MJ, Salt DE (2011) Structure and evolution of the plant cation diffusion facilitator family of ion transporters. BMC Evol Biol 11:1–13

Gygi SP, Rochon Y, Franza BR, Aebersold R (1999) Correlation between protein and mRNA abundance in yeast. Mol Cell Biol

Hallgren J, Tsirigos KD, Pedersen MD, et al (2022) DeepTMHMM predicts alpha and beta transmembrane proteins using deep neural networks. bioRxiv.

Hantke K (2001) Bacterial zinc transporters and regulators. In: Maret W (ed) Zinc Biochemistry, Physiology, and Homeostasis: Recent Insights and Current Trends. Springer Netherlands, Dordrecht, pp 53–63

Harding HP, Zhang Y, Ron D (1999) Protein translation and folding are coupled by an endoplasmic-reticulum-resident kinase. Nature 397:271–274.

Harding RW (1974) The Effect of Temperature on Photo-induced Carotenoid Biosynthesis in *Neurospora crassa*. Plant Physiol 54:142–147.

Harris ED (2002) Cellular transporters for zinc. Nutr Rev 60:121–124.

He L, Girijashanker K, Dalton TP, et al (2006) ZIP8, member of the solute-carrier-39 (SLC39) metal-transporter family: characterization of transporter properties. Mol Pharmacol 70:171–180.

Heintzen C, Liu Y (2007) The *Neurospora crassa* Circadian Clock. Academic Press, pp 25–66

Herbig A, Bird AJ, Swierczek S, et al (2005) Zap1 activation domain 1 and its role in controlling gene expression in response to cellular zinc status. Mol Microbiol 57:834–846.

Hetz C (2012) The unfolded protein response: Controlling cell fate decisions under ER stress and beyond. Nat Rev Mol Cell Biol 13:89–102.

Higgins CF (1992) ABC transporters: from microorganisms to man. Annu Rev Cell Biol 8:67–113

Himeno S, Yanagiya T, Fujishiro H (2009) The role of zinc transporters in cadmium and manganese transport in mammalian cells. Biochimie 91:1218–1222.

Hirano T, Murakami M, Fukada T, et al (2008) Roles of zinc and zinc signaling in immunity: zinc as

an intracellular signaling molecule. Adv Immunol 97:149–176

Hoch E, Lin W, Chai J, et al (2012) Histidine pairing at the metal transport site of mammalian ZnT transporters controls Zn2+ over Cd2+ selectivity. Proc Natl Acad Sci U S A 109:7202–7207.

Hojyo S, Miyai T, Fujishiro H, et al (2014) Zinc transporter SLC39A10/ZIP10 controls humoral immunity by modulating B-cell receptor signal strength. Proc Natl Acad Sci 111:11786–11791

Holm L (2022) Dali server : structural unification of protein families. 50:210–215.

Honda S, Eusebio-Cope A, Miyashita S, et al (2020) Establishment of *Neurospora crassa* as a model organism for fungal virology. Nat Commun 11:5627.

Huang L, Kirschke CP, Gitschier J (2002) Functional characterization of a novel mammalian zinc transporter, ZnT6. J Biol Chem 277:26389–26395

Huang L, Tepaamorndech S (2013) The SLC30 family of zinc transporters–a review of current understanding of their biological and pathophysiological roles. Mol Aspects Med 34:548–560

Huang L, Yu YY, Kirschke CP, et al (2007) Znt7 (Slc30a7)-deficient mice display reduced body zinc status and body fat accumulation. J Biol Chem 282:37053–37063

Hussain D, Haydon MJ, Wang Y, et al (2004) P-type ATPase heavy metal transporters with roles in essential zinc homeostasis in Arabidopsis. Plant Cell 16:1327–1339

Inoue H, Nojima H, Okayama H (1990) High efficiency transformation of *Escherichia coli* with plasmids. Gene 96:23–28.

Inoue K, Matsuda K, Itoh M, et al (2002) Osteopenia and male-specific sudden cardiac death in mice lacking a zinc transporter gene, Znt5. Hum Mol Genet 11:1775–1784

Itsumura N, Inamo Y, Okazaki F, et al (2013) Compound heterozygous mutations in SLC30A2/ZnT2 results in low milk zinc concentrations: a novel mechanism for zinc deficiency in a breast-fed infant. PLoS One 8:e64045

Ivey FD, Kays AM, Borkovich KA (2002) Shared and Independent Roles for a G Protein and Adenylyl Cyclase in Regulating Development and Stress Responses in *Neurospora crassa*. Eukaryot Cell 1:634–642.

Jeong J, Eide DJ (2013) The SLC39 family of zinc transporters. Mol Aspects Med 34:612–619.

Kambe T (2012) Chapter Eight - Molecular Architecture and Function of ZnT Transporters. In: Argüello JM, Lutsenko S (eds) Metal Transporters. Academic Press, pp 199–220

Kambe T, Matsunaga M, Takeda TA (2017) Understanding the contribution of zinc transporters in the function of the early secretory pathway. Int. J. Mol. Sci. 18

Kambe T, Narita H, Yamaguchi-Iwai Y, et al (2002) Cloning and characterization of a novel mammalian zinc transporter, zinc transporter 5, abundantly expressed in pancreatic β cells. J Biol Chem 277:19049–19055

Kambe T, Taylor KM, Fu D (2021) Zinc transporters and their functional integration in mammalian cells. J. Biol. Chem. 296

Kambe T, Tsuji T, Hashimoto A, Itsumura N (2015) The physiological, biochemical, and molecular roles of zinc transporters in zinc homeostasis and metabolism. Physiol Rev 95:749–784.

Kambe T, Weaver BP, Andrews GK (2008) The genetics of essential metal homeostasis during development. Genesis 46:214–228.

Kambe T, Yamaguchi-Iwai Y, Sasaki R, Nagao M (2004) Overview of mammalian zinc transporters. Cell Mol Life Sci 61:49–68.

Kamizono A, Nishizawa M, Teranishi Y, et al (1989) Identification of a gene conferring resistance to zinc and cadmium ions in the yeast *Saccharomyces cerevisiae*. Mol Gen Genet MGG 219:161–167.

Kaur K, Gupta R, Saraf SA, Saraf SK (2014) Zinc: The Metal of Life. Compr Rev Food Sci Food Saf 13:358–376.

Kays AM, Borkovich KA (2004) Severe impairment of growth and differentiation in a *Neurospora crassa* mutant lacking all heterotrimeric G alpha proteins. Genetics 166:1229–1240.

Kim H, Borkovich KA (2004) A pheromone receptor gene, pre-1, is essential for mating type-specific directional growth and fusion of trichogynes and female fertility in *Neurospora crassa.* Mol Microbiol 52:1781–1798.

Kim H, Wright SJ, Park G, et al (2012) Roles for receptors, pheromones, G proteins, and mating type genes during sexual reproduction in *Neurospora crassa*. Genetics 190:1389–1404

Kim MJ, Kil M, Jung JH, Kim J (2008) Roles of zinc-responsive transcription factor Csr1 in filamentous growth of the pathogenic yeast *Candida albicans*. J Microbiol Biotechnol 18:242–247

Kimura T, Kambe T (2016) The functions of metallothionein and ZIP and ZnT transporters: an overview and perspective. Int J Mol Sci 17:336

Kiranmayi P, Mohan PM (2006) Metal transportome of *Neurospora crassa*. In Silico Biol 6:169–180

Kiranmayi P, Tiwari A, Sagar KP, et al (2009) Functional characterization of tzn1 and tzn2-zinc transporter genes in *Neurospora crassa*. Biometals an Int J role Met ions Biol Biochem Med

22:411–420.

Klug A, Schwabe JWR (1995) Zinc fingers. FASEB J 9:597–604.

Ko J, Park H, Heo L, Seok C (2012) GalaxyWEB server for protein structure prediction and refinement. Nucleic Acids Res 40:294–297.

Kochańczyk T, Drozd A, Krężel A (2014) Relationship between the architecture of zinc coordination and zinc binding affinity in proteins – insights into zinc regulation. Metallomics 7:244–257.

Koh JY (2001) Zinc and disease of the brain. Mol Neurobiol 24:99–106.

Kolaj-Robin O, Russell D, Hayes KA, et al (2015) Cation Diffusion Facilitator family: Structure and function. FEBS Lett 589:1283–1295.

Kousha M, Tadi R, Soubani AO (2011) Pulmonary aspergillosis: a clinical review. Eur Respir Rev 20:156–174

Krężel A, Maret W (2016) The biological inorganic chemistry of zinc ions. Arch Biochem Biophys 611:3–19.

Krężel A, Maret W (2006) Zinc-buffering capacity of a eukaryotic cell at physiological pZn. JBIC J Biol Inorg Chem 11:1049–1062

Krezoski SK, Villalobos J, Shaw CF 3rd, Petering DH (1988) Kinetic lability of zinc bound to metallothionein in Ehrlich cells. Biochem J 255:483–491

Kronholm I, Ketola T (2018) Effects of acclimation time and epigenetic mechanisms on growth of Neurospora in fluctuating environments. Heredity (Edinb) 121:327–341.

Kumánovics A, KE P, KA O, et al (2006) YKE4 (YIL023C) encodes a bidirectional zinc transporter in the endoplasmic reticulum of *Saccharomyces cerevisiae.* J Biol Chem 281:22566–22574

Küry S, Dréno B, Bézieau S, et al (2002) Identification of SLC39A4, a gene involved in acrodermatitis enteropathica. Nat Genet 31:239–240. https://doi.org/10.1038/ng913

Laskowski RA, MacArthur MW, Moss DS, Thornton JM (1993) PROCHECK: a program to check the stereochemical quality of protein structures. J Appl Crystallogr 26:283–291.

Lee SR, Noh SJ, Pronto JR, et al (2015) The critical roles of zinc: Beyond impact on myocardial signaling. Korean J Physiol Pharmacol 19:389–399.

Letunic I, Khedkar S, Bork P (2020) SMART: recent updates, new developments and status in 2020. Nucleic Acids Res 49:D458–D460.

Li C, Xu D, Hu M, et al (2022) MaNCP1, a C2H2 Zinc Finger Protein, Governs the Conidiation Pattern Shift through Regulating the Reductive Pathway for Nitric Oxide Synthesis in the Filamentous

Fungus *Metarhizium acridum*. Microbiol Spectr 10:e0053822.

Li L, Kaplan J (2001) The Yeast Gene MSC2, a Member of the Cation Diffusion Facilitator Family, Affects the Cellular Distribution of Zinc. J Biol Chem 276:5036–5043.

Li L, Kaplant J (1998) Defects in the yeast high affinity iron transport system result in increased metal sensitivity because of the increased expression of transporters with a broad transition metal specificity. J Biol Chem 273:22181–22187.

Li M, Zhang Y, Liu Z, et al (2007) Aberrant expression of zinc transporter ZIP4 (SLC39A4) significantly contributes to human pancreatic cancer pathogenesis and progression. Proc Natl Acad Sci 104:18636–18641

Li N, Li J, Chen Y, et al (2023) Mechanism of Zn(2+) regulation of cellulase production in *Trichoderma reesei* Rut-C30. Biotechnol biofuels Bioprod 16:73.

Linke K, Wolfram T, Bussemer J, Jakob U (2003) The roles of the two zinc binding sites in DnaJ. J Biol Chem 278:44457–44466.

Liu Z, Li H, Soleimani M, et al (2008) Cd2+ versus Zn2+ uptake by the ZIP8 HCO3--dependent symporter: kinetics, electrogenicity and trafficking. Biochem Biophys Res Commun 365:814–820

Livak KJ, Schmittgen TD (2001) Analysis of relative gene expression data using real-time quantitative PCR and the 2-ΔΔCT method. Methods 25:402–408.

López-Berges MS (2020) ZafA-mediated regulation of zinc homeostasis is required for virulence in the plant pathogen *Fusarium oxysporum*. Mol Plant Pathol 21:244–249

Lorenz MC, Heitman J (1998) Regulators of pseudohyphal differentiation in *Saccharomyces cerevisiae* identified through multicopy suppressor analysis in ammonium permease mutant strains. Genetics 150:1443–1457.

Loros JJ, Dunlap JC (2001) Genetic and molecular analysis of circadian rhythms in neurospora. Annu Rev Physiol 63:757–794

Lovell MA, Smith JL, Markesbery WR (2006) Elevated zinc transporter-6 in mild cognitive impairment, Alzheimer disease, and pick disease. J Neuropathol Exp Neurol 65:489–498

Lu M, Fu D (2007) Structure of the zinc transporter YiiP. Science (80-) 317:1746–1748.

Lyons TJ, Gasch AP, Gaither LA, et al (2000) Genome-wide characterization of the Zap1p zinc-responsive regulon in yeast. Proc Natl Acad Sci U S A 97:7957–7962.

Ma Z, Li Z, Wang S, et al (2021) SLC39A10 Upregulation Predicts Poor Prognosis, Promotes

Proliferation and Migration, and Correlates with Immune Infiltration in Hepatocellular Carcinoma. J Hepatocell Carcinoma 899–912

MacDiarmid CW, Gaither LA, Eide D (2000) Zinc transporters that regulate vacuolar zinc storage in *Saccharomyces cerevisiae.* EMBO J 19:2845–2855.

MacDiarmid CW, Milanick MA, Eide DJ (2003) Induction of the ZRC1 metal tolerance gene in zinc-limited yeast confers resistance to zinc shock. J Biol Chem 278:15065–15072.

Maddi A, Bowman SM, Free SJ (2009) Trifluoromethanesulfonic acid-based proteomic analysis of cell wall and secreted proteins of the ascomycetous fungi *Neurospora crassa* and *Candida albicans*. Fungal Genet Biol 46:768–781.

Madi L, McBride SA, Bailey LA, Ebbole DJ (1997) rco-3, a gene involved in glucose transport and conidiation in *Neurospora crassa*. Genetics 146:499–508

Mani R, St. Onge RP, Hartman IV JL, et al (2008) Defining genetic interaction. Proc Natl Acad Sci 105:3461–3466.

Maret W (2013) Zinc biochemistry: from a single zinc enzyme to a key element of life. Adv Nutr 4:82–91.

Maret W (2017) Zinc in Cellular Regulation: The Nature and Significance of "Zinc Signals." Int J Mol Sci 18.

Maret W (2004) Exploring the zinc proteome. J Anal At Spectrom 19:15–19

Maret W (2015) Analyzing free zinc(II) ion concentrations in cell biology with fluorescent chelating molecules. Metallomics 7:202–211.

Margolin BS, Freitag M, Selker EU (1997) Improved plasmids for gene targeting at the his-3 locus of *Neurospora crassa* by electroporation. Fungal Genet Rep 44:34–36.

Martel G, Hevi C, Kane-Goldsmith N, Shumyatsky GP (2011) Zinc transporter ZnT3 is involved in memory dependent on the hippocampus and perirhinal cortex. Behav Brain Res 223:233–238.

Mäser P, Thomine S, Schroeder JI, et al (2001) Phylogenetic Relationships within Cation Transporter Families of Arabidopsis. Plant Physiol 126:1646–1667.

McAllister BB, Dyck RH (2017) Zinc transporter 3 (ZnT3) and vesicular zinc in central nervous system function. Neurosci Biobehav Rev 80:329–350

McCluskey K (2003) The fungal genetics stock center. from molds to Mol 52:245–262

McCluskey K, Wiest A, Plamann M (2010a) The fungal genetics stock center: A repository for 50 years of fungal genetics research. J Biosci 35:119–126.

McCormick NH, Kelleher SL (2012) ZnT4 provides zinc to zinc-dependent proteins in the trans-Golgi network critical for cell function and Zn export in mammary epithelial cells. Am J Physiol Physiol 303:C291–C297

Miller GL (1959) Use of dinitrosalicylic acid reagent for determination of reducing sugar. Anal Chem 31:426–428

Miller J, McLachlan AD, Klug Ajte (1985) Repetitive zinc-binding domains in the protein transcription factor IIIA from Xenopus oocytes. EMBO J 4:1609–1614

Mishra C, Keskar S, Rao M (1984) Production and properties of extracellular endoxylanase from *Neurospora crassa.* Appl Environ Microbiol 48:224–228.

Mitsis T, Efthimiadou A, Bacopoulou F, et al (2020) Transcription factors and evolution: An integral part of gene expression (Review). World Acad Sci J 2:3–8.

Miyabe S, Izawa S, Inoue Y (2001) The Zrc1 is involved in zinc transport system between vacuole and cytosol in *Saccharomyces cerevisiae*. Biochem Biophys Res Commun 282:79–83.

Miyabe S, Izawa S, Inoue Y (2000) Expression of ZRC1 coding for suppressor of zinc toxicity is induced by zinc-starvation stress in Zap1-dependent fashion in *Saccharomyces cerevisiae*. Biochem Biophys Res Commun 276:879–884.

Mocchegiani E, Bertoni-Freddari C, Marcellini F, Malavolta M (2005) Brain, aging and neurodegeneration: Role of zinc ion availability. Prog Neurobiol 75:367–390.

Montagne C (1843) Quatrieme centurie plantes cellulaires exotiques nouvelles. Decades VIII, IX, X. Ann Sci Nat Bot, Ser 2 20:339–352

Montanini B, Blaudez D, Jeandroz S, et al (2007) Phylogenetic and functional analysis of the Cation Diffusion Facilitator (CDF) family: Improved signature and prediction of substrate specificity. BMC Genomics 8.

Montenegro-Montero A, Goity A, Larrondo LF (2015) The bZIP transcription factor HAC-1 is involved in the unfolded protein response and is necessary for growth on cellulose in *Neurospora crassa*. PLoS One 10.

Moreno MÁ, Ibrahim-Granet O, Vicentefranqueira R, et al (2007) The regulation of zinc homeostasis by the ZafA transcriptional activator is essential for *Aspergillus fumigatus* virulence. Mol Microbiol 64:1182–1197

Morgan LW, Feldman JF (2001) Epistatic and synergistic interactions between circadian clock mutations in *Neurospora crassa*. Genetics 159:537–543.

Mouriño-Pérez RR (2013) Septum development in filamentous ascomycetes. Fungal Biol Rev 27:1–9.

Myers SA (2015) Zinc Transporters and Zinc Signaling: New Insights into Their Role in Type 2 Diabetes. Int J Endocrinol 2015:167503.

Nanda A, Mohapatra DBB, Mahapatra APK, et al (2021) Multiple comparison test by Tukey's honestly significant difference (HSD): Do the confident level control type I error. Int J Stat Appl Math 6:59–65.

Navarro-Sampedro L, Yanofsky C, Corrochano LM (2008) A genetic selection for *Neurospora crassa* mutants altered in their light regulation of transcription. Genetics 178:171–183.

Nelson MA, Metzenberg RL (1992) Sexual development genes of *Neurospora crassa*. Genetics 132:149–162

Nicholas KB, Nicholas HB, Deerfield DW (1997) GeneDoc: Analysis and visualization of genetic variation

Nicolson TJ, Bellomo EA, Wijesekara N, et al (2009) Insulin storage and glucose homeostasis in mice null for the granule zinc transporter ZnT8 and studies of the type 2 diabetes-associated variants. Diabetes 58:2070–2083.

Nies DH (2003) Efflux-mediated heavy metal resistance in prokaryotes. FEMS Microbiol Rev 27:313–339.

Nies DH, Silver S (1995) Ion efflux systems involved in bacterial metal resistances. J Ind Microbiol 14:186–199

Nishida K, Hasegawa A, Nakae S, et al (2009) Zinc transporter Znt5/Slc30a5 is required for the mast cell–mediated delayed-type allergic reaction but not the immediate-type reaction. J Exp Med 206:1351–1364

Nobile CJ, Nett JE, Hernday AD, et al (2009) Biofilm matrix regulation by *Candida albicans* Zap1. PLoS Biol 7.

Noh H, Paik HY, Kim J, Chung J (2014) The alteration of zinc transporter gene expression is associated with inflammatory markers in obese women. Biol Trace Elem Res 158:1–8

Nolte C, Gore A, Sekler I, et al (2004) ZnT-1 expression in astroglial cells protects against zinc toxicity and slows the accumulation of intracellular zinc. Glia 48:145–155.

Ohana E, Hoch E, Keasar C, et al (2009) Identification of the Zn2+ binding site and mode of operation of a mammalian Zn2+ transporter. J Biol Chem 284:17677–17686

Olesen RH, Hyde TM, Kleinman JE, et al (2016) Obesity and age-related alterations in the gene expression of zinc-transporter proteins in the human brain. Transl Psychiatry 6:e838–e838

Olmedo M, Ruger-Herreros C, Luque EM, Corrochano LM (2010) A complex photoreceptor system mediates the regulation by light of the conidiation genes con-10 and con-6 in *Neurospora crassa*. Fungal Genet Biol 47:352–363.

Outten CE, O'Halloran T V. (2001) Femtomolar sensitivity of metalloregulatory proteins controlling zinc homeostasis. Science (80-) 292:2488–2492.

Ouyang S, Beecher CN, Wang K, et al (2015) Metabolic impacts of using nitrogen and copper-regulated promoters to regulate gene expression in *Neurospora crassa*. G3 Genes, Genomes, Genet 5:1899–1908.

Padilla-López S, DA P (2006) *Saccharomyces cerevisiae* lacking Btn1p modulate vacuolar ATPase activity to regulate pH imbalance in the vacuole. J Biol Chem 281:10273–10280

Pal D, Sharma U, Singh SK, Prasad R (2014) Association between ZIP10 gene expression and tumor aggressiveness in renal cell carcinoma. Gene 552:195–198

Pall ML (1993) The use of Ignite (Basta;glufosinate;phosphinothricin) to select transformants of bar-containing plasmids in *Neurospora crassa*. Fungal Genet Rep 40:58.

Palmiter RD, Cole TB, Findley SD (1996a) ZnT-2, a mammalian protein that confers resistance to zinc by facilitating vesicular sequestration. EMBO J 15:1784–1791

Palmiter RD, Cole TB, Quaife CJ, Findley SD (1996b) ZnT-3, a putative transporter of zinc into synaptic vesicles. Proc Natl Acad Sci 93:14934–14939

Palmiter RD, Findley SD (1995) Cloning and functional characterization of a mammalian zinc transporter that confers resistance to zinc. EMBO J 14:639–649.

Palmiter RD, Huang L (2004) Efflux and compartmentalization of zinc by members of the SLC30 family of solute carriers. Pflugers Arch Eur J Physiol 447:744–751.

Park HS, Yu JH (2012) Genetic control of asexual sporulation in filamentous fungi. Curr Opin Microbiol 15:669–677.

Park S, Lee K (2004) Inverted Race Tube Assay for Circadian Clock Studies of the Neurospora Accessions. Fungal Genet Rep 51:12–14.

Patrushev N, Seidel-Rogol B, Salazar G (2012) Angiotensin II requires zinc and downregulation of the zinc transporters ZnT3 and ZnT10 to induce senescence of vascular smooth muscle cells. PLoS One 7:e33211

Patzer SI, Hantke K (1998) The ZnuABC high-affinity zinc uptake system and its regulator Zur in *Escherichia coli*. Mol Microbiol 28:1199–1210.

Paulsen IT, Saier MH (1997) A novel family of ubiquitous heavy metal ion transport proteins. J Membr Biol 156:99–103.

Payen A de (1843) Extrait d'un rapport adresse a M. Le Marechal Duc de Dalmatie, Ministre de la Guerre, President du Conseil, sur une alteration extraordinaire du pain de munition. Ann Chim Phys 3rd Ser 9:5–21

Paysan-Lafosse T, Blum M, Chuguransky S, et al (2023) InterPro in 2022. Nucleic Acids Res 51:D418–D427

Pereira RC, Said S (2009) Alterations in growth and branching of *Neurospora crassa* caused by sub-inhibitory concentrations of antifungal agents. Rev Argent Microbiol 41:39–44

Perkins DD (1992) Neurospora: the organism behind the molecular revolution. Genetics 130:687

Perkins DD, Barry EG (1977) The Cytogenetics of Neurospora. In: Caspari EW (ed). Academic Press, pp 133–285

Persans MW, Nieman K, Salt DE (2001) Functional activity and role of cation-efflux family members in Ni hyperaccumulation in *Thlaspi goesingense*. Proc Natl Acad Sci 98:9995–10000

Pettersen EF, Goddard TD, Huang CC, et al (2004) UCSF Chimera—a visualization system for exploratory research and analysis. J Comput Chem 25:1605–1612

Plesofsky-Vig N, Brambl R (1985) Heat shock response of *Neurospora crassa*: protein synthesis and induced thermotolerance. J Bacteriol 162:1083–1091.

Podar D, Scherer J, Noordally Z, et al (2012) Metal selectivity determinants in a family of transition metal transporters. J Biol Chem 287:3185–3196

Potapova T V, Golyshev SA (2016) Revisiting a Special Structural Order of a Growing Tip of the *Neurospora crassa* Hypha. Fungal Genomics Biol 6:3–6.

Pound LD, Sarkar SA, Benninger RKP, et al (2009) Deletion of the mouse Slc30a8 gene encoding zinc transporter-8 results in impaired insulin secretion. Biochem J 421:371–376.

Prasad AS, Halsted JA, Nadimi M (1961) Syndrome of iron deficiency anemia, hepatosplenomegaly, hypogonadism, dwarfism and geophagia. Am J Med 31:532–546

Prasad AS, Miale Jr A, Farid Z, et al (1963) Zinc metabolism in patients with the syndrome of iron deficiency anemia, hepatosplenomegaly, dwarfism, and hypogonadism. J Lab Clin Med 61:537–549

Qiao W, Mooney M, Bird AJ, et al (2006) Zinc binding to a regulatory zinc-sensing domain monitored in vivo by using FRET. Proc Natl Acad Sci 103:8674–8679

Quadri M, Federico A, Zhao T, et al (2012) Mutations in SLC30A10 cause parkinsonism and dystonia with hypermanganesemia, polycythemia, and chronic liver disease. Am J Hum Genet 90:467–477

Raju NB (1982) Easy methods for fluorescent staining of Neurospora nuclei. Fungal Genet Rep 29:24–25

Raju NB (1992) Genetic control of the sexual cycle in Neurospora. Mycol Res 96:241–262.

Ramachandran GN, Sasisekharan V (1968) Conformation of Polypeptides and Proteins. Adv Protein Chem 23:283–437.

Rand JD, Grant CM (2006) The thioredoxin system protects ribosomes against stress-induced aggregation. Mol Biol Cell 17:387–401.

Rasmussen CG, Glass NL (2005) A Rho-type GTPase, rho-4, is required for septation in *Neurospora crassa*. Eukaryot Cell 4:1913–1925.

Rasmussen CG, Glass NL (2007) Localization of RHO-4 Indicates Differential Regulation of Conidial versus Vegetative Septation in the Filamentous Fungus *Neurospora crassa*. Eukaryot Cell 6:1097–1107.

Raulin J (1869) Chemical studies on vegetation. Ann Sci Nat 11:93–99

Ren X, Feng C, Wang Y, et al (2023) SLC39A10 promotes malignant phenotypes of gastric cancer cells by activating the CK2-mediated MAPK/ERK and PI3K/AKT pathways. Exp Mol Med 55:1757–1769.

Rensing C, Mitra B, Rosen BP (1997) The zntA gene of *Escherichia coli* encodes a Zn (II)-translocating P-type ATPase. Proc Natl Acad Sci 94:14326–14331

Riquelme M, Yarden O, Bartnicki-Garcia S, et al (2011) Architecture and development of the *Neurospora crassa* hypha–a model cell for polarized growth. Fungal Biol 115:446–474

Roberts AN, Berlin V, Hager KM, Yanofsky C (1988) Molecular analysis of a *Neurospora crassa* gene expressed during conidiation. Mol Cell Biol 8:2411–2418.

Rodriguez-Amaya DB, Kimura M (2004) HarvestPlus handbook for carotenoid analysis. International Food Policy Research Institute (IFPRI) Washington

Romano N, Macino G (1992) Quelling: transient inactivation of gene expression in *Neurospora crassa* by transformation with homologous sequences. Mol Microbiol 6:3343–3353

Ruger-Herreros C, Corrochano LM (2020) Conidiation in *Neurospora crassa*: vegetative reproduction by a model fungus. Int Microbiol 23:97–105

Ruis H, Schüller C (1995) Stress signaling in yeast. BioEssays 17:959–965.

Ryan FJ, Beadle GW, Tatum EL (1943) THE TUBE METHOD OF MEASURING THE GROWTH RATE OF NEUROSPORA. Am J Bot 30:784–799

Rzhetsky A, Nei M (1993) Theoretical foundation of the minimum-evolution method of phylogenetic inference. Mol Biol Evol 10:1073–1095.

Saiki RK, Gelfand DH, Stoffel S, et al (1988) Primer-Directed Enzymatic Amplification of DNA with a Thermostable DNA Polymerase. Science (80-) 239:487–491.

Sambrook and Russell (2001) Molecular cloning: a laboratory manual. New York Cold Spring Harb

Sawyer JT, Lukaczyk T, Yilla M (1994) Dithiothreitol treatment induces heterotypic aggregation of newly synthesized secretory proteins in HepG2 cells. J Biol Chem 269:22440–22445.

Scarborough GA (2002) Molecular Mechanism of the P-Type ATPases. J Bioenerg Biomembr 34:235–250.

Scheuner D, Song B, McEwen E, et al (2001) Translational control is required for the unfolded protein response and in vivo glucose homeostasis. Mol Cell 7:1165–1176.

Schindelin J, Arganda-Carreras I, Frise E, et al (2012) Fiji: an open-source platform for biological-image analysis. Nat Methods 9:676–682.

Schmit JC, Brody S (1976) Biochemical genetics of *Neurospora crassa* conidial germination. Bacteriol Rev 40:1–41

Schneider R de O, Diehl C, Dos Santos FM, et al (2015) Effects of zinc transporters on *Cryptococcus gattii* virulence. Sci Rep 5:10104

Schneider R de O, Fogaça N de SS, Kmetzsch L, et al (2012) Zap1 regulates zinc homeostasis and modulates virulence in *Cryptococcus gattii*

Schöler A, Schüller HJ (1994) A carbon source-responsive promoter element necessary for activation of the isocitrate lyase gene ICL1 is common to genes of the gluconeogenic pathway in the yeast *Saccharomyces cerevisiae*. Mol Cell Biol 14:3613–3622.

Schweizer A, Rupp S, Taylor BN, et al (2000) The TEA/ATTS transcription factor CaTec1p regulates hyphal development and virulence in *Candida albicans*. Mol Microbiol 38:435–445.

Seidel C, Moreno-Velásquez SD, Riquelme M, Fischer R (2013) *Neurospora crassa* NKIN2, a kinesin-3 motor, transports early endosomes and is required for polarized growth. Eukaryot Cell

12:1020–1032.

Sevlever D, Mann KJ, Medof ME (2001) Differential effect of 1,10-phenanthroline on mammalian, yeast, and parasite glycosylphosphatidylinositol anchor synthesis. Biochem Biophys Res Commun 288:1112–1118.

Shao Y, Lin AH-M (2018) Improvement in the quantification of reducing sugars by miniaturizing the Somogyi-Nelson assay using a microtiter plate. Food Chem 240:898–903.

Shapiro RS, Robbins N, Cowen LE (2011) Regulatory circuitry governing fungal development, drug resistance, and disease. Microbiol Mol Biol Rev 75:213–267.

Shear CL, Dodge BO (1927) Life histories and heterothallism of the red bread-mold fungi of the *Monilia sitophila* group. US Government Printing Office Washington, DC

Sherman F (2002) Getting started with yeast. In: Guthrie C, Fink GR (eds) Guide to Yeast Genetics and Molecular and Cell Biology - Part B. Academic Press, pp 3–41

Shiu PKT, Raju NB, Zickler D, Metzenberg RL (2001) Meiotic silencing by unpaired DNA. Cell 107:905–916

Simons JF, Ferro-Novick S, Rose MD, Helenius A (1995) BiP/Kar2p serves as a molecular chaperone during carboxypeptidase Y folding in yeast. J Cell Biol 130:41–49.

Song Y, Kim S, Kim J (1995) ROK1, a high-copy-number plasmid suppressor of kem1, encodes a putative ATP-dependent RNA helicase in *Saccharomyces cerevisiae.* Gene 166:151–154.

Springer ML (1993) Genetic control of fungal differentiation: the three sporulation pathways of *Neurospora crassa*. Bioessays 15:365–374

Springer ML, Yanofsky C (1989) A morphological and genetic analysis of conidiophore development in *Neurospora crassa*. Genes Dev 3:559–571.

Starr TL, Gonc AP (2018) The major cellulases CBH-1 and CBH-2 of *Neurospora crassa* rely on distinct ER cargo adaptors for efficient ER-exit. 107:229–248.

Suhy DA, Simon KD, Linzer DIH, O'Halloran T V. (1999) Metallothionein is part of a zinc-scavenging mechanism for cell survival under conditions of extreme zinc deprivation. J Biol Chem 274:9183–9192.

Sun X, Wang F, Lan N, et al (2019) The Zn(II)2Cys6-Type Transcription Factor ADA-6 Regulates Conidiation, Sexual Development, and Oxidative Stress Response in *Neurospora crassa*. Front Microbiol 10:750.

Suutari M (1995) Effect of growth temperature on lipid fatty acids of four fungi (*Aspergillus niger,*

Neurospora crassa, *Penicillium chrysogenum*, and*Trichoderma reesei*). Arch Microbiol 164:212–216.

Suzuki T, Ishihara K, Migaki H, et al (2005) Two different zinc transport complexes of cation diffusion facilitator proteins localized in the secretory pathway operate to activate alkaline phosphatases in vertebrate cells. J Biol Chem 280:30956–30962.

Szklarczyk D, Gable AL, Lyon D, et al (2019) STRING v11: protein-protein association networks with increased coverage, supporting functional discovery in genome-wide experimental datasets. Nucleic Acids Res 47:D607–D613.

Takatani-Nakase T, Matsui C, Maeda S, et al (2014) High glucose level promotes migration behavior of breast cancer cells through zinc and its transporters. PLoS One 9:e90136

Tamura K, Stecher G, Kumar S (2021) MEGA11: Molecular Evolutionary Genetics Analysis Version 11. Mol Biol Evol 38:3022–3027.

Tanaka N, Kawachi M, Fujiwara T, Maeshima M (2013) Zinc-binding and structural properties of the histidine-rich loop of *Arabidopsis thaliana* vacuolar membrane zinc transporter MTP1. FEBS Open Bio 3:218–224

Thompson JD, Gibson TJ, Plewniak F, et al (1997) The CLUSTAL_X windows interface: flexible strategies for multiple sequence alignment aided by quality analysis tools. Oxford University Press

Tiwari A, Ngiilmei SD, Tamuli R (2018) The *NcZrg-17* gene of *Neurospora crassa* encodes a cation diffusion facilitator transporter required for vegetative development, tolerance to endoplasmic reticulum stress and cellulose degradation under low zinc conditions. Curr Genet 64:811–819.

Todd WR, Elvehjem CA, Hart EB (1933) ZINC IN THE NUTRITION OF THE RAT. Am J Physiol Content 107:146–156.

Tuschl K, Clayton PT, Gospe SM, et al (2012) Syndrome of hepatic cirrhosis, dystonia, polycythemia, and hypermanganesemia caused by mutations in SLC30A10, a manganese transporter in man. Am J Hum Genet 90:457–466

Vallee BL, Auld DS (1990) Zinc Coordination, Function, and Structure of Zinc Enzymes and Other Proteins. Biochemistry 29:5647–5659.

Vicentefranqueira R, Amich J, Marín L, et al (2018) The transcription factor ZafA regulates the homeostatic and adaptive response to Zinc starvation in *Aspergillus fumigatus*

Vicentefranqueira R, Moreno MA, Leal F, Calera JA (2005) The zrfA and zrfB genes of *Aspergillus*

fumigatus encode the zinc transporter proteins of a zinc uptake system induced in an acid, zinc-depleted environment. Eukaryot Cell 4:837–848

Vincent O, Carlson M (1998) Sip4, a Snf1 kinase-dependent transcriptional activator, binds to the carbon source-responsive element of gluconeogenic genes. EMBO J 17:7002–7008.

Vinkenborg JL, Nicolson TJ, Bellomo EA, et al (2009) Genetically encoded FRET sensors to monitor intracellular Zn2+ homeostasis. Nat Methods 6:737–740

Vogel HJ (1956) A convenient growth medium for Neurospora (Medium N). Microb Genet Bull 13:42–43

Vogel HJ (1964) Distribution of lysine pathways among fungi: evolutionary implications. Am Nat 98:435–446

Wang K, Zhou B, Kuo Y-M, et al (2002) A novel member of a zinc transporter family is defective in acrodermatitis enteropathica. Am J Hum Genet 71:66–73

Wang X, Wu Y, Zhou B (2009) Dietary zinc absorption is mediated by ZnT1 in *Drosophila melanogaster.* FASEB J 23:2650–2661

Wang Z, Feng LS, Matskevich V, et al (2006) Solution structure of a Zap1 zinc-responsive domain provides insights into metalloregulatory transcriptional repression in *Saccharomyces cerevisiae.* J Mol Biol 357:1167–1183.

Waterhouse A, Bertoni M, Bienert S, et al (2018) SWISS-MODEL: homology modelling of protein structures and complexes. Nucleic Acids Res 46:W296–W303.

Waters BM, Eide DJ (2002) Combinatorial control of yeast FET4 gene expression by iron, zinc, and oxygen. J Biol Chem 277:33749–33757

Wei Y, Fu D (2006) Binding and transport of metal ions at the dimer interface of the *Escherichia coli* metal transporter YiiP. J Biol Chem 281:23492–23502

Westergaard M, Mitchell HK (1947) Neurospora V. A synthetic medium favoring sexual reproduction. Am J Bot 573–577

Wijesekara N, Dai FF, Hardy AB, et al (2010) Beta cell-specific Znt8 deletion in mice causes marked defects in insulin processing, crystallisation and secretion. Diabetologia 53:1656–1668.

Wilson S, Bird AJ (2016) Zinc sensing and regulation in yeast model systems. Arch Biochem Biophys 611:30–36.

Wu CY, Bird AJ, Chung LM, et al (2008) Differential control of Zap1-regulated genes in response to zinc deficiency in *Saccharomyces cerevisiae*. BMC Genomics 9:1–17.

Wu Y-H, Frey AG, Eide DJ (2011) Transcriptional regulation of the Zrg17 zinc transporter of the yeast secretory pathway. Biochem J 435:259–266

Yamasaki S, Sakata-Sogawa K, Hasegawa A, et al (2007) Zinc is a novel intracellular second messenger. J Cell Biol 177:637–645.

Yang J, Zhang Y (2015) I-TASSER server: New development for protein structure and function predictions. Nucleic Acids Res 43:W174–W181.

Yang M, Derbyshire MK, Yamashita RA, Marchler-Bauer A (2020) NCBI's Conserved Domain Database and Tools for Protein Domain Analysis. Curr Protoc Bioinforma 69:e90.

Yao R, Li R, Huang Y (2023) Zinc homeostasis in *Schizosaccharomyces pombe*. Arch Microbiol 205:126.

Yin S, Duan M, Fang B, et al (2022) Zinc homeostasis and regulation: Zinc transmembrane transport through transporters.

ZALOKAR M (1954) Studies on biosynthesis of carotenoids in *Neurospora crassa*. Arch Biochem Biophys 50:71–80.

Zhang L-H, Wang X, Zheng Z-H, et al (2010) Altered expression and distribution of zinc transporters in APP/PS1 transgenic mouse brain. Neurobiol Aging 31:74–87

Zhang T, Liu J, Fellner M, et al (2017) Crystal structures of a ZIP zinc transporter reveal a binuclear metal center in the transport pathway. Sci Adv 3:e1700344

Zhang T, Sui D, Hu J (2016) Structural insights of ZIP4 extracellular domain critical for optimal zinc transport. Nat Commun 7:11979.

Zhao H, Butler E, Rodgers J, et al (1998) Regulation of zinc homeostasis in yeast by binding of the ZAP1 transcriptional activator to zinc-responsive promoter elements. J Biol Chem 273:28713–28720.

Zhao H, Eide D (1996a) The yeast ZRT1 gene encodes the zinc transporter protein of a high-affinity uptake system induced by zinc limitation. Proc Natl Acad Sci U S A 93:2454–2458.

Zhao H, Eide D (1996b) The ZRT2 gene encodes the low affinity zinc transporter in *Saccharomyces cerevisiae*. J Biol Chem 271:23203–23210.

Zhao H, Eide DJ (1997) Zap1p, a metalloregulatory protein involved in zinc-responsive transcriptional regulation in *Saccharomyces cerevisiae.* Mol Cell Biol 17:5044–5052.

Zhao Y, Antoniou-Kourounioti RL, Calder G, et al (2020) Temperature-dependent growth contributes to long-term cold sensing. Nature 583:825–829.

Zheng W, Zhang C, Li Y, et al (2021) Folding non-homologous proteins by coupling deep-learning contact maps with I-TASSER assembly simulations. Cell Reports Methods 1:100014.

Zhou M, Hu C, Yin Y, et al (2022) Experimental Evolution of Multidrug Resistance in N*eurospora crassa* under Antifungal Azole Stress. J Fungi 8:. https://doi.org/10.3390/jof8020198

Zhou PB, Thiele DJ (1991) Isolation of a metal-activated transcription factor gene from *Candida glabrata* by complementation in *Saccharomyces cerevisiae*. Proc Natl Acad Sci 88:6112–6116.

Zhu Z, Thiele DJ (1996) A Specialized Nucleosome Modulates Transcription Factor Access to a C. glabrata Metal Responsive Promoter. Cell 87:459–470.

Zubko EI, Zubko MK (2014) Deficiencies in mitochondrial DNA compromise the survival of yeast cells at critically high temperatures. Microbiol Res 169:185–195.

PUBLICATIONS, CONFERENCES AND WORKSHOP

Publications:

1. **Serena Ngiimei D,** Ranjan Tamuli. The CDF family of zinc transporters *zrc-1, msc-2*, and *zrg-17* genetically interact to maintain zinc homeostasis in *Neurospora crassa*. Journal of Bioscience (2024) 49:12 DOI: 10.1007/s12038-023-00398-4.

2. Megha Rasaily, **Serena Ngiimei D**, Rahul Kumar Thaosen, Surabhi Gupta, Sangeeta Deka, Ranjan Tamuli. Methods for the detection of intracellular calcium in filamentous fungi. MethodX (Revised version submitted).

3. **Serena Ngiimei D**, Ranjan Tamuli. ZAP-1, a C2H2 zinc finger transcription factor is essential for *Neurospora crassa* to thrive under zinc-depleted conditions (Manuscript under preparation).

Conferences presentations:

1. **Ngiimei D S**, Tiwari A and Tamuli R (2018) Cellular role of zinc transporter in *Neurospora crassa*. 10th International Conference on Yeast Biology: Model Yeasts to Fungal Pathogen, Jawaharlal Nehru University, New Delhi, India, February 8 -11, 2019.
2. **Ngiimei D S** and Tamuli R (2019) Understanding the molecular mechanism of Zinc transporters in *Neurospora crassa.* XI International Conference on Biology of Yeasts and Filamentous Fungis (ICBYFF ’19), School of Life sciences, University of Hyderabad, Hyderabad, India November 27−29, 2019.
3. **Ngiimei D S** and Tamuli R (2022) Zinc signaling and regulation of cellular functions in *Neurospora crassa.* Molecular Intricacies of Plant Associated Microorganisms (MIPAM), CDFD, Hyderabad, February 17- 20, 2022.

4. **Ngiimei D S** and Tamuli R (2022) Cation diffusion facilitator family of zinc transporters *zrg-17*, *msc-2* and *zrc-1* interact genetically to maintain zinc homeostasis in *Neurospora crassa.* Asian Mycological Congress, Thailand Science Park, Pathum Thani, Thailand. August 3−5, 2022.

Workshops:

1. **Ngiimei D S (2019)** Workshop cum lecture series on "Skill Development in Molecular Strategies for Understanding Biodiversity and Human Diseases". Bioinformatics Centre, NEHU, Shillong (NEHU- CSIR IGIB collaboration) February 28 – March 2, 2019.

J Biosci (2024)49:12
DOI: 10.1007/s12038-023-00398-4
Indian Academy of Sciences

CDF family of zinc transporters ZRC-1, MSC-2, and ZRG-17 are involved in survival at high zinc conditions, vegetative development, and cellulase utilization in Neurospora crassa

SERENA NGIIMEI D and RANJAN TAMULI*

Department of Biosciences and Bioengineering, Indian Institute of Technology Guwahati, Guwahati 781 039, India

*Corresponding author (Email, ranjantamuli@iitg.ac.in, ranjan.tam@gmail.com)

MS received 30 April 2023; accepted 7 September 2023

The cation diffusion facilitator (CDF) family of zinc transporters plays a crucial role in zinc homeostasis in eukaryotes, including fungi. Here, we investigated the cell functions and genetic interactions of CDF zinc transporters zrc-1 and msc-2 in Neurospora crassa. The Dzrc-1 mutant could not grow in a high-zinc environment, indicating that the zinc transporter protein ZRC-1 was essential for growth in high-zinc conditions. However, the deletion of msc-2 did not show any severe phenotypic defects. Furthermore, we studied the genetic interactions of the zinc transporters using the CDF double mutants. Previously, zrg-17 was reported to be critical, where the Dzrg-17 mutant showed defects in both vegetative development and asexual sporulation. Interestingly, the Dmsc-2;Dzrg-17 double mutant showed phenotypes similar to the wild type, and restored the phenotypic defects of the Dzrg-17 mutation. However, the Dzrc-1;Dmsc-2 and Dzrc-1;Dzrg-17 double mutants continue to display phenotypic defects like their parental single mutants. The double mutant Dzrc-1;Dzrg-17 showed severe vegetative growth defects, including slow growth, short aerial hyphae, narrowed septation, and defective asexual sporulation. In addition, aerial hyphae development of the Dzrc-1;Dmsc-2 and Dzrc-1;Dzrg-17 double mutants were reduced under endoplasmic reticulum stress. Thus, this study revealed the cell functions and genetic interactions of zrc-1, msc-2, and zrg-17 for vegetative development and tolerance to stress conditions in N. crassa.

Keywords. Cation diffusion facilitator (CDF); cellulase; conidiation; Neurospora crassa; zinc homeostasis

2 INTRODUCTION

After iron, zinc is the second most abundant metal found in living organisms and is an essential structural component of many proteins belonging to cellular signaling pathways (Bird and Wilson 2020; Kambe et al. 2021; Clemens 2022). Zinc is redox inactive, and therefore, zinc binding to DNA does not cause any damage (Vallee and Auld 1990). Many of these proteins acquire their zinc as they pass through the secretory pathways, which are then secreted from cells; for example, the availability of a high amount of zinc in secretory vesicles is crucial for the packaging of insulin granules in pancreatic islet b-cells (Dodson and Steiner 1998; Nicolson et al. 2009; Pound et al. 2009; Wijesekara et al. 2010). The modulation of NMDA and GABA receptors through direct zinc signaling in mammalian brain cells has also been reported (Cuajungco and Lees 1997; Mocchegiani et al. 2005; Amico-Ruvio et al. 2011). Thus, a low concentration of zinc is harmful to the cell because $Zn^{2?}$ is a vital metal cofactor and signal transducer. However, excess zinc levels have adverse effects on cells, such as protein aggregations, which consequently lead to the dysfunction of proteins (Cousins et al. 2006; Kambe et al. 2008). Zinc toxicity also resulted in neuronal cell death during pathological conditions in a rat model (Koh 2001). Therefore, it is essential to maintain cellular zinc homeostasis in the cytoplasm, endoplasmic reticulum (ER), and subcellular organelles for proper cell functions. The maintenance of zinc homeostasis is regulated by various transporter proteins that maintain $Zn^{2?}$ levels by release and uptake (Eide 2006). In eukaryotes, zinc transporter proteins belong to two major groups of proteins, namely, the Zrt-Irt-like protein family (ZIP) and the cation diffusion facilitator (CDF)/ zinc transporter (ZnT) family. The ZIP family proteins enable the uptake or release of zinc from intracellular stores, whereas the transport of zinc out of the cell or into the lumen of intracellular compartments is accomplished by the CDF family members (Eide 2006; Kambe et al. 2017).

CDF is a ubiquitous family of proteins identified in bacteria, archaea, and eukaryotes, which mediates metal homeostasis (Paulsen and Saier 1997; Nies 2003; Eide 2006; Kambe et al. 2017). In Saccharomyces cerevisiae, zinc transporters Zrt1p and Zrt2p are involved in the uptake of zinc into the cytoplasm (Zhao and Eide 1996a, b; Gaither and Eide 2001), and Zrt3p is involved in zinc transport from the vacuole in response to zinc deficiency in the cytoplasm (MacDiarmid et al. 2000). Alternatively, when the cytoplasmic zinc level goes high, Zrc1p (zinc resistance conferring) transports extra zinc into the vacuoles for storage and, therefore, acts as a suppressor of zinc toxicity (Miyabe et al. 2001). In addition, transmembrane proteins Msc2p (meiotic sister chromatid recombination 2) and Zrg17p (zinc-regulated gene), localized in the ER, form a heteromeric complex and mediate zinc transport in ER (Ellis et al. 2005). Similarly, in Schizosaccharomyces pombe, Zhf1 (zinc homeostasis factor), a homolog of Zrc1p, transports zinc into the ER, while Cis4 (chloride and immunosuppressant sensitive) (Clemens et al. 2002) and Zrg17, respective homologs of Msc2p and Zrg17p, form a complex that localizes to the cis-Golgi, and transports zinc from the cytosol into the respective compartments (Boch et al. 2008; Choi et al. 2018). In fungal pathogens, Candida albicans, the CaZrt1 and CaZrt2 zinc transporters localized in the plasma membrane, are essential for zinc uptake, and CaZrc1 is required for survival under high zinc, and maintaining zinc homeostasis is crucial for virulence (Crawford et al. 2018; Soares et al. 2020; Bellotti et al.

Supplementary Information: The online version contains supplementary material available at https://doi.org/10.1007/s12038-023-00398-4.

http://www.ias.ac.in/jbiosci
Published online: 05 January 2024

2022). Likewise, in Candida parapsilosis, CpZrt21, a homolog of Zrt2, plays an important role in zinc uptake, while the CpZrc1 vacuolar-localized zinc transporter is essential for zinc detoxification and might play a role in virulence (Taka´cs et al. 2022). The majority of these zinc transporter proteins are regulated by the zinc-responsive transcription factor Zap1p. Zap1p binds to a zinc-responsive element (ZRE), an 11 bp consensus sequence, present in the target gene promoter to upregulate gene expression in low-zinc environments (Zhao and Eide 1997; Eide 2009).

Fungal morphology is significantly affected by zinc concentrations in the culture medium (Raulin 1869). The zinc ion is a metal cofactor in several proteins; thus, zinc concentration affects their production and folding (Linke et al. 2003). Suboptimal zinc concentrations can lead to protein misfolding, resulting in ER stress, affecting the functioning of the ER. In response to ER stress conditions, distinct physiological processes are initiated in the cell, such as the unfolded protein response (UPR), that assist the ER in combating the accumulation of misfolded proteins (Harding et al. 1999; Xu et al. 2005; Hetz 2012). Msc2p of S. cerevisiae, which is localized in the ER membrane, is responsible for transporting zinc into the ER from the cytoplasm. Thus, the mutation in MSC2 leads to ER stress, which activates the UPR system under low-zinc conditions (Ellis et al. 2004). Furthermore, ZRG-17 in N. crassa is crucial for ER stress tolerance under lowzinc conditions (Tiwari et al. 2018).

In N. crassa, seven putative zinc transporters belonging to the ZIP family, and nine zinc transporters belonging to the CDF family, have been identified (Kiranmayi and Mohan 2006). The knockout mutant of N. crassa zrg-17 (member of CDF family) showed several zinc-suppressible phenotypes such as slow growth rate, short aerial hyphae, and defects in asexual sporulation (Tiwari et al. 2018). Previous studies (Montanini et al. 2007) have shown the presence of two putative zinc transporters NCU03145 (zrc-1) and NCU07262 (msc-2) belonging to the CDF family in N. crassa. Therefore, in this study, we investigated the role of these two CDF family zinc transporter proteins, ZRC-1 and MSC-2 of N. crassa, in fungal growth under different conditions by studying their knockout phenotypes. Moreover, we generated the double mutants of Dzrc-1, Dmsc-2, and Dzrg-17 in combination to further investigate the phenotypic effects of these genes. We found that ZRC-1 was critical for vegetative development under high-zinc conditions. The double mutant Dmsc-2;Dzrg-17 exhibits phenotypes similar to the wild type, indicating an epistatic interaction. Additionally, the double mutant Dzrc1;Dzrg-17 showed defects in conidiation, and both Dzrc-1;Dzrg-17 as well as Dzrc-1;Dmsc-2 double mutants were unable to grow in a medium containing cellulose, indicating the importance of these zinc transporters in combating ER stress.

Table 1. Primers used in this study

Sl. No.	Primer name	Gene targeted	Sequence (5^0-3^0)	Source
1.	5HPHR	hph	ATCCACTTAACGTTACTGAAATC	Deka et al. 2011
2.	HI-ZRC-1 SN	zrc-1 knockout	GGGAGGTGGTTCTTATGCTC	This study
3.	HI-MSC-2 SN	msc-2 knockout	CGCCAGTCCTGTAAGGACCA	This study
4.	Zrg-17-KOC-F	zrg-17 knockout	GTTTCGAGTCGTCCTCGTTG	Tiwari et al. 2018
5.	q-con-10 FW	con-10 for RT-PCR	CCAAGGAAGAGGTTCAGGCC	Barman and Tamuli 2017
6.	q-con-10-RV	con-10 for RT-PCR	TTGCCGCCCTTGGAAGCAAT	Barman and Tamuli 2017
7.	q-B-tub-FW	B-tubulin for RT-PCR	CCCAAGAACATGATGGCTGC	Barman and Tamuli 2017
8.	q-B-tub-RV	B-tubulin for RT-PCR	TTGTTCTGAACGTTGCGCATC	Barman and Tamuli 2017
9.	RT-NCU07262 FW	msc-2 for RT-PCR	CCAAGTTCACTGCGTTTCTG	This study
10.	RT-NCU07262 RV	msc-2 for RT-PCR	AGGAGACCGAGGGAATCTG	This study
11.	RT-NCU03145 FW	zrc-1 for RT-PCR	TCCAAGTGATGCTGGCGATC	This study
12.	RT-NCU03145 RV	zrc-1 for RT-PCR	CGTAGGAGAACTGATCTGTTG	This study

3 MATERIALS AND METHODS

3.1 Neurospora crassa strains, media, growth, crosses, and maintenance

Neurospora crassa wild type strains 74-OR23-1V A (FGSC 2489) and ORS-SL6 a (FGSC 4200), mutant strains DNCU03145::hph matA (FGSC 12277), DNCU07262::hph mat a (FGSC 11540), and

DNCU01254::hph mat a (FGSC 18311) were obtained from the Fungal Genetics Stock Center (FGSC), University of Missouri, Kansas City, MO 64110 (McCluskey et al. 2010). The procedures for the growth and maintenance of strains were as described previously (Davis and de Serres 1970). The opposite mating types of the single mutants were crossed using the synthetic crossing medium (SCM) (Westergaard and Mitchell 1947), to generate double mutants. Ascospores from the crosses were germinated by heat shock at 60C for 1 h and then plated on a medium containing 0.05% fructose, 0.05% glucose, 2% sorbose (FGS), and 2% Bacto agar (Davis and de Serres 1970). The progeny containing hygromycin resistance cassette (hph) was selected using FGS agar supplemented with hygromycin B (220 lg/mL). Confirmation of the F_1 progenies to generate double mutants was done by PCR using gene-specific primers (table 1) along with reverse primer 5HPHR (supplementary figure 1). Routine cultures and strains were grown on 1X Vogel's (Vogel 1956, 1964) glucose medium (VG) with 1.5%

D-glucose as a carbon source and 2% Agar powder Bacto grade (Himedia) for the solid medium. The concentration of zinc in the medium was 17 lM (unless stated otherwise). Media containing different concentrations of zinc were labeled as low-zinc Vogel's glucose (LZVG) and contained 100 lM EDTA, but devoid of zinc in trace element in 1X Vogel's stock solution. LZVG supplemented with 1 lM, 100 lM, and 1000 lM of $ZnCl_2$ were labeled as LZVG1 (zinc limiting), LZVG100 (low zinc), and LZVG1000 (high zinc), respectively.

3.2 Vegetative growth, aerial hyphae, and time course conidiation study

For radial colony growth assay, a *1 cm diameter of a mycelial agar plug was harvested from 3-day-old cultures of each strain and inoculated at the center of 90-mm Petri dishes and 250 mL flasks containing VG agar and LZVG agar media. The flasks were incubated at 30C for 3 days in the dark and then for

an additional 4 days under light at room temperature. To measure aerial hyphae height, *10^6 conidia/mL of each strain were inoculated in test tubes under different VG liquid (without agar) media and incubated in the dark for 3 days at 30C followed by 4 days at room temperature under light, and the aerial hyphae height was then measured. To study the time course conidiation assay, mycelial plugs were inoculated in 55-mm Petri dishes containing VG agar medium and incubated in the dark at 30C. After 12 h post-inoculation, conidia were harvested using sterile distilled water at every 12 h intervals until 72 h. Counting of conidia was performed using a hemocytometer.

3.3 Microscopy

To visualize internal septations, strains were grown on VG agar medium for 12 h at 30C. Agar blocks with the hyphal tip were placed on a glass slide and stained with calcofluor white (0.1%; CFW; Sigma-Aldrich) for 10 to 20 min. The samples were then observed under a microscope (AxioVert.A1 FL-LED, Carl Zeiss) using a DAPI filter with an exposure time of 400 ms. Further, septa length and width were estimated using ImageJ software (rsbweb.nih.gov/ij). For visualization of septation under a field emission scanning electron microscope (FESEM), samples were prepared as described by Seale (1973). The strains were freshly grown in VG liquid medium for 18 h. Mycelium was incorporated on a thin glass slide and dried at 40C for 8 h to 10 h. After drying, the glass slide was mounted onto the stub, coated with gold, and observed under an FESEM (Gemini 300, Carl Zeiss).

3.4 Endoplasmic reticulum stress and cellulose degradation assay

To study ER stress, we used dithiothreitol (DTT, molar mass=154.253 g/mol). We measured the aerial hyphae height at different concentrations (0.5 mM, 1 mM, and 2 mM) of DTT and compared the growth of the wild type and the mutant strains in control VG. To check whether the mutants could grow on cellulose as the sole carbon source, we replaced glucose with 1.5% cellulose (w/v) in Vogel's glucose media to prepare Vogel's Cellulose (VC), and different concentrations of zinc were supplemented externally. The Low Zinc Vogel's Cellulose (LZVC) media contained 100 lM EDTA and without zinc in the trace element added to the 50X VGN stock solution. Additionally, this medium was supplemented with either 1 lM $ZnCl_2$ (referred to as LZVC1) or 1000 lM $ZnCl_2$ (referred to as LZVC1000). The strains were first grown in VG agar for 3 days in the dark at 30C and then transferred to light for 2 days. Conidia were freshly harvested using sterile distilled water, and *10^6 conidia/mL were inoculated in a 250 mL flask containing different media and incubated at 30C with shaking at 180 rpm for 7 days. The mycelial masses were harvested and dried at 60C for 1 h, and dry weights were measured. Estimation of glucose and protein accumulation in the supernatant was done as described previously (Mishra et al. 1984; Starr and Gonc 2018).

3.5 RNA isolation and quantitative real-time PCR analysis

To analyze the expression of genes, *10^6 conidia/mL of the wild type were inoculated in different media (VG, LZVG1, and LZVG1000) and incubated for 16 h at 30C with shaking at 180 rpm, and then the mycelial masses were collected and crushed into powder using a mortar-pestle and liquid nitrogen. RNA was isolated using TRIzol reagent (Life Technologies, USA), and cDNA was synthesized using a VersoTM cDNA Synthesis Kit (Thermo Fisher Scientific, USA) following the manufacturer's protocol. RNA of N. crassa strains in submerged culture was isolated as previously described (Barman and Tamuli 2017). Quantitative real-time PCR (qRT-PCR) analysis was performed using

the sequence-specific primer pairs (table 1), a PowerUp™ SYBR™ Green Master Mix (Applied Biosystem, USA), and a 7500 Real-time PCR System (Applied Biosystems, City, State, USA) as per the manufacturer's protocol. The target gene's relative expression levels were calculated using the 2^{-DDCT} method (Livak and Schmittgen 2001). b-tubulin expression was used as the control.

3.6 Statistical analysis

All experiments reported in this manuscript were carried out at least three times. The results are presented as means±standard deviation. GraphPad Prism 10.0.0 was used to conduct statistical analyses of the differences between the groups using either one- or two-way ANOVA with Tukey's post hoc analysis methods.

4 RESULTS

4.1 N. crassa ZRC-1 zinc transporter is required for survival in high-zinc conditions

The N. crassa NCU03145 and NCU07262 genes encode the ZRC-1 and MSC-2 proteins, respectively, which are members of the CDF zinc transporters family (Montanini et al. 2007). The ZRC-1 and MSC-2 proteins contain six potential transmembrane domains (TMDs), and show 39.14% and 44.93% sequence identities to the Zrc1p and Msc2p homologs of S. cerevisiae, respectively (supplementary figure 2). We investigated the phenotypes of the N. crassa Dzrc-1 and Dmsc-2 mutants under different zinc concentrations to investigate the cell functions of zrc-1 and msc2. The Dzrc-1 and Dmsc-2 mutants were viable in the standard VG liquid media, suggesting that zrc-1 and msc-2 are non-essential genes (figure 1A). To test the effect of the zinc limiting condition, EDTA (100 lM) was added as a zinc-chelating agent (Zhao and Eide

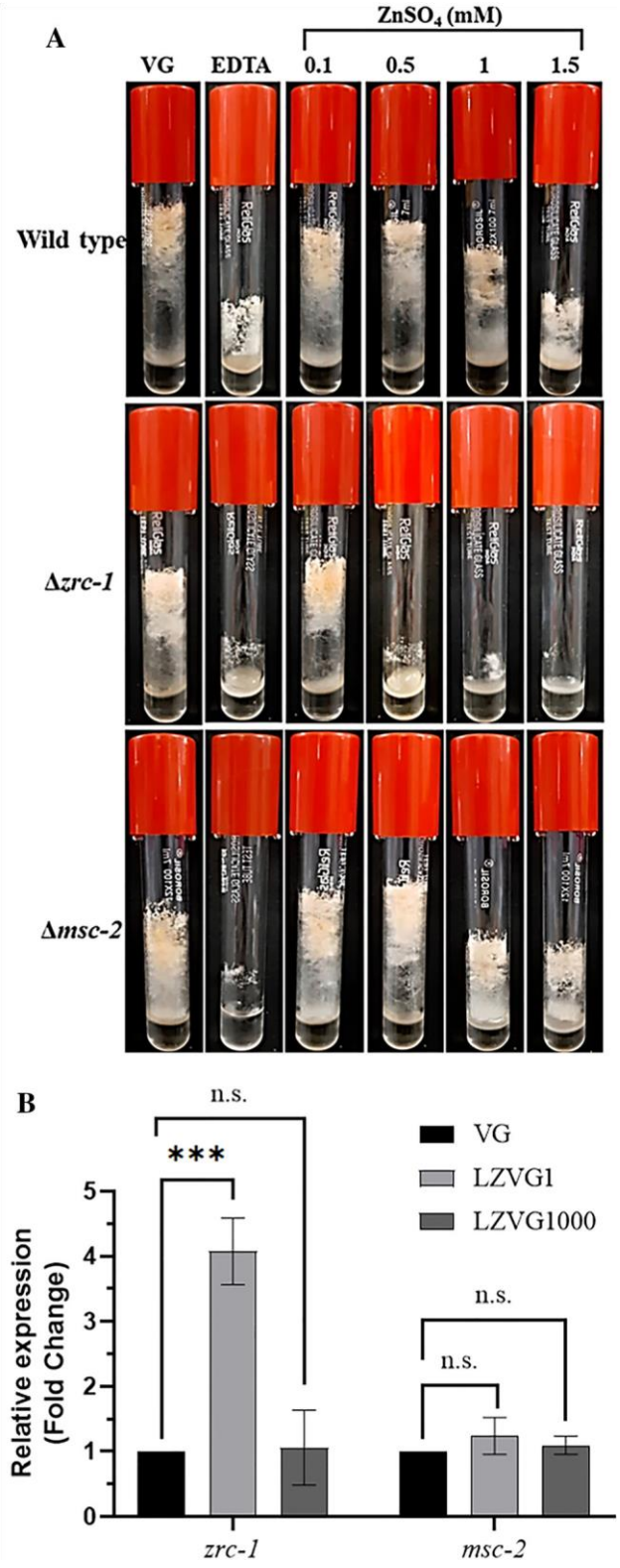

1996a) in the medium. In the zinc limiting condition (LZVG1), both Dzrc-1 and Dmsc-2 displayed a reduced growth phenotype, which was restored by adding zinc into the medium (figure 1A). The Dzrc-1 mutant did not produce any aerial hyphae with increasing

[b]Figure 1. Effect of various zinc concentrations on Dzrc-1 and Dmsc-2 mutants. (A) Aerial hyphae of strains under zinc limiting conditions (EDTA) and different concentrations of zinc (0.1 mM, 0.5 mM, 1 mM, 1.5 mM). (B) Expression analysis of msc-2 and zrc-1: RNA from wild type were extracted from three different media; VG, LZVG1, LZVG1000, and expression were studied by qRT-PCR on three biological replicates. The relative expressions of the zrc-1 and msc-2 genes were normalized to the expression of b-tubulin in LZVG1 and LZVG1000, and values were compared with the expression in normal growth condition, VG. Error bars indicate the average standard deviation calculated from data from three independent experiments. The asterisks represent significant difference when comparing the expressions with the wild type, as measured by twoway ANOVA analysis with Tukey's post hoc test with p\0.001 (***); n.s. not statistically significant (nonsignificant).

concentration of zinc, and concentrations beyond 0.5 mM were lethal to the Dzrc-1 mutant (figure 1A), suggesting that zrc-1 plays a role in survival in highzinc conditions in N. crassa. However, the wild type and Dmsc-2 mutant showed aerial hyphae growth in the medium containing up to 1.5 mM zinc. In addition, the Dzrc-1 and Dmsc-2 mutants showed no defects in sexual development and fertility (supplementary table 2; supplementary figure 3). Furthermore, the expression of zrc-1 in the LZVG1 condition was *3fold higher than cells grown in VG and high-zinc (LZVG1000) conditions (figure 1B); however, msc-2 expression was not significantly altered in low-zinc (LZVG100) and high-zinc (LZVG1000) conditions tested (figure 1B). These results suggested that zrc-1, but not msc-2, gene expression is regulated by zinc concentration.

4.2 zrc-1, msc-2, and zrg-17 genetically interact for vegetative development under different zinc conditions

To study the genetic interactions of zrc-1, msc-2, and zrg-17 zinc transporters in N. crassa, we generated the Dzrc-1;Dmsc-2, Dmsc-2;Dzrg-17, and Dzrc-1;Dzrg-17 double mutants and studied their phenotypes at different concentrations of zinc (table 2; figure 2). The Dzrc1;Dmsc-2 double mutant showed phenotypes similar to its parental single mutants; however, the growth rate was decreased in LZVG1000, which was more evident in the flask than on the Petri dish, and this could be due to a greater extended period of incubation. Interestingly, the slow growth phenotype of Dzrg-17 was masked in the Dmsc-2;Dzrg-17 double mutant that showed colony morphology like the wild type in all the tested zinc concentrations (figure 2), suggesting that msc-2 is epistatic to zrg-17. However, the Dzrc-1;Dzrg17 double mutant showed severe growth defects in both low- and high-zinc conditions (table 2; figure 2A, B). Additionally, aerial hyphae growth was significantly reduced in the Dzrc-1 single mutant but only moderately reduced in the Dzrc-1;Dmsc-2 double mutant when grown in LZVG1000 (figure 2C). The Dmsc-2;Dzrg-17 double mutant did not show any distinctive difference in aerial hyphae height when compared with the wild type in all the tested concentrations of zinc. Furthermore, Dzrc-1;Dzrg-17 could not produce aerial hyphae either in LZVG1 or LZVG1000 media. However, the zrc-1, msc-2, and zrg-17 single and double mutants were not sensitive to osmotic (NaCl and KCl) and pH stresses (pH 3.8 and 7.8), azole drugs (fluconazole and itraconazole), or temperature (20C and 40C) conditions (supplementary figure 4). Taken together, these results suggest that zrc-1, msc-2, and zrg-17 genetically interact and play critical roles in vegetative development and tolerance to low- and highzinc concentrations in N. crassa.

4.3 Double mutant Dzrc-1;Dzrg-17 showed defects in septation, early conidiation, and inappropriate conidiation under submerged condition

In S. cerevisiae, Zrc1p, Msc2p, and Zrg17p are required for transporting zinc into the ER, and mutations in MSC2 and ZRG17 hyperactivate the UPR system in low-zinc conditions, indicating the likelihood

Figure 2. Vegetative development of the N. crassa strains.[c] (A) Colony morphology of the mutant strains on 90 mm Petri dishes under different concentrations of zinc. The agar plug was inoculated and incubated at 30C in the dark for 21 h. Images were taken 21 h postinoculation. (B) The flask morphology of mutant strains was examined in different concentrations of zinc. Theagarplugwasinoculatedandincubatedat30Cfor3daysin the dark and at room temperature for 2 days in the light. (C) Aerial hyphae of strains. The conidial suspensions (10^6 conidia/mL) were inoculated in VG liquid containing different concentrations of zinc and incubated at 30C in the dark for 3 days and at room temperature for 2 days in the light.

of protein misfolding (Ellis et al. 2004, 2005). The Dtzn1 and Dtzn1;Dtzn2 mutants in N. crassa exhibited an aconidiation phenotype (Kiranmayi et al. 2009), while the Dzrg-17 mutant exhibited slow growth rate, short aerial hyphae, increased hyphal branching, early and enhanced conidiation, and delayed conidial germination (Tiwari et al. 2018). Furthermore, the Dzrc1;Dzrg-17 mutant showed severe growth retardation in low-zinc conditions (figure 2A). Therefore, we investigated if the slow growth phenotype of the Dzrc1;Dzrg-17 mutants was due to a defect in septa formation and conidiation defect. We used a fluorescent blue dye CFW which binds to the cellulose and chitin of the cell wall (Seidel et al. 2013; Boyce et al. 2016) to visualize and estimate septa length and hyphal width. The Dzrc-17, and Dzrc-1;Dzrg-17 mutants had severely reduced hyphal width and septation length (table 3; figure 3A). In addition, the Dzrg-17 and Dzrc1;Dzrg-17 mutants developed significant constriction in the septation site compared with the wild type as revealed by the FESEM analysis (figure 3B).

Table 2. Average colony growth rates of the N. crassa strains

	Average growth rate (cm/h)[a]			
Strains	VG	LZVG1	LZVG100	LZVG1000
Wild type	0.38±0.01	0.32±0.01	0.36±0.03	0.36±0.01
Dzrc-1	0.37±0.01	0.36±0.01 (*)	0.37±0.02	0.30±0.02
Dmsc-2	0.38±0.04	0.34±0.04	0.35±0.05	0.36±0.02
Dzrg-17	0.20±0.02 (*)	0.17±0.01 (*)	0.20±0.02 (*)	0.2±0.02 (*)
Dzrc-1; Dmsc-2	0.4±0.02	0.32±0.035	0.37±0.05	0.32±0.01
Dmsc-2; Dzrg-17	0.37±0.02	0.33±0.02	0.36±0.03	0.35±0.01
Dzrc-1; Dzrg-17	0.20±0.02 (*)	0.17±0.01 (***)	0.20±0.02 (*)	0.16±0.02 (*)

[a] Results are shown as means±standard deviation for three independent experiments (n=3) with p\0.05 (*), and \0.001 (***) compared with the wild-type strain as measured by two-way ANOVA with Tukey's post hoc tests.

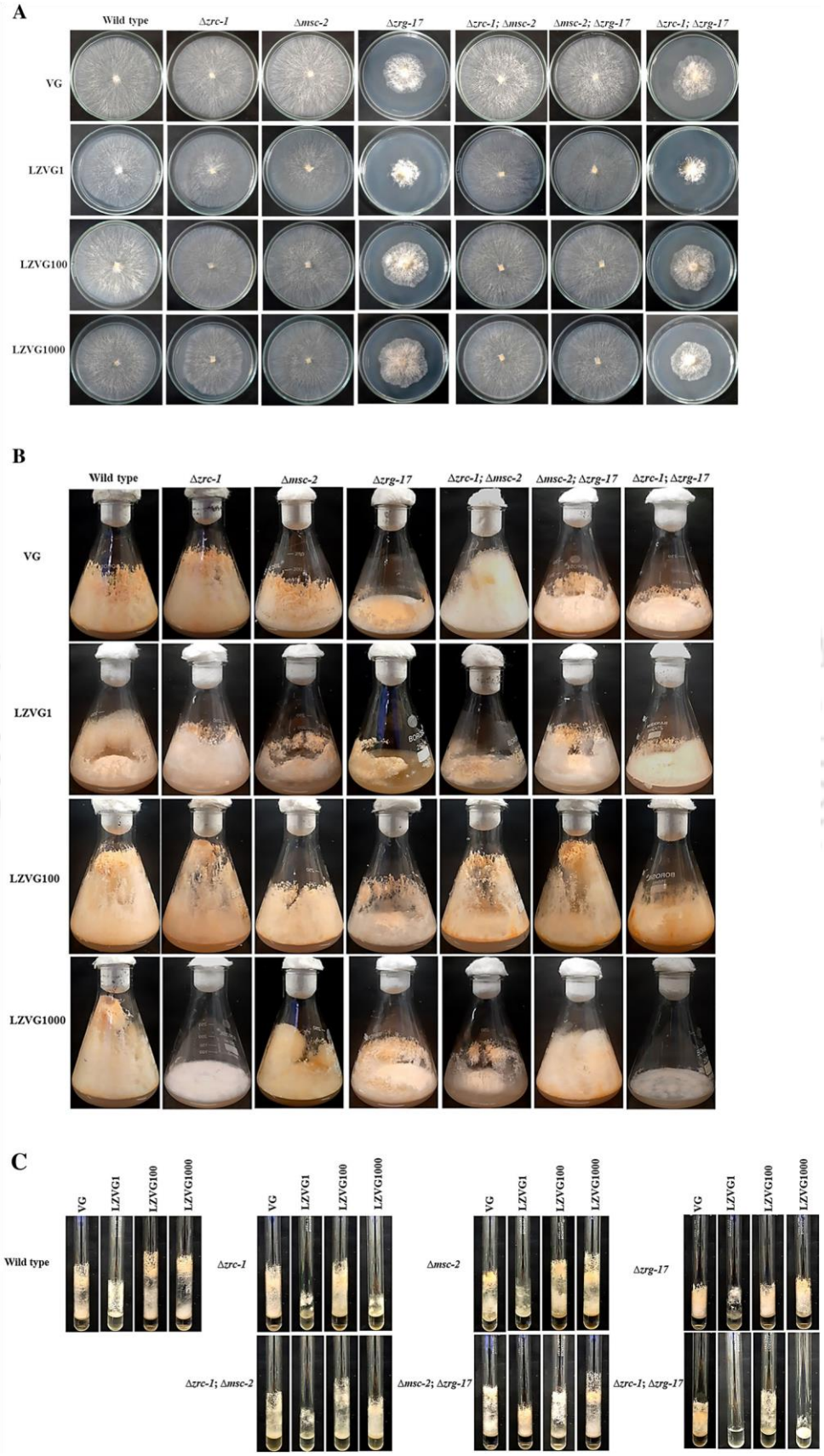
A
Wild type
Δzrc-1
Δmsc-2
Δzrg-17
Δzrc-1; Δmsc-2
Δmsc-2; Δzrg-17
Δzrc-1; Δzrg-17
VG
LZVG1
LZVG100
LZVG1000
B
Wild type
Δzrc-1
Δmsc-2
Δzrg-17
Δzrc-1; Δmsc-2
Δmsc-2; Δzrg-17
Δzrc-1; Δzrg-17
VG
LZVG1
LZVG100
LZVG1000
C
VG
LZVG1
LZVG100
LZVG1000
Wild type
Δzrc-1
Δmsc-2
Δzrg-17
Δzrc-1; Δmsc-2
Δmsc-2; Δzrg-17
Δzrc-1; Δzrg-17

Table 3. Septation length and hyphal width

	Average length (lm)[a]		Septation length (lm)[a]	
Strains	Hyphal width (n=30)	Septation length (n=30)	Maximum	Minimum
Wild type	10.33±2.4	81±26	135.99	32.85
Dzrg-17	7±3 (**)	28.83±10.53 (***)	57.937	16.68
Dzrc-1; Dzrg-17	7±2.6 (**)	32±10.75 (***)	52.66	19.06

[a] Results are shown as means±standard deviation for three independent experiments (n=3) with p\0.01 (**), and \0.001 (***) compared with the wild-type strain as measured by one-way ANOVA with Tukey's post hoc tests.

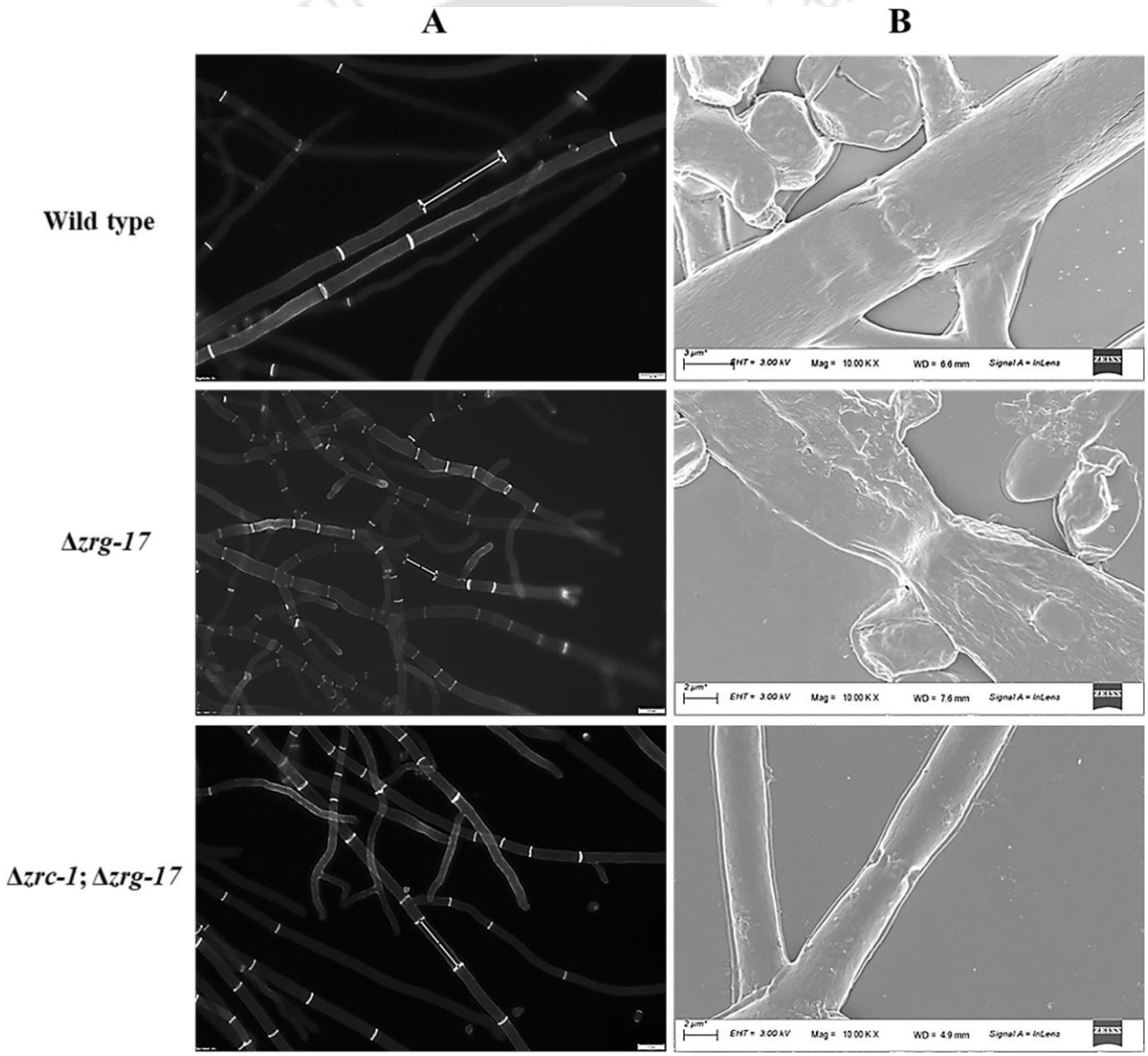

Figure 3. Imaging of hyphal cross walls. (A) Visualization of septa of N. crassa strains using calcofluor (CFW) staining. The strains were grown on VG agar for 12 h at 30C and visualized under a microscope using a DAPI filter. Scale bar, 20 lm. (B) FESEM of septation of N. crassa strains. The difference in structure in the area of septation of the wild type and the Dzrg17 and Dzrc-1;Dzrg-17 mutants are visible in the FESEM micrograph.

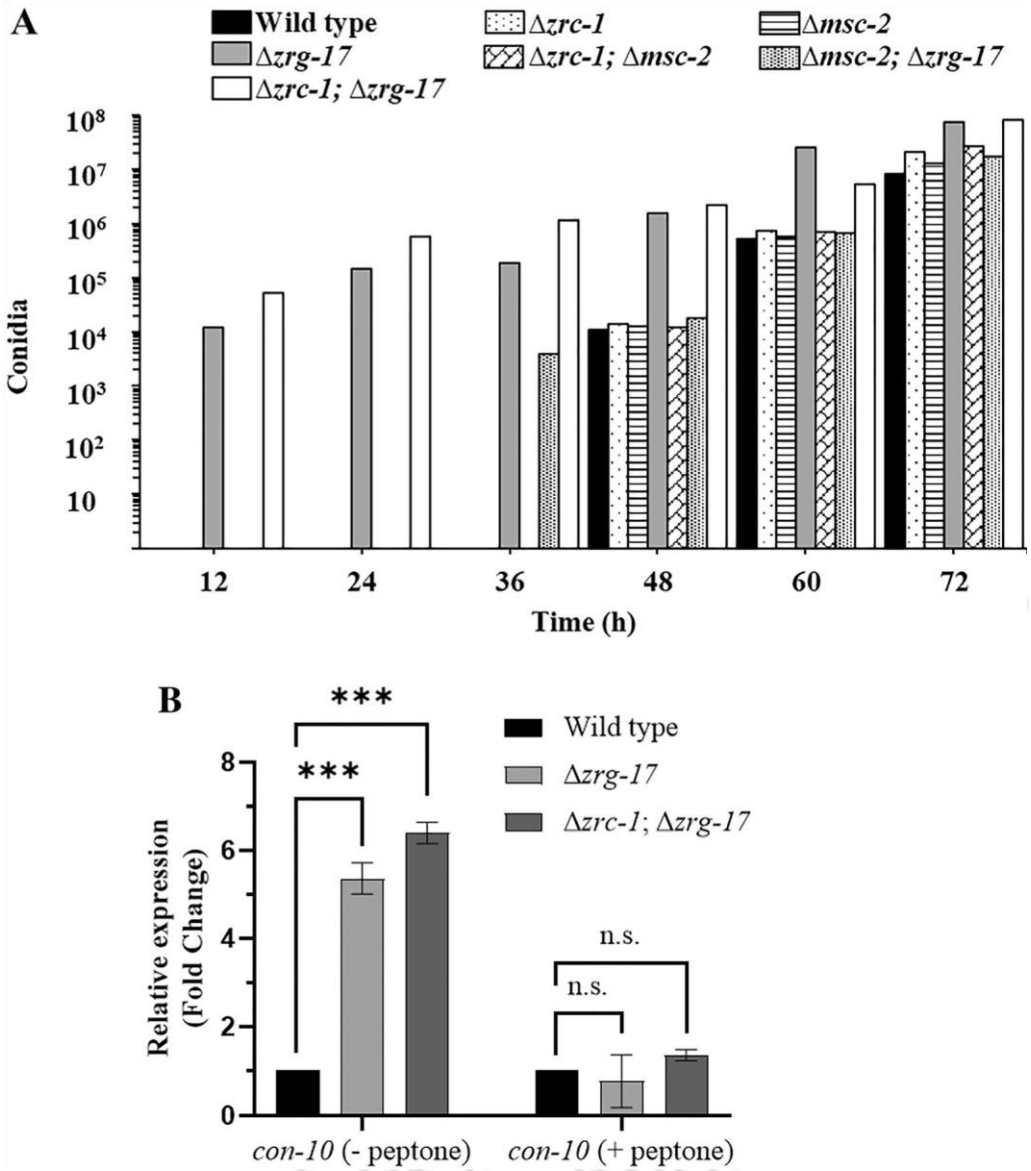

Figure 4. Asexual sporulation in the Dzrc-1;Dzrg-17 mutant. (A) Time course conidiation. N. crassa strains were inoculated in VG agar, and conidia were harvested in 12 h intervals until 72 h; the harvested conidia were counted using a hemocytometer. (B) The con-10 gene expression. The expression of the con-10 gene was determined by qRT-PCR on three biological replicates. The relative expression of the con-10 gene was normalized with the expression of b-tubulin, and values were compared with that of the wild type. Error bars indicate the standard deviation calculated from the data of three independent experiments. The asterisks represent significant difference when comparing the expressions with the wild type, as measured by two-way ANOVA analysis with Tukey's post hoc test with p\0.001 (***); n.s. not statistically significant
(non-significant).

Moreover, in a time course conidiation assay, conidia production in the Dzrg-17 and Dzrc-1;Dzrg-17

mutants was as early as 12 h; the Dmsc-2;Dzrg-17 mutant produced conidia by 36 h, while the wild type, Dmsc-2, and Dzrc-1, and Dzrc-1;Dmsc-2 strains were able to produce conidia only after 48 h of inoculation (figure 4A). Furthermore, in a submerged culture of 16 h, the Dzrg-17 and Dzrc-1;Dzrg-17 mutants showed abundant conidiophores, unlike the wild type.

In N. crassa, conidiation is triggered by nutrient deprivation, and therefore, to suppress inappropriate conidiation, nutrient-rich peptone is added to the medium (Springer and Yanofsky 1989; Kays et al. 2000). Hence, the addition of 2% peptone in the medium rescued the conidiation in submerged culture, and the mutants were able to form mycelial mass like the wild type (supplementary figure 5). In addition, we found that the conidiation-specific con-10 gene (Roberts et al. 1988; Navarro-Sampedro et al. 2008; Park and Yu 2012) was overexpressed in the Dzrg-17 and Dzrc-1;Dzrg-17 mutants in submerged culture; however, expression was similiar to the wild type when peptone was supplemented to the medium (figure 4B). Therefore, the inappropriate conidiation in the submerged culture condition of the Dzrg-17 and Dzrc-1; Dzrg-17 mutants was consistent with the overexpression of con-10, suggesting that ZRG-17 is involved in the proper expression of con-10.

4.4 Double mutants Dzrc-1;Dmsc-2 and Dzrc-1; Dzrg-17 showed defects in cellulose utilization

In N. crassa, ZRG-17 is reported to be crucial for survival under ER stress (induced by DTT and tunicamycin) and the Dzrg-17 mutant showed a slower growth rate and impaired protein secretion in cellulose medium (Tiwari et al. 2018). Therefore, we exposed the double mutants in stress linked to ER (DTT and cellulose) to determine if these genes act in the same or parallel pathways or if there is any functional redundancy within the zinc transporters. We tested the effect of DTT, which induces ER stress by inhibiting the formation of disulfide bonds and disrupting protein folding (Freedman 1995; Feige and Hendershot 2011) on the mutants of zinc transporters. The Dzrc-1;Dmsc-2 and Dzrc-1;Dzrg-17 double mutants displayed stunted hyphae and reduced growth rates of 29% and 24%, respectively (figure 5A). The wild type showed reduced growth of 45% in the medium supplemented with 2 mM DTT, while the Dzrc-1, Dmsc-2, and Dmsc2;Dzrg-17 mutants showed growth like the wild type (figure 5A). ER stress is also caused by glucose deprivation, causing interference with N-linked protein glycosylation (Scheuner et al. 2001). Therefore, we further replaced glucose with cellulose in the medium to test the effect of a glucose-deprived environment. We cultured the wild type, the Dzrc-1, Dmsc-2, and Dzrg-17 single mutants, and the Dzrc-1;Dmsc-2, Dmsc2;Dzrg-17, and Dzrc-1;Dzrg-17 double mutants in crystalline cellulose (Avicel) liquid medium with varying zinc concentrations. The Dzrc-1, Dmsc-2 single mutant and the Dmsc-2;Dzrg-17 double mutant strains were able to degrade cellulose like the wild type in all the conditions tested, except the Dzrc-1 mutant, which was unable to form any mycelial mass in the LZVC1000 medium (figure 5B). However, the growth of the Dzrg-17, Dzrc-1;Dmsc-2 and Dzrc-1;Dzrg-17 mutants was dramatically impaired in all concentrations of zinc (figure 5B). These results were consistent

Figure 5. Effect of the conditions inducing endoplasmic reticulum stress on N. crassa strains. (A) ER stress assay. The ability of the strains to produce aerial hyphae under different concentrations of DTT was checked, 10^6 conidia/mL conidial suspension was inoculated in VG liquid media containing different concentrations of DTT (0.5 mM, 1 mM, and 2 mM) and incubated at 30C, 3 days in the dark and 2 days under the light, and the aerial hyphae height of the strains were measured. Error bars indicate the standard deviations calculated from the data of three independent replicates. (B) Degradation of cellulose in different concentrations of zinc. Approximately, 10^6 conidia/mL conidial suspension was inoculated in 50 mL Vogel's

cellulose liquid media (VC, replacing glucose with 1.5% cellulose) containing different concentrations of zinc (LZVC1, LZVC100, LZVC1000), in a 250 mL flask and incubated at 30C, at 180 rpm for 7 days. (C) Cellulase activity of the strains. The glucose released in the supernatant in the medium under different conditions of varying zinc concentrations was measured using D-glucose as standard by 3, 5-dinitrosalicylic acid (DNSA), a reducing agent used to determine the reducing sugar present in samples. (D) Protein concentrations of the strains in different zinc concentrations were measured by Bradford assay. Results are shown as means±standard deviation for three independent experiments (n=3). The asterisks represent significant difference when comparing with the wild type, as measured by twoway ANOVA analysis with Tukey's post hoc test with p\0.05 (*),\0.01 (**), and\0.001 (***).

with their biomass accumulation in a liquid culture (table 4). It is possible that the Dzrc-1;Dmsc-2 and Dzrc-1;Dzrg-17 mutants secrete reduced levels of cellulase enzyme, which could explain the inability of these mutants to germinate and form biomass in the medium. To confirm this, we measured cellulase activity by measuring the amount of glucose. The wild type, Dmsc-2, Dzrc-1, and Dmsc-2;Dzrg-17 mutant strains had higher concentrations of glucose and protein in the supernatant (figure 5C, D). However, the Dzrg-17, Dzrc-1;Dmsc-2 and Dzrc-1;Dzrg-17 mutants secreted severely low amounts of glucose and protein in the supernatant, which was consistent with their phenotype (figure 5C, D). These results demonstrated the requirement of the CDF zinc transporters in cellulose degradation.

4.5 ZRC-1 and MSC-2 show similarities to Escherichia coli YiiP

The experimental structures of ZRC-1 and MSC-2 of N. crassa were not available in the protein databank

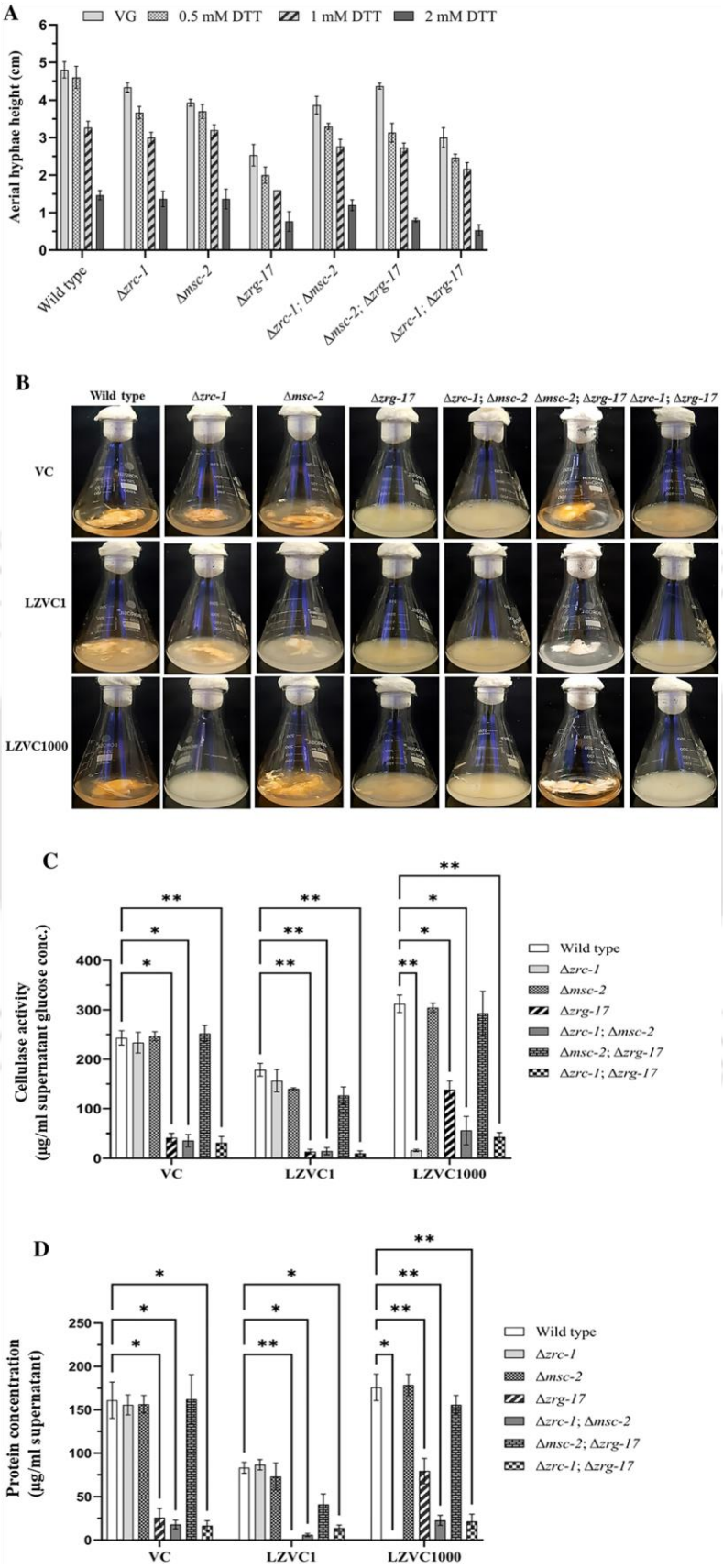
A
VG
0.5 mM DTT
1 mM DTT
2 mM DTT
Aerial hyphae height (cm)
Wild type
Δzrc-1
Δmsc-2
Δzrg-17
Δzrc-1; Δmsc-2
Δmsc-2; Δzrg-17
Δzrc-1; Δzrg-17
B
Wild type
Δzrc-1
Δmsc-2
Δzrg-17
Δzrc-1; Δmsc-2
Δmsc-2; Δzrg-17
Δzrc-1; Δzrg-17
VC
LZVC1
LZVC1000
C
Cellulase activity
(μg/ml supernatant glucose conc.)
VC
LZVC1
LZVC1000
Wild type
Δzrc-1
Δmsc-2
Δzrg-17
Δzrc-1; Δmsc-2
Δmsc-2; Δzrg-17
Δzrc-1; Δzrg-17
D
Protein concentration
(μg/ml supernatant)
VC
LZVC1
LZVC1000
Wild type
Δzrc-1
Δmsc-2
Δzrg-17
Δzrc-1; Δmsc-2
Δmsc-2; Δzrg-17
Δzrc-1; Δzrg-17

Table 4. Biomass accumulation in strains

	Biomass weight (mg/dry weight)[a]		
Strains	VC	LZVC1	LZVC1000
Wild type	714±31.7	363±55	868±34
Dzrc-1	676±73.7	418±40	-
Dmsc-2	662±75.1	432±44	637±29
Dzrg-17	-	-	118±41 (***)
Dzrc-1;Dmsc-2	-	-	-
Dmsc-2;Dzrg-17	689±35.8	342±37	737±22
Dzrg-17;Dzrc-1	-	-	-

[a] Results are shown as means±standard deviation for three independent experiments (n=3) with p\0.001 (***) compared with the wild-type strain as measured by two-way ANOVAwith Tukey's post hoc tests.

(PDB). The only zinc transporter with available X-ray crystallography structure is the Escherichia coli YiiP (Lu and Fu 2007), which showed 18.92% and 23.01% sequence identities to the ZRC-1 and MSC-2 proteins, respectively; therefore, we used YiiP as a template for homology modeling. The E. coli CDF metal transporter YiiP is a ferrous-iron efflux pump (FieF: P69380) of 300 amino acid residues localized on the plasma membrane (Chao and Fu 2004). In YiiP, the residues present within the transmembrane helix 2 and 5 were found to be involved with zinc, where Asp45 and Asp49 of TM helix 2 and His153 and Asp157 of TM helix 5 form a 'DDHD' motif involved in the interaction of zinc (Lu and Fu 2007). In addition, the zincinteracting residues of YiiP were found partially conserved in ZRC-1 and MSC-2 despite their minimal sequence identities. Protein structure prediction was performed using the Iterative Threading ASSEmbly Refinement (I-TASSER) suite that uses threading and ab initio methods (Yang and Zhang 2015; Zheng et al. 2021). The best predicted structures of ZRC-1 and MSC-2 were refined using GalaxyWEB (Ko et al. 2012) to improve structural quality (figures 6 and 7), and the final structure was validated based on the Ramachandran plot (Ramachandran and Sasisekharan 1968) obtained using PROCHECK (Laskowski et al. 1993). After the refinement process, residues in the most favored regions increased from 70.2% to 86.1% in ZRC-1 (supplementary figure 6A), and from 62.7% to 82.2% in MSC-2 (supplementary figure 6B). Structural alignment between YiiP and the modeled structures of ZRC-1 and MSC-2 was performed using the Dali webserver (Holm 2022). The RMSD between the modeled structures with YiiP were 2.8 A˚for ZRC-1 and 2.6 A˚ for MSC-2, which shows the significance of the similarity in the structures. Based on the structural alignment between YiiP and ZRC-1 and MSC-2, we found that the residue forming a 'DDHD' motif in YiiP was partially conserved as 'HDHD' in ZRC-1 and MSC-2 (supplementary figure 7). The conservation of these zinc-binding motifs in ZRC-1 and MSC-2 as in YiiP indicated that these residues were involved in zinc binding. To further validate the results obtained from the structural alignment, we superimposed the predicted ZRC-1 and MSC-2 structures on YiiP and visualized the structures using PyMOL (figure 6B, D; figure 7B, D). Therefore, the N. crassa ZRC-1 and MSC-2 show structural similarities to the E. coli YiiP.

5 DISCUSSION

The CDF family of zinc transporters is essential for cellular zinc homeostasis. In this study, we investigated cell functions of the CDF family of zinc transporter proteins ZRC-1, ZRG-17, and MSC-2 in N. crassa. The Dzrc-1 mutant was viable and unable to survive at 0.5 mM $ZnSO_4$, whereas the wild type was able to grow at even higher concentrations of zinc (1.5 mM $ZnSO_4$), indicating that ZRC-1 is necessary for survival under high-zinc conditions. Unexpectedly, the expression of zrc-1 was more elevated in low-zinc than in high-zinc conditions, and we identified a putative ZRE consensus sequence at the promoter region of zrc-1 (supplementary table 1), indicating that ZAP-1 might play a role in zrc-1 regulation. In S. cerevisiae and C. neoformans, overexpression of Zrc1p showed resistance to high zinc (Kamizono et al. 1989; Cho et al. 2018). At the same time, ZRC1 expression was upregulated in a Zap1p-dependent manner in zinclimited cells, and when zinc was added to the medium, this induction was repressed (Miyabe et al. 2001). The upregulation of ZRC1 was to rescue the cell from undergoing 'zinc shock', which is the sudden influx of zinc into the cytosol due to the activation of ZIP proteins in zinc-depleted conditions in S. cerevisiae and C. neoformans (Zhao and Eide 1997; MacDiarmid et al. 2000; Cho et al. 2018). ZAP-1-dependent regulations under low-zinc conditions in fungal systems were also reported in Aspergillus fumigatus (Miyabe et al. 2000; MacDiarmid et al. 2003; Moreno et al. 2007; Amich and Calera 2014; Vicentefranqueira et al. 2018), Candida albicans (Kim et al. 2008; Nobile et al. 2009), and Fusarium oxysporum (Lo´pez-Berges 2020). In N. crassa, the Dmsc-2 mutant exhibited no significant phenotypic differences compared with the wild type. The S. cerevisiae Msc2p, which is localized in the ER

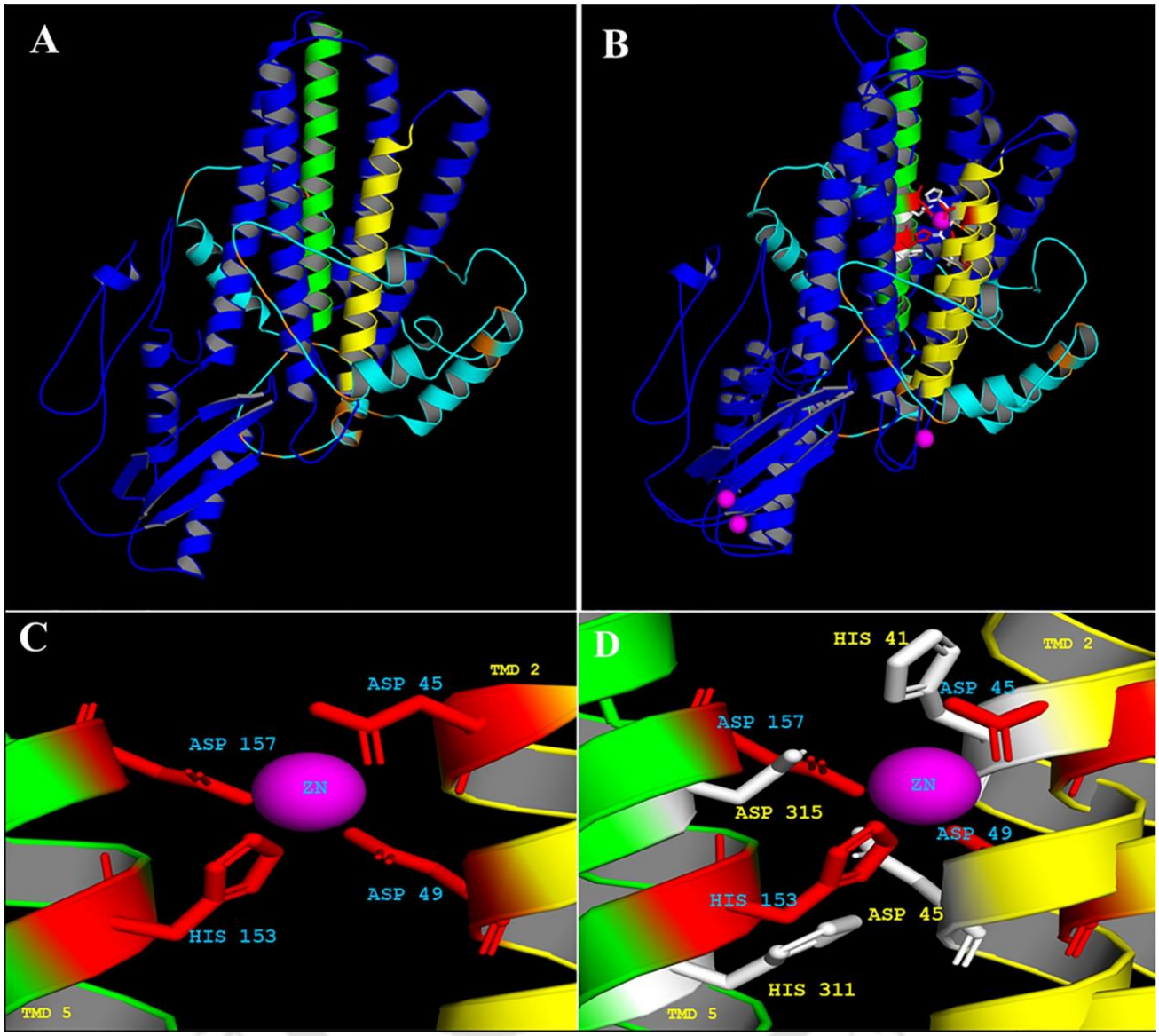

Figure 6. Homology modeling and structure validation of ZRC-1. (A) Modelled structure of ZRC-1. The ZRC protein is shown in blue; TM helixes 2 and 5 are shown in yellow and green, respectively; the regions that are structurally not aligned with YiiP (PDB ID: 3H90, Chao and Fu 2004) are shown in cyan; and the histidine residues within that region are highlighted in orange. (B) Superimposed image of YiiP and the modeled ZRC-1; the residues of ZRC-1 that are aligned with the zincinteracting residues of YiiP are shown in white. (C) The zinc-interacting site of YiiP shows the 'DDHD' motif present within the TM helix 2 and 5 of YiiP. (D) The superimposed image of the zinc-interacting site of YiiP with ZRC-1. The probable zinc-interacting residues in the 'HDHD' motif of ZRC-1 are shown based on its alignment with YiiP.

membrane, is responsible for transporting zinc into the ER from the cytoplasm (Ellis et al. 2004). Despite its crucial role in maintaining zinc homeostasis in S. cerevisiae, the expression of MSC2 was independent of zinc (Lyons et al. 2000; Wu et al. 2008). Similarly, zinc concentration did not affect msc-2 expression in N. crassa (figure 1B). These results suggested that cell functions of MSC-2 and ZRC-1 are conserved in S. cerevisiae and N. crassa.

To investigate the genetic interactions among CDF zinc transporters, we generated the Dzrc-1;Dmsc-2, Dmsc-2;Dzrg-17, and Dzrc-1;Dzrg-17 double mutants and investigated their phenotypes on a medium containing different concentrations of zinc for vegetative developments. In both low- and high-zinc environments, the double mutant Dzrc-1;Dzrg-17 exhibited additive phenotypes that led to defects in vegetative and asexual reproduction. Similarly, the Dzrc-1;Dmsc-2

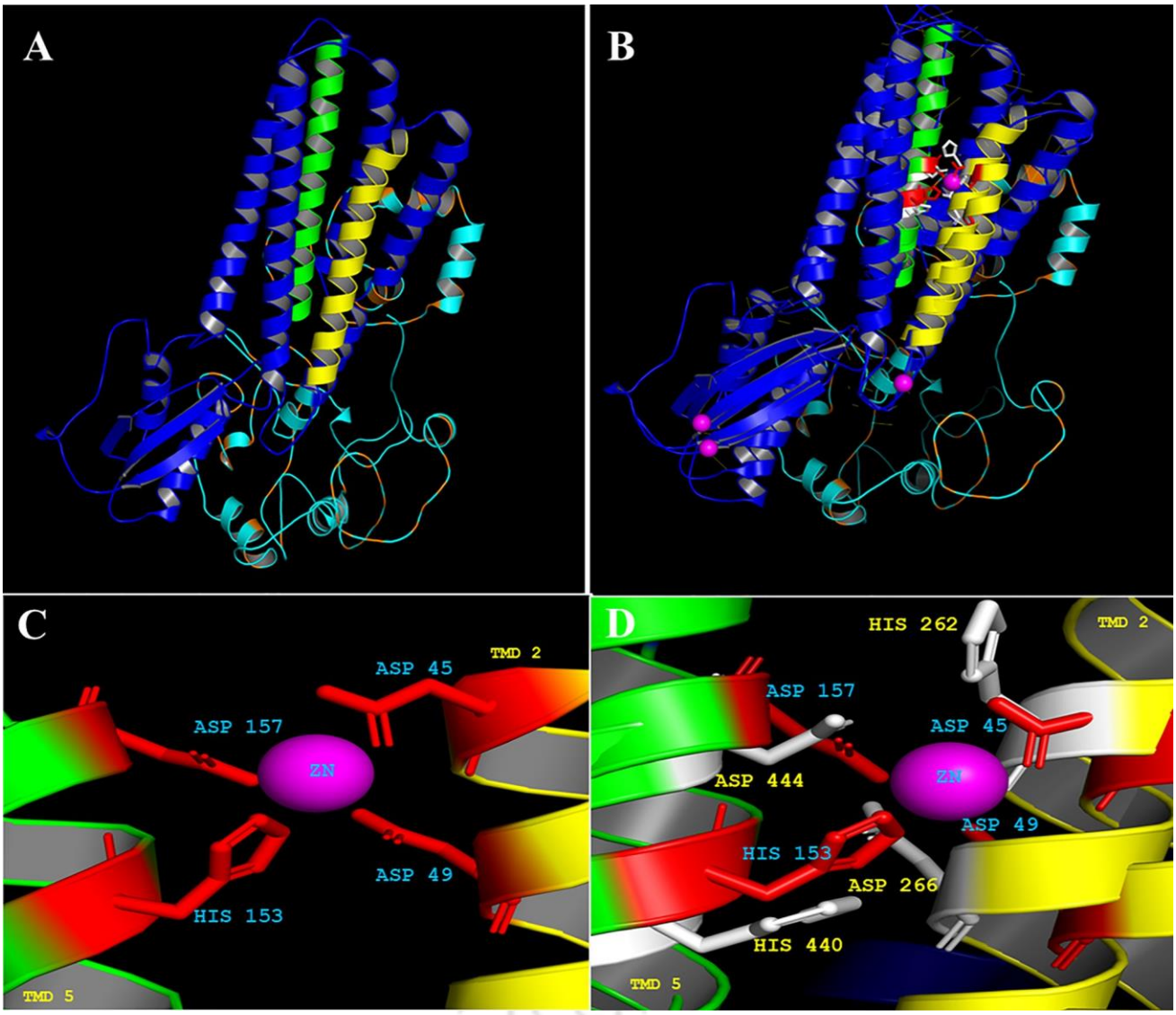

Figure 7. Homology modeling and structure validation of MSC-2. (A) Modeled structure of MSC-2. The MSC-2 protein is shown in blue; TM helixes 2 and 5 are shown in yellow and green, respectively; the regions that are structurally not aligned with YiiP (PDB ID: 3H90, Chao and Fu 2004) are shown in cyan; and the histidine residues within that region are highlighted in orange. (B) Superimposed image of YiiP and the modeled MSC-2; the residues of MSC-2 that are aligned with the zincinteracting residues of YiiP are shown in white. (C) The zinc-interacting site of YiiP. The residues in the 'DDHD' motif present within the TM helix 2 and 5 of YiiP are shown. (D) The superimposed image of the zinc-interacting site of YiiP with MSC-2. The probable zinc-interacting residues in the 'HDHD' motif of MSC-2 are shown based on its alignment with YiiP.

double mutant showed phenotypes corresponding to the parental single mutant Dzrc-1 in high-zinc condition (figure 2). However, double deletion of both msc-2

and zrg-17 restored the zrg-17 single-mutant defects in growth, cellulose degradation, and asexual sporulation (figures 2, 4, and 5). Therefore, Dzrg-17 mutation rescued the Dmsc-2 mutant, suggesting a possible antagonistic interaction between msc-2 and zrg-17. Similarly, Zrg17p and Msc2p in S. cerevisiae and Zrg17 and Cis4 in S. pombe form a heteromeric complex and transport zinc into the secretory pathways

(Ellis et al. 2005; Fang et al. 2008; Choi et al. 2018). The effect of the simultaneous deletion of zrc-1, msc-2, and zrg-17 is not known. Therefore, we screened progenies ([200) from Dzrc-1;Dmsc-2 mat A crossed with Dzrg-17 mat a, to generate triple mutants lacking zrc-1, msc-2, and zrg-17; however, we could not obtain a single viable triple mutant. A viable triple mutant would indicate a possible of functional redundancy of these genes, while the inability to obtain viable progeny might suggest an essential role of these in transporting zinc necessary for survival in N. crassa.

The Dzrc-1;Dzrg-17 double mutant showed a shorter septum length, resulting in more septation and distorted aerial hyphae. Moreover, Dzrc-1;Dzrg-17 showed conidiation defects, such as early and enhanced immature conidiation and inappropriate conidiation in submerged culture. The Dzrc-1;Dzrg-17 mutant produced asexual sporulation that was correlated with the increased expression of the con-10 gene (figure 4B), which was shown to be highly expressed in the conidiation process in N. crassa (Roberts et al. 1988). Correlation between the release of immature conidia and short aerial hyphae was also reported in the Ddcc-1 mutant (Barba-Ostria et al. 2011), and the Dplc1;DsplA2 and Dplc-1;Dcpe-1 double mutants (Barman and Tamuli 2017). In N. crassa, the multinucleated cell hyphae possess septa or crosswalls, allowing the passage of organelles, including nuclei (Potapova and Golyshev 2016). These septations provide structural integrity of the hyphae and also play crucial roles in developmental processes such as asexual sporulation and protoperithecia formation (Riquelme and Bartnicki-Garcia 2004; Rasmussen and Glass 2007;

Mourin˜o-Pe´rez 2013). These results highlight the significance of CDF zinc transporters and the potential genetic interactions between zrc-1, msc-2, and zrg-17 in N. crassa during septa development and proper conidiation.

ER stress activates distinct physiological processes like unfolded protein response or apoptosis in the cell depending on the stress intensity (Xu et al. 2005; Hetz 2012). In addition, cellulose as a substrate causes a glucose-deprived condition, triggering the secretion of an array of enzymes; such loads of enzymes compromise the ER folding capacity, triggering ER stress (Montenegro-Montero et al. 2015; Starr and Gonc 2018; Collier et al. 2020). The ER proteins Zrg17p and Msc2p, along with the vacuolar proteins Zrc1p and Zot1p, were significant for ER function by regulating zinc homeostasis in S. cerevisiae (Ellis et al. 2004, 2005). The Dzrg-17 mutant of N. crassa could not grow under ER stress induced by DTT and was unable to degrade cellulose (Tiwari et al. 2018). Therefore, to elucidate the roles of CDF in ER function, strains were exposed to ER stress mediated by DTT and cellulose as a carbon source. The double mutants Dzrc-1;Dmsc-2 and Dzrc-1;Dzrg-17 produced retarded aerial hyphae in the DTT-containing medium and were not able to utilize Avicel, producing negligible or no biomass (figure 5). Further, we measured the glucose amount and protein concentrations released in the supernatant of the strains and compared the mutants with the wild type. The

estimated glucose released with protein concentration corresponds to the growth of the strains in the provided conditions. This suggested the involvement of CDF zinc transporters and their genetic interactions in the normal growth of N. crassa. Structural prediction of the N. crassa ZRC-1 and MSC-2 using the only available X-ray crystallography structure of YiiP (Lu and Fu 2007) as a template revealed the conserved 'DDHD/HDHD' motif necessary for interaction with zinc (figures 6 and 7). In conclusion, this work suggested that ZRC-1 functions in zinc detoxification required for survival under highzinc conditions, and MSC-2 might be involved in assisting zinc transportation in N. crassa. Further studies will reveal their molecular interacting partners and structure–function relationships.

ACKNOWLEDGEMENTS

We thank the Fungal Genetics Stock Center (FGSC), Kevin McCluskey, and Aric Wiest for generously waiving charges for some of the strains. We also thank Dr. Anand Tiwari for initial help in this work. SN was financially supported by a Research Fellowship from the Ministry of Human Resource Development (MHRD), Government of India. We acknowledge the MHRD, IIT Guwahati, Department of Biotechnology (DBT) NER twinning grant BT/PR24473/NER/95/737/ 2017 to RT, and Science and Engineering Research Board (SERB) Start-up grant for Young Scientists, YSS/2014/000174, to AT, for partial financial support.

Declarations

Conflict of Interest The authors declare that they have no conflict of interest.

REFERENCES

Amich J and Calera JA 2014 Zinc acquisition: a key aspect in Aspergillus fumigatus virulence. Mycopathologia 178 379–385

Amico-Ruvio SA, Murthy SE, Smith TP, et al. 2011 Zinc effects on NMDA receptor gating kinetics. Biophys J. 100 1910–1918

Barba-Ostria C, Lled´ıas F and Georgellis D 2011 The Neurospora crassa DCC-1 protein, a putative histidine kinase, is required for normal sexual and asexual development and carotenogenesis. Eukaryot. Cell 10 1733–1739

Barman A and Tamuli R 2017 The pleiotropic vegetative and sexual development phenotypes of Neurospora crassa arise from double mutants of the calcium signaling genes plc-1, splA2, and cpe-1. Curr. Genet. 63 861–875

Bellotti D, Miller A, Rowin´ska-Zyrek M,_ et al. 2022 $Zn^{2?}$ and $Cu^{2?}$ binding to the extramembrane loop of Zrt2, a zinc transporter of Candida albicans. Biomolecules 12 121

Bird AJ and Wilson S 2020 Zinc homeostasis in the secretory pathway in yeast. Curr. Opin. Chem. Biol. 55 145–150

Boch A, Trampczynska A, Simm C, et al. 2008 Loss of Zhf and the tightly regulated zinc-uptake system SpZrt1 in Schizosaccharomyces pombe reveals the delicacy of cellular zinc balance. FEMS Yeast Res. 8 883–896

Boyce KJ, Cao C, and Andrianopoulos A 2016 Twocomponent signaling regulates osmotic stress adaptation via sskA and the high-osmolarity glycerol MAPK pathway in the human pathogen Talaromyces marneffei. mSphere 1 e00086-15

Chao Y and Fu D 2004 Thermodynamic studies of the mechanism of metal binding to the Escherichia coli zinc transporter YiiP. J. Biol. Chem. 279 17173–17180

Cho M, Hu G, Caza M, et al. 2018 Vacuolar zinc transporter Zrc1 is required for detoxification of excess intracellular zinc in the human fungal pathogen Cryptococcus neoformans. J. Microbiol. 56 65–71

Choi S, Hu YM, Corkins ME, et al. 2018 Zinc transporters belonging to the Cation Diffusion Facilitator (CDF) family have complementary roles in transporting zinc out of the cytosol. PLoS Genet. 14 e1007262

Clemens S 2022 The cell biology of zinc. J. Exp. Bot. 73 1688–1698

Clemens S, Bloss T, Vess C, et al. 2002 A transporter in the endoplasmic reticulum of Schizosaccharomyces pombe cells mediates zinc storage and differentially affects transition metal tolerance. J. Biol. Chem. 277 18215–18221

Collier LA, Ghosh A and Borkovich KA 2020 Heterotrimeric G-protein signaling is required for cellulose degradation in Neurospora crassa. mBio 11 e02419– e02420

Cousins RJ, Liuzzi JP and Lichten LA 2006 Mammalian zinc transport, trafficking, and signals. J. Biol. Chem. 281 24085–24089

Crawford AC, Lehtovirta-morley LE, Alamir O, et al. 2018 Biphasic zinc compartmentalisation in a human fungal pathogen. PLoS Pathog. 14 e1007013

Cuajungco MP and Lees GJ 1997 Zinc metabolism in the brain: Relevance to human neurodegenerative disorders. Neurobiol. Dis. 4 137–169

Davis RH and de Serres FJ 1970 Metabolism of amino acids and amines Part A. Methods Enzymol. 17 79–143

Deka R, Kumar R, and Tamuli R 2011 Neurospora crassa homologue of Neuronal Calcium Sensor-1 has a role in growth, calcium stress tolerance, and ultraviolet survival. Genetica 139 885–894

Dodson G and Steiner D 1998 The role of assembly in insulin's biosynthesis. Curr. Opin. Struct. Biol. 8 189–194

Eide DJ 2006 Zinc transporters and the cellular trafficking of zinc. Biochim. Biophys. Acta Mol. Cell Res. 1763 711–722

Eide DJ 2009 Homeostatic and adaptive responses to zinc deficiency in Saccharomyces cerevisiae. J. Biol. Chem. 284 18565–18568

Ellis CD, Wang F, MacDiarmid CW, et al. 2004 Zinc and the Msc2 zinc transporter protein are required for endoplasmic reticulum function. J. Cell Biol. 166 325–335

Ellis CD, MacDiarmid CW and Eide DJ 2005 Heteromeric protein complexes mediate zinc transport into the secretory pathway of eukaryotic cells. J. Biol. Chem. 280 28811–28818

Fang Y, Sugiura R, Ma Y, et al. 2008 Cation diffusion facilitator Cis4 is implicated in golgi membrane trafficking via regulating zinc homeostasis in fission yeast. Mol. Biol. Cell 19 1295–1303

Feige MJ and Hendershot LM 2011 Disulfide bonds in ER protein folding and homeostasis. Curr. Opin. Cell Biol. 23 167–175

Freedman RB 1995 The formation of protein disulphide bonds. Curr. Opin. Struct. Biol. 5 85–91

Gaither LA and Eide DJ 2001 Eukaryotic zinc transporters and their regulation. Biometals 14 251–270

Harding HP, Zhang Y and Ron D 1999 Protein translation and folding are coupled by an endoplasmic-reticulumresident kinase. Nature 397 271–274

Hetz C 2012 The unfolded protein response: Controlling cell fate decisions under ER stress and beyond. Nat. Rev. Mol. Cell Biol. 13 89–102

Holm L 2022 Dali server: structural unification of protein families. Nucleic Acids Res. 50 210–215

Kambe T, Weaver BP and Andrews GK 2008 The genetics of essential metal homeostasis during development. Genesis 46 214–228

Kambe T, Matsunaga M and Takeda TA 2017 Understanding the contribution of zinc transporters in the function of the early secretory pathway. Int. J. Mol. Sci. 18 2179

Kambe T, Taylor KM and Fu D 2021 Zinc transporters and their functional integration in mammalian cells. J. Biol. Chem. 296 100320

Kamizono A, Nishizawa M, Teranishi Y, et al. 1989
Identification of a gene conferring resistance to zinc and cadmium ions in the yeast Saccharomyces cerevisiae. Mol. Gen. Genet. 219 161–167

Kays AM, Rowley PS, Baasiri RA, et al. 2000 Regulation of conidiation and adenylyl cyclase levels by the Galpha protein GNA-3 in Neurospora crassa. Mol. Cell. Biol. 20 7693–7705

Kim MJ, Kil M, Jung JH, et al. 2008 Roles of zincresponsive transcription factor Csr1 in filamentous growth of the pathogenic yeast Candida albicans. J. Microbiol. Biotechnol. 18 242–247

Kiranmayi P and Mohan PM 2006 Metal transportome of Neurospora crassa. In Silico Biol. 6 169–180

Kiranmayi P, Tiwari A, Sagar KP, et al. 2009 Functional characterization of tzn1 and tzn2-zinc transporter genes in Neurospora crassa. Biometals 22 411–420

Ko J, Park H, Heo L, et al. 2012 GalaxyWEB server for protein structure prediction and refinement. Nucleic Acids Res. 40 294–297

Koh JY 2001 Zinc and disease of the brain. Mol. Neurobiol. 24 99–106

Laskowski RA, MacArthur MW, Moss DS, et al. 1993 PROCHECK: a program to check the stereochemical quality of protein structures. J. Appl. Crystallogr. 26 283–291

Linke K, Wolfram T, Bussemer J, et al. 2003 The roles of the two zinc binding sites in DnaJ. J. Biol. Chem. 278 44457–44466

Livak KJ and Schmittgen TD 2001 Analysis of relative gene expression data using real-time quantitative PCR and the 2^{-DDC}T method. Methods 25 402–408

Lo´pez-Berges MS 2020 ZafA-mediated regulation of zinc homeostasis is required for virulence in the plant pathogen Fusarium oxysporum. Mol. Plant Pathol. 21 244–249 Lu M and Fu D 2007 Structure of the zinc transporter YiiP. Science 317 1746–1748

Lyons TJ, Gasch AP, Gaither LA, et al. 2000 Genome-wide characterization of the Zap1p zinc-responsive regulon in yeast. Proc. Natl. Acad. Sci. USA 97 7957–7962

MacDiarmid CW, Gaither LA and Eide D 2000 Zinc transporters that regulate vacuolar zinc storage in Saccharomyces cerevisiae. EMBO J. 19 2845–2855

MacDiarmid CW, Milanick MA and Eide DJ 2003 Induction of the ZRC1 metal tolerance gene in zinc-limited yeast confers resistance to zinc shock. J. Biol. Chem. 278 15065–15072

McCluskey K, Wiest A and Plamann M 2010 The fungal genetics stock center: A repository for 50 years of fungal genetics research. J. Biosci. 35 119–126

Mishra C, Keskar S and Rao M 1984 Production and properties of extracellular endoxylanase from Neurospora crassa. Appl. Environ. Microbiol. 48 224–228

Miyabe S, Izawa S and Inoue Y 2000 Expression of ZRC1 coding for suppressor of zinc toxicity is induced by zincstarvation stress in Zap1-dependent fashion in Saccharomyces cerevisiae. Biochem. Biophys. Res. Commun. 276 879–884

Miyabe S, Izawa S and Inoue Y 2001 The Zrc1 is involved in zinc transport system between vacuole and cytosol in Saccharomyces cerevisiae. Biochem. Biophys. Res. Commun. 282 79–83

Mocchegiani E, Bertoni-Freddari C, Marcellini F, et al. 2005 Brain, aging and neurodegeneration: Role of zinc ion availability. Prog. Neurobiol. 75 367–390

Montanini B, Blaudez D, Jeandroz S, et al. 2007 Phylogenetic and functional analysis of the Cation Diffusion Facilitator (CDF) family: Improved signature and prediction of substrate specificity. BMC Genomics 8 107

Montenegro-Montero A, Goity A and Larrondo LF 2015 The bZIP transcription factor HAC-1 is involved in the unfolded protein response and is necessary for growth on cellulose in Neurospora crassa. PLoS One 10 e013141

Moreno MA´ , Ibrahim-Granet O, Vicentefranqueira R, et al. 2007 The regulation of zinc homeostasis by the ZafA transcriptional activator is essential for Aspergillus fumigatus virulence. Mol. Microbiol. 64 1182–1197

Mourin˜o-Pe´rez RR 2013 Septum development in filamentous ascomycetes. Fungal Biol. Rev. 27 1–9

Navarro-Sampedro L, Yanofsky C and Corrochano LM 2008 A genetic selection for Neurospora crassa mutants altered in their light regulation of transcription. Genetics 178 171–183

Nicolson TJ, Bellomo EA, Wijesekara N, et al. 2009 Insulin storage and glucose homeostasis in mice null for the granule zinc transporter ZnT8 and studies of the type 2 diabetes-associated variants. Diabetes 58 2070–2083

Nies DH 2003 Efflux-mediated heavy metal resistance in prokaryotes. FEMS Microbiol. Rev. 27 313–339

Nobile CJ, Nett JE, Hernday AD, et al. 2009 Biofilm matrix regulation by Candida albicans Zap1. PLoS Biol. 7 e1000133

Park HS and Yu JH 2012 Genetic control of asexual sporulation in filamentous fungi. Curr. Opin. Microbiol. 15 669–677

Paulsen IT and Saier MH 1997 A novel family of ubiquitous heavy metal ion transport proteins. J. Membr. Biol. 156 99–103

Potapova TV and Golyshev SA 2016 Revisiting a special structural order of a growing tip of the Neurospora crassa hypha. Fungal Genomics Biol. 6 3–6

Pound LD, Sarkar SA, Benninger RKP, et al. 2009 Deletion of the mouse Slc30a8 gene encoding zinc transporter-8 results in impaired insulin secretion. Biochem. J. 421 371–376

Ramachandran GN and Sasisekharan V 1968 Conformation of polypeptides and proteins. Adv. Protein Chem. 23 283–437

Rasmussen CG and Glass NL 2007 Localization of RHO-4 indicates differential regulation of conidial versus vegetative septation in the filamentous fungus Neurospora crassa. Eukaryot. Cell 6 1097–1107

Raulin J 1869 Chemical studies on vegetation. Ann. Sci. Nat. 11 93–99

Riquelme M and Bartnicki-Garcia S 2004 Key differences between lateral and apical branching in hyphae of Neurospora crassa. Fungal Genet. Biol. 41 842–851

Roberts AN, Berlin V, Hager KM, et al. 1988 Molecular analysis of a Neurospora crassa gene expressed during conidiation. Mol. Cell Biol. 8 2411–2418

Scheuner D, Song B, McEwen E, et al. 2001 Translational control is required for the unfolded protein response and in vivo glucose homeostasis. Mol. Cell 7 1165–1176

Seale T 1973 Life cycle of Neurospora crassa viewed by scanning electron microscopy. J. Bacteriol. 113 1015–1025

Seidel C, Moreno-Vela´squez SD, Riquelme M, et al. 2013 Neurospora crassa NKIN2, a kinesin-3 motor, transports early endosomes and is required for polarized growth.
Eukaryot. Cell 12 1020–1032

Soares LW, Baila˜o AM, de Soares CMA, et al. 2020 Zinc at the host-fungus Interface: How to uptake the metal? J. Fungi 6 305

Springer ML and Yanofsky C 1989 A morphological and genetic analysis of conidiophore development in Neurospora crassa. Genes Dev. 3 559–571

Starr TL and Gonc AP 2018 The major cellulases CBH-1 and CBH-2 of Neurospora crassa rely on distinct ER cargo adaptors for efficient ER-exit. Mol Microbiol. 107 229–248

Taka´cs T, Ne´meth MT, Bohner F, et al. 2022 Characterization and functional analysis of zinc trafficking in the human fungal pathogen Candida parapsilosis. Open Biol. 12 220077

Tiwari A, Ngiilmei SD and Tamuli R 2018 The NcZrg-17 gene of Neurospora crassa encodes a cation diffusion facilitator transporter required for vegetative development, tolerance to endoplasmic reticulum stress and cellulose degradation under low zinc conditions. Curr. Genet. 64 811–819

Vallee BL and Auld DS 1990 Zinc coordination, function, and structure of zinc enzymes and other proteins. Biochemistry 29 5647–5659

Vicentefranqueira R, Amich J, Mar´ın L, et al. 2018 The transcription factor ZafA regulates the homeostatic and adaptive response to zinc starvation in Aspergillus fumigatus. Genes 9 318

Vogel HJ 1956 A convenient growth medium for Neurospora (Medium N). Microb. Genet. Bull. 13 42–43

Vogel HJ 1964 Distribution of lysine pathways among fungi: evolutionary implications. Am. Nat. 98 435–446

Corresponding editor: PN RANGARAJAN

Westergaard M and Mitchell HK 1947 Neurospora V. A synthetic medium favoring sexual reproduction. Am. J. Bot. 573–577

Wijesekara N, Dai FF, Hardy AB, et al. 2010 Beta cellspecific Znt8 deletion in mice causes marked defects in insulin processing, crystallisation and secretion. Diabetologia 53 1656–1668

Wu CY, Bird AJ, Chung LM, et al. 2008 Differential control of Zap1-regulated genes in response to zinc deficiency in Saccharomyces cerevisiae. BMC Genomics 9 1–17

Xu C, Bailly-Maitre B and Reed JC 2005 Endoplasmic reticulum stress: Cell life and death decisions. J. Clin. Invest. 115 2656–2664

Yang J and Zhang Y 2015 I-TASSER server: New development for protein structure and function predictions. Nucleic. Acids Res. 43 174–181

Zhao H and Eide D 1996a The yeast ZRT1 gene encodes the zinc transporter protein of a high-affinity uptake system induced by zinc limitation. Proc. Natl. Acad. Sci. USA 93 2454–2458

Zhao H and Eide D 1996b The ZRT2 gene encodes the low affinity zinc transporter in Saccharomyces cerevisiae. J. Biol. Chem. 271 23203–23210

Zhao H and Eide DJ 1997 Zap1p, a metalloregulatory protein involved in zinc-responsive transcriptional regulation in Saccharomyces cerevisiae. Mol. Cell Biol. 17 5044–5052

Zheng W, Zhang C, Li Y, et al. 2021 Folding nonhomologous proteins by coupling deep-learning contact maps with I-TASSER assembly simulations. Cell Rep. Methods 1 100014